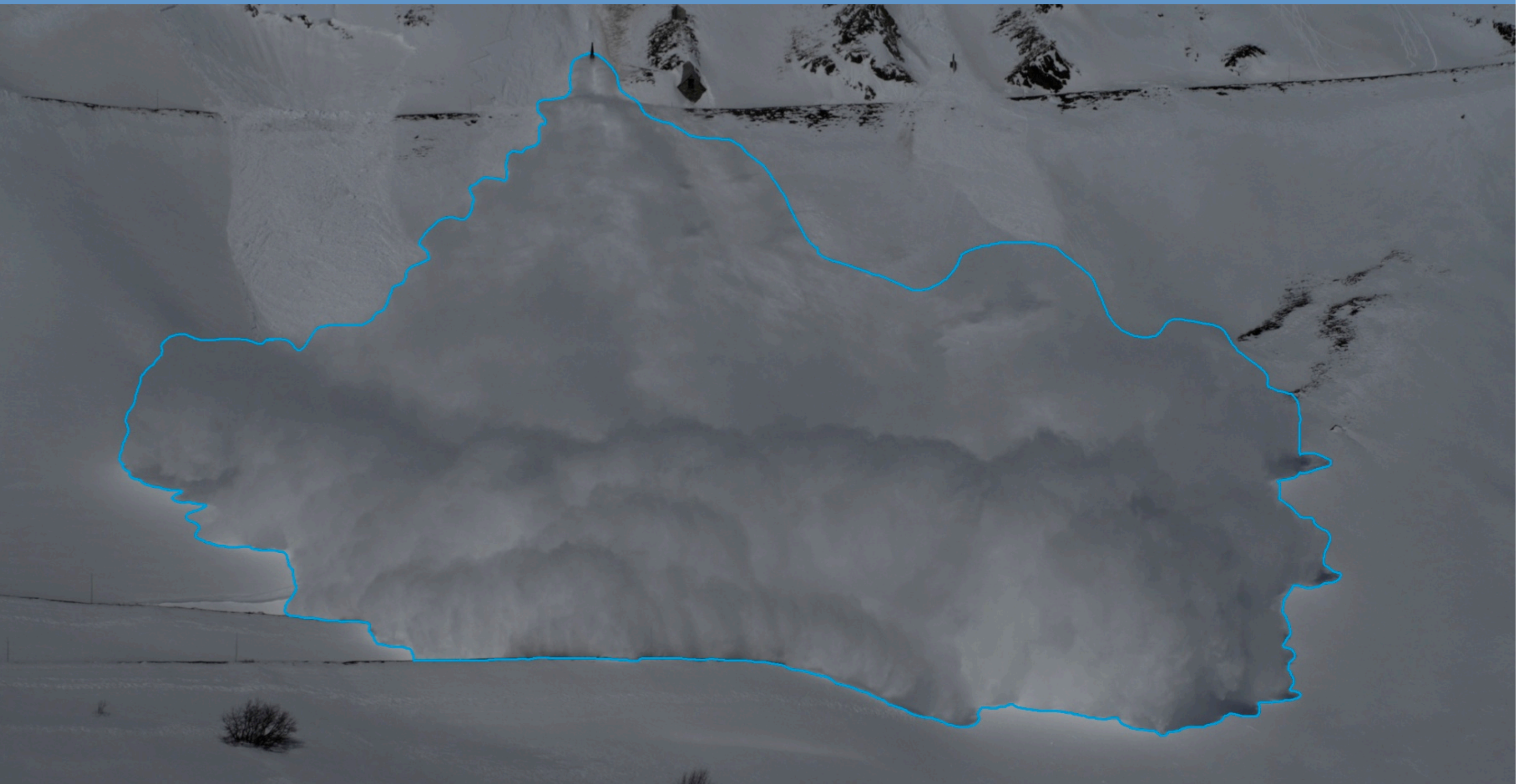

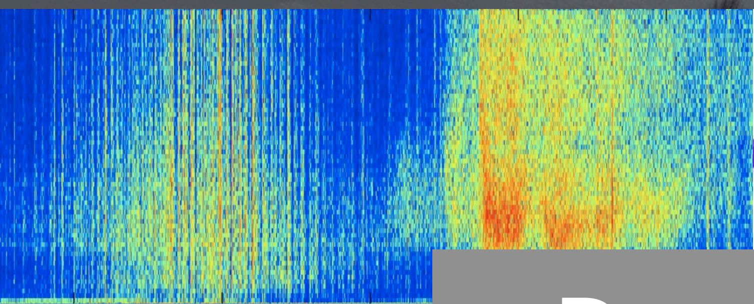

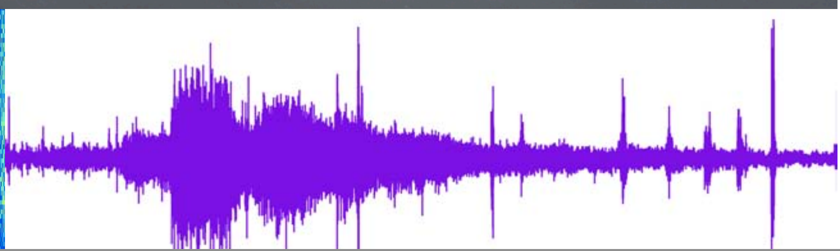

Development of acoustic monitoring for alpine mass movements

Institute of Mountain Risk Engineering
University of Natural Resources and Life Sciences, Vienna

Development of Acoustic Monitoring for Alpine Mass Movements

A PhD thesis submitted

for the degree of

Doctor rerum naturalium technicarum

presented by Arnold Kogelnig

Supervisor:

Univ. Prof. DI Dr. Johannes Hübl

Prof. Titular Dra. Emma Suriñach Cornet

Institute of Mountain Risk Engineering

University of Natural Resources and Applied Life Sciences

Vienna, 2012

Cover photograph*: Artificial released snow avalanche at the Col du Lautaret test site (Cemagref, France), February 2007. Picture taken by Arnold Kogelnig.*

Back cover photograph: *Debris flow surge, pictured at the Jiangjia Gully observation station (China) by Johannes Hübl, summer 2007.*

Literature Citation: Kogelnig, A. (2012): Development of acoustic monitoring for alpine mass movements, PhD thesis, University of Natural Resources and Life Sciences Vienna (BOKU), Institute of Mountain Risk Engineering

Dedicated to my family, for their support
during all the years of studying
and writing my thesis.

A good scientist is not a person who gives the right answers,
he's one who asks the right questions.
Claude Lévi-Strauss, 1964

Stay hungry, Stay foolish!

Steve Jobs, Stanford University, 2005

Contents

List of Figures

List of Tables

Acknowledgements

Finally I reached this long awaited point; this is the end of my PhD thesis. It would have never been possible to come even close to the end of this study without the help of numerous people. Many thanks to all accompanying me on my journey!

I have been very fortunate with my supervisors. I would like to thank Johannes Hübl, for giving me the opportunity to accomplish this thesis, for the financial support and for always giving me the freedom to follow my ideas.

I want to express my deeply felt thanks to Emma Suriñach, co-supervisor of my thesis, for spending numerous hours teaching me the fundamentals of signal analysis and geophysics. Without her guidance and support I would have been lost. Her endurance and patience with me is admirable.

Furthermore I owe my deepest gratitude to Ignasi Vilajosana for the many things that I have learnt from him, for his ability to explain things clearly and simplly, for pushing me during the last 4 years and for his friendship. His enthusiasm and his inspiration are contagious!

My sincere thanks goes to the whole research group at the UB Barcelona at the Department of Geodynamics and Geophysics for making my stays there so easy.

During my thesis many people supported me here at the Institute of Mountain Risk Engineering among them Roland Kaitna, Monika Stanzer, Michael Chiari, and Christian Scheidl. Thank you for all the lunch times, break times and discussions we have shared! I feel very grateful to Sven Fuchs for his wise advise and his open ear whenever I had a question.

Especially I would like to mention my teammates from the small but very vital snow and avalanche research group here at the Institute of Mountain Risk Engineering. Michael Bacher for introducing me to the world of science and giving me the opportunity to ski in La Grave during my master thesis. Alexander Prokop for all those adventures in Lech am Arlberg and Thomas Wiesinger, for bringing a little bit Swiss style to our institute. Thank you for sharing the passion and love for snow with me! I cannot forget to thank Reinhold Totschnig for sharing the office with me and to always have an answer to my daily questions.

For this research, data were essential and I collected a lot of data. Gathering data from random alpine processes is truly a demanding task. Many people helped with this especially I would like to thank:

Friedrich Zott for his help with all the instrumentation 24/7 through all the years, his support has made this work possible. How can I forget all those late night discussions about life, wives and children?

Brian McArdell, Christoph Graf and Catherine Berger from the WSL for giving me the possibility to come to the Illgraben torrent and for the support with installing and maintaining the equipment. Thank you for sharing your data with me!

Special thanks go to Betty Sovilla and Francois Dufour for letting me work at the VDLS test site. It was very encouraging to work with Betty in Davos, thank you for sharing your time and data with me, this was a key point to finish this study. Especially I have to thank Martin Hiller for his support and patience installing the equipment at VDLS all the years. He is a legend.

This study has been supported by the BOKU DOC grants 2008, the Spanish national project “Nuevas Tecnologías y métodos para la detección y caracterización de movimientos de masa (aludes de nieve, corrientes de derrubios y desprendimientos de rocas) CGL2010-18609 (NUTESA)” and the Spanish national project „Development and application of quantitative methods and techniques to characterize, detect and prevent mass movements (snow avalanches, debris flow and rock fall) CGL2006-06596/BTE (DALMASA)”.

Furthermore I want to thank the official referees Gloria Furdada and Marcel Hürlimann for taking the time and assessing this thesis and Emily Procter for helping me out with the English.

Finally I want to thank my family. The encouragement and unconditional support from my beloved wife Barbara is a never-ending source of energy for me. For all that, and for being everything I am not, she has my everlasting love. A special thought is devoted to my parents, my sister Alexandra and my grandmother for endless support; they deserve far more credit than I can give them. To them I dedicated this thesis.

Motivation

Due to the fast socio-economic development in alpine regions, processes like debris flows or snow avalanches (alpine mass movements), which occur at the intersection between the natural environment and the environment formed and controlled by human activity, pose a continued threat to people and property. Governmental agencies try to protect settlements and traffic routes by active measures (e.g., retention dams, snow bridges, etc.) and/or passive measures (e.g., land use planning, evacuations, closing of roads and railways in case of acute danger). These measures, and in particular the passive approaches, require reliable information from monitoring and detection systems. Knowledge of specific parameters of the phenomena, such as occurrence/frequency, size, velocity, etc., can assist regional or local authorities who are responsible for the control of such hazards.

Although different monitoring systems already exist, such as geophones, radar, ultrasonic sensors (flow depth), etc., a reliable monitoring system has yet to be developed. The harsh alpine environment makes it difficult to find appropriate and sustainable monitoring locations for the equipment. Most of the present methods need sensors placed in close proximity to or in/above the process itself, which leads to expensive structures and continuous maintenance to ensure steadiness and stability (Graf et al., 2006; Bessason et al., 2007; Badoux et al., 2009).

The scientific field of acoustics covers the study of mechanical waves propagating in gases (ultra-, audible- and infrasound), liquids (hydroacoustic) and solids (seismic waves) that can be monitored with specific sensors distant from the source.

This study presents a new approach to monitor alpine mass movements using a combination of two acoustic sensors: seismometers/geophones and infrasound microphones. Both sensors have been individually used in many previous studies. Seismic sensors such as geophones and seismometers have already been used for monitoring natural hazards (e.g., Sabot et al., 1998; Arattano, 1999; Suriñach et al., 2001; Suriñach et al., 2005; Vilajosana et al., 2008). Infrasound technology has been used recently for the development of automatic detection systems for snow avalanches and debris flows (Adam et al., 1997; Zhang et al., 2004; Chou et al., 2007; Scott et al., 2007). However, the potential combination of infrasonic and seismic sensors for monitoring natural hazards, which could take advantage of the benefits of both sensor technologies, has not been evaluated to date. Both seismic and infrasonic signals are mechanical waves that are often generated by the same physical phenomena. Additionally, the Earth's surface is not opaque to mechanical waves, either those propagating upward from within the Earth's solid interior or those propagating down from the atmosphere (Arrowsmith et al., 2010). As a consequence, the aim of the present work is an in-depth, combined study considering both the infrasonic and the seismic wave field generated by alpine mass movements.

A detailed analysis of seismic and infrasonic signals generated by snow avalanches and debris flows monitored at different locations in the Austrian and Swiss Alps will be presented. Additionally, we compare our data with other measurements, such as flow depth (for debris flows) or flow velocity and pressure (snow avalanches), for the interpretation, verification and validation of the seismic and infrasonic data.

References

Arrowsmith, S., Johnson, J., Drob, D. and Hedlin M. (2010): The seismoacoustic wavefield: A new paradigm in studying geophysical phenomena, Reviews of Geophysics, 48, RG4003, doi:10.1029/2010RG000335.

Adam, V., Chritin, V., Rossi, M. and Bolognesi, R. (1997): Acoustic detection system for operational avalanche forecasting, in: International Snow Science Workshop, Banff, Alberta, 149–153

Arattano, M. (1999): On the use of seismic detectors as monitoring and warning systems for debris flows, Natural Hazards and Earth System Sciences, 20,197–213

Badoux, A., Graf, C., Rhyner, J., Kuntner, R. and McArdell, B. (2009): A debris-flow alarm system for the alpine Illgraben catchment: design and performance, Natural Hazards and Earth System Sciences, 49, 517–539

Bessason, B., Eirìksson, G., Thoŕorinsson, Ò., Thoŕorinsson, A. and Einarsson, S. (2007): Automatic detection of avalanches and debris flows by seismic methods, Journal of Glaciology, 53, 461–472

Chou, H., Cheung, Y. and Zhang, S. (2007): Calibration of infrasound monitoring system and acoustic characteristics of debris-flow movement by field studies. In: Chenglung C, Major J (eds.) Debris-flow hazards mitigation: mechanics, prediction, and assessment. Millpress, Rotterdam, 571–580

Graf, C., Badoux, A., McArdell, B., Dufour, F., Rhyner, J. and Kuntner, R. (2006): A warning system for natural hazards in summer at the Illgraben, 4th Swiss Geoscience Meeting, Bern

Sabot, F., Naaim, M., Granada, F., Suriñach, E., Planet, P. and Furdada, G. (1998): Study of avalanche dynamics by seismic methods, image processing techniques and numerical models, Annals of Glaciology, 26, 319–323

Scott, E., Hayward, C., Kubichek, R., Hamann, J., Comey, R., Pierre, J. and Mendenhall, T. (2007): Single and multiple sensor identification of avalanche-generated infrasound, Cold Regions Science and Technology, 47, 159–170

Suriñach, E., Furdada, G., Sabot, F., Biescas, B. and Vilaplana, J. (2001): On the characterization of seismic signals generated by snow avalanches for monitoring purposes, Annals of Glaciology, 32, 268–274

Suriñach, E., Vilajosana, I., Khazaradze, G., Biescas, B., Furdada, G. and Vilaplana, J. (2005): Seismic detection and characterization of landslides and other mass movements, Natural Hazards and Earth System Sciences, 5, 791–798

Vilajosana, I., Suriñach, E., Abellán, A., Khazaradze, G., Garcia, D. and Llosa, J. (2008): Rockfall induced seismic signals: case study in Montserrat, Catalonia, Natural Hazards and Earth System Sciences, 8(4), 805–812.

Zhang, S., Hong, Y. and Yu, B. (2004): Detecting infrasound emission of debris flow for warning purposes, International Symposium Interpraevent VII, Riva, Trient, 359–364

Chapter 1

Introduction

Infrasound waves are low frequency (< 20 Hz) pressure fluctuations in the air and seismic waves are the counterpart, i.e. elastic waves travelling through the ground. In the last decades infrasound and seismic sensors have been used in many different studies for monitoring natural and artificial phenomena from distant locations (Benioff et al., 1951; Salway, 1978; Johnson, 2003; La Rocca et al., 2004).

One of the first possible observations of naturally-occurring infrasound originated from the eruption of the volcano on the Indonesian island Krakatoa in 1883 and from the Great Siberian Meteorite in 1909, when infrasonic waves circled the globe several times and were recorded on barometers worldwide (Strachey, 1888). Comparing arrival times, scientists were able to reconstruct the source by the progress of radiating pressure waves sometimes passing a monitoring station several times.

In the 1950s infrasonic sensing technology was developed to monitor nuclear explosions. Once the United States developed satellite technology to monitor nuclear explosions, infrasound research efforts declined. International adoption of the Comprehensive Nuclear-Test-Ban Treaty (CTBT) in the 1990s sparked renewed interest in infrasound monitoring (Comey and Mendenhall, 2004).

Nowadays, the most important use of infrasound technology is a global monitoring based on the CTBT, which bans all nuclear explosions in the atmosphere, oceans and underground. In the current international monitoring regime, a seismic network provides the tool for monitoring underground tests, the associated infrasound network is designed for monitoring atmospheric tests, and the hydroacoustic network allows for monitoring of tests in the oceans (Arrowsmith et al., 2010). As part of this International Monitoring System (IMS) a global network of 60 infrasound-monitoring stations has been established (Brachet et al., 2010).

In the last decades infrasound sensors attracted interest of the scientific community for their ability to monitor different natural phenomena remotely. For example, some studies have analysed infrasonic emission and propagation from volcanic explosions (Johnson, 2003), atmospheric pressure changes associated with earthquakes (Watada at al., 2006), infrasound signals generated from high speed trains hitting a tunnel (Iida et al., 2007), infrasound signals produced by ocean swell (Garces et al., 2003), infrasound signals produced by explosions (Hagerty et al., 2002), infrasound signals produced by jets (Le Pichon et al., 1995), infrasound associated with large rock and ice avalanches (Kenneth et al., 2005), as well as many more.

Seismic sensors on the other hand are most commonly used for discrimination and analysis of assumed stationary, point-source phenomena such as explosions and earthquakes. Nowadays, networks of seismographs continuously monitor the seismic environment of the planet, allowing global earthquakes (Nakamura, 1988) and tsunami warnings (Kanamori et al., 2008), as well as the recording of a variety of seismic signals arising from non-earthquake sources such as explosions (Evernden et al., 1986) or cryospheric events associated with large icebergs and glaciers (Amundson et al., 2008).

Infrasound and seismic technology has also proven to be suitable for monitoring rapid alpine mass movements. Saint-Lawrence and Williams (1976) were one of the first to show that snow avalanches generate seismic signals. Seismic signals of snow avalanches have been studied intensively since the 1990s focusing mainly on two purposes: a) development of early warning systems (Leprette et al., 1998; Bessason et al., 2007; Navarre et al., 2009) and b) improved understanding of snow avalanche characteristics (flow type, size, length, etc.) through the generated seismic signals (Sabot et al., 1998; Suriñach et al., 2000; Suriñach et al., 2001). This was achieved mainly through the investigation of the time and frequency evolution of the seismic signals (Biescas et al., 2003). Recently, seismic studies of snow avalanches have shown that it is possible to determine avalanche speed (Vilajosana et al., 2007a) and seismic energy emission (Vilajosana et al., 2007b), two physical parameters that are important for characterizing snow avalanches.

The first attempt using infrasound and seismic sensors for monitoring snow avalanches was performed by Harrison (1976), who detected weak, high frequency seismic signals but no infrasonic signals. The acoustic sensors used were not effective at detecting frequencies above about 0.3 Hz and it was noted that if the seismic and infrasonic signals have a common cause, it would probably be necessary to use microphones with a frequency response between 2 Hz and 20 Hz (Bedard et al., 1988). In the 1980s Bedard et al. (1988, 1989) continued the work of Harrison (1976) and studied the infrasonic emissions of snow avalanches. Infrasonic research activities have continually increased since then with a focus mainly towards detection of snow avalanches using predefined threshold values, cross correlation or beam forming algorithms (e.g., Bedard, 1994; Chritin et al., 1996; Comey and Mendenhall, 2004; Scott et al., 2007). However, few studies exist (Firstov et al., 1992; Naugolnykh and Bedard, 2002) related to the source of infrasound signals from snow avalanches.

In addition to snow avalanches, one of the most harmful processes in alpine environments are debris flows. Various previous studies on debris flows (e.g., Okuda et al., 1980; Wu et al., 1990; Hadley and Lahusen, 1991; Marchi et al., 2002; Arattano, 2003; Huang et al. 2003, 2007) have already shown that it is possible to detect and monitor these processes using seismic signal analysis.

Infrasonic detection of debris flows has also sparked the interest of the scientific community. For example, in China and Taiwan first studies have been conducted using custom-made infrasound microphones (Zhang et al., 2004; Chou et al., 2007), showing promising detection capabilities. Infrasound debris flow monitoring is still in its early years compared to the efforts that have been made for snow avalanches.

As mentioned above many previous studies using infrasound and seismic sensors focused primarily on the detection of snow avalanches or debris flows (e.g., Zhang et al., 2004; Scott et al., 2007). To design a reliable detection system it is important to understand the source of the signal, the propagation in the atmosphere and the evolution of the signal in the time and frequency domain; none of the past studies analysed these aspects in detail. The author’s intention is to analyze the infrasound and seismic signals emitted by alpine mass movements to gather information about the characteristics of the process and the source of the signals. Furthermore we want to present a theory about the source of infrasound waves of snow avalanches, and compare the theoretically calculated data with our measurements.

This study is structured as follows: Chapter 2 gives a short introduction to the alpine processes monitored, including snow avalanches, debris flows and debris floods. The theoretical background on infrasound and seismic signals and their propagation and attenuation is provided in Chapter 3. Understanding the propagation and attenuation mechanisms of seismic and infrasonic waves in the study conditions is crucial for the interpretation of the recorded seismic and infrasonic signals. Moreover, in Chapter 3 a brief description of the possible mechanisms that cause infrasonic emissions from mass movements is presented. In Chapter 4 key points for choosing a test site are summarized. Chapter 5 gives an overview of the different sensors and data acquisition systems used for monitoring. Chapter 6 introduces the data analysis methodology used, and the time, frequency and time-frequency methods are explained.

Chapter 7 constitutes the first principle part of this work. Infrasound and seismic signals of debris flows are analysed and compared with flow height measurements. It is demonstrated that debris flows emit low frequency infrasonic signals that can be monitored and correlated with seismic signals. During the passage of the debris flow, several surges were identified by ultrasonic gauges and detected in the time series and the running spectra of infrasonic data. This work allowed us to correlate specific signal features with characteristics of the flow. The main contents of this part have been published in Kogelnig et al. (online first). Chapter 8 presents the continuation of the analysis presented in Chapter 7; further acoustic data of debris flows and also debris floods are discussed. In addition, signals monitored at locations in China are presented, which demonstrated that the sensor locations and equipment setups were less preferable. The main contents of this chapter have been published in Kogelnig et al. (2011a). Chapter 9, the second principle part of this work, presents results obtained from monitoring infrasound and seismic signals emitted by snow avalanches. Comparing the seismic and acoustic data with flow velocity measurements the source of the infrasound signals could be identified and reproduced. Infrasound and seismic sensors not only detected the avalanches but were also sensitive to different flow regimes. The main contents of this part have been published in Kogelnig et al. (2011b). Chapter 10 then presents an overview, summarizing the most important acoustic characteristics of snow avalanches and debris flows. In Chapter 11 different common known sources of infrasound signals are presented. Infrasound and seismic data are analysed in detail and their main characteristics are identified.

Chapter 12 presents the final conclusions of the entire study and in Chapter 13 an outlook of further implications of infrasound and seismic sensors is given. The references are given add the end of every chapter.

References

Amundson, J., Truffer, M., Lüthi, M., Fahnestock, M., West M. and Motyka R. (2008): Glacier, fjord, and seismic response to recent large calving events, Jakobshavn Isbræ, Greenland, Geophysical Research Letters, 35, L22501, 1-5, doi:10.1029/2008GL035281

Arattano, M. (2003): Monitoring the presence of the debris-flow front and its velocity through ground vibrations detectors, Proceedings of the Third International Conference on Debris-Flow Hazards Mitigation: Mechanics, Prediction and Assessment, Millpress, Rotterdam, 2, 731-743.

Arrowsmith, S., Johnson, J., Drob, D. and Hedlin M. (2010): The seismoacoustic wavefield: A new paradigm in studying geophysical phenomena, Reviews of Geophysics, 48, RG4003, doi:10.1029/2010RG000335.

Bedard, A., Greene, G., Intrieri, J. and Rodriguez, R. (1988): On the Feasibility and Value of Detecting and Characterizing Avalanches Remotely by Monitoring Radiated Sub-Audible Atmospheric Sound at Long Distances, in Proceedings: A Multidisciplinary Approach to Snow Engineering, Santa Barbara, CA, 1-9

Bedard, A. (1989): Detection of avalanches using atmospheric infrasound, in: Proceedings of the Western Snow Conference, edited by: Shafer, B., Western Snow Conference, Colorado State University, 52–58

Bedard, A. (1994): An Evaluation of Atmospheric Infrasound for Monitoring Avalanches, Proceedings; 7th International Symposium on Acoustic Sensing and Associated Techniques of the Atmosphere and Oceans, Boulder, CO

Benioff, H., Ewing, E. and Press, F. (1951): Sound wave in the atmosphere generated by a small earthquake, Proceedings of the National Academy of Sciences of the United States of America, 37, 600-603.

Bessason, B., Eirìksson, G., Thoŕorinsson, Ò., Thoŕorinsson, A. and Einarsson, S. (2007): Automatic detection of avalanches and debris flows by seismic methods, Journal of Glaciology, 53, 461–472

Biescas, B., Dufour, F., Furdada, G., Khazaradze, G. and Suriñach, E. (2003): Frequency content evolution of snow avalanche seismic signals, Surveys in Geophysics, 24, 447–464

Brachet, N., Brown, D., Le Bras, R., Cansi, Y., Mialle, P. and Coyne, J. (2010): Monitoring the Earth's Atmosphere with the Global IMS Infrasound Network, in: Infrasound Monitoring for Atmospheric Studies, edited by: Le Pichon, A., Blanc, E. and Hauchecorne, A., Springer, 77-119

Comey, R. and Mendenhall, T. (2004): Recent Studies Using Infrasound Sensors to Remotely Monitor Avalanche Activity, in: Proceedings of the International Snow Science Workshop, Jackson Hole, Wyoming, 640–646

Chritin, V., Rossi, M., Bolognesi, R. (1996): Acoustic Detection System for Operational Avalanche Forecasting, in: Proceedings of the International Snow Science Workshop, Banff, Alberta.

Chou, H., Cheung, Y. and Zhang, S. (2007): Calibration of infrasound monitoring system and acoustic characteristics of debris-flow movement by field studies, in: Chenglung, C., Major, J. (eds.) Debris-flow Hazards Mitigation: Mechanics, Prediction, and Assessment, Millpress, Rotterdam, 571–580

Comey, R. and Mendenhall, T. (2004): Recent Studies Using Infrasound Sensors to Remotely Monitor Avalanche Activity, in: International Snow Science Workshop, Jackson Hole, Wyoming, 640–646

Evernden, J., Archambeau C. and Cranswick E. (1986): An evaluation of seismic decoupling and underground nuclear test monitoring using high-frequency seismic data, Reviews of Geophysics, 24(2), 143–215, doi:10.1029/RG024i002p00143

Firstov, P., Sukhanov, L., Pergament, V., and Rodionovskiy, M. (1992): Acoustic and seismic signal from snow avalanches, Transactions (Doklady) of the U.S.S.R., Academy of Sciences: Earth Science Sections, 312, 67–71

Garcés, M., Hetzer, C., Merrifield, M., Willis, M. and Aucan J. (2003): Observations of surf infrasound in Hawai'i, Geophysical Research Letters, 30(24), 2264, doi:10.1029/2003GL018614

Hadley, K. and Lahusen R. (1991): Deployment of an acoustic flow monitor system and examples of its application at Mount Pinatubo, Philippines (abstract), Eos Trans, AGU, 72(44), F67

Hagerty, M., Kim, W. and Martysevich, P. (2002): Infrasound detection of large mining blasts in Kazakhstan, Pure and Applied Geophysics, 159, 1063–1079, doi:10.1007/s00024-002-8673-3

Harrison, J. (1976): Seismic Signals from Avalanches, Chapter 7 in: Avalanche Release and Snow Characteristics, San Juan Mountain, Colorado, Final Report San Juan Avalanche Project, Institute of Arctic and Alpine Research, U. of Colorado, Boulder, CO, Editors: R. L. Armstrong and J. D. Ives, 145-152

Huang, C., Yin, H. and Shieh, C. (2003): Experimental study of the underground sound generated by debris flow, in: Proceedings of the Third International Conference on Debris-Flow Hazards Mitigation: Mechanics, Prediction and Assessment, Millpress, Rotterdam, 2, 731-743

Huang, C., Yin, H., Chen, C., Yeh, C. and Wang C. (2007): Ground Vibrations produced by rock motions and debris flow, Journal of Geophysical Research, 112, F02014, doi:10.1029/2005JF000437.

Iida, M., Kikuchi K. and Takami H. (2007): Infrasound Generated by a High-Speed Train Running Through a Short Tunnel, Journal of Low Frequency Noise, Vibration and Active Control, 26(3), 177-194

Johnson, J. (2003): Generation and propagation of infrasonic airwaves from volcanic explosions, Journal of Volcanology and Geothermal Research, 121,1–14

Kanamori, H. and Rivera, L. (2008): Source inversion of W-phase: speeding up seismic tsunami warning, Geophysical Journal International, 175, 222–238

Kenneth, M., Wilson, C., Olson, J. and Szuberla C. (2005): Infrasound Associated with Mt. Steller Avalanche, Inframatics, 12, December 2005, 4-7

Kogelnig, A., Hübl, J., Suriñach, E., Vilajosana, I. and McArdell, B. (online first): Infrasound produced by debris flow: propagation and frequency content evolution, Natural Hazards, doi:10.1007/s11069-011-9741-8

Kogelnig, A., Hübl, J., Suriñach, E., Vilajosana, I., Zhang, S., Yun, N. and McArdell, B. (2011a): A study of infrasonic signals of debris flows, in: Genevois, R., Hamilton, D. and Prestininzi, A. (Eds.), Italian Journal of Engineering Geology and Environment - Book, 563- 572, ISBN: 1825-6635; ISSN 978-88-95814-46-9

Kogelnig, A., Suriñach, E., Vilajosana, I., Hübl, J., Sovilla, B., Hiller, M. and Dufour, F. (2011b): On the complementariness of infrasound and seismic sensors for monitoring snow avalanches, Natural Hazards and Earth System Sciences, 11(8), 2355-2370

La Rocca, M., Galluzzo, D., Saccorotti, G., Tinti, S., Cimini, G. and Del Pezzo, E. (2004): Seismic signals associated to landslides and to tsunami at Aeolian islands, Italy, Geophysical Research Abstracts, Vol. 6, 00738

Le Pichon, A., Garcés, M., Blanc, E., Barthélémy, M. and Drob, D. (2001): Acoustic propagation and atmosphere characteristics derived from infrasonic waves generated by the Concorde, Journal of the Acoustical Society of America, 111 (1), 629-641

Leprettre, B., Martin, N., Glangeaud, F. and Navarre, J. (1998): Three-Component Signal Recognition Using Time, Time-Frequency and Polarization Information-Application to Seismic Detection of Avalanches, IEEE Transactions on Signal Processing, 46, 83–102

Marchi L., Arattano M. and Deganutti, A. (2002): Ten years of debris-flow monitoring in the Moscardo Torrent (Italian Alps), Geomorphology, 46(1-2), 1-17

Nakamura, Y. (1988): On the urgent earthquake detection and alarm system, in: Proceedings of ninth world conference on earthquake engineering, Tokyo, Japan, 7, 673-678

Naugolnykh, K. and Bedard, A. (2002): A model of the avalanche infrasonic radiation, in: Geoscience and Remote Sensing Symposium, 2, 871–872, doi:10.1109/IGARSS.2002.1025713

Navarre, J., Bourova, E., Roulle, J. and Deliot, Y. (2009): The seismic detection of avalanches: an information tool for the avalanche forecaster, in: Schweizer, J. and A. van Herwijnen, (eds.) Proceedings of the International Snow Science Workshop, 27 September–2 October 2009, Davos, Switzerland. Davos, WSL Institute for Snow and Avalanche Research SLF, 379–383.

Okuda, S., Okunishi, K. and Suwa, H. (1980): Observation of debris flow at Kamikamihori Valley of Mt. Yakedade, Excursion Guidebook of the Third Meeting of IGU commission on Field Experiment in Geomorphology, 127-130

Sabot, F., Naaim, M., Granada, F., Suriñach, E., Planet, P. and Furdada, G. (1998): Study of avalanche dynamics by seismic methods, image processing techniques and numerical models, Annals of Glaciology, 26, 319–323

Saint-Lawrence, Y. and Williams, T. (1976): Seismic signals associated with avalanches, Journal of Glaciology, 17, 521–526

Salway, A. (1978): A Seismic and Pressure Transducer System for Monitoring Velocities and Impact Pressure of Snow Avalanches, Arctic Antarctic and Alpine Research, 10, 769–774

Scott, E., Hayward, C., Kubichek, R., Hamann, J., Comey, R., Pierre, J. and Mendenhall, T. (2007): Single and multiple sensor identification of avalanche-generated infrasound, Cold Regions Science and Technology, 47, 159–170

Strachey, R. (1888): On the air waves and sounds caused by the eruption of Krakatoa in August, 1883, in: The Eruption of Krakatoa and Subsequent Phenomena, edited by G. J. Symons, 57–88,Trubner, London.

Suriñach, E., Sabot, F., Furdada G. and Vilaplana, J. (2000): Study of seismic signals of artificially released snow avalanches for monitoring purposes, Physics and Chemistry of the Earth, 25(9), 721–727

Suriñach, E., Furdada, G., Sabot, F., Biescas, B. and Vilaplana, J. (2001): On the characterization of seismic signals generated by snow avalanches for monitoring purposes, Annals of Glaciology, 32, 268–274

Vilajosana, I., Khazaradze, G., Suriñach, E., Lied, E. and Kristensen, K. (2007a): Snow avalanche speed determination using seismic methods, Cold Regions Science and Technology, 49, 2–10

Vilajosana, I., Suriñach, E., Khazaradze, G., and Gauer, P. (2007b): Snow avalanche energy estimation from seismic signal analysis, Cold Regions Science and Technology, 50, 72–85

Watada, S., Kunugi, T., Hirata, K., Sugioka, H., Nishida, K., Sekiguchi, S., Oikawa, J., Tsuji, Y. and Kanamori, H. (2006): Atmospheric pressure change associated with the 2003 Tokachi-Oki earthquake, Geophysical Research Letters, 33, L24306, doi: 10.1029/2006GL027967.

Wu, J., Kang, Z., Tian, L. and Zhang, S. (1990): Observation and investigation of debris flows at Jiangjia Gully in Yunnan Province (China), Science Press, Beijing, China

Zhang, S., Hong, Y. and Yu, B. (2004): Detecting infrasound emission of debris flow for warning purposes, International Symposium Interpraevent VII, Riva, Trient, 359–364

Chapter 2

Alpine mass movements

Snow avalanches

Snow avalanches are a natural phenomenon that often threaten traffic routes and infrastructure and cause many casualties in alpine regions. In this study seismic and infrasonic signals generated by different snow avalanches monitored at the Swiss (SLF) dynamic test site at Vallée de la Sionne (VDLS) (Ammann, 1999; Barbolini and Issler, 2006) are presented. Typical for this site are mixed snow avalanches that often generate a well-developed powder part, but wet snow avalanches also occur in early winter or spring.

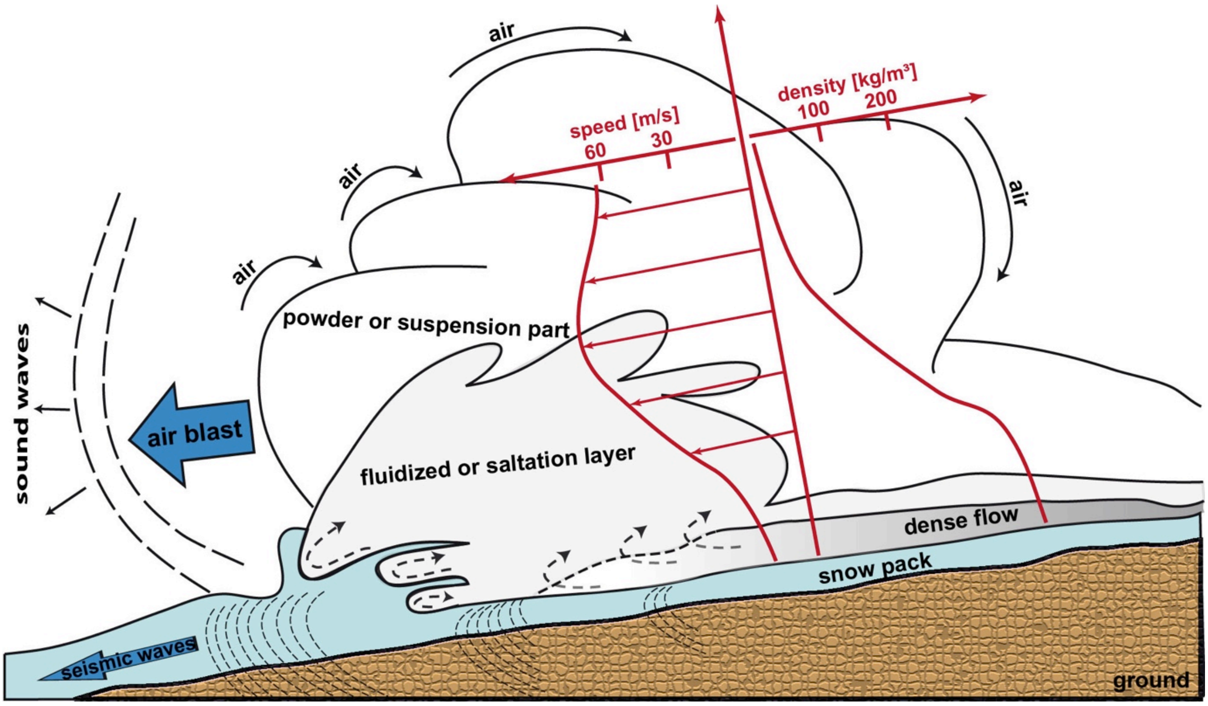

Figure 1: Cross section of a mixed snow avalanche, indicating the different parts (modified after McClung and Schaerer, 2006 and Gauer et al., 2008). The sources of seismic and acoustic emissions are also indicated.

Mixed snow avalanches are generally described as a three-layered structure (Fig. 1). A dense flow layer is usually present at the bottom of the avalanche (Sovilla et al., 2008a), and is characterized by a high snow density (200 kg/m^3 to 400 kg/m^3) and snow particles that have persistent contact with each other or with the bed surface (frictional flow regime) (McClung and Schaerer, 2006). With an increase in avalanche speed, particles at the surface of the dense flow are lifted due to the shear stress produced by the interaction with the air above, and a fluidized layer is created. Stresses are primarily transmitted by particle collisions and particle inertia (Gauer et al., 2008). If the snow is dry and the avalanche speed is sufficiently high

(>10 m/s), a snow "dust" cloud of low density (approx. 10 kg/m^3) covers the exterior of the avalanche core (McClung and Schaerer, 2006). Small particles are suspended by turbulent eddies of air generated by the friction of the flowing snow interacting with the ambient air. This powder cloud or suspension layer is thought to behave like a turbulent flow of a Newtonian fluid (Gauer et al., 2008).

Figure 2: Numerous levees and snow deposition of a wet avalanche flow in the lower avalanche path at the Vallée de la Sionne experimental site taken on 15.01.2010. View is from the shelter (see Chapter 9).

Wet snow avalanches are constituted by wet snow, i.e. snow around the melting temperature (0°C). Compared to dry snow avalanches, the density of a wet snow avalanche is considerable higher due to the higher water content. One of the consequences of the increased density is the higher friction at the sliding surface compared to dry/mixed flow avalanches (Fig. 2). Another consequence is that the speed and run out distances of wet snow avalanches are usually less than that of dry snow avalanches for equivalent mass and fall height (McClung and Schaerer, 2006). Moreover, no turbulent dust cloud of suspended material is formed during wet snow avalanche motion. Despite the points mentioned above the destructive force of wet snow avalanches is considered similar to that of dry/mixed snow avalanches (McClung and Schaerer, 2006).

In the last decades the avalanche community has focused efforts in the development of avalanche simulation models and a better understanding of the phenomena through theoretical and experimental studies. Avalanche-dynamic models have been increasingly used in land-use planning and for the design of protecting structures able to resist avalanche impact (Christen et al., 2010). These models have been improved by taking more and more processes into account to better describe snow avalanche motion. To continue refining these models and develop more robust avalanche physical descriptions, it is essential to obtain more information on avalanche dynamics. In addition to this, increased human activity and exposed infrastructure increases the necessity of well-developed and functioning early warning systems (Zschau and Küppers, 2003).

In order to increase knowledge about the dynamics of moving snow avalanches researchers were interested in field experiments at different scales (e.g., chute and full scale experiments). In the last decades the measuring equipment at the main test sites in Europe have been adapted (Ammann, 1999; Lied et al., 2002). For example, test sites were equipped with monitoring systems to get new insights on the avalanche physical parameters (e.g., front velocity, flow depth, mass balance) (Sovilla et al., 2008b; Kern et al., 2009). In addition, further development of remote sensing technologies and methodologies based on Doppler radar (Gauer et al., 2007a; Rammer et al., 2007), seismic sensors (Suriñach et al., 2001) and infrasound sensors (Scott et al., 2007) has occurred. However, acquiring data on high-speed phenomena still remains a challenge. The description of the avalanche behaviour needs to be supported by physical observations measured during chute- (Kern et al., 2004) and full-scale experiments (Sovilla et al. 2008b, Gauer et al., 2007b). Classical methods such as image processing techniques give useful information on the shape and velocity of the avalanche, but they cannot track the internal structure. Non-intrusive methods (e.g., Doppler radar) give access to the internal structure of an avalanche but the obtained signals are difficult to interpret (Issler, 2003). Static sensors for measuring the impact pressure or snow density are also of common use but they only yield information at fixed places and the interpretation needs supplementary information (velocity measurements, density) (Gauer et al., 2007a). Over the last ten years, a new generation of instruments has been used to study snow avalanches. Radar techniques have been improved to yield more accurate speed estimates (Gauer et al., 2007a; Rammer et al., 2007). Development of commercially available laser scanning systems has allowed accurate measurements on avalanche mass balance (Prokop, 2008; Prokop, 2009), which was inconceivable some years ago. Ground-based SAR radars have also been used to monitor avalanche activity (Martinez et al., 2005).

Another successfully used instrument for monitoring and detecting snow avalanches are infrasound and seismic sensors (e.g., Suriñach et al., 2001; Scott et al. 2007). They have been used for snow avalanche studies in Europe and the USA to monitor avalanche activity (Bedard, 1994; Suriñach et al., 2000; Bessason et al., 2007). These sensors allow monitoring from a remote place not affected by the avalanche activity and information can be obtained continuously from the avalanche initiation in the starting zone until the end of avalanche motion in the run out zone.

In this study seismic and infrasonic signals generated by different snow avalanches monitored at the Swiss dynamic test site at Vallée de la Sionne (VDLS) are presented. The scope of the present work is to better understand the avalanche phenomena through analysis of the infrasound and seismic wavefield emitted. As will be shown in the following chapters relevant information on the nature of the phenomena can be obtained.

Debris flows - Debris floods

Processes like debris flows, debris floods, or bed load transport are widespread phenomena in alpine regions where they repeatedly cause damage of infrastructure or even provoke lose of life.

Debris flows generally occur when masses of poorly sorted sediment, agitated and saturated with water, move down slopes (Iverson, 1997). Both solid and fluid forces strongly influence the motion, distinguishing debris flows from related phenomena such as rock avalanches, turbidity currents, and sediment-laden water floods.

Whereas solid-grain interactions dominate momentum transfer in avalanches, and fluid turbulence dominates momentum transfer in turbidity currents and floods, solids and fluids must transfer momentum synergistically to sustain the type of motion that characterizes debris flows (Iverson, 1997).

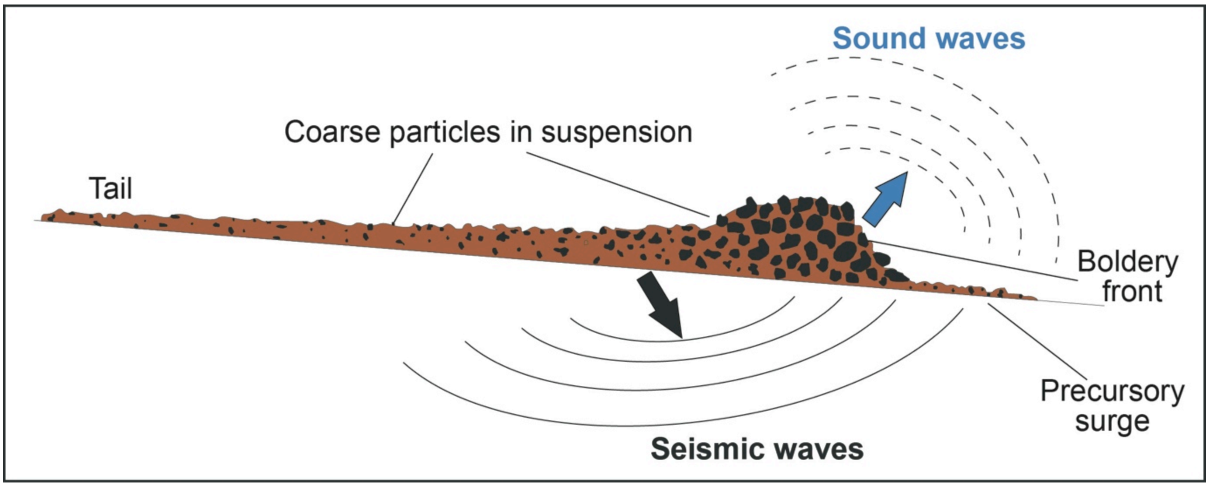

Figure 3: Cross section of a debris flow (modified after Hungr et al., 2001). The characteristic steep front commonly formed by boulders is indicated, followed by a thinner tail. The sources of seismic and acoustic emissions are also indicated.

Debris flows are generally described as very rapid to extremely rapid flows (velocities up to 20 m/s) that move down a slope in a series of waves or surges. The key characteristic of a debris flow is the presence of an established channel or regular confined path (Hungr et al., 2001), and this distinguishes debris-flow processes from debris avalanches and hillslope debris flows (Hutchinson, 1988). Materials involved in debris flows range from clay to boulders several meters in diameter (Hungr et al., 2001). Commonly, an abrupt bore forms the head of the flow, followed by a tapering body and a thin, more watery tail (Iverson, 1997) (Fig. 3). The presence of a well-defined and recognizable front, dominated by boulders and organic material such as timber, seems therefore to be characteristic for every debris flow (Arattano, 2000). As a result of the surging behaviour and the building of coarse surge fronts, peak discharges of debris flows are up to 40 times higher than those of extreme floods (Hungr et al., 2001).

The term debris flood has been applied by Aulitzky (1980) to cases of massive bedload transport characterized by a limited maximum grain size, a limited thickness of deposits and gently sloping deposition areas. Thus, debris floods are very rapid surging flows of water, heavily charged with debris, in a steep channel (Hungr et al., 2001). However, the main driving force in a debris flood is the drag force of water, and thus the peak discharge of a debris flood is comparable to that of a water flood. Evidence for such a limited discharge in channels is that the deposition areas clearly contrast with those of debris flows, which have peak discharges tens of times greater than major floods (VanDine, 1985). Therefore, according to Hungr et al. (2001), peak discharge is suggested as the most reliable criterion to distinguish between debris flows and debris floods. Despite the differences mentioned above, both debris flows and debris flood are considered to have a similar destructive power.

In the last decades research on debris flows has focused efforts in the development of debris flow simulation models and better understanding of the phenomena through theoretical and experimental studies. Analyses of different solid-fluid mixtures, ranging from pure granular to viscous characteristics, provide a foundation for a comprehensive debris-flow theory, whereas experiments provide data that reveal the strengths and limitations of theoretical models (Major and Pierson, 1992; Iverson, 1997). To keep on refining these models and develop a more robust debris-flow physical description, it is essential to obtain more information on debris-flow dynamics. Additionally, the increased human activity and exposed infrastructure underline the importance of the development of reliable early warning systems.

These needs forced the development of remote sensing technologies and methodologies based on seismometers (Okuda et al., 1979; Arattano, 1999; and many others), ground vibration sensors (Zhang, 1993; Itakura et al., 1997, 2000; Hurlimann et al., 2003; and many others), infrasound sensors (Zhang et al., 2004; Chou et al. 2007) and methods to measure the velocity of debris-flow with image processing techniques (Inaba et al., 1997; Uddin et al., 1999; Arattano and Marchi, 2000; Genevois et al., 2001). Static sensors on the other hand measure the impact pressure or flow density often in combination with complementary information from remote sensors (e.g., video recordings, velocity measurements) (Genevois et al., 2000). The main observation sites in Europe have been permanently upgraded with new sensor technologies in order to gather monitoring data or develop reliable warning systems (Hurlimann et al., 2003; Marchi et al., 2002; Cho et al., 2008).

In addition to the monitored data of real events, chute experiments provide a basis for observation of different physical parameters under predetermined boundary conditions (e.g., Iverson, 1997). A comprehensive summary and review of debris-flow monitoring devices and methods can be found in Itakura et al. (2005).

Acoustic sensors have been successfully used for monitoring debris-flow events in previous studies. Infrasound sensors were implemented for monitoring debris flows in China and Taiwan. Seismic monitoring of debris-flow activity was mainly developed in Italy and Japan (Arattano, 1999; Itakura et al., 2000; Suwa et al., 2000). Both sensor types allow monitoring from a remote place not affected by the debris-flow activity.

For this study debris flows and debris floods at two different test sites (Lattenbach, Austria; Illgraben Switzerland), representing typical steep and small debris flow catchments, were monitored. The scope of the present work is to demonstrate the potential of infrasound sensors for monitoring debris flows and to better understand debris flows and debris floods through monitoring with a combination of infrasound and seismic sensors.

References

Ammann, W. (1999): A new Swiss test-site for avalanche experiments in the Vallée de la Sionne Valais, Cold Regions Science and Technology, 30, 3–11

Arattano, M. (1999): On the use of seismic detectors as monitoring and warning systems for debris flows, Natural Hazards and Earth System Sciences, 20,197–213

Arattano, M. (2000): On debris flow front evolution along a torrent, Natural Hazards and Earth System Sciences, 25(9), 733–740

Arattano, M. and Marchi, L. (2000): Video-derived velocity distribution along a debris flow surge, Physics and Chemistry of the Earth, Part B, 25, 781–784

Aulitzky, H. (1980): Preliminary two-fold classification of debris torrents, International Symposium Interpraevent IV, Bad Ischl, Austria, 285-309 (translated to English by G. Eisbacher)

Barbolini, M. and Issler, D. (2006): Avalanche Test Sites and Research Equipment in Europe: An Updated Overview, Final-report deliverable D8, SATSIE avalanche studies and model validation in Europe

Bedard, A. (1994): An Evaluation of Atmospheric Infrasound for Monitoring Avalanches, Proceedings; 7th International Symposium on Acoustic Sensing and Associated Techniques of the Atmosphere and Oceans, Boulder, CO

Bessason, B., Eirìksson, G., Thoŕorinsson, Ò., Thoŕorinsson, A. and Einarsson, S. (2007): Automatic detection of avalanches and debris flows by seismic methods, Journal of Glaciology, 53, 461–472

Cho, C., Chou, P., Chung, Y., King, C., Tsai, M., Lee, B. and Chou T. (2008): Wireless Sensor Networks for Debris Flow Observation, in: Proceedings 2nd International Conference on Urban Disaster Reduction, IEEE Xplore, 615-617

Chou, H., Cheung, Y. and Zhang, S. (2007): Calibration of infrasound monitoring system and acoustic characteristics of debris-flow movement by field studies, in: Chenglung, C., Major, J. (eds.) Debris-flow Hazards Mitigation: Mechanics, Prediction, and Assessment, Millpress, Rotterdam, 571–580

Christen, M., Kowalski, J. and Bartelt, P. (2010): RAMMS: Numerical simulation of dense snow avalanches in three dimensional terrain, Cold Regions Science and Technology, 63, 1–14, doi:10.1016/j.coldregions.2010.04.005

Gauer, P., Kern, M., Kristensen, K., Lied, K., Rammer, L. and Schreiber, H. (2007a): On pulsed Doppler radar measurements of avalanches and their implication to avalanche dynamics, Cold Regions Science and Technology, 50, 55–71

Gauer, P., Issler, D., Lied, K., Kristensen, K., Iwe, H., Lied, E., Rammer, L. and Schreiber, H. (2007b): On full-scale avalanche measurements at the Ryggfonn test site, Norway, Cold Regions Science and Technology, 49(1), 39–53

Gauer, P., Issler, D., Lied, K., Kristensen, K. and Sandersen, F. (2008): On snow avalanches flow regimes: Inferences from observations and measurements, in: Proceedings International Snow Science Workshop, 717–723, Whistler

Genevois, R., Tecca, P., Breti, M. and Simoni, A. (2000): Debris-flow in the Dolomites: Experimental data from a monitoring system, in: Debris-Flow Hazards Mitigation: Mechanics, Prediction, and Assessment, edited by: Wieczorek, G. F. and Naeser, N. D., Proc. 2nd Intern. Conf., Taipei, Taiwan, 16–18 August 2000, Rotterdam, Balkema Press, 283–291

Genevois, R., Gaigaro, A. and Tecca, P. R. (2001): Image analysis for debris flow properties estimation, Physics and Chemistry of the Earth, Part C, 26, 623–631

Hungr, O., Evans, S., Bovis, M. and Hutchinson, J. (2001): A review of the classification of landslides of the flow type, Environmental and Engineering Geoscience, 7(3), 221–238, doi:10.2113/gseegeosci.7.3.22

Hurlimann, M., Rickenmann, D. and Graf, D. (2003): Field and monitoring data of debris-flow events in the Swiss Alps, Canadian Geotechnical Journal, 40, 161–175

Hutchinson, J. (1988): General Report: morphological and geotechnical parameters of landslides in relation to geology and hydrogeology. In: Bonnard, C. (Editor), Proceedings, Fifth International Symposium on Landslides, A.A: Balkema, Rotterdam, 1, 3-36

Inaba, H., Uddin, M. S., Itakura, Y. and Kasahara, M. (1997): Surface velocity vector field measurement of debris flow based on spatio temporal derivative space method, in: Debris-Flow Hazards Mitigation: Mechanics, Prediction, and Assessment, edited by: Chen, C. L., Proc. First Intern. Conf., San Francisco, USA, 7–9 August 1997, New York, ASCE, 757–766

Issler, D., (2003): Experimental information on the dynamics of dry-snow avalanches, in: Hutter, K. and N. Kirchner (eds.), Dynamic Response of Granular and Porous Materials under Large and Catastrophic Deformations, Lecture Notes in Applied and Computational Mechanics 11, Springer, 109–160

Itakura, Y., Koga, Y., Takahama, J. and Nowa, Y. (1997): Acoustic detection sensor for debris-flow, in: Debris-Flow Hazards Mitigation: Mechanics, Prediction, and Assessment, edited by: Chen, C. L., Proc. First Intern. Conf., San Francisco, USA, 7–9 August 1997, New York, ASCE, 747–756

Itakura, Y., Fujii, N. and Sawada, T. (2000): Basic characteristics of ground vibration sensors for the detection of debris-flow, Physics and Chemistry of the Earth, Part B, 25, 717–720

Itakura, Y., Inaba, H. and Sawada T. (2005): A debris flow monitoring devices and methods bibliography, Natural Hazards and Earth System Sciences, 5, 971-977

Iverson, R. (1997): The physics of debris flow, Reviews of Geophysics, 35(3), 245–296

Kern, M., Tiefenbacher, F. and McElwaine J. (2004): The rheology of snow in large chute flows, Cold Regions Science and Technology, 39, 181–192

Kern, M., Bartelt, P., Sovilla, B. and Buser, O. (2009): Measured shear rates in large dry and wet snow avalanches, Journal of Glaciology, 55, 327–338

Lied, K., Moe, A., Kristensen, K. and Issler, D. (2002): Ryggfonn: Snow Avalanche Research Program SIP-6: Full scale avalanche test site and the effect of the catching dam, Tech. Rep. NGI report 581200-35, Norwegian Geotechnical Institute, Oslo

Major, J. and Pierson, T. (1992): Debris flow rheology: experimental analysis of fine-grained slurries, Water Resources Research, 28, 841-857

Marchi L., Arattano M. and Deganutti, A. (2002): Ten years of debris-flow monitoring in the Moscardo Torrent (Italian Alps), Geomorphology, 46(1-2), 1-17

Martinez, A., Fortuny, J. and Gruber, U. (2005): Monitoring of the snow cover with a ground-based synthetic aperture radar, European Association of Remote Sensing Laboratories, eProceedings, 4, 171-178

McClung, D. and Schaerer, P. (2006): The Avalanche Handbook, The Mountaineers Books

Okuda, S., Suwa, H., Okunishi, K., Yokoyama, K., Ogawa, K. and Hamana, S. (1979): Synthetic observation on debris-flow, Part 5, Observation at Valley Kamikamihorisawa of Mt. Yakedade in 1978, Annuals of Disaster Prevention Research Institute, Kyoto University, 22B-1, 157–204

Prokop, A. (2008): Assessing the applicability of terrestrial laser scanning for spatial snow depth measurements, Cold Regions Science and Technology, 54(3), 155-163

Prokop, A (2009): Terrestrial laser scanning for snow depth observations: An update on technical developments and applications, in: Schweizer, J. and Herwijnen, A. van (Eds.), ISSW 09 - International Snow Science Workshop: Proceedings, 192-196

Rammer, L., Kern, M., Gruber, U. and Tiefenbacher, F. (2007): Comparison of avalanche-velocity measurements by means of pulsed Doppler radar, continuous wave radar and optical methods, Cold Regions Science and Technology, 50, 35–54

Scott, E., Hayward, C., Kubichek, R., Hamann, J., Comey, R., Pierre, J. and Mendenhall, T. (2007): Single and multiple sensor identification of avalanche-generated infrasound, Cold Regions Science and Technology, 47, 159–170

Sovilla, B., Schaer, M., Kern, M. and Bartelt, P. (2008a): Impact pressures and flow regimes in dense snow avalanches observed at the Vallée de la Sionne test site, Journal of Geophysical Research, 113, 1–14, doi:10.1029/2006JF000688

Sovilla, B., Schaer, M. and Rammer, L. (2008b): Measurements and analysis of full-scale avalanche impact pressure at the Vallèe de la Sionne test site, Cold Regions Science and Technology, 51, 122–137

Suriñach, E., Sabot, F., Furdada G. and Vilaplana, J. (2000): Study of seismic signals of artificially released snow avalanches for monitoring purposes, Physics and Chemistry of the Earth, 25(9), 721–727

Suriñach, E., Furdada, G., Sabot, F., Biescas, B. and Vilaplana, J. (2001): On the characterization of seismic signals generated by snow avalanches for monitoring purposes, Annals of Glaciology, 32, 268–274

Suwa, H., Yamakoshi, T. and Sato, K. (2000): Relationship between debris-flow discharge and ground vibration, in: Debris-Flow Hazards Mitigation: Mechanics, Prediction, and Assessment, edited by: Wieczorek, G. F. and Naeser, N. D., Proceedings 2nd International Conference, Taipei, Taiwan, 16-18 August 2000, Rotterdam, Balkema Press, 311–318

Uddin, M. S., Inaba, H., Itakura, Y., Yoshida, Y. and Kasahara, M. (1999): Adaptive computer-based spatial filtering method for more accurate estimation of the surface velocity of debris-flow, Applied Optics, 38, 6714–6721

VanDine, D. (1985): Debris flows and debris torrents in the southern Canadian Cordillera, Canadian Geotechnical Journal, 22, 44-68

Zhang, S. (1993): A Comprehensive Approach to the Observation and Prevention of Debris Flow in China, Natural Hazards, 7, 1-23

Zhang, S., Hong, Y. and Yu, B. (2004): Detecting infrasound emission of debris flow for warning purposes, International Symposium Interpraevent VII, Riva, Trient, 359–364

Zschau, J. and Küppers, A. (2003): Early warning systems for natural disaster reduction, Springer, Berlin

Chapter 3

Background on infrasound and seismic waves

In physics, a wave is a disturbance that travels through space and time, accompanied by the transfer of energy. Acoustic waves, such as infrasound and seismic signals, are mechanical waves, which are in fact wavelike representation of propagations of pressure- or density fluctuations in different elastic mediums such as gases, liquids and solids (Tipler, 1994). Understanding the basic physical properties of wave theory is fundamental when using infrasound and seismic sensors to study the source of a phenomenon. Additionally, if analyzing the infrasound and seismic wavefield coupling effects have to be considered at the solid-gas boundary between the lithosphere and the atmosphere.

Infrasound Waves

Infrasound waves are longitudinal pressure fluctuations in the air, which occupy a relatively narrow band in the low frequency acoustic spectrum (0.001 Hz to 20 Hz), too low to be perceived by the human ear. Longitudinal waves are alternating pressure deviations from the equilibrium pressure, causing local regions of compression and rarefaction in direction of propagation. Frequencies just below 20 Hz are termed near-infrasound, and frequencies just below about 1 Hz are known as far-infrasound. The speed of the waves in the air is about 344 m/s (at standard temperature and pressure), which is about the same as that of audible sound. The speed of propagation is determined by the properties of the air, and not by the frequency or amplitude of the waves.

Infrasound can travel thousands of kilometers and still be detectable. This is due to the frequency-dependency of atmospheric attenuation. The atmosphere is absorbing high-frequency sound waves (audible and ultrasound) more than low-frequency waves (infrasound) (Pilger and Bittner, 2009). Wave propagation is affected by different mechanisms that modify the amplitude and the frequency of the waves (Spreading losses and Absorption losses). These mechanisms modify the amplitude and frequency of a sound wave and eventually lead to its energy diminishment by converting it to heat. The dominant loss mechanism for infrasound at long-range propagation is due to absorption processes in the atmosphere (Le Pichon et al., 2002; Drob and Piccone, 2003). Monitoring infrasound waves at regional distances (< 5 km) from the source one has to consider uniform spherical spreading loss, energy loss due to absorption in the atmosphere is small (Albert and Orcutt, 1990; Johnson, 2003).

Spreading losses

Uniform spherical spreading refers to the spreading of acoustic energy as a result of the expansion of the wave front, most important it is independent of frequency (Evans et al., 1972). As the waves propagate, the wave front expands and the energy is spread over a larger and larger area. As the total energy stays constant, the area expands and the energy in one unit of area decreases. Uniform spherical spreading effects depend on the type of wave (spherical, cylindrical, planar). For example, a surface pressure source typically expands like a sphere. On the other hand, a line source propagates as cylindrical wave front. The geometry and the characteristics of the medium where the wave propagates determine which is the best approximation (Crighton, 1975). In the atmosphere, as sound propagates away from the source, the waves are refracted and diffracted by the structure of the atmosphere. At long distances, focusing and ducting occur in the atmosphere and the geometric sound pattern of a spherical wave becomes more cylindrical (Pilger and Bittner, 2009). Generally, when monitoring at local distances (< 5 km) the effects of focusing and ducting are negliable on the wave propagation because parameters such as air temperature, air density and sound speed can be assumed as constant.

In this study we consider the monitored alpine mass movements as moving spherical sound sources. According to the inverse-distance law for spherical spreading, $\Delta P \propto 1/r$ (ΔP is the pressure decrease and r the distance) (e.g., Tipler, 1994).

In practice, the sound pattern generated by a surface sound source does not often develop the theoretically expected 3-D sphere shape (depending on landscape, surfaces etc.). If there are for example reflective surfaces in the wave field, then the reflected waves will add to the directed waves and higher amplitudes at a field location will be recorded than the inverse distance law predicts (Stubbs, 2005).

Nonuniform spreading losses including reflection by finite boundaries, refraction by nonuniform atmosphere, and diffraction (scattering) by nonstationary atmosphere also contribute to energy loss (Evans et al., 1972). However, the more variable effects of nonuniform spreading are irrelevant to this work.

Absorption losses

Sound propagating from a source is subject to absorption by the atmosphere and absorption by the ground and ground cover. The variable effects of sound absorption by the atmosphere are described in Chapter 8 and are hence not discussed here. In the following we will focus on sound absorption by ground, ground cover and most important, if monitoring snow avalanches, snow cover.

The main effect of the interaction between the wave and the ground is energy loss. If sound waves are propagating over ground, the interaction with the surface and surfaces irregularities will cause various i.) Reflections increasing the destructive interferences. For example, sharp and porous surfaces (thick grass) will produce high absorption whereas smooth and hard surfaces (asphalt surfaces) may result in lower absorption (Albert and Orcutt, 1990). Moreover, high frequencies are generally more affected than low frequencies due to the dependence of the wavelength on the size of the irregularity (Embleton et al., 1976; Albert and Orcutt, 1990) ii.) Refractions, which are the change in direction of a wave due to a change in its speed (Tipler, 1994). This is most commonly observed when a wave passes from one medium to another at any angle other than 90° or 0°. Refraction is described by Snell's law, which states that the angle of incidence Θ_1 is related to the angle of refraction Θ_2 (Becker and Güdesen, 2000). However, for the purpose of this study refractions effects have not been considered.

Most people experience in an environment covered with snow a low noise level, which illustrates the silencing effect a strong absorbing snow layer has (Albert and Orcutt, 1990; Albert et al., 2008). This effect shows that the presence of snow produce effects on sound propagation, which can be perceived by human beings. In order to understand this phenomenon previous studies (Nicolas et al. 1985; Santana and Olsen, 2004; Albert et al., 2008) analysed the effect of snow on sound propagation.

For example Albert et al. (2008) performed a series of experiments using blank pistol shots as a sound source. Snow cover is considered as a rigid porous material with parameters such as density, grain size, snow depth etc. influencing the snow cover permeability and in consequence the acoustic attenuation, which is a function of frequency. Albert et al. (2008) reported that high frequencies are strongly attenuated by the snow cover, in contrast to low frequencies (< 50 Hz), which in some cases (usually for shallow snow) are even enhanced. In general, any acoustic signal measured when a snow cover is present will be low pass filtered. Please note that the studies of Albert et al. (2008) included maximum snow depths of 60 cm.

More in relation to infrasound waves, Santana and Olsen (2004) studied the effects of snow cover on infrasonic signal levels at I53US (Fairbanks, Alaska), a station of the International Monitoring System (IMS). She compared the mean infrasound signal level with snow cover in winter for a period of four months to data gathered in summer and found no significant change. During the four months period she reported continuous snow cover above the sensor with a maximum snow depth of 51 cm.

It can be concluded that a snow cover of up to 60 cm has no absorption effects on low frequency infrasound signals. In one of the experiments performed during this study one sensor did not report any significant change in infrasound amplitude during 2 months. The sensor was located in the ski resort in Lech am Arlberg (Tyrol, Austria). A field observation revealed that the snow level above the infrasound sensor exceeded 1.5 m. The snow directly above the sensors had a high density due to the high snow level and the wind exposure at the site. Signals with low energy as e.g., small avalanches could eventually be hard to identify. In consequence, a high snow level above the infrasound sensor may present problems, but as far as the authors know, has not been investigated in a specific study yet. A low snow cover over the sensors can be ensured if the sensors are setup in a forest or underneath bushes, which prevent extreme snow depth and additionally act as a natural protection to wind.

The source of infrasound waves of alpine mass movements

Infrasound emissions of alpine mass movements have already been the subject of earlier studies (e.g., Zhang et al., 2004; Arnoult, et al., 2005; Scott et al., 2007). However, few of them discuss the possible sources of infrasonic emissions of these phenomena. For example, infrasound emissions of debris flows have been studied in (Zhang et al., 2004; Chou et al., 2007) and the origin of infrasound emitted by snow avalanches was briefly discussed in Firstov et al. (1992) and Naugolnykh and Bedard (2002). In the following, an introduction about the theory behind acoustic radiation from a moving source is given in view of debris flows or snow avalanches as sound source.

Acoustic emissions generated by moving sources have been widely studied in the last decade (Proudman, 1952; Lighthill, 1952, 1954; Curle, 1955; Ffowcs Williams, 1963,1977; Ffowcs Williams and Hawkings, 1969; Crighton, 1975). Most of the studies concluded that sound emissions from moving sources represent only a small fraction of the total energy in the flow. As a consequence, direct detection and description of sound generation presents a difficult task. This is particularly true in a free field condition and at low subsonic speeds (Lighthill, 1954), as is the case in snow avalanche or debris flow studies.

Ffowcs Williams and Hawkings (1969) derived a governing equation to describe the sound field generated by a moving source in a free field condition, i.e., the so-called Ffowcs Williams-Hawkings equation (Lee and Wang, 2010):

$$\begin{aligned}\left[\frac{1}{c_0^2}\frac{\partial^2}{\partial t^2}-\nabla^2\right]p\left(\vec{x}_0,t\right)=\frac{\partial}{\partial t}\left\{\rho_0\upsilon_n\left(\vec{x}_s,t\right)\delta\left(f\right)\right\}-\frac{\partial}{\partial x_i}\left\{p\left(\vec{x}_s,t\right)\hat{n}\delta\left(f\right)\right\}\\+\frac{\partial^2}{\partial x_i\partial x_j}\left\{T_{ij}H\left(f\right)\right\}\end{aligned} \quad (1)$$

where $\vec{x}_0$ and $\vec{x}_s$ represent the position of the observer and the sound source, respectively, both of which are time t dependent. The function f represents the geometry of the surface of the moving sound source. The term ρ_0 is the fluid density and c_0 is the speed of sound in air. This equation can be viewed as a classical wave equation where the non-homogenous terms on the right-hand side of the equation act as source terms of the sound field. These source terms $p\left(\vec{x}_s,t\right)$, $\upsilon_n\left(\vec{x}_s,t\right)$ and T_{ij} represent the surface pressure, the outward normal speed on the surface and the Lighthill's stress tensor (Lighthill, 1952), respectively. The Heaviside function $H\left(f\right)$ and Dirac delta function $\delta\left(f\right)$ are used under the generalized function framework as described by Ffowcs Williams and Hawkings (1969).

From the physical point of view, the first right-hand side term represents the volume displaced by the flow body, the second term accounts for the force produced by the flow motion into the surrounding air, and the third term accounts for the acoustic emissions produced by the turbulent part of the flow, if present. We expect that the stress tensor T_{ij} is not negligible (high Reynolds stresses) (Lighthill, 1952), in which case, the third term in Eq. 1 would be important and a process with a larger turbulent part would cause higher infrasonic emissions than a process with a smaller turbulent part.

Following Lighthill (1952), Firstov et al. (1992) suggested that the intensity emitted (sound by unit mass of a turbulent medium per unit time) would be proportional to the Lighthill eight power law for a single eddy (Lighthill, 1952). In Firstov et al. (1992) the acoustic source was considered static and was generated by a single eddy. A more realistic approach is to consider snow avalanches or debris flows as non-stationary sound sources where turbulence is convected at a mean speed U. The process motion will cause two effects on the sound emissions in relation to the static approach suggested by Firstov et al. (1992): a change in frequency and a change of effective source length in the direction of motion. This was shown first by Lighthill (1954) and was afterwards corrected by Ffowcs Williams (1963) to account for the finite source volume. According to this, the intensity generated by a moving turbulent source would be (Ffowcs Williams, 1963):

$$I \approx \frac{\rho^2 U^8}{\rho_0 a_0^5} \left(\frac{D}{|y|} \right)^2 \frac{1}{|1 - M \cos\theta|^5} \qquad (2)$$

where I is the intensity, ρ the fluid density, ρ_0 the atmospheric density, a_0 the atmospheric speed of sound, U the flow speed, D the flow dimension, y the distance travelled by the sound wave and M the Mach number $M = (U / a_0)$.

As the radiated wave field (infrasound) fluctuates in time in the same way as T_{ij} (source), the source and the sound have the same time scale (i.e. frequency) corrected by $(1 - M \cos\theta)$, where $\cos\theta$ indicates the direction between source motion and acoustic propagation.

In consequence, infrasound emissions of alpine mass movements are depending on the presence of a well-developed, turbulent flow part. Following Eq. 2**,** the emission intensity of the turbulent part is proportional to the eighth power of the flow speed corrected by the Mach number and by the flow dimension. For example dry/mixed snow avalanches with a full-developed turbulent powder part are expected to have higher infrasonic emissions than a wet dense flow avalanche or a debris flow.

Seismic Waves

Seismic waves are elastic waves of energy that travel through the earth. Both natural and human-made sources of deformational energy can produce seismic waves, elastic disturbances that expand spherically outward from the source as a result of transient stress imbalances in the ground (Thorne and Wallace, 1995). The physics governing seismic wave propagation have been well known since the early 19th century. The fundamental laws of linear elastic mechanics predict that solid bodies react to excitation by propagating energy in the form of elastic waves (e.g. Stein and Wylesession, 2003). Similar to sound waves the velocity at which the seismic waves propagate is depending on the propagating medium. In consequence, a deterministic link between the travel time of the wave from source to receiver and the mechanical properties of the material crossed by its ray path exists. In general, the propagation velocity of elastic waves in solids is one order of magnitude higher than in gases (Thorne and Wallace, 1995).

Seismic waves travelling in the earth can be divided into 4 different types: Body Waves (P stands for Primary and S for Secondary Waves) and Surface Waves (Love- and Rayleigh- Waves) (Udias, 1999). Primary Waves are longitudinal or pressure waves in contrast to Secondary Waves, which are transverse waves, alternating shear stress at right angle to the direction of propagation. Primary waves travel faster than Secondary Waves and are thus the first motion to be detected form any source in an elastic solid (Thorne and Wallace, 1995).

Rayleigh and Love waves are surface waves and result form the interaction of Body Waves with the surface. Rayleigh Waves are made of longitudinal and transverse particle motion and Love Waves, which appear in the presence of discontinuities, form a horizontal line perpendicular to the direction of propagation (i.e. are transverse waves) (Udias, 1999). Due to their higher speed, the P- and S-waves generated by an earthquake arrive before the surface waves. However, the particle motion of surface waves is larger than that of body waves, so the surface waves tend to cause more damage.

Seismic waves attenuate following the main mechanism described above for infrasound. The most important of them are geometrical spreading and anelastic attenuation (internal frictional losses) in the ground, which is frequency dependent (Aki and Richards, 1980).

Previous studies exist investigating the source of seismic signals from alpine mass movements (Arattano, 1999; Biescas et al., 2003; Brodsky et al., 2003; Suriñach et al., 2005; Vilajosana et al., 2007). Brodsky et al. (2003) showed that landslides generate seismic waves by both shearing and loading the surface as the mass moves from a steep to a shallow slope. Arattano (1999) monitored debris flows using geophones and concluded that the presence of boulders in the turbulent front of debris flows is expected to generate particularly intense ground vibrations. The main sources of the seismic energy generated by snow avalanches are the basal friction produced by the dense body inside the flow in contact with the ground or snow cover and the changes in the slope of the path (Suriñach et al., 2000; Biescas et al., 2003; Vilajosana et al., 2007; Schneider et al., 2010 for rock-ice avalanches). Wet snow avalanches generate especially large and long signals owing to the high-density snow and the relatively slow speed of propagation. In contrast, powder snow avalanches produce comparatively smaller seismic amplitudes because of the low-density snow and high speed of propagation (Biescas et al., 2003).

Earlier studies showed that superficial waves are predominant in the seismic signals recorded of alpine mass movements (Vilajosana et al., 2007). In general, P- and S Waves are not observed when monitoring alpine mass movements, except rocks of significant size are present in the process. The relative position between the sensor and the mass movement and the characteristics of the site influence the seismic signal recorded. Seismic site effects were studied for seismic signals generated by mass movements previously (Suriñach et al., 2001).

Coupling effects

Ground to air coupling effects

Ground to air coupling effects correspond to the generation of atmospheric disturbances by ground motion (Fig. 4) and as a result similar acoustic and seismic signals are observed in collocated seismic and acoustic sensors. This correlation between seismic and acoustic waves can be explained by the passing of Rayleigh waves, producing ground coupled pressure waves in the air (Arrowsmith et al., 2010).

Sound waves produced by vertical ground motions have been observed previously mostly in relation to earthquakes (e.g., Bedard, 1971; Artru et al., 2004; Starovoit and Martysevich, 2005; Watada et al., 2006; Arrowsmith et al., 2009) and underground explosions (Arrowsmith et al., 2008; Che et al., 2009). In these studies the coupling mechanism could be explained as the combination of pressure changes in the air caused by vertical ground motion and also the mechanical sensitivity of the microphone (Bedard, 1971; Alcoverro et al., 2005). A very comprehensive overview of the seismoacoustic wave field from source to receiver can be found in Arrowsmith et al. (2010).

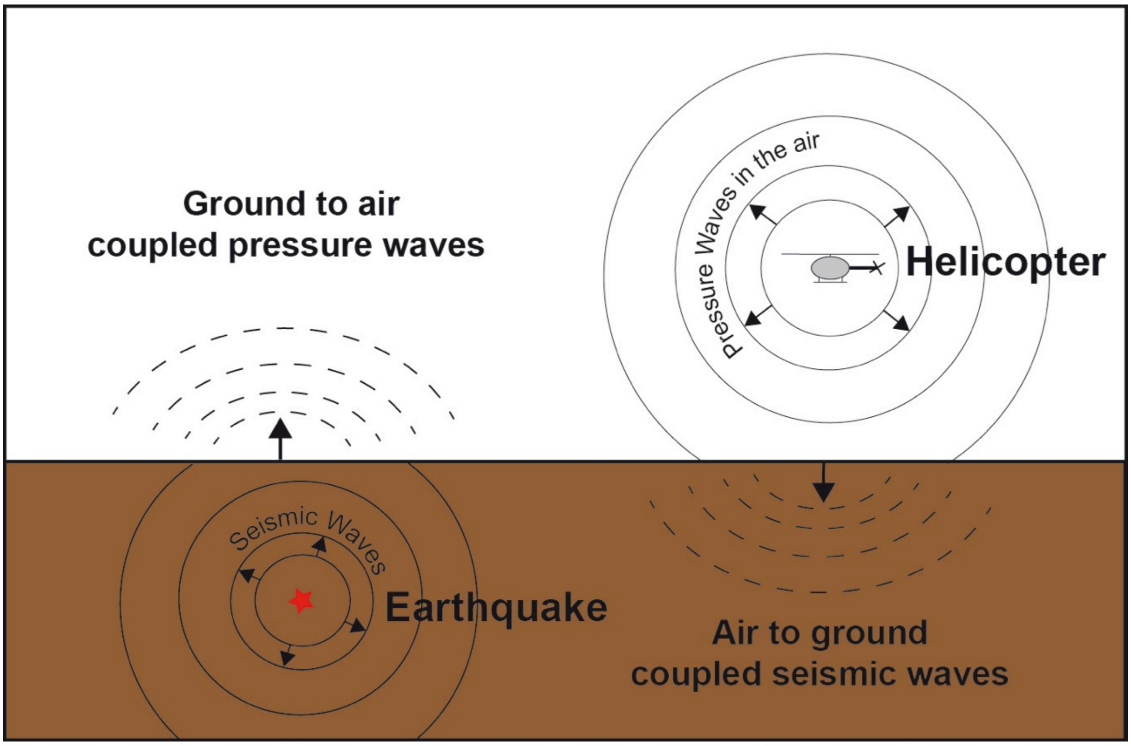

Figure 4: Sketch of the two principle coupling effects: i.) Ground to air coupling caused e.g. by an earthquake and ii.) Air to ground coupling caused e.g. by a helicopter.

According to Watada et al. (2006) the atmospheric disturbances caused by earthquakes are often modeled by a simple relationship between ground velocity and the pressure change at the surface with an assumption that the time scale of the vertical motion is short compared to the acoustic cut-off period. Ground motion is related to the excess pressure in a homogenous fluid medium through (e.g., Lighthill, 1978): $p = \rho c_s w$. Where p is the excess pressure, ρ is the air density, c_s is the sound velocity and w is the velocity of the ground motion.

Mass movements as superficial seismogenic sources (e.g., Suriñach et al., 2001; Vilajosana et al., 2007) mainly produce superficial waves and in consequence the effects of ground to air coupling have to be considered when analyzing the data of collocated seismic and acoustic sensors. For example, as presented in Chapter 9, seismic and infrasonic signals of snow avalanches have similar wave packages, which can be attributed to coupling effects.

Air to ground coupling effects

Air to ground coupling corresponds to the generation of seismic waves by pressure fluctuations in the air (Fig. 4). In the 80`s Sabatier et al. (1986) had studied theoretically and experimentally the generation of seismic waves induced by an incident acoustic wave in a ground surface (sand and loess).

Air to ground coupling in the near field (< 270 m) has been investigated in detail by Albert and Orcutt (1989) using pistol shots as a source of sound. Their observations have shown that an acoustic source will cause two different kinds of seismic wave arrivals at geophones buried in the ground. The largest amplitude signal is caused by the passage of the airwave, which travels primarily through the atmosphere (at the speed of sound) and couples locally into the ground, inducing seismic surface waves. An earlier arrival was also recorded for body waves, induced in the ground immediately under the source, since they travel at higher subsurface seismic wave velocity, but their amplitudes were one to two orders of magnitude lower than those of the later arriving air wave.

Another example is large meteoroids, which can generate seismoacoustic signals as they interact with Earth´s atmosphere. When the resultant airwave impinges on the ground, it can couple into the solid Earth, generating seismic waves (Arrowsmith et al., 2010). Edwards et al. (2008) provide an excellent review of seismic observations of meteoroids.

Becker and Güdesen (2000) described passive sensing techniques with acoustics on the battlefield and reported about air to ground coupling from helicopter signals using collocate microphones and geophones. Similar observations have been reported by Sikora et al. (2009) and Van Herwijnen and Schweizer (2011), who found signals produced by helicopters and propeller airplanes in the seismic data, conducting snow avalanche seismic studies, using geophones and collocated microphones.

In Chapter 9 of this study high infrasonic amplitudes with a spindle shape that could be attributed to the powder part of an avalanche are described. Simultaneously the authors observed this spindle shape with the same arrival time and length in the filtered seismic time series. In consequence, it can be concluded that infrasound waves propagating in the atmosphere induced locally vibrations in the ground big enough to be recorded by seismometers. As mentioned in the previous chapter these coupling effects have to be considered when analyzing the data of collocated seismic and acoustic sensors.

References

Aki, K. and Richards, P. (1980): Quantitative Seismology, A Series of Books in Geology,1, W.H. Freeman and Company, New York, USA

Albert, D. and Orcutt, J. (1989): Observations of low frequency acoustic to seismic coupling in the summer and winter, Journal of the Acoustical Society of America, 86(1), 352-359

Albert, D. and Orcutt, J. (1990): Acoustic pulse propagation above grassland and snow: Comparison of theoretical and experimental waveforms, Journal of the Acoustical Society of America, 87 (1), 93-100

Albert, D., Decato, S. and Carbee, D. (2008): Snow cover effects on acoustic sensors, Cold Regions Science and Technology, 52, 132–145

Alcoverro, B., Martysevich, P. and Starovoit, Y. (2005): Mechanical sensitivity of microbarometers MB2000 (DASE, France) and Chaparral5 (USA) to vertical and horizontal ground motion, Inframatics, 9, March 2005, 1-10

Arattano, M. (1999): On the use of seismic detectors as monitoring and warning systems for debris flows, Natural Hazards and Earth System Sciences, 20,197–213

Arnoult, K., Wilson, C., Olson, J. and Szuberla, A. (2005): Infrasound associated with Mt. Steller Avalanche, Inframatics, 12, December 2005, 4-7

Arrowsmith, S., Hedlin, M., Stump, B. and Arrowsmith, M. (2008): Infrasonic signals from large mining explosions, Bulletin of the Seismological Society of America, 98(2), 768-777 doi:10.1785/0120060241.

Arrowsmith, S., Burlacu, R., Whitaker, R. and Randall G. (2009): A repeating secondary source of infrasound from the Wells, Nevada, earthquake sequence, Geophysical Research Letters, 36, L11817, doi:10.1029/2009GL038363.

Arrowsmith, S., Johnson, J., Drob, D. and Hedlin M. (2010): The seismoacoustic wavefield: A new paradigm in studying geophysical phenomena, Reviews of Geophysics, 48, RG4003, doi:10.1029/2010RG000335.

Artru, J., Farges, T. and Lognonné P. (2004): Acoustic waves generated from seismic surface waves: propagation properties determined from Doppler sounding observations and normal-mode modelling, Geophysical Journal International, 158, 1067–1077

Becker, G. and Güdesen, A. (2000): Passive sensing with acoustics on the battlefield, Applied Acoustics, 59, 149-178

Bedard, A. (1971): Seismic response of infrasonic microphones, Journal of Research of the National Bureau of Standards, C, Engineering and Instrumentation, 75(1), 41-45

Biescas, B., Dufour, F., Furdada, G., Khazaradze, G. and Suriñach, E. (2003): Frequency content evolution of snow avalanche seismic signals, Surveys in Geophysics, 24, 447–464

Brodsky, E., Gordeev, E. and Kanamori, H. (2003): Landslide basal friction as measured by seismic waves, Geophysical Research Letters, 30(24), 2236, doi:10.1029/2003GL018485

Che, I., Shin, J. and Kang, I. (2009): Seismo-acoustic location method for small-magnitude surface explosions, Earth Planets Space, 61, e1–e4

Chou, H., Cheung, Y. and Zhang, S. (2007): Calibration of infrasound monitoring system and acoustic characteristics of debris-flow movement by field studies, in: Chenglung, C., Major, J. (eds.) Debris-flow Hazards Mitigation: Mechanics, Prediction, and Assessment, Millpress, Rotterdam, 571–580

Crighton, D. (1975): Basic Principles of Aerodynamic Noise Generation, Progress in Aerospace Sciences, 16, 31–96

Curle, N. (1955): The influence of solid boundaries upon aerodynamic sound, Proceedings of the Royal Society London A, 231(1187), 505–514, doi: 10.1098/rspa.1955.0191

Drob, D. and Picone, J. (2003): Global morphology of infrasound propagation, Journal of Geophysical Research, 108(21), 4680, doi:10.1029/2002JD003307

Edwards, W., Eaton, D. and Brown, P. (2008): Seismic observations of meteors: Coupling theory and observations, Reviews of Geophysics, 46, RG4007, doi:10.1029/2007RG000253

Embleton, T., Piercy, J. and Olson, N. (1976): Outdoor sound propagation over ground of finite Impedance, Journal of the Acoustical Society of America, 59(2), 267-277

Evans, L., Bass, H. and Sutherland, L. (1972): Atmospheric absorption of sound: theoretical predictions, Journal of the Acoustical Society of America, 51 (5), 1565-1575

Firstov, P., Sukhanov, L., Pergament, V. and Rodionovskiy, M. (1992): Acoustic and seismic signal from snow avalanches, Transactions (Doklady) of the U.S.S.R., Academy of Sciences: Earth Science Sections, 312, 67–71

Ffowcs Williams, J. (1963): The noise from Turbulence Convected at High Speed, Philosophical Transactions of the Royal Society of London A, 255(1061), 469–503, doi: 10.1098/rsta.1963.0010

Ffowcs Williams, J. and Hawkings, D. (1969): Sound Generation by Turbulence and Surfaces in Arbitrary Motion, Philosophical Transactions of the Royal Society of London A, 264(1151), 321–342, doi:10.1098/rsta.1969.0031

Ffowcs Williams, J. (1977): Aeroacoustics, Annual Review of Fluid Mechanics, 9, 447–468, doi: 10.1146/annurev.fl.09.010177.002311

Johnson, J. (2003): Generation and propagation of infrasonic airwaves from volcanic explosions, Journal of Volcanology and Geothermal Research, 121,1–14

Kogelnig, A., Hübl, J., Suriñach, E., Vilajosana, I. and McArdell, B. (online first): Infrasound produced by debris flow: propagation and frequency content evolution, Natural Hazards, doi:10.1007/s11069-011-9741-8

Lee, P. and Wang, J. (2010): The simulation of acoustic radiation from a moving line source with variable speed, Applied Acoustics, 71, 931–939

Le Pichon, A., Garcés, M., Blanc, E., Barthélémy, M. and Drob, D. (2001): Acoustic propagation and atmosphere characteristics derived from infrasonic waves generated by the Concorde, Journal of the Acoustical Society of America, 111 (1), 629-641

Lighthill, M. (1952): On sound generated aerodynamically I, General Theory, Proceedings of the Royal Society A, 211(1107), 564–587

Lighthill, M. (1954): On sound generated aerodynamically II. Turbulence as a source of sound, Proceedings of the Royal Society A, 222(1148), 1–32

Lighthill, J. (1978): Waves in Fluids, Cambridge University Press, New York

Naugolnykh, K. and Bedard, A. (2002): A model of the avalanche infrasonic radiation, in: Geoscience and Remote Sensing Symposium, 2, 871–872, doi:10.1109/IGARSS.2002.1025713

Nicolas, J., Berry, J. and Daigle, G. (1985): Propagation of sound above a finite layer of snow, Journal of the Acoustical Society of America, 77, 67–73

Pilger, C. and Bittner, M. (2009): Infrasound from tropospheric sources: impact on mesopause temperature?, Journal of Atmospheric and Solar-Terrestrial Physics, 71(8-9), 816–822, doi:10.1016/j.jastp.2009.03.008

Proudman, I. (1952): The generation of noise by isotropic turbulence, Proceedings of the Royal Society A, 214(1116), 119-132, doi: 10.1098/rspa.1952.0154

Santana, V. and Olson, J. (2004): A Study of the Effects of Snow Cover on Infrasonic Signal Levels: Variations in the RMS Levels, Inframatics, 7, September 2004, 22-25

Sabatier, J., Bass, H. and Bolen, L. (1986): Acoustically induced seismic waves, Journal of the Acoustical Society of America, 80(2), 646-649

Schneider, D., Bartelt, P., Caplan-Auerbach, J., Christen, M., Huggel, C. and McArdell, B. (2010): Insights into rock-ice avalanche dynamics by combined analysis of seismic recordings and a numerical avalanche model, Journal of Geophysical Research, 115, doi:10.1029/2010JF001734

Scott, E., Hayward, C., Kubichek, R., Hamann, J., Comey, R., Pierre, J. and Mendenhall, T. (2007): Single and multiple sensor identification of avalanche-generated infrasound, Cold Regions Science and Technology, 47, 159–170

Sikora, T., Kogelnig, A., Vilajosana, I., Suriñach, E., Hiller, M. and Dufour, F. (2009): Monitoring of snow avalanches - a new approach to measuring flow induced vibrations in the ground and in the air, Geophysical Research Abstracts, Vol. 11, EGU2009-12327

Stein, S. and Wylesession, M. (2003): An Introduction to seismology, earthquakes and earth structure, Blackwell Publishing

Stubbs, C. (2005): Tactical infrasound, Technical report, The MITRE Corporation, Department of the Army United States Army Intelligence and Security Command National Ground Intelligence Center, Charlottesville, Virginia

Suriñach, E., Sabot, F., Furdada G. and Vilaplana, J. (2000): Study of seismic signals of artificially released snow avalanches for monitoring purposes, Physics and Chemistry of the Earth, 25(9), 721–727

Suriñach, E., Furdada, G., Sabot, F., Biescas, B. and Vilaplana, J. (2001): On the characterization of seismic signals generated by snow avalanches for monitoring purposes, Annals of Glaciology, 32, 268–274

Suriñach, E., Vilajosana, I., Khazaradze, G., Biescas, B., Furdada, G. and Vilaplana, J. (2005): Seismic detection and characterization of landslides and other mass movements, Natural Hazards and Earth System Sciences, 5, 791–798

Starovoit, Y. and Martysevich P. (2005): Different observed mechanisms of correlation between seismic and pressure signals, Inframatics, 9, March 2005, 11-16

Thorne, L. and Wallace, T. (1995): Modern Global Seismology, Academic Press, San Diego, USA

Tipler, P. (1994): Physics for scientists and engineers, Worth Publishers Inc., New York, USA

Udías, A. (1999): Principles of Seismology, Cambridge University Press

VanHerwijnen, A. and Schweizer, J. (2011): Seismic sensor array for monitoring an avalanche start zone: design, deployment and preliminary results, Journal of Glaciology, 57(202), 267-276

Vilajosana, I., Suriñach, E., Khazaradze, G., and Gauer, P. (2007): Snow avalanche energy estimation from seismic signal analysis, Cold Regions Science and Technology, 50, 72–85

Watada, S., Kunugi, T., Hirata, K., Sugioka, H., Nishida, K., Sekiguchi, S., Oikawa, J., Tsuji, Y. and Kanamori, H. (2006): Atmospheric pressure change associated with the 2003 Tokachi-Oki earthquake, Geophysical Research Letters, 33, L24306, doi: 10.1029/2006GL027967

Zhang, S., Hong, Y. and Yu, B. (2004): Detecting infrasound emission of debris flow for warning purposes, International Symposium Interpraevent VII, Riva, Trient, 359–364

Chapter 4

Test sites

For this study existing, with a variety of sensors equipped test sites have been used: Lattenbach torrent, Tyrol, Austria (debris flows), Illgraben torrent, Valais, Switzerland (debris flows), Vallée de la Sionne (VDLS), Valais, Switzerland (snow avalanches). A detailed description of the test sites can be found in the respective chapters (Chapters 7 to 9). The selected test sites allowed comparison with data from other measurements, which facilitates our data interpretation and verification. Moreover we could benefit from the existing infrastructure in terms of power supply, data storage and network connection, which shortened installation work a lot and decreased equipment costs.

Throughout the progress of this study it became clear that the desire of monitoring alpine mass movements such as snow avalanches or debris flows presents a variety of problems due to the high alpine regions of occurrence and the random frequency of the processes. Installing high sensitive measuring equipment that works reliably and continuously is not always an easy task. The harsh alpine environment makes it difficult to find appropriate and sustainable locations for the monitoring devices. The positions of the monitoring stations have to be chosen in order to meet the requirements of the specific studies. Key aspects of choosing a monitoring location are:

- The requirements of the sensors used
- Easy access all time of year for maintenance
- Sufficient hours of solar radiation per day for energy supply
- Reception of mobile network or other possibilities of remote control and data transmission

It is common that problems with power supply, data storage and data transmission significantly minimize the possible sensor locations.

Furthermore it is clear that experimental studies always demand a frequent presence at the site for control and maintenance of the equipment, which has to be considered when choosing a test site.

Lattenbach torrent, Tyrol, Austria (debris flows)

The Austrian monitoring site for debris flow observation is the Lattenbach catchment (5.3 km^2), located near the villages of Pians and Grins in Tyrol, Austria (Fig. 5). The

Lattenbach torrent is an observation site for debris flows operated by the Institute of Mountain Risk Engineering (BOKU, Vienna) in cooperation with the Austrian Service for Torrent and Avalanche Control (WLV) (Hübl and Moser 2006).

The test site consists of two main monitoring locations, one is near the village of Grins (MS Grins) and the other one is down in the valley in the village of Pians (MS Pians). Infrasound sensors have first been installed in 2008. The setup of the acoustic equipment changed over the years and detailed information can be found in the following Chapter 5. The main parameters, which are measured at MS Grins include seismic vibrations, infrasound signals, flow depth with two ultrasonic gauges, and video recordings. Down in the valley at MS Pians radar data (for speed estimation), flow depth with an ultrasonic gauge and videos are recorded. In addition, meteorological data (precipitation, air temperature, air moisture and radiation) are recorded at two stations in the upper catchment, indicated in Figure 5.

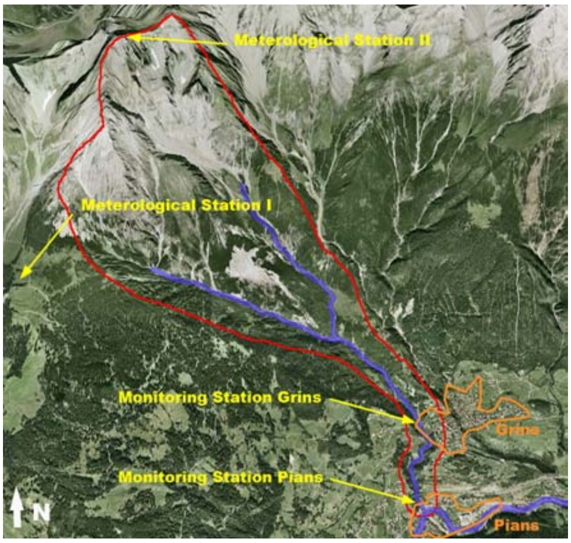

Figure 5: Overview of the Lattenbach catchment (red). The villages of Pians and Grins are indicated in orange. The Lattenbach torrent (blue) joins the Sanna river (blue) in the village of Pians. The locations of the monitoring stations are indicated in yellow (Picture taken from Google Earth).

Illgraben torrent, Valais, Switzerland (debris flows)

In addition to the Austrian test site, debris flow monitoring was also performed at the Illgraben torrent. This is one of the most active debris flow catchments in the Alps, where up to seven debris flow events occur per year with a great variability of flow properties. The Illgraben catchment (9.5 km^2) is located near the village of Susten in

Valais, Switzerland (Fig. 6) and is characterized by highly fractured bedrock and has therefore unlimited sediment supply (Badoux et al., 2009).

The Swiss Federal Institute for Forest, Snow and Landscape Research (WSL) operates the debris flow observation station at the Illgraben since the year 2000. The monitoring system records data such as flow velocity, pressure of the flowing part, total event volume, seismic data and video recordings. In total 29 check damns spread across the Illgraben channel (Fig. 6). Check dam 9, 10 and 27 are instrumented for measurements of flow depth. In addition sensors at check dam 9 and 10 are used as a trigger for the instrumentation further downstream. Infrasound sensors were first installed in summer 2008. The setup of the acoustic monitoring equipment for this study changed over the years and detailed information can be found in the following Chapter 5 and 7.

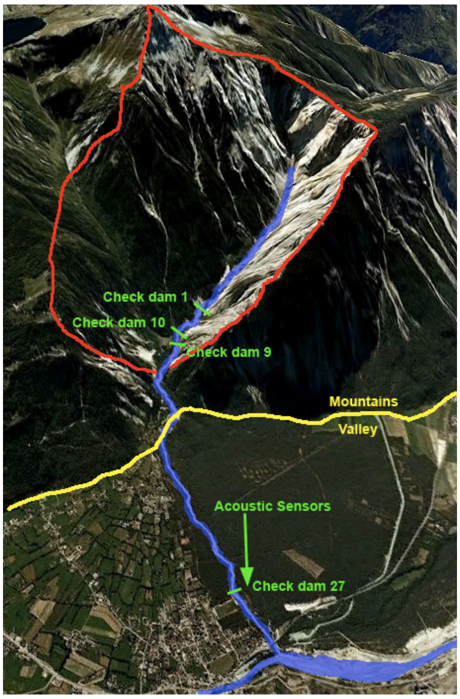

Figure 6: Overview of the Illgraben torrent (blue). The catchment area is marked in red, the borderline between the mountains and the Rhone valley is indicated in yellow. The check dams and the position of the sensors are highlighted.

Vallée de la Sionne, Valais Switzerland (snow avalanches)

The full-scale avalanche experimental site Vallée de la Sionne (VDLS) is operated by the Swiss Institute for Snow and Avalanche Research (SLF) since 1997. It is situated above the town of Sion, in Valais, Switzerland.

Avalanches start from three main release areas, indicated in Figure 7 with the abbreviations PR (Pra Roua), CB1 (Crêta Besse 1), and CB2 (Crêta Besse 2), and follow a partially channeled track down to the La Sionne river (Barbolini and Issler, 2006). Three caverns were installed along the avalanche track for various measurements. In the two upper caverns (A, B) geophones are installed, which are used to trigger the monitoring system in case of natural snow avalanches. Additionally, near cavern C a 20 m high mast is mounted with velocity and pressure sensors. Information about the sensors at the mast is given in Sovilla et al. (2008) and Kern et al. (2009).

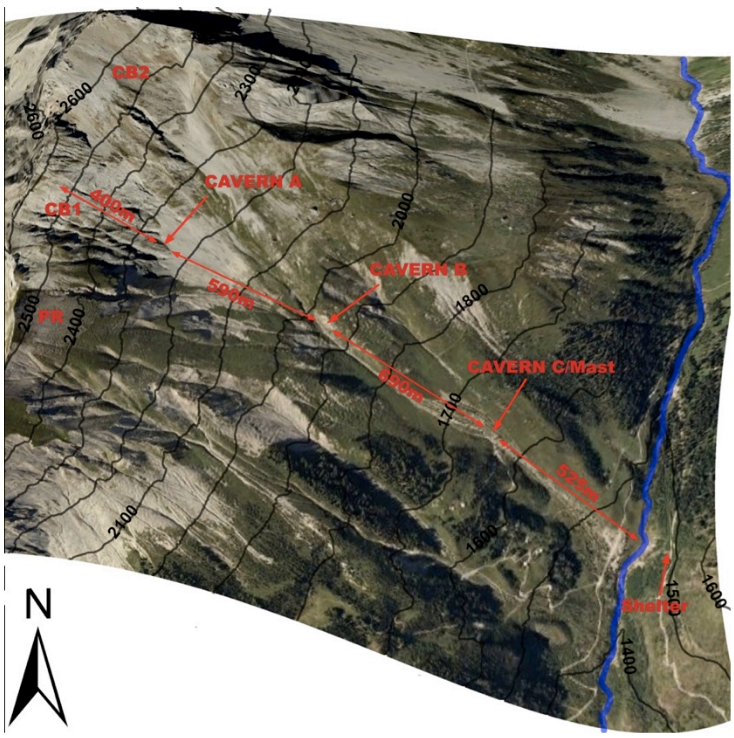

Figure 7: Overview of the VDLS test site. Caverns A, B and C are marked. The 20 m instrumented pylon is located near cavern C. The VDLS data acquisition systems are located in a shelter opposite the slope. Release areas are indicated as Pra Roua (PR), Crêta-Besse (CB1) and Crêta -Besse 2 (CB2). The La Sionne river is shown in blue (source: Google Earth).

A concrete shelter construction just opposite to the avalanche track allows human observation of artificially released snow avalanches, hosts additional monitoring equipment and serves also as data storage center. For an artificial avalanche release the transfer of the test team to the shelter is provided by helicopter with a landing platform on the roof to secure fast entrance to the shelter in case of increased avalanche danger (Ammann, 1999). The site has been equipped for seismic monitoring of snow avalanche signals since the year 1998 (Sabot et al., 1998; Suriñach, 2004). Infrasound (IS) sensors were first installed in 2008, close to the seismic sensor near the shelter. The setup of the acoustic monitoring equipment for this study changed over the years, detailed information can be found in the following Chapter 5 and 9.

References

Ammann, J. (1999): A new Swiss test-site for avalanche experiments in the Vallée de la Sionne/Valais, Cold Regions Science and Technology, 30, 3–11

Badoux, A., Graf, C., Rhyner, J., Kuntner, R. and McArdell, B. (2009): A debris-flow alarm system for the alpine Illgraben catchment: design and performance, Natural Hazards and Earth System Sciences, 49, 517–539

Barbolini, M. and Issler, D. (2006): Avalanche Test Sites and Research Equipment in Europe: An Updated Overview, Final-report deliverable D8, SATSIE avalanche studies and model validation in Europe

Hübl, J. and Moser, M. (2006): Risk management in Lattenbach: a case study from Austria. In: Lorenzi, G., Brebbia, C., Emmanouloudis, D. (eds.) Monitoring, Simulation, Prevention and Remediation of Dense and Debris Flows, WIT Press, Southamption, 333-342

Kern, M., Bartelt, P., Sovilla, B. and Buser, O. (2009): Measured shear rates in large dry and wet snow avalanches, Journal of Glaciology, 55, 327–338

Sabot, F., Naaim, M., Granada, F., Suriñach, E., Planet, P. and Furdada, G. (1998): Study of avalanche dynamics by seismic methods, image processing techniques and numerical models, Annals of Glaciology, 26, 319–323

Sovilla, B., Schaer, M. and Rammer, L. (2008): Measurements and analysis of full-scale avalanche impact pressure at the Vallée de la Sionne test site, Cold Regions Science and Technology, 51, 122–137

Suriñach, E. (2004): Spanish avalanche research: Experimental sites and seismic measurements, in: Snow and Avalanche Test Sites, edited by Naaim, M. and Naaim-Bouvet, F., 71–183, Cemagref

Chapter 5

Equipment

In this chapter an overview over the different infrasound sensors, seismic sensors and dataloggers used during this study is given. Their characteristics and key points that have to be considered when choosing and installing monitoring equipment is summarized and an overview of the sensors organized by year and test site is given in Table 1 for debris flows and Table 2 for snow avalanches.

To avoid problems with the data acquisition system in advance, first of all, the sensors have to be carefully chosen in accordance with the phenomena monitored and the objectives of the study. Secondly, the characteristics of the datalogger have to measure up the characteristics of the sensors. From the experiences gathered throughout this study it can be concluded that it is always advisable to i) stream all data of different sensors on the same datalogger to avoid problems with time synchronization, ii) provide regular monitoring if the system's functionality through remote control and iii) ensure the possibility to store all data on the datalogger or a nearby server in case of failure in data transmission. The data obtained is always a combination of the characteristics of the sensors and the datalogger used. Inadequate equipment can influence the output significantly.

Alpine mass movements were expected to emit infrasound signals with maximum amplitudes of up to 10 Pa, and with frequencies up to 20 Hz. The seismic signals were expected to have amplitudes between 10^{-7} m/s and 10^{-3} m/s and frequencies up to 50 Hz. For the purpose of this study, monitoring the acoustic signals of alpine mass movements, all data were continuously monitored with a sampling rate of 100 Hz. Throughout this study we tried to optimize the equipment (sensors and dataloggers) in view of the points mentioned above.

Dataloggers

The datalogger is an electronic device that records data of one or more sensors connected. The data can be stored internally on a hard disk or continuously streamed to a server. The datalogger is the key element of every monitoring system, which collects the data from the sensors and supply it for further use. Therefore the datalogger has to be chosen carefully in accordance to the specifications of the sensor and the data storage capabilities. The most important specification is the dynamic input range and the resolution of the datalogger; it has to fit to the specification of the sensor. Otherwise peak amplitudes will be cut by the datalogger or the resolution of the equipment will be affected. Throughout the progress of this study different dataloggers were used. For the summer setup monitoring debris flows at Lattenbach and Illgraben torrent the Campbell CR1000 (dynamic input range +/- 5 V) was used. In winter at the VDLS test site the Reftek DAS 130 (dynamic input range +/- 9 V) was implemented for monitoring snow avalanches.

Please note that the dynamic input range of the CR1000 is limited to +/- 5 V and therefore it can only be used with the Chaparral Model 24 infrasound sensor if a resistor and a bidirectional 5V diode on the digitizer input is implemented and consequently the output range of the Chaparral Model 24 is reduced to +/- 4.5 volts.

Figure 8 shows infrasound data monitored with the Chinese microphone MK 224 and an unknown datalogger. Obviously the dynamic input range of the datalogger was too small, cutting the peaks of the signal (some indicated by red arrows). Please note that this is not a problem of the microphone but of the datalogger.

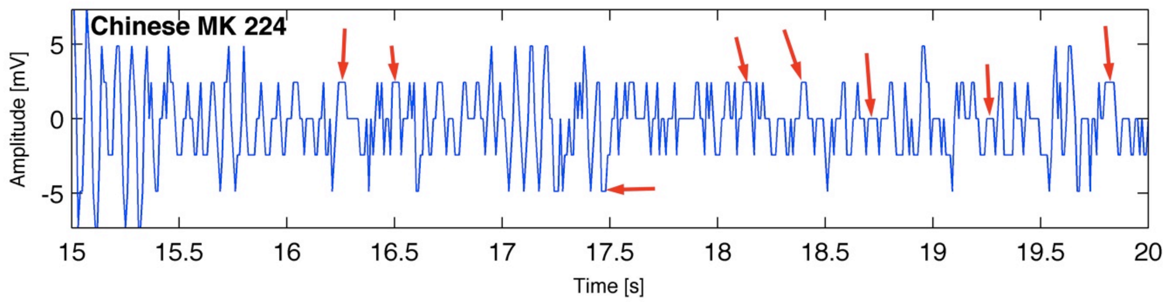

Figure 8: Time series of infrasound signals monitored with the Chinese microphone MK224 (sensitivity 50mv/Pa) and an unknown datalogger. The red arrows mark peaks of the signal that have been cut by the datalogger.

Infrasound sensors

Figure 9 gives an overview of the different infrasound sensors, which were used throughout this study. First of all it seems necessary to the author to explain the main difference between the two kinds of infrasound sensors available: absolute sensors ("barometers") and differential sensors ("microphones").

- Absolute sensors compare atmospheric pressure with a known reference in pressure (mostly a vacuum) enclosed in a sealed cavity.
- Differential sensors compare present atmospheric pressure with an averaged image of the atmospheric pressure. They measure the pressure difference between the inside and outside of a cavity connected with a small leak. They

use the same principle as microphones and are sometimes called infrasound microphones (Ponceau and Bosca, 2010). Differential infrasound sensors can achieve very low noise (i.e. signal to noise ratio). Their main drawbacks are their sensitivity to environment due to their low frequency acoustic behaviour and the lack of accurate calibration technology suited to them (Ponceau and Bosca, 2010). All sensors used in this study were differential pressure sensors.

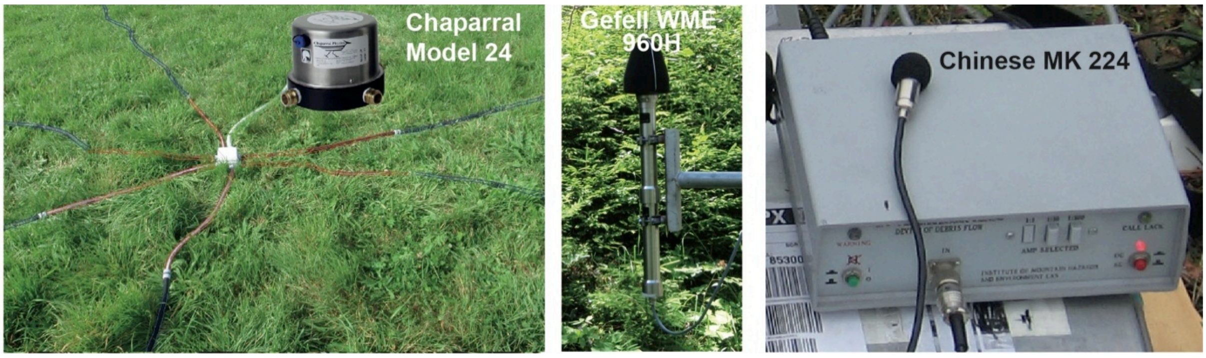

Figure 9: Images of the different infrasound sensors used during this study (see Tables 1 and 2).

The sensors used in the first step of our study were custom-made infrasound capacity microphones MK 224, developed by the Acoustics Institute, Chinese Academy of Science (CAS), with a frequency range of 3 Hz to 200 Hz and a sensitivity of 50 mV/Pa. These sensors showed good potential for monitoring snow avalanches and debris flows but were constructed for indoor use. For safety and convenience reasons, the equipment has to be placed indoors in China. To adapt the sensors for outdoor use in Europe, they have always been placed in weather-proof housing (see Fig. 11). To improve the signal-to-noise ratio and to dampen wind noise, these sensors were connected to a porous garden hose setup, which acted as a spatial wind noise reduction system for the winter setup (see following section).

The second infrasound microphone used was a ‘‘Gefell WME 960H’’ with a frequency range from 0.5 Hz to 20 kHz and a sensitivity of 50 mV/Pa. This is a commercially available product, which had the advantage of a bigger frequency range and could be mounted outdoors without the need for any additional measures.

Throughout the progress of the study the number of sensors available and especially the low sensitivity of 50 mV/Pa was considered as a limitation.

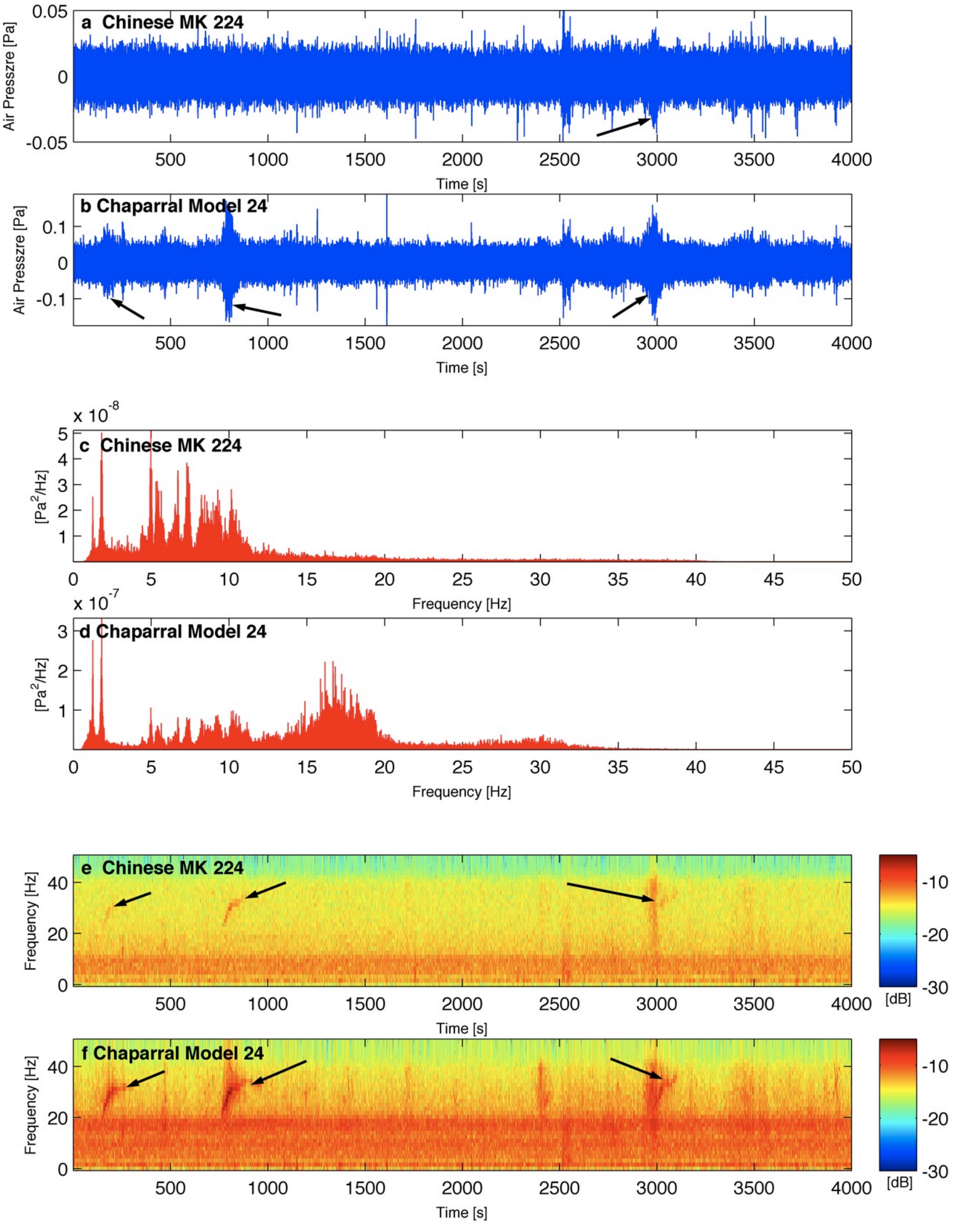

Figure 10: Comparison of infrasound data from the Chinese MK 224 and the Chaparral Model 24 sensor monitored at the Illgraben test site in 2010 using the same datalogger. (a) Time series Chinese MK 224; (b) Time series Chaparral Model 24; (c) Total spectrum Chinese MK 224; (d) Total spectrum Chaparral Model 24; (e) Running spectrum Chinese MK 224; (f) Running spectrum Chaparral Model 24; The black arrows indicate signal associated with airplanes.

The third type of sensors used were Chaparral Model 24 infrasound sensors with a frequency range of 0.1 Hz to 50 Hz and a sensitivity of 2V/Pa. These sensors were connected to a porous garden hose setup, which acted as a spatial wind noise reduction system (see following section).

Figure 10 shows a comparison of data simultaneously monitored with the Chinese microphone MK 224 and the Chaparral Model 24 infrasound sensor, both connected to the Campbell CR 1000 datalogger. Both sensors were collocated at the Illgraben torrent in spring 2010. Different times and dates were chosen and they all showed the same result. The higher sensitivity of the Chaparral Model 24 allows monitoring of signals with lower amplitudes. The time series of the Chaparral Model 24 sensor (Fig. 10b) presents some wave packages of higher amplitude associated with airplanes in the area (marked by arrows), which are not visible in the time series of the Chinese microphone MK224 (Fig. 10a).

In the running spectrum of the Chaparral Model 24 (Fig. 10f) signals associated with airplanes are visible, whereas in the running spectrum of the Chinese MK 224 (Fig. 10e) only weak signals are observable (marked by arrows). Unfortunately no debris flow or snow avalanche event could be monitored with both sensors simultaneously to allow comparisons of the relative detection capabilities of both sensors.

The total spectra of the signals of both sensors (Fig. 10c, d) depict a similar frequency distribution with the Chaparral Model 24 having high energy in the frequency band 15 Hz to 20 Hz, which are not present in the Chinese MK 224. The source of this high energy is unknown but can most probably be attributed to atmospheric background noise.

The mechanical sensitivity (i.e. the sensitivity to ground motion) of the Chaparral Model 5 infrasound sensor has been investigated in a previous study (Alcoverro et al., 2005) and shown to be negligibly low. It has to be noted that the mechanical sensitivity of the infrasound sensors used in this study is unknown, but for the Chaparral Model 24, we have considered it as negligibly low, following the work of Alcoverro et al. (2005) and information given by the manufacturer.

Porous garden hose noise reduction filter

It has been well known for a long time that noise increases on microphones and microbarometers with increasing winds. Wind is caused by spatial differences in atmospheric pressure and is a common part of the diurnal meteorological cycles in most parts of the world. Wind is intimately related to atmospheric turbulence. There are two types of turbulence: convective and mechanical. Convective turbulence is driven by thermal instability and is the predominant mechanism of mixing in the troposphere. Mechanical turbulence is created by the interaction of the wind with topography and ground based objects. It is well known that the interaction of wind with objects can lead to acoustic energy radiation (Walker and Hedlin, 2010).

Most infrasound studies conducted in recent years (e.g., Scott et al. 2007; Edwards et. al., 2007; Assink et al., 2008) have used microporous hoses (Fig. 11) originally designed for irrigation, as a spatial wind noise reduction system. These hoses are often encased in a perforated PEHD pipe and placed on the ground. The PEHD pipe (not shown in Fig. 11) should protect the micropores of the hoses from obstruction due to small particles. Depending on the objective, configurations vary from linear porous hoses to circular ones, all connected to a central or end infrasound sensor.

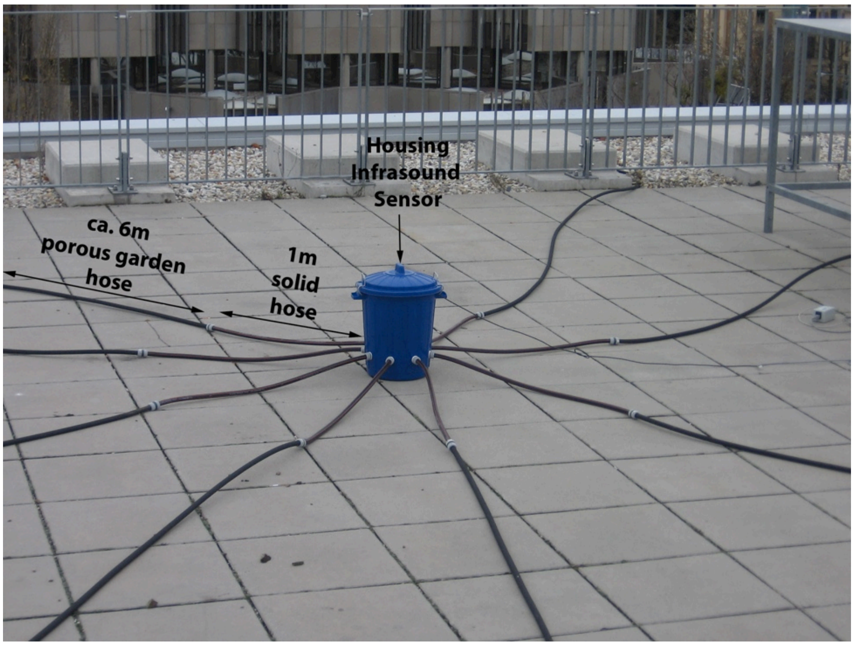

Figure 11: Overview of the star aligned porous garden hose setup. The Chinese MK224 infrasound sensor is placed in the center in a weatherproof housing.

The effect of a linear porous hose wind noise reduction filter can be explained as follows: As the signal wave front propagates along the length of the hose toward the sensor, a running acoustic wave presumably propagates inside the hose at the same speed. As a result, pressure variations are integrated along the entire length of the hoses. There are presumably destructive interferences in incoherent wind noise for turbulences that are smaller than either the length of the hose for linear configurations or the aperture for areal configurations (Walker and Hedlin, 2010). Therefore uncorrelated pressure variations, for example due to wind, sum incoherently and are reduced. Although noise and the signal of interest might have the same time and frequency, the noise, which is most commonly due to wind turbulence, is incoherent over shorter length scales (Hedlin and Berger, 2001).

Disadvantages of this system are the time delay that increases as the aperture of the filter increases and the micro porosity of the hoses degrades with time and exposure to UV radiation. Therefore hoses have to be checked on a regular basis. Additionally, the setup of the hoses is time and space consuming. In wintertime this garden hose setup is covered by snow, which provides an additional buffer from ambient noise and wind (Scott and Lance, 2002).

For the present study the configuration consisted of a star aligned (6 to 8 hoses) garden hose setup, with a length of about 7 m, whilst the first meter was a solid hose (Fig. 11). Simple garden hose connecters (e.g. Gardena) were used for the connection of the hoses.

Summary

The different infrasound sensors mentioned above have all advantages and disadvantages, for each monitoring applications thorough assessment is needed to choose the more appropriate sensor.

The highly sensitive Chaparral Model 24 sensor is the most powerful tool for monitoring snow avalanches and debris flows. It can be installed with a spatial wind noise reduction system and covered by snow ($h < 1$ m). The high sensitivity (2 V/Pa) ensures technical capacity to detect also small amplitude infrasound signals. The disadvantage of this system is the time and space consuming installation of the star aligned porous garden hose setup.

The Gefell WME 960H is a compact unit, most suitable for monitoring in wind protected locations as no spatial wind noise reduction system can be connected. The solid construction allows easy installation in the alpine environment. It seems most suitable for monitoring debris flows in narrow places, protected from wind through a dense forest and limited availability of space (e.g. Lattenbach torrent). But can also be used in wintertime for monitoring snow avalanches at wind protected sensor locations (e.g. forest).

Finally the custom-made Chinese MK 224 microphone presents a cheap alternative for monitoring in the vicinity of the process. Due to the high natural frequency (3 Hz) and the rigid construction the applications are limited. It seems most suitable for monitoring debris flows, where the sensor can be placed close to the torrent, ideally in a dense forest to be protected from wind (e.g. Illgraben). For outdoor use it has to be placed in a weatherproof housing, therefore the application in wintertime is limited.

Seismic sensors

Same as previously explained for the infrasound sensors the seismic equipment improved with the progress of the study. In general seismic sensors can be divided into one-dimensional geophones and one- to three-dimensional seismometers. The natural frequency and the sensitivity of the sensors are key points when choosing monitoring equipment for a study. It is very important that the natural frequency of the sensor is chosen with respect to the frequencies emitted by the phenomena.

Figure 12: Overview of the different seismic sensors used during this study.

In addition the distance source-sensor has to be considered with regard to the amplitudes and frequencies of the signals that are expected to arrive at the monitoring location. It is clear that monitoring with seismic sensors close to the process result in higher amplitudes and frequencies than monitoring 2 km away. Geophones are widely used for monitoring natural mass movements (e.g., Arattano, 1999; Kishimura and Izumi, 1997) but are recording only the vertical movement of the ground motion. As the wave field of a mass movement is 3D, the horizontal components are not recorded and in consequence part of the emitted seismic energy is not monitored. 3D seismometers record all three components of the seismic wavefield and generally have a higher sensitivity than geophones. Many previous studies have already proven the benefit of 3D seismometers for studying alpine mass movements (Suriñach et al., 2001, 2005; Vilajosana et al., 2008; etc.).

Figure 12 gives an overview of the seismic sensors used. This study started using a one-dimensional geophone of the type Sensor SM4 with a frequency range of 10 Hz to 180 Hz and a sensitivity of 28.8 V/m/s for monitoring debris flows at the Lattenbach test site. But its low natural frequency (10 Hz) was very unfavorable, as the signals below 10 Hz, important for the comparison with infrasound, were not monitored. Another geophone of type Sara GS 11 with a natural frequency of 4.5 Hz and a sensitivity of 90 V/m/s was installed 2009 for one season at Illgraben torrent. For monitoring snow avalanches at the VDLS test site and in 2010 at Illgraben and Lattenbach torrent seismometers of the type Mark L4-3D with a natural frequency of 1 Hz and a sensitivity of 277 V/m/s were used.

Table 1: Overview of the setup of the seismometers and infrasound (IS) sensors used in this study for monitoring debris flows.

Year	Lattenbach		Illgraben	
	Seismic	IS	Seismic	IS
2008	Geophone SM4 10 Hz natural frequency Sensitivity of 28.8 V/m/s	IS-Sensor Gefell WME 960H 0.5 Hz natural frequency Sensitivity of 50 mV/Pa	No sensor	IS-Sensor Chinese MK 224 3 Hz natural frequency Sensitivity of 50 mV/Pa
2009	Geophone SM4 10 Hz natural frequency Sensitivity of 28.8 V/m/s	IS-Sensor Gefell WME 960H 0.5 Hz natural frequency Sensitivity of 50 mV/Pa	Geophone GS11 4.5 Hz natural frequency Sensitivity of 90 V/m/s	IS-Sensor Chinese MK 224 3 Hz natural frequency Sensitivity of 50 mV/Pa
2010	Seismometer Mark L4-3D, 1Hz natural frequency Sensitivity of 277 V/m/s	IS-Sensor Gefell WME 960H 0.5 Hz natural frequency Sensitivity of 50 mV/Pa	Seismometer Mark L4-3D, 1Hz natural frequency Sensitivity of 277 V/m/s	IS-Sensor Chaparral Model 24 0.1Hz natural frequency Sensitivity of 2V/Pa

The monitoring location of seismic sensors has to be chosen carefully in order to minimize ambient noise due to wind (induced e.g. by roots of the trees into the ground), rain, trains, cars or other sources. Additionally, direct contact with the atmosphere should be avoided in order to decrease coupling effects with infrasound signals. This can be achieved by burying the sensor in the ground or placement in a capped hole. The work conducted throughout this study showed that the use of a three dimensional seismometer with a high sensitivity is necessary to study the seismic wave field in all three dimensions and is highly recommended for all studies including seismic waves. Geophones are a low cost tool for preliminary studies.

Table 2: Overview of the setup of the seismometers and infrasound (IS) sensors used in this study for monitoring snow avalanches at VDLS.

Year	Cavern B	Cavern C	Shelter	
2008/2009	No sensor	SEISMOMETER Mark L4-3D, 1Hz natural frequency Sensitivity 277 V/m/s	SEISMOMETER Mark L4-3D, 1Hz natural frequency Sensitivity 277 V/m/s	IS-SENSOR Gefell WME 960H 0.5Hz natural frequency Sensitivity 50mV/Pa
2009/2010	SEISMOMETER Mark L4-3D, 1Hz natural frequency Sensitivity 277 V/m/s	No sensor	SEISMOMETER Mark L4-3D, 1Hz natural frequency Sensitivity 277 V/m/s	IS-SENSOR Chaparral Model 24 0.1Hz natural frequency Sensitivity 2V/Pa
2010/2011	SEISMOMETER Mark L4-3D, 1Hz natural frequency Sensitivity 277 V/m/s	SEISMOMETER Mark L4-3D, 1Hz natural frequency Sensitivity 277 V/m/s	SEISMOMETER Mark L4-3D, 1Hz natural frequency Sensitivity 277 V/m/s	IS-SENSOR Chaparral Model 24 0.1Hz natural frequency Sensitivity 2V/Pa

References

Alcoverro, B., Martysevich, P. and Starovoit, Y. (2005): Mechanical sensitivity of microbarometers MB2000 (DASE, France) and Chaparral5 (USA) to vertical and horizontal ground motion, Inframatics, 9, March 2005, 1-10

Arattano, M. (1999): On the use of seismic detectors as monitoring and warning systems for debris flows, Natural Hazards and Earth System Sciences, 20,197–213

Assink, J., Evers, L., Holleman, I. and Paulssen, H. (2008): Characterization of infrasound from lightning, Geophysical Research Letters, 35, L15802, doi:10.1029/2008GL034193

Edwards, W., Eaton, D., McCausland, P., ReVelle, D. and Brown, P. (2007): Calibrating infrasonic to seismic coupling using the Stardust sample return capsule shockwave: Implications for seismic observations of meteors, Journal of Geophysical Research, 112, B10306, doi:10.1029/2006JB004621

Hedlin, M. and Berger, J. (2001): Evaluation of infrasonic noise reduction filters, in: Proceedings 23rd Seismic Research Review: Worldwide Monitoring of Nuclear Explosions, 121-130

Kishimura, K. and Izumi, K. (1997): Seismic signals induced by snow avalanche flow, Natural Hazards, 15, 89-100

Ponceau, D. and Bosca, L. (2010): Low-Noise Broadband Microbarometers, in: Infrasound Monitoring for Atmospheric Studies, edited by: Le Pichon, A., Blanc, E. and Hauchecorne, A., Springer, 119-141

Scott, E. and Lance, C. (2002): Infrasonic Monitoring of Avalanche Activity, in: Proceedings International Snow Science Workshop, Penticton, British Columbia

Scott, E., Hayward, C., Kubichek, R., Hamann, J., Comey, R., Pierre, J. and Mendenhall, T. (2007): Single and multiple sensor identification of avalanche-generated infrasound, Cold Regions Science and Technology, 47, 159–170

Suriñach, E., Furdada, G., Sabot, F., Biescas, B. and Vilaplana, J. (2001): On the characterization of seismic signals generated by snow avalanches for monitoring purposes, Annals of Glaciology, 32, 268–274

Suriñach, E., Vilajosana, I., Khazaradze, G., Biescas, B., Furdada, G. and Vilaplana, J. (2005): Seismic detection and characterization of landslides and other mass movements, Natural Hazards and Earth System Sciences, 5, 791–798

Vilajosana, I., Suriñach, E., Abellán, A., Khazaradze, G., Garcia, D. and Llosa, J. (2008): Rockfall induced seismic signals: case study in Montserrat, Catalonia, Natural Hazards and Earth System Sciences, 8(4), 805–812

Walker, K. and Hedlin, M. (2010): A Review of Wind-Noise Reduction Methodologies, in: Infrasound Monitoring for Atmospheric Studies, edited by: Le Pichon, A., Blanc, E. and Hauchecorne, A., Springer, 119-141

Chapter 6

Data analysis

The methods used for data treatment in this study have been presented in previous publications (Sabot et al., 1998; Biescas et al., 2003; Suriñach et al., 2005; Vilajosana et al., 2007). In line with their results, the data has been processed as following.

First, the raw signals were converted into physical parameters, velocity of the ground (m/s) for seismic signals and air pressure (Pa) for infrasound signals, important to allow comparison with other data and publications. The signals were filtered (1 Hz to 40 Hz) with a 4th order Butterworth band-pass filter to homogenize the data. Furthermore, data were analysed using detailed time series analysis. Different wave packets in the time series allow us to determine different sections.

Total spectra using FFT (Fast Fourier Transformation) were used to analyze frequency content of different sections. Total spectra represent the energy distribution with respect to frequency of a stationary signal.

Since we expected the snow avalanche and debris flow signals to evolve in time as the process develops and approaches the sensors, we used running spectra to investigate the frequency time evolution of the signal. The running spectra were calculated using the Short Time Fourier Transformation with a Hanning Window (length 128 samples) and an overlap of 50% (64 samples). Using a sampling rate of 100 Hz this implies a window length of 1.28 s and an overlap of 0.64 s. In order to study the signals with more detail, if necessary, we decreased the window length to 64 samples with an overlap of 32 samples, or even smaller. The running spectrum represents the evolution in time of the frequency content of the signal. The spectral amplitudes of the signals (in this study normalized in dB for better representation) are defined by the different colors of the color bar, red corresponding to the highest and blue to the lowest amplitudes. In the different running spectra figures of this study different color scales were used to better represent each signal.

For the data interpretation we benefitted from the work of Biescas et al. (2003) and Suriñach et al. (2005) that associated an increase in the seismic amplitudes in the time series with the avalanche approaching the sensor. This is also reflected in an increase and the presence of higher frequencies in time giving a triangular shape in the running spectra in the seismic data. These features are due to the wave attenuation phenomenon (Stein and Wylesession, 2003; Suriñach et al., 2005).

As previously described we used total spectra to study the signal energy with respect to frequency. In order to study and compare the signal shape and amplitudes of seismic and infrasound data, within the most energetic frequency band or the frequency band of specific interest, signals were filtered with a 4th order Butterworth band-pass filter in different frequency spectra (e.g. 1 Hz to 3 Hz).

References

Biescas, B., Dufour, F., Furdada, G., Khazaradze, G. and Suriñach, E. (2003): Frequency content evolution of snow avalanche seismic signals, Surveys in Geophysics, 24, 447–464

Stein, S. and Wylesession, M. (2003): An Introduction to seismology, earthquakes and earth structure, Blackwell Publishing

Sabot, F., Naaim, M., Granada, F., Suriñach, E., Planet, P. and Furdada, G. (1998): Study of avalanche dynamics by seismic methods, image processing techniques and numerical models, Annals of Glaciology, 26, 319–323

Suriñach, E., Vilajosana, I., Khazaradze, G., Biescas, B., Furdada, G. and Vilaplana, J. (2005): Seismic detection and characterization of landslides and other mass movements, Natural Hazards and Earth System Sciences, 5, 791–798

Vilajosana, I., Khazaradze, G., Suriñach, E., Lied, E. and Kristensen, K. (2007): Snow avalanche speed determination using seismic methods, Cold Regions Science and Technology, 49, 2–10

Chapter 7

Infrasound produced by debris flow: Propagation and frequency content evolution

Kogelnig, A., Hübl, J., Suriñach, E., Vilajosana, I. and McArdell, B.

Published in: *Natural Hazards,* online first*, doi:10.1007/s11069-011-9741-8*

Abstract

Rapid mass movements such as avalanches, debris flows and rock fall are periodic or episodic phenomena that occur in alpine regions. Recent studies have shown that debris flows generate characteristic signals in the low frequency infrasonic spectrum (4 Hz to 15 Hz). Infrasound can travel thousands of kilometers and can still be detectable. This characteristic provides a basis for the development of wide area automated monitoring systems that can operate in locations unaffected by the activity of the process. This study focuses on the infrasound vibrations produced by a debris flow at the Lattenbach torrent, Tyrol (Austria) and by two events at the Illgraben torrent, Canton of Valais (Switzerland). The Lattenbach torrent is a very active torrent, which is located in the west of Tyrol in a geologic fault zone between the Silvrettakristallin and the Northern Limestone Alps. It has a large supply of loose sediment. The Illgraben torrent, which is well known for its frequent sediment transport and debris flow activity, has been equipped with instruments for debris flow monitoring since the year 2000. This study shows that debris flow emits low frequency infrasonic signals that can be monitored and correlated with seismic signals. During the passage of the debris flow, several surges were identified by ultrasonic gauges and detected in the time series and the running spectra of infrasonic data. In the following pages the paper Kogelnig et al. (online first) is fully reproduced in an easy reading format.

Introduction

Owing to the rapid socio-economic development of mountain areas, processes like debris flows, debris floods or bed load transport, at the intersection between the natural environment and human activity, constitute an increasing hazard to live and property. Monitoring debris flow torrents is essential for mitigating these hazards and gaining more knowledge about the processes. Different types of ground vibration detectors (accelerometers, velocimeters, geophones, seismometers) have already been used by several researchers around the world to monitor seismic signals from debris flows (e.g., Arattano, 1999; Marchi et al, 2002). In this study, we combine seismic and infrasound monitoring. Infrasound monitoring systems are used for detection of snow avalanches (e.g., Bedard, 1994; Scott and Lance, 2002; Scott et al., 2006), volcanic explosions (e.g., Johnson, 2003) and atmospheric studies (e.g., Le Pichon et al., 2010). There exist only a few studies on infrasound measurements of debris flows (Zhang et al., 2004; Chou et al., 2007). For natural hazard monitoring purposes, seismic waves as well as infrasonic waves have advantages and disadvantages. The advantages include independence from weather conditions with respect to visibility, no structural need for sustainability and monitoring from a remote location unaffected by the process. Problems arise from noise induced by e.g. wind or human activity, which can mask the debris flow signal or by signal attenuation and dispersion in the propagation medium. The relative position between the mass movement (acting as a signal source) and the sensor and the characteristics of the site influence the recorded signal.

The Lattenbach torrent (Tyrol, Austria) and the Illgraben torrent (Valais, Switzerland) were selected for our study because they are both very active torrents with frequent debris flow activity and have already been equipped with instruments for debris flow monitoring in previous studies (Graf et al., 2006; Hübl and Moser, 2006). We present data from infrasonic monitoring of debris flow at Lattenbach and we correlate infrasonic and seismic signals with flow height measurements to confirm the infrasonic measurements. Furthermore infrasonic signals of two events at Illgraben will be correlated with flow height measurements and the results will be discussed. The aim of this work is to provide new insights into the potential of the infrasound sensor (in combination with seismic sensors) for monitoring torrential hazards.

Infrasound propagation and attenuation

The aim of the following section is to briefly summarize the most important factors that influence sound propagation and attenuation in the atmosphere and to apply them to infrasound monitoring over short distances (< 5km). Infrasound signals (0.01-20Hz) are longitudinal pressure waves that travel through the air with a velocity of 343 m/s (standard temperature and pressure (STP)), which is approximately that of audible sound. Infrasound signals generated by mass movements have a specific amplitude and occupy a relatively noise free band in the low frequency acoustic spectrum. Infrasound can travel thousands of kilometers and still be detectable owing to the frequency-dependence of atmospheric attenuation. The atmosphere absorbs high-frequency (audible and ultra-) sound more than low-frequency (infra-) sound (Pilger and Bittner, 2009). The attenuation reduces the amplitude of the sound signal converting the energy of the acoustic wave into heat. The most commonly used unit for measuring sound amplitudes is the Sound Pressure Level (dBSPL), which is defined following Günther et al. (2002) as:

$$dB_{SPL} = 20\log\left(\frac{p}{p_0}\right) \quad (3)$$

where p (Pa) is the sound pressure that is measured and p_0 is the reference sound pressure ($2\text{x}10^{-5}$Pa). Pressure perturbations from alpine mass movements (≈3 Pa) are infinitesimal with respect to the ambient atmospheric pressure (≈10^{-5} Pa). In our case, the pressure perturbation can be treated as a linear elastic wave rather than a non-linear shock wave (according to Johnson, (2003)). Sound propagation through the atmosphere is dependent on two forms of energy loss: Spreading loss and Absorption loss.

Spreading loss

Uniform spherical spreading (Inverse-Distance Law) loss refers to the spreading of acoustic energy as a result of the expansion of the wave fronts and it is independent of frequency. The geometrical sound pattern generated by a surface pressure source typically expands as a sphere. As sound propagates away from the source the waves are refracted and diffracted by the structure of the atmosphere. At long distances, focusing and ducting occur in the atmosphere and the geometric sound pattern becomes more cylindrical (Pilger and Bittner, 2009). However, in this study, we are dealing with spherical spreading because we are monitoring close (< 5km) to the source. According to the Inverse-Distance Law for spherical spreading, $\Delta P \propto 1/r$ (ΔP is the pressure decrease and r the distance) (e.g., Tipler, 1994). Thus:

$$\Delta dB_{SPL} = 20\log\left(\frac{r_2}{r_1}\right) \quad (4)$$

where ΔdB_{SPL} is the change in the sound pressure level, and r_1 (near) and r_2 (far) represent the change in distance. Hence, a change of a factor of 10 in the distance leads to 20 dB attenuation. In practice, the sound pattern generated by a surface sound source does not often develop the theoretically expected 3-D sphere shape (e.g. depending on landscape etc.) with the result that the geometrical loss is less than that expected for 3-D spreading (Stubbs, 2005).

Nonuniform spreading loss including reflection by finite boundaries, refraction by nonuniform atmosphere and diffraction (scattering) by non-stationary atmosphere also contributes to energy loss. However, the more variable effects of nonuniform spreading are irrelevant to this work. The dominant loss mechanism for infrasound is due to absorption processes in the atmosphere as explained in the following subsection.

Absorption loss

Sound propagating from a source is subject to absorption by the atmosphere and absorption by the ground and ground cover. If sound propagates over ground, attenuation depends on the surface because of the acoustic energy loss from reflection. Smooth, hard surfaces will produce little absorption whereas thick grass may result in higher absorption. High frequencies are generally more attenuated than low frequencies (Drob and Picone, 2003).

Energy loss due to absorption by the atmosphere can be divided into classic absorption and molecular relaxation. The latter is a result of a loss mechanism inherent in molecular gases. As a sound wave progresses in a molecular gas, part of the compressional energy is stored in the internal degrees of freedom of the molecules (Bass et al., 1972). Molecular relaxation loss is associated with redistribution of translational or internal energy of the molecules, which requires time and a phase lag. The molecular relaxation loss breaks down into rotational loss and vibrational relaxation loss (vibration of nitrogen and oxygen molecules that account for 99.03% of air). The amount of absorption depends on the temperature and humidity of the atmosphere. The most important factor is humidity because the vibrational relaxation frequencies of nitrogen and oxygen largely depend on the amount of water vapor in the atmosphere (Huang et al., 2008). Vibrational relaxation is the most potent attenuation process in the lower atmosphere but exerts only a minor influence on the infrasound given that the lower atmosphere attenuation is generally weak (Pilger and Bittner, 2009).

The classic absorption effects are a result of the transport processes that occur in a gas i.e. viscosity, heat conduction, and molecular diffusion (Bass et al., 1972). Because the Stokes-Kirchoff loss viscosity and the thermal conductivity of the air increase with temperature, the main region of attenuation is the thermosphere where the temperature increase is due to solar radiation (Pilger and Bittner, 2009). In classic acoustic attenuation, amplitude decay due to transmission loss through the atmosphere is proportional to the square of the frequency (Johnson, 2003):

$$\Delta P = P_0 e^{-(\alpha_t f^2/\rho_a)r} \tag{5}$$

where ΔP_o is the original pressure fluctuation, α_t is the total attenuation coefficient, ρ_a is the density of the air, r is the distance from the source, and f is the frequency (Hz). The total attenuation coefficient α_t considers classic loss, rotational relaxation loss, diffusion loss and the molecular vibrational relaxation loss.

This coefficient α_t can be specified in many convenient formulations, depending on the application, but a general form following (Sutherland and Bass, 2004) is:

$$\alpha_t = \alpha_{cr} + \alpha_{diff} + \sum_i \left\{ \left[A_{\max,i} / c \right] * \left[\left(2 * f^2 / f_{vib} \right) / \left(1 + \left(f / f_{vib,i} \right)^2 \right) \right] \right\} \tag{6}$$

where α_{cr} is the combined attenuation coefficient for classic loss and rotational relaxation loss, α_{diff} is the attenuation coefficient for diffusion loss and $A_{max,i}$ is the maximum loss per wavelength for the i^{th} molecular vibration relaxation component with a relaxation frequency f_{vib}, f is the frequency and c is the speed of sound. The speed of sound in air depends on temperature $c = \left(\gamma RT / M\right)^{1/2}$ (Blackstock, 2000), where γ is the specific heat ratio, T the background temperature, R the gas constant and M the molecular mass. Higher temperatures produce higher speeds of sound. Under conditions of low wind and reasonable temperature gradients, the effects of sound speed variations can be neglected for infrasound monitoring purposes at regional distances (< 5 km). Inserting values, α_t varies for 10 Hz from 2 x10^{-1}dB/km in dry air to 2x10^{-3} dB/km with 100% humidity, according to Bass et al. (1972). These small values suggest that attenuation of infrasound due to absorption in the atmosphere is nearly insignificant in the lower atmosphere even at global distances (Johnson, 2003).

In summary, infrasound propagation at regional distances (< 5km) is subject to uniform spherical spreading loss; energy loss due to absorption of the atmosphere is small and frequency dependent.

Lattenbach experimental site: characteristics and sensors

The catchment area (5.3 km^2) of the Lattenbach torrent is located in the tectonic borderline between Silvrettakristallin and the Northern Limestone Alps. Debris flows are commonly triggered from the unstable slopes, dominated by Phyllite and so-called "Wettersteinkalke". The upper zone is at 2968m asl and the lower zone where the Lattenbach torrent joins the Sanna river is at 828m asl (Fig. 13). In the lower zone lies the village of Pians, where numerous buildings are exposed to the risk of debris flow events due to the blockage of the bridge of the federal highway and/or to the overburdening of the channel because of the limited transportation capacity of the channel. Aside from regular flood events with bedload transport in spring and summer, there were three debris flows and one sediment transport process within the last four years (01/09/08, 20/06/07, 30/08/07 and 22/08/05, respectively).

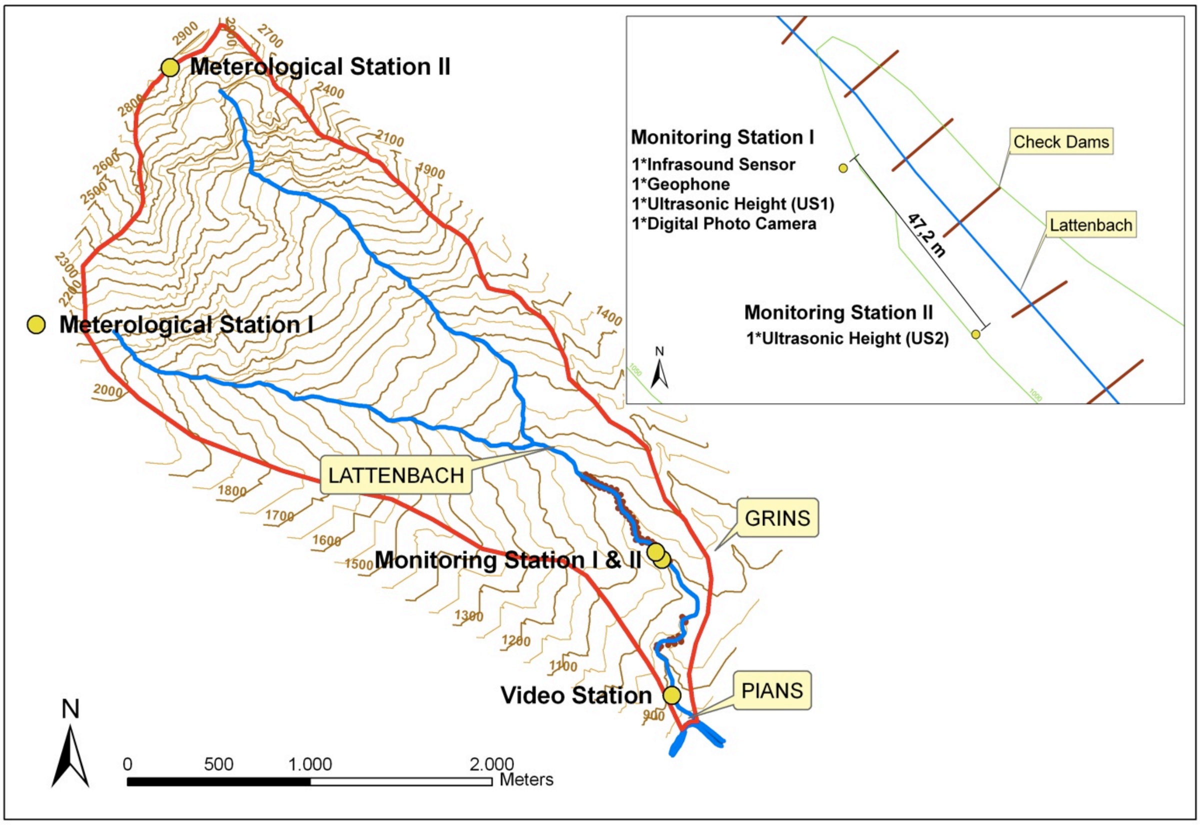

Figure 13: Overview of the Lattenbach catchment with all monitoring stations. It consists of 2 meteorological stations at the top of the mountain, monitoring station I and II (top right) in the transition zone and a video station in Pians at the lowest part.

The parameters, which are currently measured during an event, include the seismic vibrations induced by the materials in motion recorded by a geophone, low frequency fluctuations in the air detected by an infrasound microphone, the flow depth (2*ultrasonic gauges US1 and US2, 47.2 m apart), the mean flow velocity (using the ultrasonic gauges) and meteorological data (e.g. amount and intensity of precipitation, air temperature, air moisture and radiation (Fig. 13). Since July 2008 the data have been automatically transferred using a modem and GSM technology to BOKU, Vienna. The position of the monitoring station (see Fig. 13) was chosen taking into account the full development of the debris flow, easy access (the upper catchment is inaccessible) and sufficient hours of solar radiation per day for energy supply. The meteorological data have been monitored further upstream (≈ 4 km) at the so-called "Dawinalpe" (Meteorological Station I and II, see Fig. 13), which is very exposed to meteorological influences. About 950 m downstream in the village of Pians is another monitoring station including a digital video camera. The infrasound sensor used was a "Gefell WME 960H" with a frequency range from 0.5 Hz to 20 kHz and a sensitivity of 50 mV/Pa. The geophone "Sensor SM4" has a frequency range of 10Hz to 180Hz and a sensitivity of 28.8 V/m/s. The data were acquired with a Campbell Scientific CR1000 data-logger. The infrasonic and seismic signals were recorded with a sampling frequency of 100 Hz and the ultrasonic gauge recorded with 1 Hz. The infrasound sensor and the geophone were mounted close to each other near the US1 ultrasonic sensor. Other characteristics of the site that facilitates good monitoring are:

1) Proximity to the flow path, which guarantees a low ground attenuation of the seismic signals.

2.) Same data-logger for all sensors (US1, US2, Infrasound, Geophone and Digital Camera) which ensures time correlation.

3.) Protection of the sensors from wind due to the surrounding dense forest, which ensures low background noise in the infrasonic data (see Fig. 14).

4.) Seismic and infrasound sensors at the same site, which allows us to compare the signals.

Lattenbach data analysis

The event discussed in this paper is a viscous debris flow (according to the classification of Takahashi (2007)) of 1 September 2008. Its duration (time with flow height above 30 cm) was 867 s, the peak discharge was up to 380 m^3/s and the maximum flow velocity was 7 m/s. The total amount of volume was 14000 m^3. The data were analyzed with Running Spectra (RS) using the Short Time Fourier Transformation with a Hanning Window (length 128 samples) and an overlap of 50% and Power Spectrum (PS) to obtain the frequency range. The latter method represents the energy distribution with respect to frequency of a stationary signal. Since we expected the debris flow signals to evolve in time as the debris flow develops and approaches the sensors, we used the RS to investigate the frequency time evolution of the acoustic debris flow signal. The RS represents the evolution in time of the frequency content of the signal. The spectral amplitudes of the signals (in this study normalized in dB for better representation) are defined by the different colors of the color bar, red corresponding to the highest and blue to the lowest amplitudes. In the different RS figures of this study different color scales were used to better represent each signal. Figure 14 and 15 show an example of RS, time series and PS of background noise data at the site.

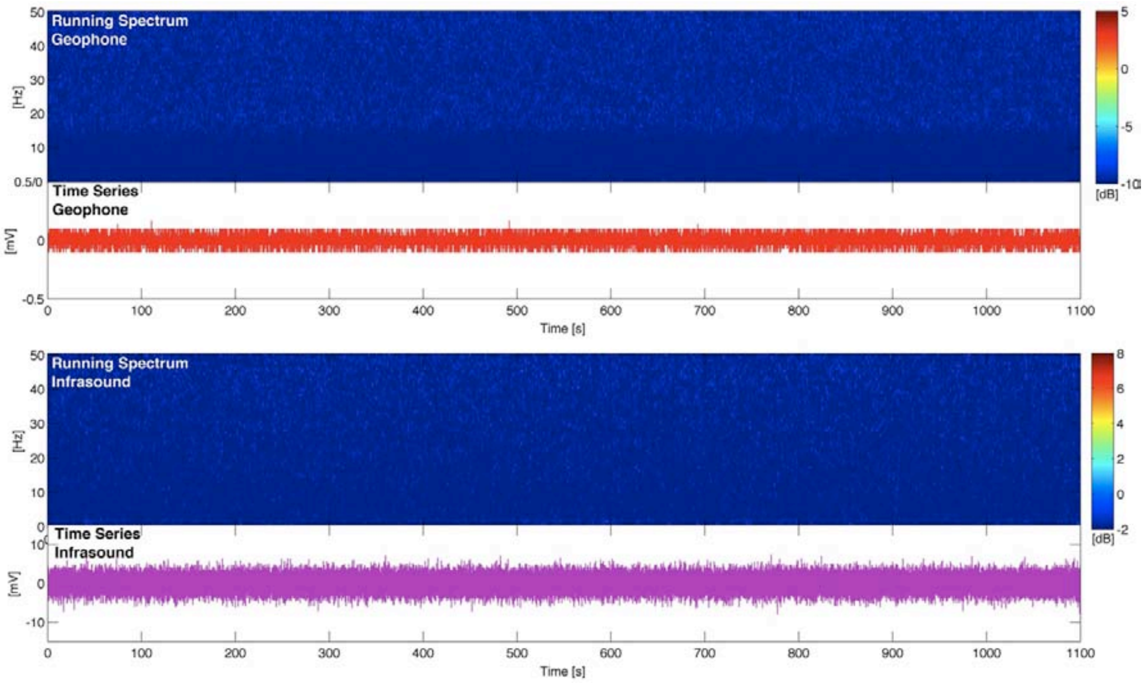

Figure 14: Example of running spectra (RS) and time series of background noise on 30/07/2008 starting at 3 a.m. at Lattenbach. The seismic amplitudes are 100 times and the infrasonic amplitudes 50 times smaller compared to the debris flow event. Top Graph: Geophone; Bottom Graph: Infrasound sensor. Seismic and infrasound signals in mV of the respective equipment.

Different days and times were chosen to study the background noise of the Lattenbach site and they all provide approximately the same results. It may be concluded that the monitoring point is appropriate given the very little background noise observed in the seismic and infrasonic measurements.

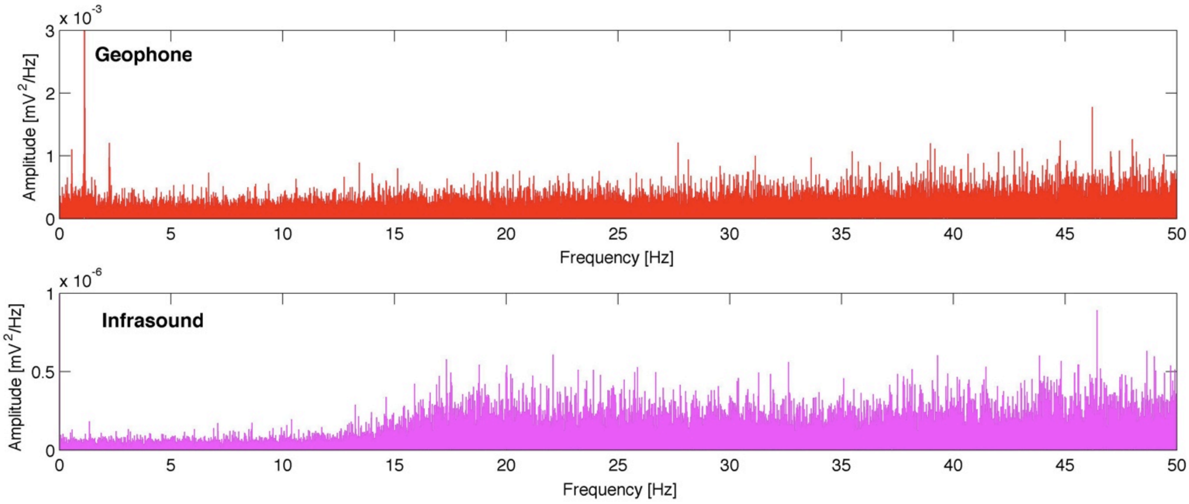

Figure 15: Example of power spectra (PS) of seismic (top) and infrasound (bottom) background noise on 30/07/08, starting at 3 a.m. at Lattenbach.

This low noise could be a consequence of the protection of the site from wind owing to its location in a thick forest and its distance from large human settlements. There is a small village (Grins) and a bridge nearby but these do not affect the noise level in the sensors.

Figure 16 gives an overview of the time series of the debris flow event. Debris flows are generally described to move down slope in a series of waves or surges. Commonly, an abrupt bore forms the head of the flow, followed by a tapering body and a thin, more watery tail (Iverson, 1997). The presence of a well-defined and recognizable front seems therefore to be a characteristic common to every debris flow (Arattano, 2000). Ultrasonic gauges are a reliable device to monitor these steep and well-defined fronts. The ultrasound sensors at the Lattenbach torrent start recording when the flow height reaches 30 cm. In the ultrasonic data (see Fig. 16 and 17, top graph US1), several surges passing the monitoring station are visible. These surges also produced corresponding peaks in the infrasonic and seismic data. It should be noted that a relationship between ground vibrations and discharge had already been observed by other authors (Itakura et al., 1997). In the magnified time series (see Fig. 17), the arrows indicate a possible first arrival of the signal at the different sensors. It is assumed that the first surge passed the monitoring station when the ultrasonic gauges started recording, which is at 650 s in the time series.

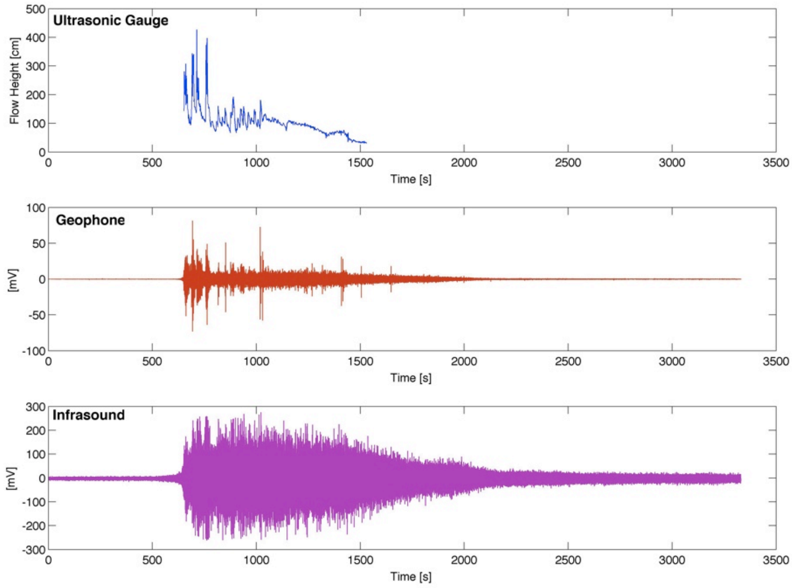

Figure 16: Time series measurements of the debris flow event at Lattenbach on 01/09/08 starting at 06:50 p.m. Top graph: Flow height (US1 sensor); Middle graph: Geophone sensor; Bottom graph: Infrasound sensor. Seismic and infrasound signal in mV of the respective equipment. Geophone sensitivity 28.8V/m/s, infrasound sensitivity 50mV/Pa.

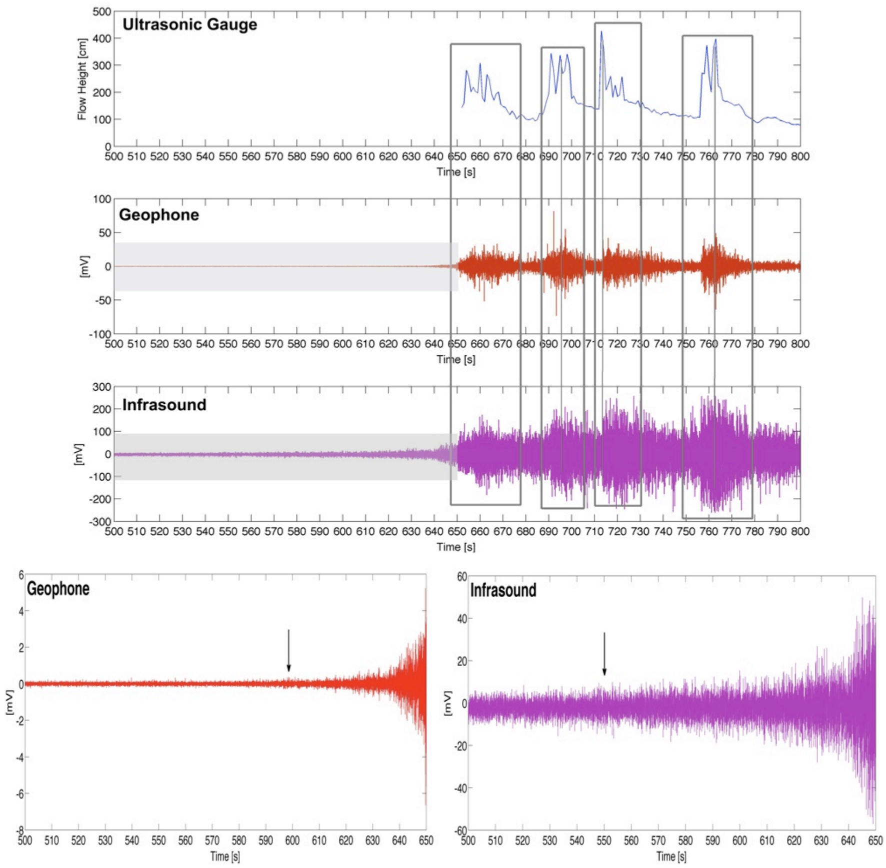

Figure 17: Magnified time series (500-800 s) of the Lattenbach signal on 01/09/08. The origin of time is corresponding to Figure 16. The rectangles mark different surges. Bottom: The grey shadowed area at the top (500-650 s) is magnified. The arrows indicate the beginning of the debris flow signal.

As a result, geophone and infrasound sensors detect the phenomenon before it reaches the sensors; in the case of the geophone, 50 s before, and in the case of the infrasound sensor, 90s before. The determination of this detection time depends on the signal-to-noise ratio and the sensitivity of the equipment.

An experiment was carried out to determine the seismic speed (at least its order of magnitude) at the Lattenbach torrent by employing three geophones over a varying distance (maximum of 50 m) and a sledgehammer (5 kg) to create a signal source. The geophones were installed in a hole in the ground after removing the top (humus) layer and then covering with soil. The seismic speed obtained from the superficial layer is approximately 465 m/s, which is a little higher than the speed of sound in the air (≈ 343 m/s at 20 °C). This speed would lead to a difference in the time propagation between the seismic and sound waves of 0.8 s in 1000 m, which is negligible.

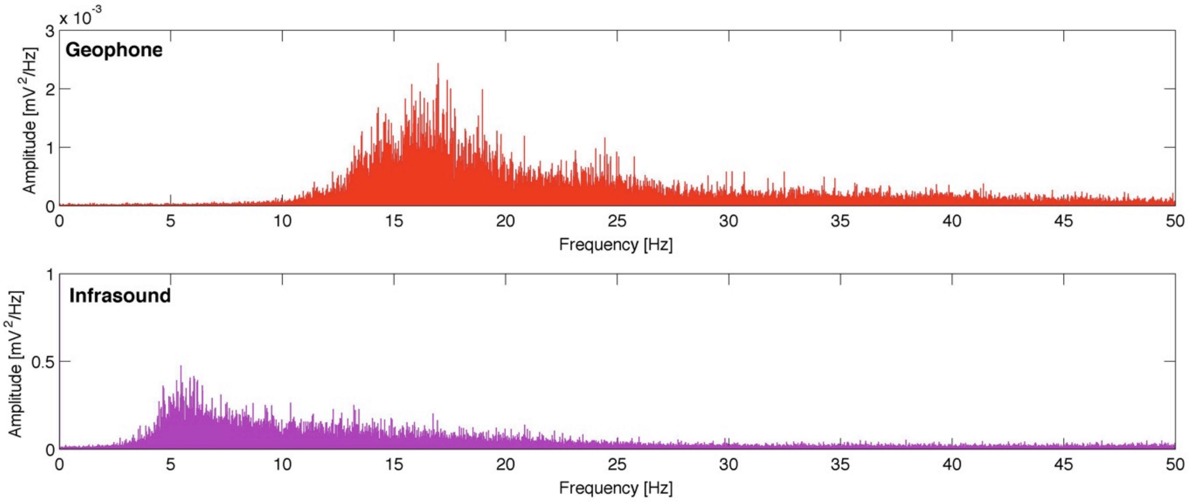

Figure 18: PS of the complete Lattenbach signal on 01/09/08 starting at 06:50 p.m. presented in Figure 16. Top Graph: Geophone frequencies centered at 17 Hz, note that the cut-off frequency of the geophone is 10 Hz. Bottom Graph: Infrasound with main frequency content around 6Hz.

The maximum amplitudes in the infrasonic signal during a surge reach values up to 240 mV, which given the sensitivity of the Gefell infrasound microphone (50 mV/Pa), corresponds to a pressure fluctuation of 4.8 Pa. This is in agreement with the results obtained by Zhang et al. (2004), who monitored pressure fluctuation between 0.5 to 4 Pa for viscous debris flows in the Jiangjia Gully, China. In the audible sound range, pressure fluctuations of up to 4 Pa correspond to heavy vehicles, a waterfall or a jackhammer.

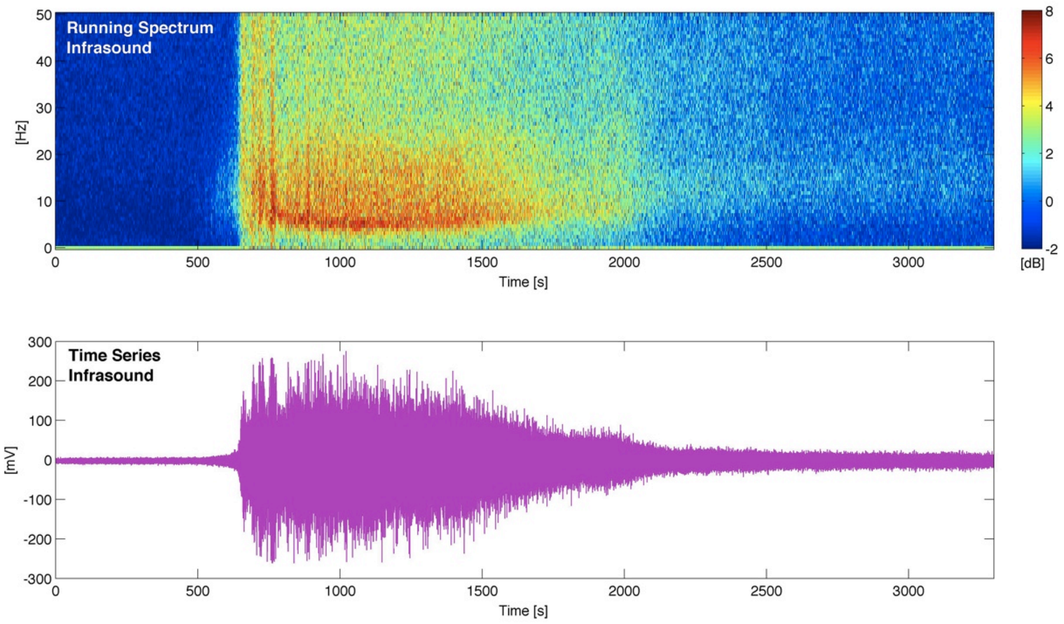

Figure 19: Infrasound data: Top graph RS; Bottom graph time series. The origin of time is corresponding to Figure 16.

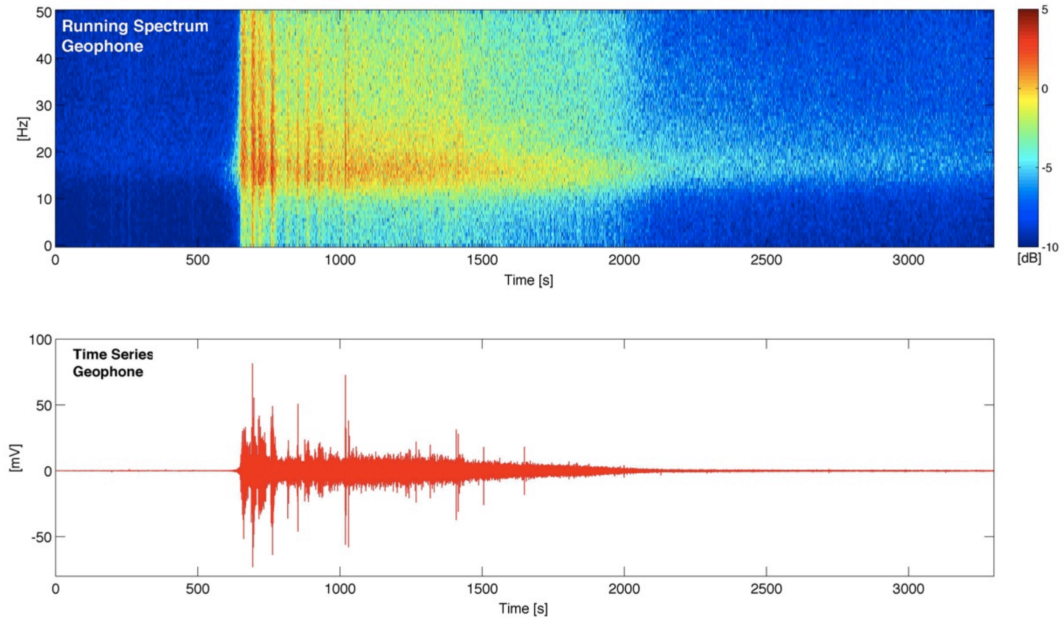

Figure 20: Geophone data: Top graph RS; Bottom graph time series. For comparison with infrasound note that the cut-off frequency of the geophone is 10Hz. The origin of time is corresponding to Figure 16.

The PS (Fig. 18) of the signal presented in Figure 16 shows that, at the Lattenbach torrent, the main frequency content for infrasonic debris flow signals is centered at 6 Hz whereas it is at 17 Hz for seismic signals. Infrasound is expected to be generated by the violent surge front and the collision (or abrasion) between debris flow and the channel loose boundary (Chou et al., 2007). The viscous debris flows at the

Lattenbach torrent are similar to the debris flows at Jiangjia Gully monitored by Zhang et al. (2004) and they show a similar infrasonic frequency distribution (centered at 6 Hz). Chou et al. (2007) monitored stony debris flows in Houyenchan, Taiwan with infrasonic frequencies between 5 Hz to 15 Hz and concluded that viscous debris flows emit lower frequencies and that stony debris flows intensify the infrasound energy at higher frequencies.

An examination of the RS of the seismic and infrasonic signals from the Lattenbach torrent (Fig. 19 and Fig. 20) sheds light on the process. As stated above, the PS (Fig. 18) indicates that the seismic debris flow signal has predominant frequencies around 17 Hz whereas the infrasonic signal is centered around 6 Hz. The RS of the signals show that this frequency content varies in time. The frequencies of the infrasonic and seismic signals increase rapidly when the debris flow moves towards the sensor, attaining the highest frequencies and amplitudes when the debris flow passes over the sensor (Fig. 21).

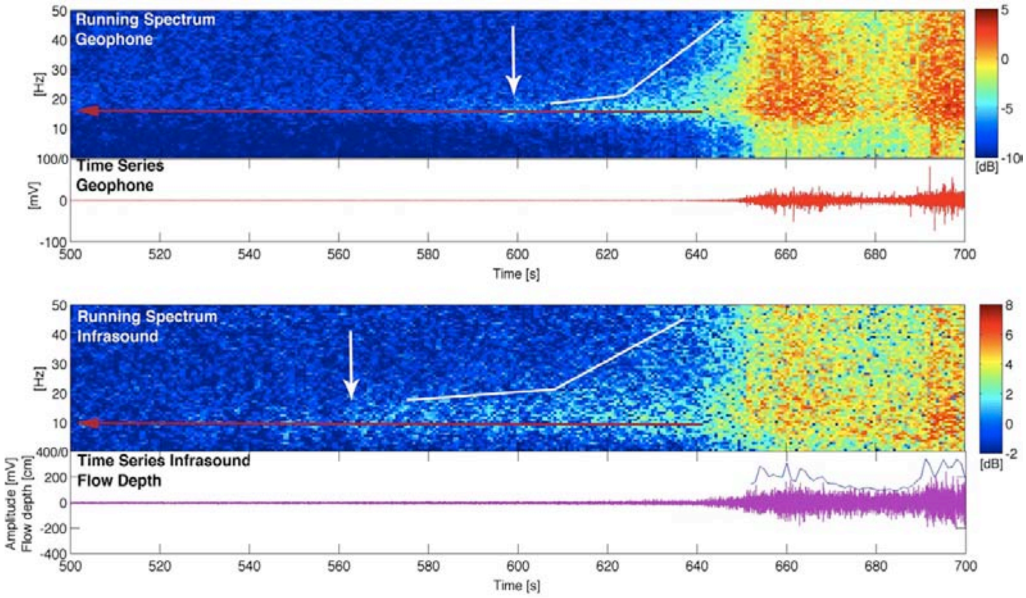

Figure 21: Geophone (top) and infrasound (bottom) RS from 500-700 s. The blue line in the infrasound time series is the flow depth indicating the time when the debris flow is passing the monitoring station (≈ 650 s). A first confirmation of the signal arrival can be seen in the geophone at ≈ 600 s and in the infrasound at ≈ 560 s or even before (white arrows). The white lines indicate the increase in frequencies, which corresponds to "signal onset SON". Seismic and infrasound signal in mV of the respective equipment. Geophone sensitivity 28.8 V/m/s, infrasound sensitivity 50 mV/Pa.

This characteristic can be used to identify the passage of a mass movement with acoustic sensors without the need for additional measurements. The exact time (650 s, Fig. 17 top) that the surge passes the station is detected by the ultrasonic gauges.

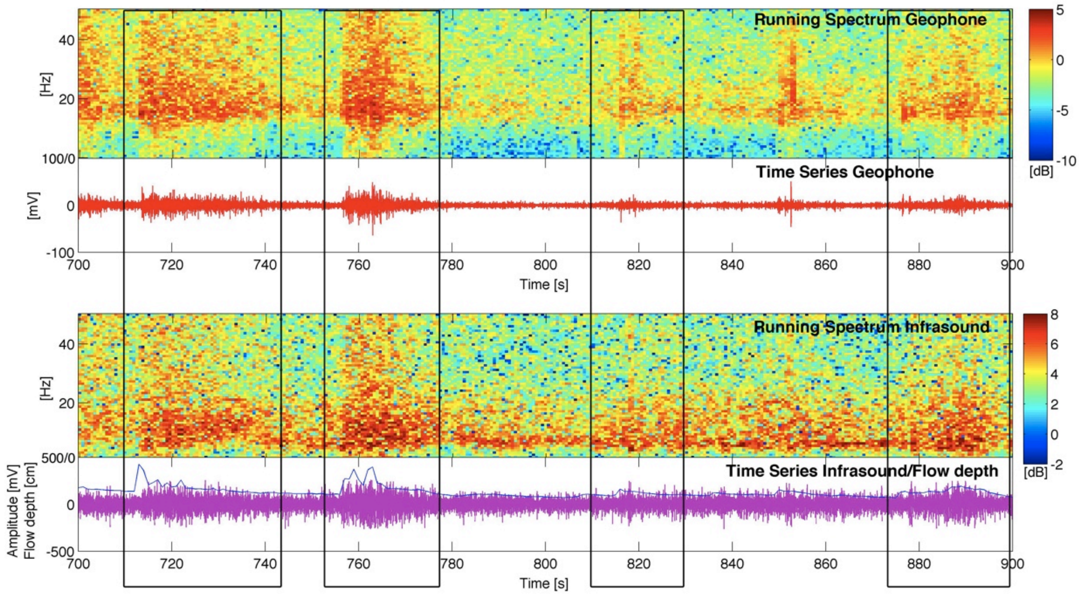

Figure 22: Geophone (top) and infrasound (bottom) RS from 700-900 s. Different debris flow surges, marked by the grey rectangles, pass the station ("signal body SBO"). The seismic signal represents the surges more clear in the time series as well as in the RS compared to infrasound. The blue line in the infrasound time series is the flow depth. Seismic and infrasound signal in mV of the respective equipment. Sensitivity geophone 28.8 V/m/s, infrasound sensitivity 50 mV/Pa.

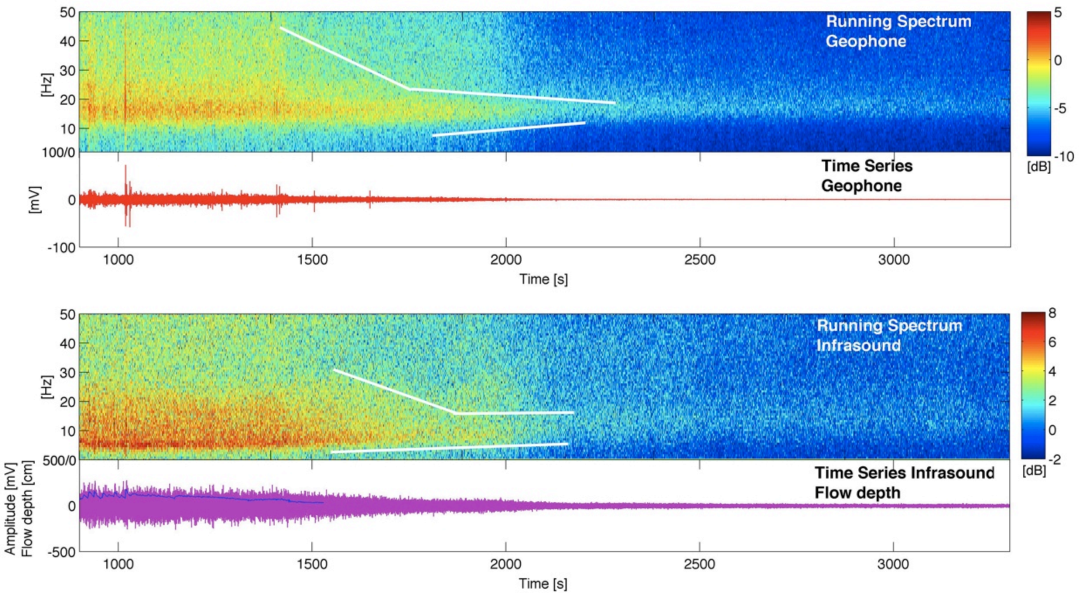

Figure 23: Geophone (top) and infrasound (bottom) RS from 900-end s. Seismic and infrasound signals seem to have a similar shape and end at the same time, although at different frequencies. The white lines indicate the decrease in frequencies, which would correspond to "signal tail STA". The blue line in the infrasound time series is the flow depth ending when the flow reaches a depth under 30 cm. Seismic and infrasound signal in mV of the respective equipment. Geophone sensitivity 28.8 V/m/s, infrasound sensitivity 50 mV/Pa.

The frequency content tends to decrease again (Fig. 23) when the debris flow moves downstream far from the monitoring station. This variation of the frequency content is observed not only for the whole debris flow but also for the different individual surges of the debris flow (see Fig. 22).

One explanation for the variation of the frequencies over time in the seismic part is the anaelastic attenuation of the seismic waves propagating in the Earth, which depends on the frequency (Biescas et al., 2003). This means that high frequencies attenuate faster than low frequencies. This observation, which is also detected in the seismic signals of snow avalanches and landslides, is related to the fact that all these phenomena are masses in movement that behave as moving vibration sources, as pointed out in Suriñach et al. (2005). To describe the behaviour of the RS of the debris flow signals, we divided the RS into three parts. We adopted the terminology proposed in Vilajosana (2008) for the RS of snow avalanche signals: "signal onset (SON)" (see Fig. 21) corresponding to the time/section before the debris flow passes the monitoring station, "signal body (SBO)" (see Fig. 22) for the time/section when the different surges pass the station and "signal tail (STA)" (see Fig. 23) for the time of the surges moving further downstream.

Like seismic waves, high frequency sound waves in the air attenuate faster than low frequency waves. Another contribution to the increase in high frequencies in the seismic and infrasound parts could be the Doppler Effect, which is the change in the frequency of a wave generated at a source for an observer in a relative movement to the source. In our case, the source is in motion whereas the sensor is fixed. The decrease in distance, with the change in velocity, between the moving source and the sensor induces an increase in the frequencies observed at the sensor. The Doppler effect, however, can be neglected because the speed of the debris flow is approximately constant ($v \approx 5$ m/s, variation of $\pm$ 3 m/s) and is two orders of magnitude lower than the speed of seismic waves ($\approx$ 465 m/s) and sound waves in the air ($\approx$ 343 m/s at 20°C).

The magnified RS of the section 500 s to 700 s (Fig. 21), which corresponds to the time interval just before and at the moment that the debris flow begins to pass the monitoring station, yields further information about the arrival time of the signals (see white arrows). It can be observed that the early seismic frequencies are centered around 16 Hz (see red arrow in Fig. 21 top) whereas the infrasonic frequencies are around 10 Hz (see red arrow in Fig. 21 bottom). The infrasonic waves tend to have a much lower frequency content compared with the seismic signals in general (see Fig. 18) and especially in the SON section where there is not much signal energy above 10 Hz in the infrasonic RS (Fig. 21). It should be borne in mind, however, that the cut-off frequency of the geophone is around 10 Hz and therefore the low frequency part in the seismic is not monitored. Observation of the first arrivals (see white arrows in Fig. 21) shows that a gap of approximately 40 s between the seismic (≈ 600 s) and the infrasonic signals (≈ 560 s) can be determined. As stated above, the geophone detects the debris flow 50 s and the infrasound sensor 90 s before the surge passes the monitoring station (Fig. 17). Multiplying these time gaps by the average flow velocity of 6 m/s (obtained from the ultrasonic gauges), an upstream distance of 300 m for the geophone and 540 m for the infrasound sensor is obtained. One explanation for the time gap observed between the infrasonic and seismic detection of the debris flow could be that, owing to attenuation, only the low frequency part (below 10 Hz) of the seismic signals generated 540 m upstream of the monitoring station reaches the geophone, and it is not captured by the geophone because of its high cut-off frequency (10 Hz). Huang et al. (2008) showed that the spatial decay rate of sound in the air is much smaller than that of ground vibrations. To verify and reproduce this observation, further debris flows must be monitored using a geophone with a wide range of low frequencies.

Illgraben study: site characteristics and sensors

The Illgraben catchment (9.5 km^2) extends from the summit of the Illhorn (2716 m asl) to the Rhône valley (ca. 610 m asl) (Schlunegger et al., 2009). Forty-four percent of the catchment is covered with bedrock and debris deposits, 42% by forest, and 14% by grassland (Badoux et al., 2009). The catchment is located in highly fractured bedrock that forms a large anticline within the northern steep limb of the Penninic nappe stack (Schlunegger et al., 2009). The main channel of the Illgraben torrent flows approx. 1400 m to the northeast through the active part before reaching check dam 1 (48 m fall height) and 1600 m before leaving the mountains (at the Bhutan bridge) and entering the Rhône valley (Fig. 24). In total, there are 29 check dams spread across the channel. Check dams 2 to 29 have fall heights varying from one to seven meters, some of which are completely covered with sediment deposits or are destroyed. The mean slope of the channel in the upper mountainous part is 21 % and in the Rhône valley around 10 %. Every year three to five debris flows as well as several debris floods are caused by intense summer thunderstorms that pose a threat to the village of Susten at the confluence of Illgraben torrent and the Rhône River.

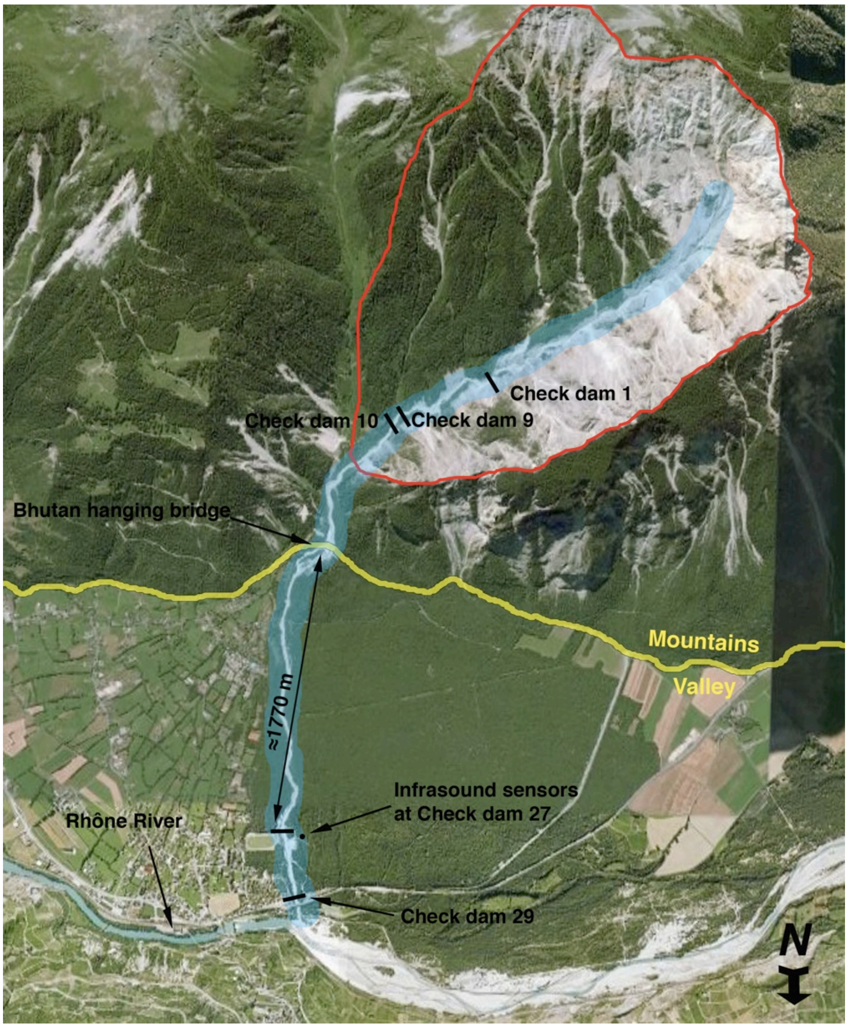

Figure 24: Overview of the Illgraben torrent (in blue), the thin red line marks the catchment area and the yellow line marks the boarder between mountains and Rhône valley (Picture taken from Google Earth).

Two infrasound capacity microphones, developed by Acoustics Institute, Chinese Academy of Science (CAS) with a frequency range of 3 Hz to 200 Hz and a sensitivity of 50 mV/Pa, were placed close to check dam 27 (Fig. 24) owing to the inaccessibility of the upper catchment. One of them (IS1) was equipped with a spatial wind noise reduction system consisting of 6 star aligned porous garden hoses. The other one (IS2) was placed close to IS1 to evaluate the "hose array". Unfortunately, data acquisition of IS2 encountered problems and as a consequence these data were not used. The data of both sensors were monitored with a Campbell

Scientific CR23 data-logger with 50 Hz and stored on a Xplore iX104 C3 tablet computer that runs continuously. Additionally, we used the data of ultrasonic gauges (for flow depth, sampling rate 1 Hz) at check dams 1, 9 and 27, operated by the Swiss Federal Institute for Forest, Snow and Landscape Research (WSL). Unfortunately, no geophone data are available at this study site.

Illgraben data analysis

The first "Illgraben" event discussed in this paper is the debris flow that occurred on 31 August 2008 at approx. 8:15 p.m. The front velocity based on flow depth measurements between check dams 27 and 29 (distance 467 m) was 1.89 m/s and the maximum flow depth at check dam 27 was approx. 0.9 m. The second event studied is the debris flood that took place on 19 August 2008 at 08:55 p.m. The difference between debris flow and debris flood is blurred. A larger bulk density characterizes debris flows and debris floods have a higher water content that is also visible at the surge front (Hungr et al., 2001). As in the case of the Lattenbach data, signals were analyzed with Running Spectra (RS) using the Short Time Fourier Transformation with a Hanning Window (length 128 samples) and an overlap of 50% and Power Spectra (PS) to obtain the frequency range.

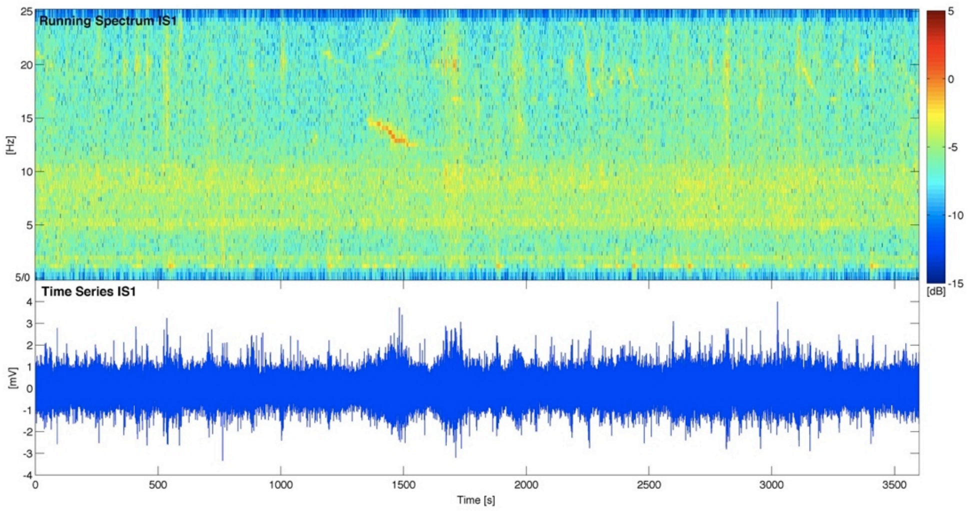

Figure 25: Example of RS and time series of infrasonic background noise on 06/08/08 starting at 10:55 a.m. at Illgraben. Data were filtered with a 4th order Butterworth bandbass filter between 1 Hz to 24 Hz. Note that the amplitudes are 50 times smaller compared to that of debris flow signal (see Fig. 27). Infrasound signal in mV of the respective equipment.

The data were filtered with a 4th order Butterworth band bass filter between 1-24Hz to eliminate interfering low frequency background noise. Inherent in all the Illgraben data is a dominant low frequency sinusoidal wave (≈0.5Hz) of unknown origin. Figures 25 and 26 show an example of the infrasound background noise at the Illgraben site. Note that there is more "noise" than at the Lattenbach site. This noise could be attributed to the Rhône River or the highway nearby. Nevertheless, the amplitudes of the background noise are low with respect to the debris flow event (see Fig. 27).

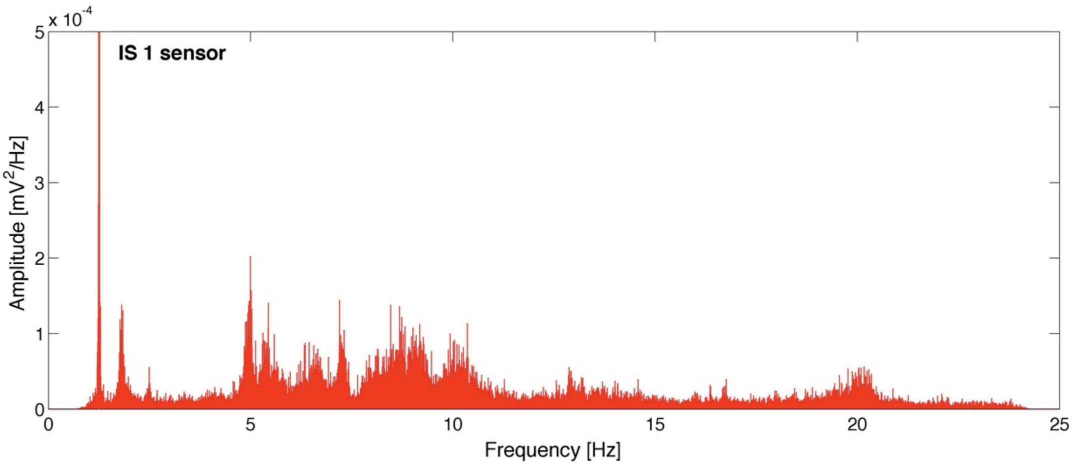

Figure 26: Example of PS of infrasonic background noise on 06/08/08 starting at 10:55 a.m. at Illgraben. Data were filtered with a 4th order Butterworth bandbass filter between 1 Hz to 24 Hz.

Figure 27 shows the infrasound signal of the debris flow event on 31 August 2008. From the ultrasonic gauge we know that the debris flow passed check dam 1 at ca. 07:50:50 p.m. (accuracy of ±1min due to installation issues), check dam 9 at 08:00:00 p.m. and check dam 27 at 08:16:24 p.m. These data lead to a flowing time of 984s from check dam 9 to check dam 27, which are at a distance of 2694 m apart. As a consequence, the average speed obtained is 2.8 m/s in this section. Observation of the running spectra of the infrasonic data shows an increase in frequencies at around 635 s before the debris flow passes check dam 27 (marked by oblique black lines). There is also a slight increase in amplitudes, which is observable in the time series in the same section. This part corresponds to section SON as defined in Section 4. At 08:16:24 p.m. the debris flow passes the infrasound sensor and section SBO starts. Thereafter, as the debris flow depth decreases, the infrasonic frequency content falls again (section STA).

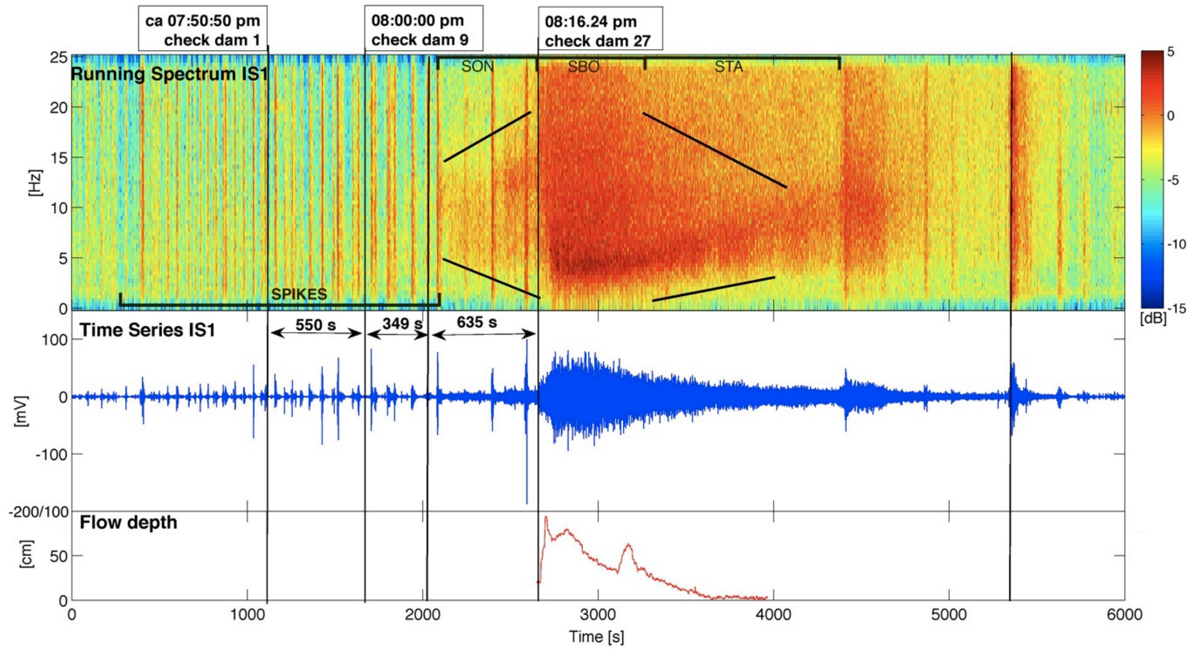

Figure 27: RS (top), Time Series (middle) and Flow Depth (bottom) of the debris flow on 31/08/08 at Illgraben, IS1 sensor. Infrasound data were filtered with a 4th order Butterworth bandbass filter between 1-24Hz. Infrasound signal in mV of the respective equipment.

Figure 27 also illustrates a series of spikes, before section SON, whose origin is unclear. While it is not possible to identify these spikes owing to the unavailability of information, it may be hypothesized that they correspond to a thunderstorm over the area. The triggering mechanism of the debris flow at the Illgraben torrent is unknown because of the inaccessibility of the upper catchment (Badoux et al., 2009). However, in the light of historical evidence and ongoing studies, it is likely that such events are triggered by short periods of high-intensity rainfall. A time gap of 635 s before the debris flow passes check dam 27 is observed from section SON. This time corresponds to a distance of 1738 m upstream of the monitoring station. This distance was calculated considering a constant velocity for the flow of 2.73 m/s. To obtain this velocity value, we used the distance from check dam 9 to 27 (2694 m) and the time (984 s obtained from the ultrasonic gauges) that the debris flow employs in covering this distance.

This upstream distance corresponds to a point near the Bhutan Bridge or to the transition of the mountainous area to the Rhône valley (see yellow line in Fig. 24). It may therefore be concluded that the infrasound microphone, placed at check dam 27 can detect the debris flow when it leaves the mountains and enters the flat valley. The time delay of the signal arrival owing to the speed of sound in air (≈ 343 m/s at

20°C) must be considered for a more accurate monitoring or for warning purposes when using infrasound. The distance from check dam 1 to 27 is approximately 3389 m. Consequently, an infrasound signal travelling at approx. 343 m/s needs 10 s to cover this distance and 8 s for the distance between check dam 9 and check dam 27 (2694 m).

The PS shown in Figure 28 illustrates that the main frequency content for infrasonic debris flow signals is between 3 to 8 Hz at the Illgraben torrent. This correlates strongly with the infrasonic frequency content obtained at the Lattenbach torrent (Fig. 18) and with that obtained by Zhang et al. (2004) for viscous debris flows. In addition, Figure 28 shows the evolution of the signal frequency as the debris flow moves towards the infrasonic sensor. Section SON has a frequency content from 5 to 15 Hz (red lines), section SBO from 3 to 7 Hz (blue lines) and section STA from 4 to 10 Hz (yellow lines). The spikes before the onset of the signal (Fig. 27) do not have a characteristic frequency range (green lines). The maximum signal amplitudes in the time series at Illgraben reach values up to 100 mV, which corresponds to pressure fluctuations of 2 Pa (infrasound sensor sensitivity is 50 mV/Pa). This is only half the value reached at the Lattenbach torrent. This difference can be attributed to a) the event size (total amount of volume is unknown for Illgraben) and b) the difference in terrain.

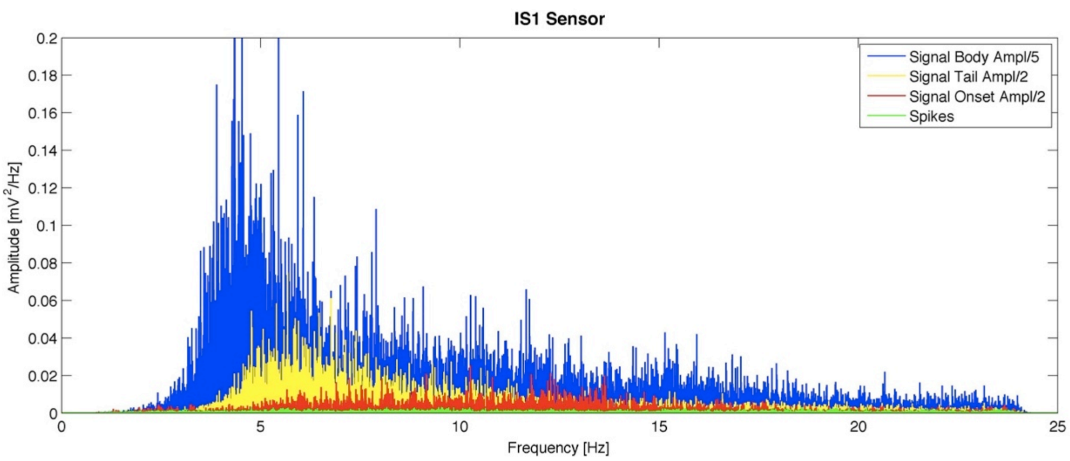

Figure 28: PS of the different parts of Illgraben infrasonic debris flow signal on 31/08/08 presented in Figure 27. Data were filtered with a 4th order Butterworth bandbass filter between 1-24 Hz. In order to represent all the spectra in one figure, amplitudes [mV^2/Hz] were reduced as defined in the legend.

The monitoring station at the Lattenbach torrent is located in a narrow alpine gorge that leads to a channeling of the sound waves, whereas at the Illgraben torrent the monitoring station is placed in the wide-open Rhône valley, which favors the geometrical spreading of the signal.

The second event studied at this site is the debris flood (according to the classification of Hungr et al. (2001)) of 19 August 2008 (Fig. 29). The exact time that the debris flood passes the monitoring station is not known because of the low sampling frequency (average over 10 min) of the ultrasonic gauge. The black line in Figure 29, which indicates that the flow passes the monitoring station at 08:03:48 p.m., was chosen considering the increase in amplitudes in the infrasonic data.

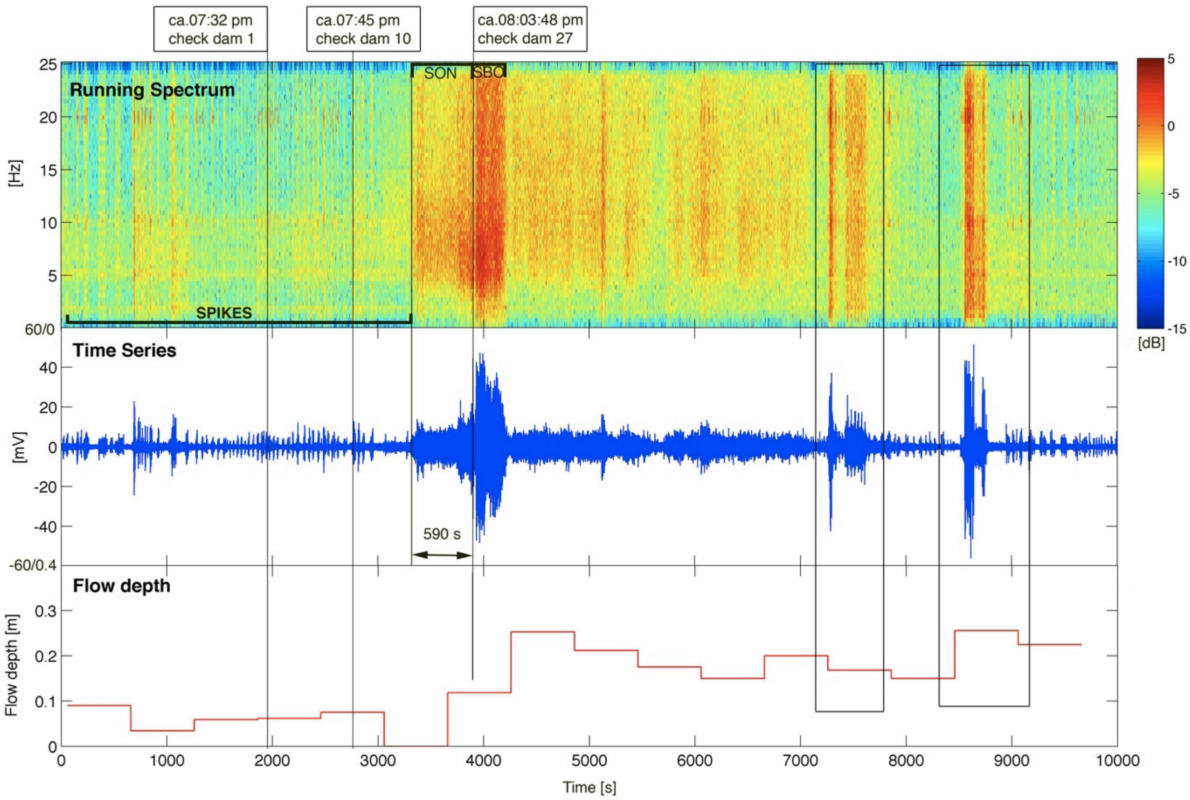

Figure 29: RS (top), time series (middle) and flow depth (bottom) of the debris flood on 19/08/08, IS1 sensor. The flow depth data available are corresponding to an average over 10 minutes. Infrasound signal in mV of the respective equipment.

One important characteristic observed in the signals from the events discussed above and in the seismic monitoring of other mass movements such as avalanches (e.g., Vilajosana et al., 2007) is a marked increase in the amplitudes and the frequencies when the mass movement passes over the sensor. Although the flow depth of this event was fairly small (max 0.3 m) it has a behaviour similar to that of the event of 31 August 2008. There is an increase in frequencies (see RS Fig. 29) and also in amplitudes (time series Fig. 29) about 590 s before the flow passes sensor IS1 at check dam 27 (section SON). Section SBO is fairly short in time (about 200 s) but still identifiable. Section STA is absent not only in the RS but also in the time series. This absence could be due to the passage of only a single surge. However, this observation is not confirmed by the ultrasonic flow depth data. More debris floods must be recorded with a higher sampling frequency of the ultrasonic gauge to gain further insights into the process.

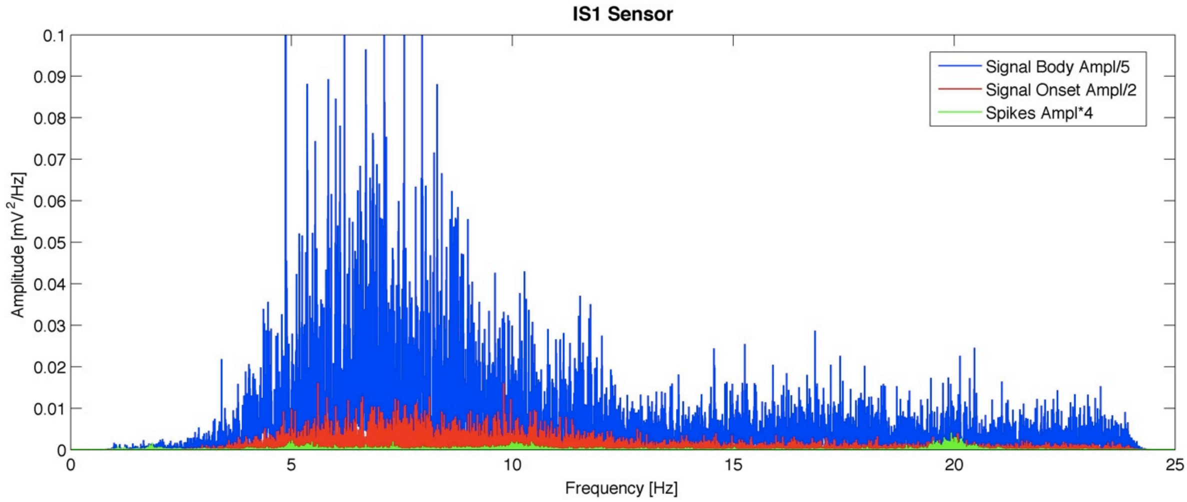

Figure 30: PS of the different parts of Illgraben infrasonic debris flood signal on 19/08/08 presented in Figure 29. Data were filtered with a 4th order Butterworth bandbass filter between 1 Hz to 24 Hz. In order to represent all the spectra in one figure, amplitudes [mV^2/Hz] were reduced as defined in the legend.

Comparison of the PS of the infrasound signals of the debris flow on 31/08/08 (Fig. 25) and that of the debris flood on 19/08/08 (Fig. 30) shows that the frequency content of SBO section (5 Hz to 10 Hz) of the debris flood is slightly higher than that of the SBO section (3 Hz to 7 Hz) of the debris flow. One explanation for the different peak frequencies could be that a debris flood has a higher water content and a finer sediment concentration than a debris flow. Moreover, the debris flood event (flow depth 0.3 m) in our case was smaller than the debris flow (flow height 1 m). Further debris flows/floods with different rheological characteristics should be monitored to draw some conclusions in this regard.

Conclusions

Low frequency vibrations in the ground and in the air produced by debris flows, and one debris flood were analyzed and compared. At the Lattenbach torrent we employed one infrasound sensor, one geophone and two ultrasonic gauges. At the

Illgraben torrent, one infrasound sensor and several ultrasonic gauges were used. It may be affirmed that debris flows emit low frequency infrasonic signals that can be monitored and correlated with seismic signals. The amplitude and frequency content of the seismic and infrasound signals increase as the debris flow moves towards the sensors. During the passage of the debris flow, several surges were identified by the ultrasonic gauges. The time series and the RS of the seismic and infrasonic data also recognize these surges. The infrasound sensor detects the approaching debris flow before it passes the monitoring station. The RS analysis of seismic and infrasonic signals provides useful information for monitoring purposes and confirms the detection of the debris flow by the infrasound sensor. The RS of the seismic and infrasonic signals allows us to divide the signal into three parts: Onset, Body and Tail in a way similar to that observed previously in seismic signals of avalanches. The frequency content of the infrasonic and seismic signals is not stationary at the sensors. This is because the debris flow is a mass in motion and acts as a moving source of vibration.

Another phenomenon is observed at the Illgraben torrent. The infrasound sensor starts to detect infrasonic emissions of the torrential processes when these leave the mountains and enter the wide-open Rhône valley. The high mountain ridge seems to form a natural sound barrier with an acoustic shadow zone behind. This effect must be considered when using infrasound equipment for detecting natural hazards. The cut-off frequency of the geophones installed must be taken into account given that it can limit the observations. This was the case at the Lattenbach torrent where the cut-off frequency was 10 Hz.

Further studies are envisaged not only at the Lattenbach torrent, Austria, but also at the Illgraben torrent, Switzerland, to confirm the reproducibility of these results and to gain new insights into the source of infrasonic signals of debris flows.

References

Arattano, M. (1999): On the use of seismic detectors as monitoring and warning systems for debris flows, Natural Hazards and Earth System Sciences, 20,197–213

Arattano, M. (2000): On debris flow front evolution along a torrent, Natural Hazards and Earth System Sciences, 25(9), 733–740

Badoux, A., Graf, C., Rhyner, J., Kuntner, R. and McArdell, B. (2009): A debris-flow alarm system for the alpine Illgraben catchment: design and performance, Natural Hazards and Earth System Sciences, 49, 517–539

Bass, H., Bauer, H. and Evans, L. (1972): Atmospheric absorption of sound: Analytical expressions, Journal of the Acoustical Society of America, 52, 821-825

Bedard, A. (1994): An Evaluation of Atmospheric Infrasound for Monitoring Avalanches, Proceedings; 7th International Symposium on Acoustic Sensing and Associated Techniques of the Atmosphere and Oceans, Boulder, CO

Biescas, B., Dufour, F., Furdada, G., Khazaradze, G. and Suriñach, E. (2003): Frequency content evolution of snow avalanche seismic signals, Surveys in Geophysics, 24, 447–464

Blackstock, D. (2000): Fundamentals of Physical Acoustics, Wiley Interscience Publications

Chou, H., Cheung, Y. and Zhang, S. (2007): Calibration of infrasound monitoring system and acoustic characteristics of debris-flow movement by field studies, in: Chenglung, C., Major, J. (eds.) Debris-flow Hazards Mitigation: Mechanics, Prediction, and Assessment, Millpress, Rotterdam, 571–580

Drob, D. and Picone, J. (2003): Global morphology of infrasound propagation, Journal of Geophysical Research, 108(21), 4680, doi:10.1029/2002JD003307

Graf, C., Badoux, A., McArdell, B., Dufour, F., Rhyner, J. and Kuntner, R. (2006): A warning system for natural hazards in summer at the Illgraben, 4th Swiss Geoscience Meeting, Bern

Günther, B., Hansen, K. and Veit, I. (2002): Technische Akustik- Ausgewählte Kapitel, 7,Expert Verlag

Huang, C., Yeh, C., Chen, C. and Chang, S. (2008): Ground vibrations and airborne sounds generated by motion of rock river bed, Natural Hazards and Earth System Sciences, 8, 1139-1147

Hübl, J. and Moser, M. (2006): Risk management in Lattenbach: a case study from Austria. In: Lorenzi G, Brebbia C, Emmanouloudis D (eds.) Monitoring, Simulation, Prevention and Remediation of Dense and Debris Flows, WIT Press, Southamption, 333-342

Hungr, O., Evans, S., Bovis, M. and Hutchinson, J. (2001): A review of the classification of landslides of the flow type, Environmental and Engineering Geoscience, 7(3), 221–238, doi:10.2113/gseegeosci.7.3.22

Itakura, Y., Koga, Y., Takahama, J. and Nowa, Y. (1997): Acoustic detection sensor for debris-flow, in: Debris-Flow Hazards Mitigation: Mechanics, Prediction, and Assessment, edited by: Chen, C. L., Proc. First Intern. Conf., San Francisco, USA, 7–9 August 1997, New York, ASCE, 747–756

Iverson, R. (1997): The physics of debris flow, Reviews of Geophysics, 35(3), 245–296

Johnson, J. (2003): Generation and propagation of infrasonic airwaves from volcanic explosions, Journal of Volcanology and Geothermal Research, 121,1–14

Le Pichon, A., Blanc, E. and Hauchecorne, A. (2010): Infrasound Monitoring for Atmospheric Studies, Springer

Marchi L., Arattano M. and Deganutti, A. (2002): Ten years of debris-flow monitoring in the Moscardo Torrent (Italian Alps), Geomorphology, 46(1-2), 1-17

Pilger, C. and Bittner, M. (2009): Infrasound from tropospheric sources: impact on mesopause temperature?, Journal of Atmospheric and Solar-Terrestrial Physics, 71(8-9), 816–822, doi:10.1016/j.jastp.2009.03.008

Schlunegger, F., Badoux, A., McArdell, B., Gwerder, C., Schnydrig, D., Rieke-Zapp, D. and Molnar, P (2009): Limits of sediment transfer in an alpine debris-flow catchment, Illgraben, Switzerland, Quaternary Science Reviews, 28, 1097-1105

Scott, E. and Lance, C. (2002): Infrasonic Monitoring of Avalanche Activity, in: Proceedings International Snow Science Workshop, Penticton, British Columbia

Scott, E., Hayward, C., Colgan, T., Hamann, J., Kubichek, R., Pierre, J. and Yount, J. (2006): Practical implementation of avalanche infrasound monitoring technology for operational utilization near Teton pass Wyoming, in: Proceedings International Snow Science Workshop

Stubbs, C. (2005): Tactical infrasound, Technical report, The MITRE Corporation, Department of the Army United States Army Intelligence and Security Command National Ground Intelligence Center, Charlottesville, Virginia

Suriñach, E., Vilajosana, I., Khazaradze, G., Biescas, B., Furdada, G. and Vilaplana, J. (2005): Seismic detection and characterization of landslides and other mass movements, Natural Hazards and Earth System Sciences, 5, 791–798

Sutherland, L. and Bass, H. (2004): Atmospheric absorption in the atmosphere up to 160 km, Acoustical Society of America, 3(115), 1012-1032

Takahashi, T. (2007): Debris Flow: Mechanics, Prediction and Counter measurements, Taylor and Francis Group, London, UK

Tipler, P. (1994): Physics for scientists and engineers, Worth Publishers Inc., New York, USA

Vilajosana, I., Suriñach, E., Khazaradze, G., and Gauer, P. (2007): Snow avalanche energy estimation from seismic signal analysis, Cold Regions Science and Technology, 50, 72–85

Vilajosana, I. (2008): Seismic detection and characterization of snow avalanches and other mass movements, PhD thesis, Universitat de Barcelona, Department de Geodinámica i Geofísica, Facultat de Geologia

Zhang, S., Hong, Y. and Yu, B. (2004): Detecting infrasound emission of debris flow for warning purposes, International Symposium Interpraevent VII, Riva, Trient, 359–364

Chapter 8

A study of infrasonic signals of debris flow

Kogelnig, A., Hübl, J., Suriñach, E., Vilajosana, I., Zhang, S., Yun, N. and McArdell, B.

Published in: Genevois, R., Hamilton, D. and Prestininzi, A. (Eds.), *Italian Journal of Engineering Geology and Environment - Book*, 563- 572, ISBN: 1825-6635; ISSN 978-88-95814-46-9 (2011)

Abstract

Mass movements such as debris flows, rock fall and snow avalanches are sources of sub-audible sounds in the low frequency infrasonic and seismic spectrum. Recent studies indicated that debris flow-generated signals are of significant amplitude and occupy a relatively noise free band in the low frequency acoustic spectrum. Infrasound signals have the ability to propagate kilometers from the source, thereby allow monitoring of mass movements from a remote location. This study presents debris flow monitoring at four international sites – Lattenbach, Tyrol (Austria), Illgraben, Valais (Switzerland), and the Midui and Guxiang Glacier, Tibet (China). The infrasound sensors used were the Chinese sensor MK 224 (DFW I-III) or the German sensor (Gefell WME 960 H). The results show that debris flows emit detectable low frequency infrasonic signals (1 Hz to 20 Hz) that are correlated to seismic signals. The infrasound sensors detect the phenomena before it reaches the sensors, depending on the landscape, distances and the sensitivity of the equipment. In the following pages the paper (Kogelnig et al., 2011), which presents a continuation of the study presented in Chapter 7, is fully reproduced in an easy reading format.

Introduction

Rapid mass movements (debris flows or snow avalanches) are periodic or episodic phenomena that present a hazard for people and property in inhabited alpine areas. Although efforts to develop debris flow monitoring or warning devices have increased in the last decades (Arattano, 1999; Itakura et al., 2005; Lahusen, 2005; Badoux et al., 2009) further research is needed and only few studies exist of infrasound monitoring of such events (Zhang et al., 2004; Chou et al., 2007; Hübl et al., 2008; Chapter 7). Infrasound signals (frequency range 0.01 Hz to 20 Hz) are longitudinal pressure waves that travel through the air at a speed of 343 m/s, which is the same as that of audible sound. Infrasound signals can propagate over long distances in the atmosphere with little attenuation. This is due to selective frequency absorption of sound waves in the atmosphere – higher frequencies (e.g. audible) are absorbed more readily than lower frequencies (e.g. infrasound) (Pilger and Bittner, 2009). For debris flow monitoring seismic waves as well as infrasound, both have benefits and drawbacks. The latter is mostly noise induced from wind or human activities that mask the debris flow signal. The benefits include no structural need for sustainability and monitoring from a remote location not affected by the process activity. The quality of monitoring results will depend on the relative positioning between the mass movement and the sensors as well as the specific characteristics of the site (e.g. topography).

The aim of this study is to present further results of infrasound monitoring of debris flows at four international sites and to illustrate the potential of infrasound monitoring of alpine mass movements. The study sites included the Lattenbach torrent (Tyrol, Austria), the Illgraben torrent (Valais, Switzerland), the Midui Glacier (Tibet, China) and the Guxiang Glacier (Tibet, China). The specific equipment, setup and sensor placement differed between sites. Where available, seismic signals and flow depth data were used for comparison, correlation and validation of the infrasound data.

Lattenbach (Austria)

A debris flow event was recorded on 01.09.2008 in the Lattenbach torrent (catchment area 5.3 km^2) (overview see Fig. 31). The event had a duration of 867 s (defined as time with flow depth >30 cm), a peak discharge of 380 m^3/s and a total volume of 14000 m^3 within this time. For further details of this event, the reader is referred to Chapter 7.

Data was collected using an infrasound microphone, a geophone and two ultrasonic gauges (with an inter-distance of 47.2 m). The infrasound sensor used at this site was the Gefell WME 960H, which has a frequency range from 0.5 Hz to 20 Hz and a sensitivity of 50 mV/Pa. The geophone sensor SM4 has a frequency range from 10 Hz to 180 Hz and a sensitivity of 28.8 V/m/s. The geophone was therefore not able to register those seismic signals with a frequency less than 10 Hz, resulting in missing data. The infrasound sensor was placed in the proximity of the upstream ultrasonic gauge and the geophone for better data comparison. Furthermore, this location has previously been shown to be optimal for both infrasonic and seismic monitoring as there is minimal background noise (Chapter 7). A Campbell Scientific CR1000 data-logger was used with a sampling rate of 100 Hz. The signals were analysed with Running Spectra (RS), which present the temporal evolution of the frequency content of a signal, using the Short Time Fourier transformation with a Hanning Window (length 128 samples) and an overlap of 50%.

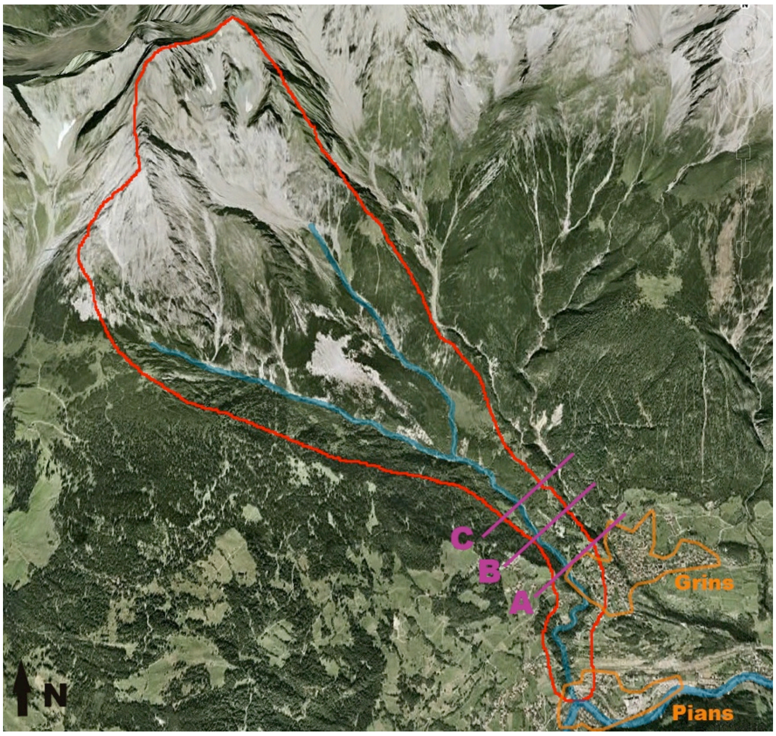

Figure 31: Overview of Lattenbach torrent - the catchment area and the affected villages of Grins and Pians are highlighted. The geophone detected the debris flow 300 m upstream (B) and the infrasound sensor 540 m upstream (C) of the actual sensor location (A) (Source: Google Earth).

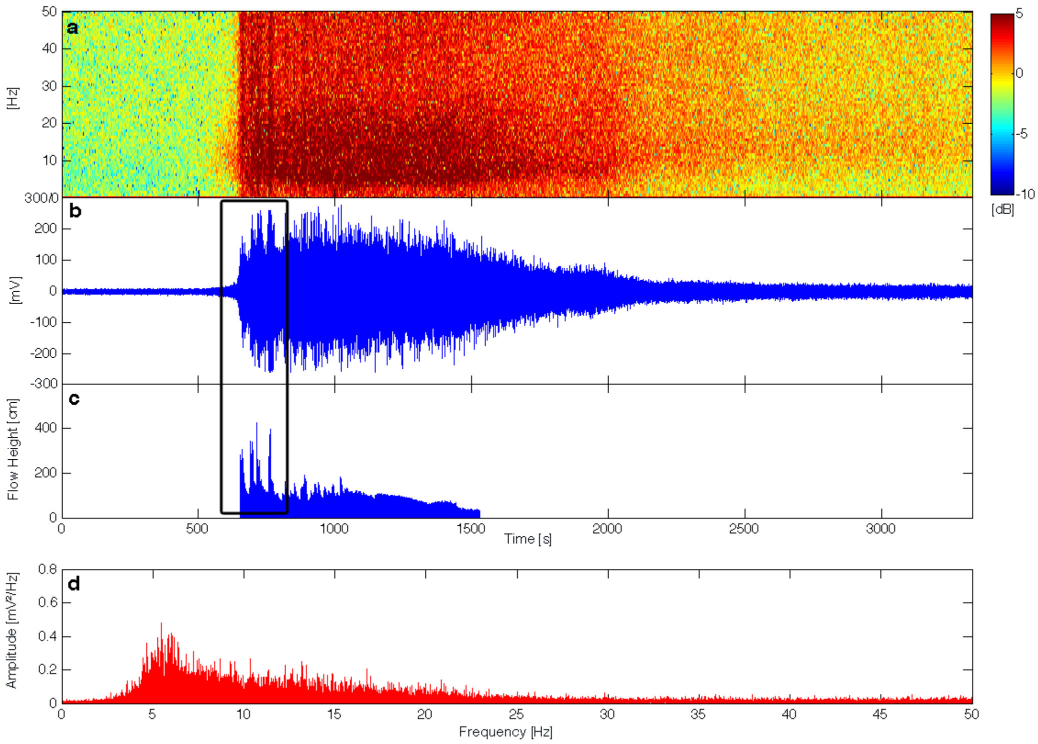

Figure 32: RS (a), time series (b), flow depth (c) and PS (d) of the infrasound signal during a debris flow on 01/09/08 in the Lattenbach torrent. Different debris flow surges are marked by the rectangle. The initiation time corresponds to Figure 33. Infrasound signal in mV, sensor sensitivity 50 mV/Pa.

Furthermore, an analysis with Power Spectra (PS) were used, which show the frequency content of a stationary signal. Debris flows are generally described as moving downhill in a series of waves or surges, whereby the flowing body has a steep front with higher material content and the flowing tail has a more gradual slope and higher water content (Iverson, 1997). These particular characteristics, which are common to all debris flows, can also be seen in the flow height data from the ultrasonic gauges as well as the seismic and infrasonic data from this event (Fig. 32 and 33, rectangles).

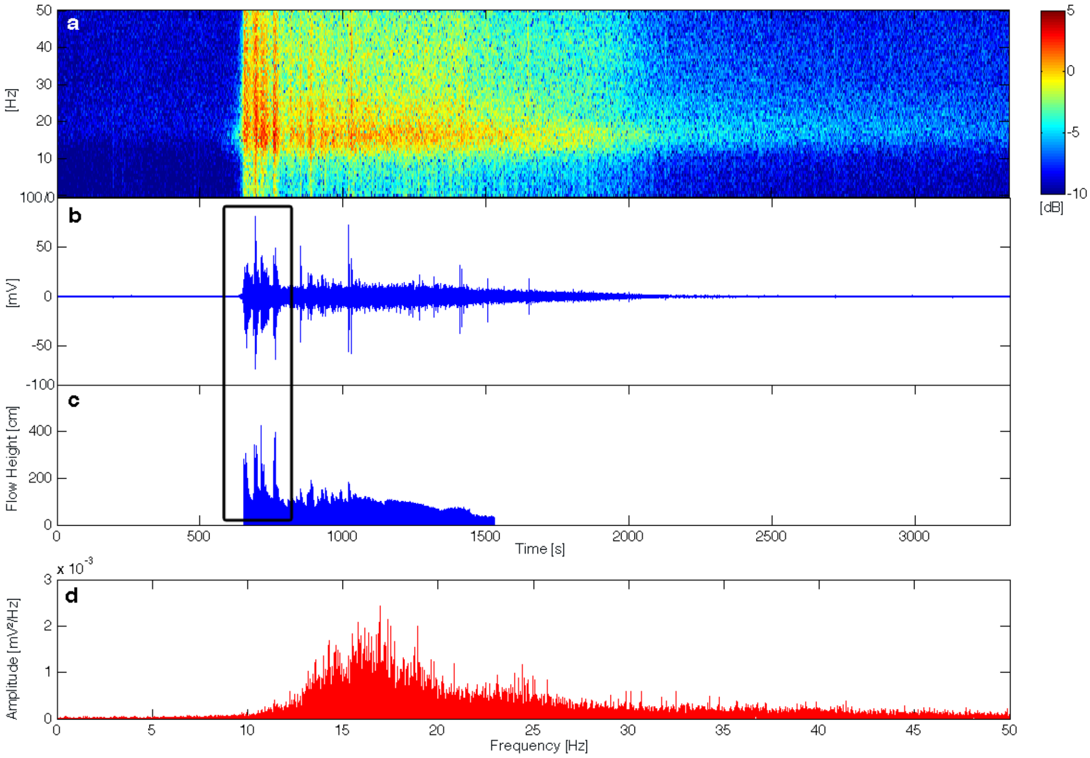

Figure 33: RS (a), time series (b), flow depth (c) and PS (d) of the seismic signal during a debris flow on 01/09/08 in the Lattenbach torrent. Different debris flow surges are marked by the rectangle. The initiation time corresponds to Figure 32. Geophone signal in mV, sensor sensitivity 28.8V/m/s.

Illgraben (Switzerland)

The Illgraben torrent is famous for its frequent sediment transport and debris flow activity. This may be accounted for by both its situation in an area of highly fractured bedrock (Badoux et al., 2009) and its size (9.5 km^2). In total there are 29 check dams located over the course of the torrent (Fig. 34). Check dam 1 has the greatest vertical height (48 m), whereas dams 2 to 29 have heights varying between 1 m and

7 m and several are either covered by sediment deposits or are destroyed. Two infrasound capacity microphones, developed by the Acoustics Institute at the Chinese Academy of Science (CAS), were placed 38 m apart in the proximity of check dam 27. These devices have a frequency range of 3 Hz to 200 Hz and a sensitivity of 50 mV/Pa. Unfortunately, this setup was not ideal as the distance between sensors was inadequate to show a difference in arrival time within the acoustic signals. Data will therefore be presented for the upstream microphone only.

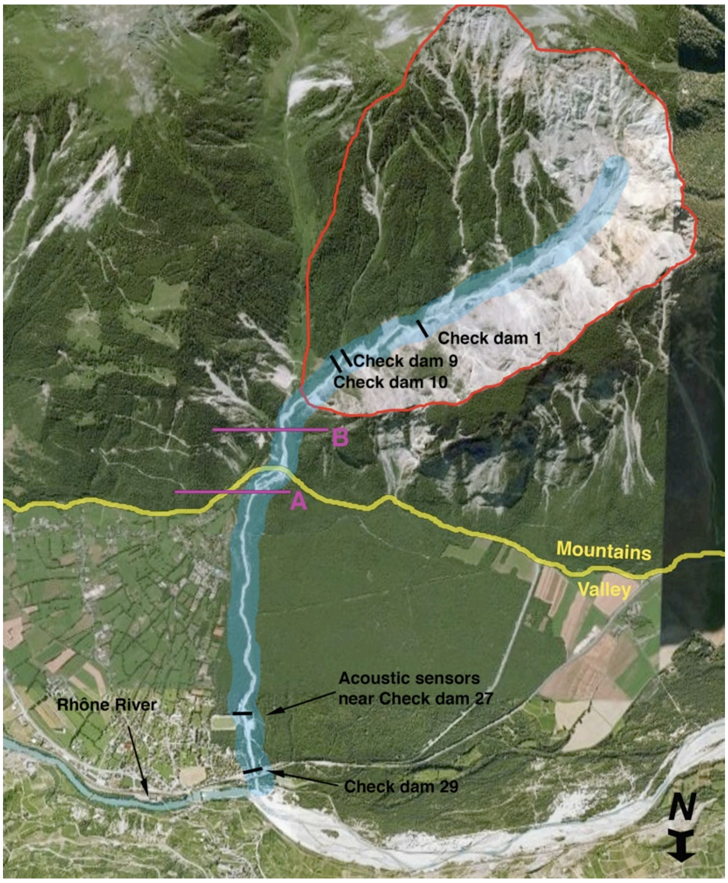

Figure 34: Overview of the Illgraben torrent - the catchment area and the boarder between mountains and Rhône valley are highlighted. The infrasound sensor detects the debris flow 1500m upstream (A) of check dam 27 and the seismic sensor 2000m upstream (B) (Source: Google Earth).

Additionally, a seismic velocimeter, model GS11, was placed near the upstream infrasound microphone. This device has a frequency range of 4.5 Hz to 100 Hz and a sensitivity of 90 V/m/s. Data from all three acoustic sensors were collected with a Campbell Scientific CR23 data-logger with a sampling rate of 100 Hz and were stored on an Xplore iX104 C3 tablet computer. Finally, ultrasonic gauges were placed at check dams 1, 10 and 27 to monitor flow depth (sampling rate 1 Hz). These gauges were operated by the Swiss Federal Institute for Forest, Snow and

Landscape Research (WSL). Data of the infrasonic and seismic background noise at the Illgraben torrent have been presented in Chapter 7; this site generates greater background noise compared to the Lattenbach torrent, but the amplitudes are nevertheless low relative to the debris flow signal. The torrential process discussed in this paper occurred on 28.07.2009. Unfortunately no video data is available of this event. Other measurements provided by the WSL like bulk density (around 1600kg/m^3) and flow depth from laser sensors (flow front was small and undular) point to a debris flood like event; the impulse frequency of the geophone (operated by WSL, mounted in the concrete of check dam 27) indicates only weak activity at the flow front which could indicate that there were not many boulders or just relatively small ones.

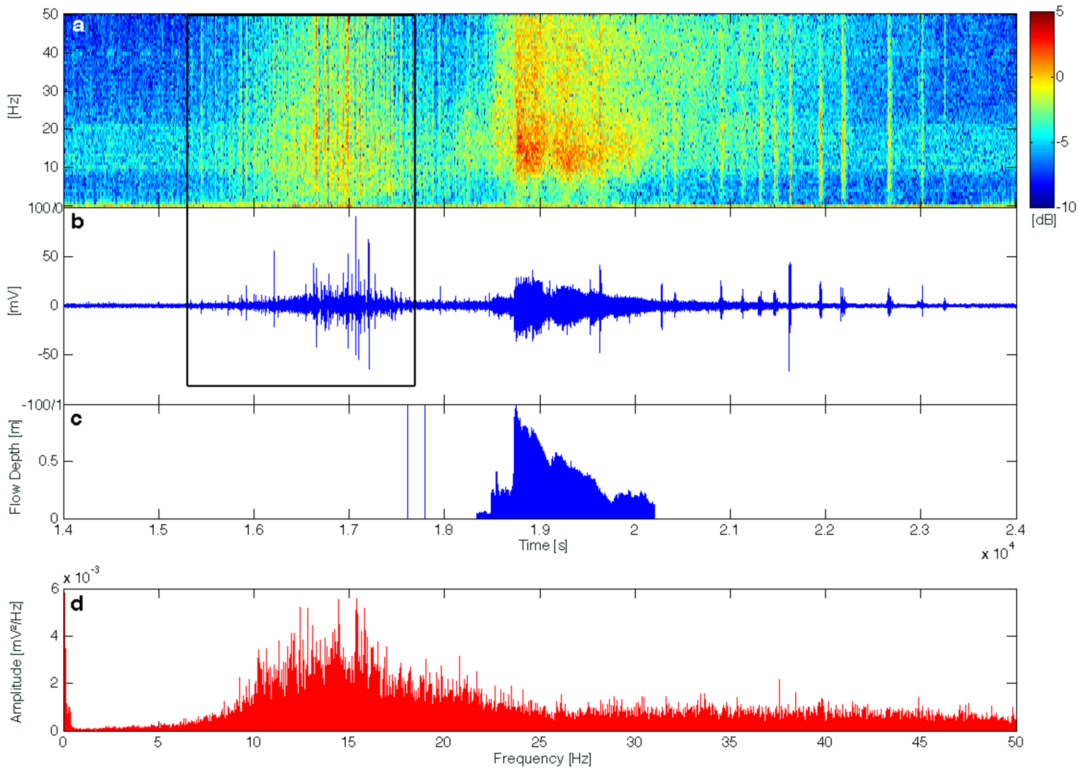

Figure 35: RS (a), time series (b), flow depth (c) and PS (d) of the infrasound signal during a debris flood on 28/07/09 in Illgraben torrent. In order to show only the debris flood frequency content a time window from 1.8-2.2x10^{4}s was chosen for the computation of the PS. Infrasound signal associated with a thunderstorm in the area are marked by the rectangle. The passing of the debris flood at check dam 1 and check dam 10 is marked by the vertical lines in the flow depth graph. Infrasound signal in mV, sensor sensitivity 50mV/Pa.

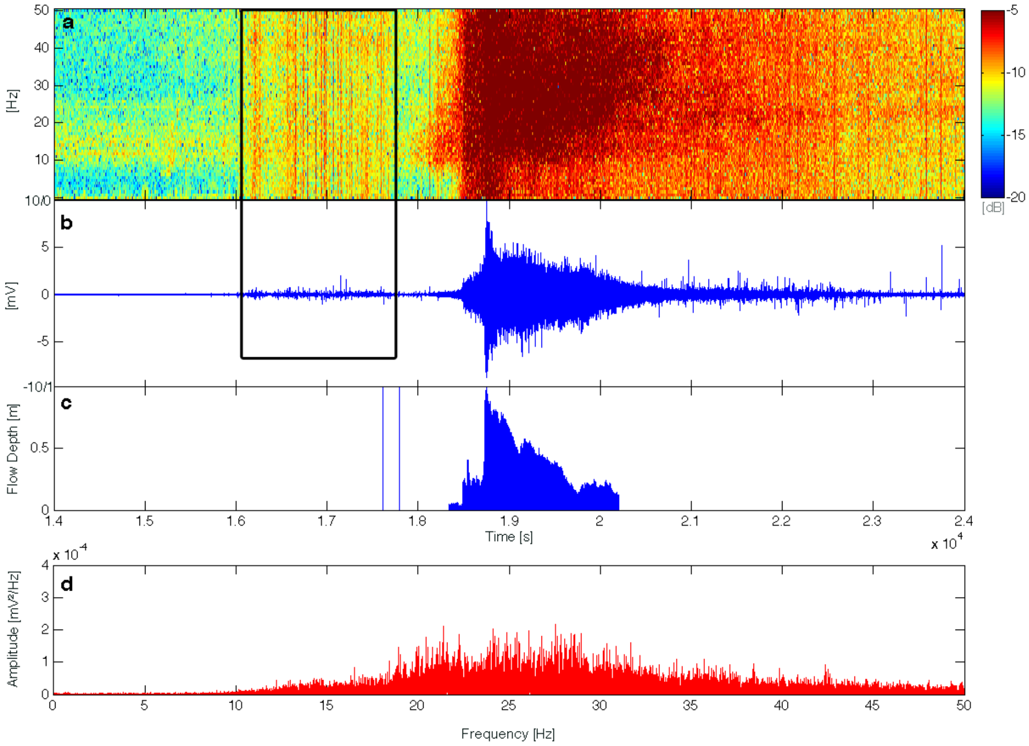

Figure 36: RS (a), time series (b), flow depth (c) and PS (d) of the seismic signal during a debris flood on 28/07/09 in the Illgraben torrent. In order to show only the debris flood frequency content a time window from 1.8-2.2x10^{4}s was chosen for the computation of the PS. Seismic signal associated with a thunderstorm in the area are marked by the rectangle. The passing of the debris flood at check dam 1 and check dam 10 is marked by the vertical lines in the flow depth graph. Geophone signal in mV, sensor sensitivity 90 V/m/s.

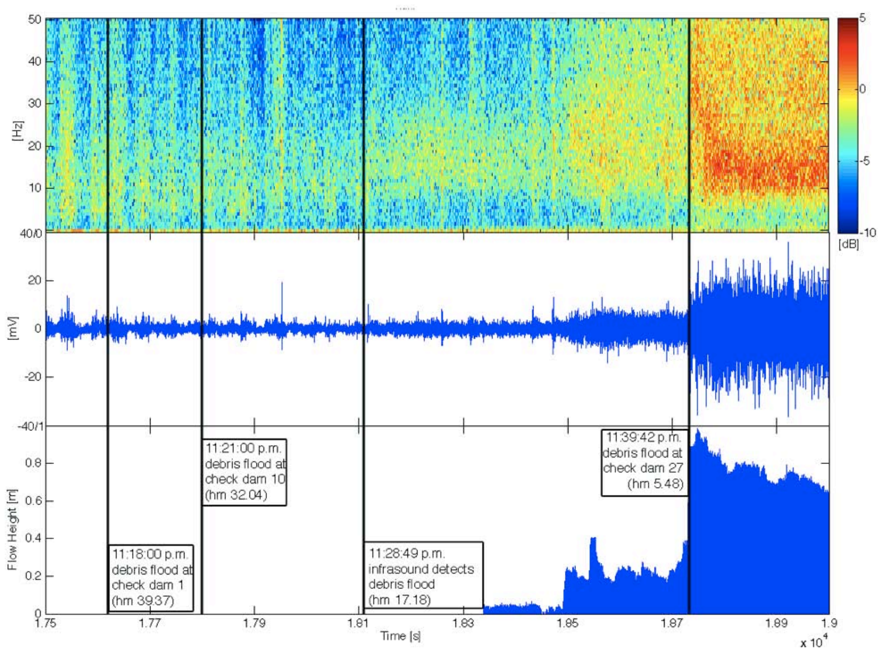

Figure 37: - Magnified section of Figure 35; the infrasound sensor detects the debris flood ca. 377s before it passes the sensor.

Without any visual information and given the evidence mentioned above it can be assumed that this event was a debris flood or an event that had a front like a debris flood and a body like a debris flow. Hence in this paper we will refer to this event as debris flood (according to the classification of Hungr et al., 2001).

The infrasound signal is shown in Figure 35 and the seismic signal in Figure 36. From the ultrasonic gauges it is known that the main surge of the debris flood passed check dam 1 at 11:18:00 pm (accuracy of +/-1 min due to installation issues), check dam 10 at 11:21:00 pm and check dam 27 at 11:39:42 pm. This corresponds to a flow duration of 1122 s between dams 10 and 27, and given that this is a known distance of 2656 m, the average flow velocity in this section can be calculated as 2.3 m/s.

The RS of the infrasound signal shows the arrival of the first debris flood signal at 11:28:49 pm (Fig. 37). There is also an observable increase in amplitude in the time series in this section. This occurs approximately 653 s before arrival at check dam 27. Assuming the above calculated average speed of 2.3 m/s, this time point corresponds to a distance of 1500 m, which happens to be the topographical transition between the mountains and valley near the Bhutan Bridge (Fig. 34, A). Previous work (Chapter 7) also reported that the infrasound microphone, when placed at check dam 27, detects the torrential processes at this location. Infrasound signals generated from debris flows are believed to be produced by the violent surge front and the collisions (or abrasion) between the flow and the channel loose boundary (Chou et al., 2007). Earlier studies (Zhang et al., 2004; Hübl et al., 2008) reported that viscous debris flows recorded in the Jiangjia Gully (China) have a frequency content of 6 Hz to 10 Hz. In contrast, Chou et al., 2007 monitored stony debris flows in Houyenchan (Taiwan) and reported frequencies between 5 Hz to 15 Hz and concluded that viscous flows emit lower frequencies than stony flows.

The PS of the infrasound signal (Fig. 35c) indicates that the main frequency content from this debris flood was between 10 Hz and 20 Hz. This differs from those results seen at the Lattenbach torrent (peak frequency ca. 6 Hz) and those reported In Chapter 7 for a previous event at the Illgraben (31.08.2008, peak frequencies from 3 Hz to 8 Hz). These results hint that debris floods produce higher peak frequencies (10 Hz to 20 Hz) than debris flows (< 10 Hz).

The RS of seismic data shows the arrival of the first debris flood signal at 11:25:13 pm (Fig. 38), which is 869 s before the debris flood passes check dam 27 and 216 s before the infrasound sensor detects the event. Applying the above distance calculation (i.e. assuming a constant flow velocity of 2.3 m/s) this corresponds to a distance of 2000 m (Fig. 34, B).

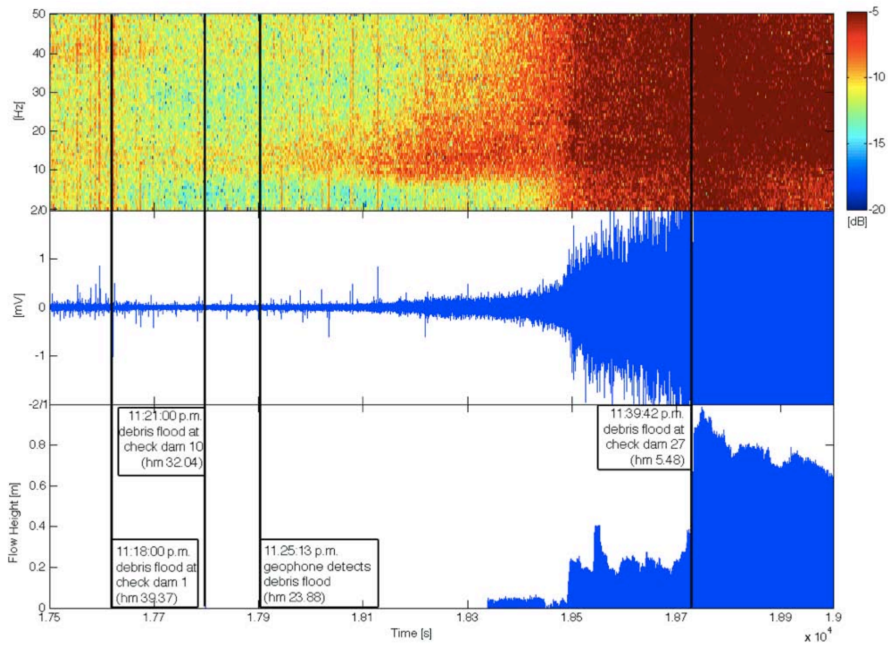

Figure 38: Magnified section of Figure 36; the geophone detects the debris flood ca 593s before it passes the sensor.

The peak frequency content in the seismic PS was 20 to 30 Hz (Fig. 36c), which, similar to the infrasound frequency content, was higher than that of the Lattenbach torrent (seismic range 10 Hz to 20 Hz).

Guxiang Glacier (China)

The Guxiang Glacier is well known for its frequent debris flow occurrences. The first sizeable event was in 1953 – the event had a peak discharge of 12600 m^3/s and a total volume of thirty million cubic meters. The flow structure was a mixture of fine sediment, stones and boulders. This event blocked the Podou Zhangpu River and formed the lake as it is now (Fig. 39). The catchment area is 24 km^2 and debris flows can be classified as viscous.

The infrasound monitoring unit DFW-I III (which includes a microphone and a data-logger) was installed at this site. The sampling rate of the unit is 100 Hz. The datalogger was developed in 2004 by the Institute of Mountain Hazards and Environment, the CAS and the Southwest Jiao Tong University. The microphone was created by the Acoustics Institute at the Chinese Academy of Science (CAS) and is a further development of the original device described in Zhang et al. (2004). It has a frequency range of 3 to 200 Hz and a sensitivity of 50 mV/Pa. For safety and convenience reasons, the equipment had to be placed in the cultural room office in the Guxiang village, approximately 5 km east of the debris flow channel (Fig. 39).

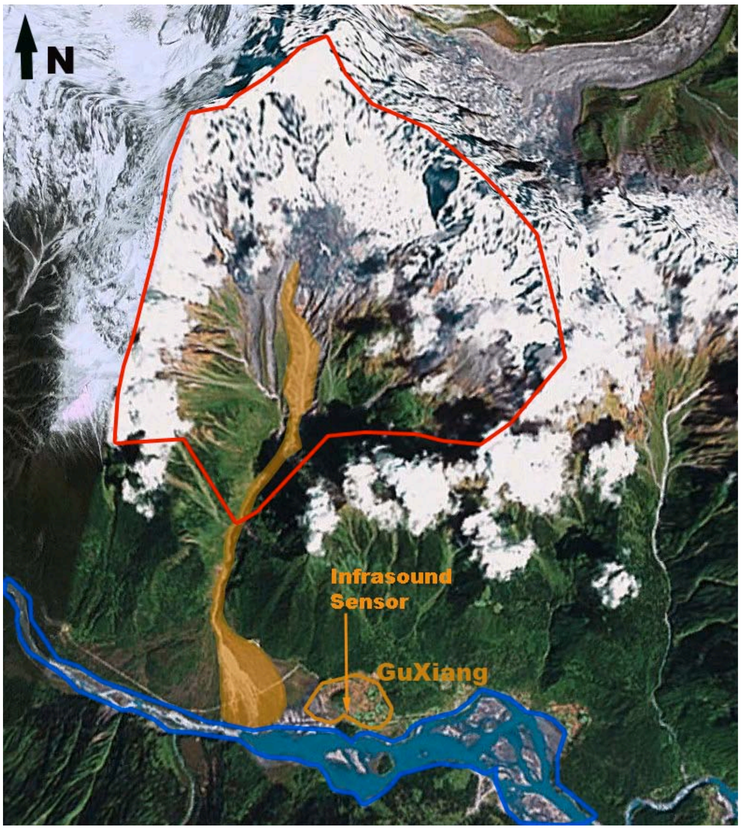

Figure 39: Overview of the Guxiang Glacier - catchment area, debris flow channel, Podou Zhangpu River and neighbouring town with sensor location indicated. Clearly observable is the lake formed by the event in 1953 (Source: Google Earth).

This setup location is less preferable compared to the European sites and resulted in lower data resolution due to both signal attenuation (an effect of distance source sensor and building interference) and increased background noise. The infrasound signal over 180 s is shown in Figure 40. Other measurements for comparison to this data were not available. Local witnesses provided anecdotal evidence of event time and date. The RS of the infrasound shows a constant signal in the frequency range from 5 to 10 Hz (Fig. 40), which is assumed to be associated with the debris flow.

This frequency range is also observable in the PS. These results correspond to the infrasonic data reported by Zhang et al. (2004) and Hübl et al. (2008) for viscous debris flows in the Jinagjia Gully (China). There is no observable increase in amplitude in the time series nor an increase in the frequency in the RS (Fig. 40), as was the case for the Lattenbach and Illgraben torrents. An increase in amplitudes and frequencies in the infrasonic signal is observed when a debris flow is moving toward the sensor, and the highest values are seen when the flow passes the sensor (Chapter 7).

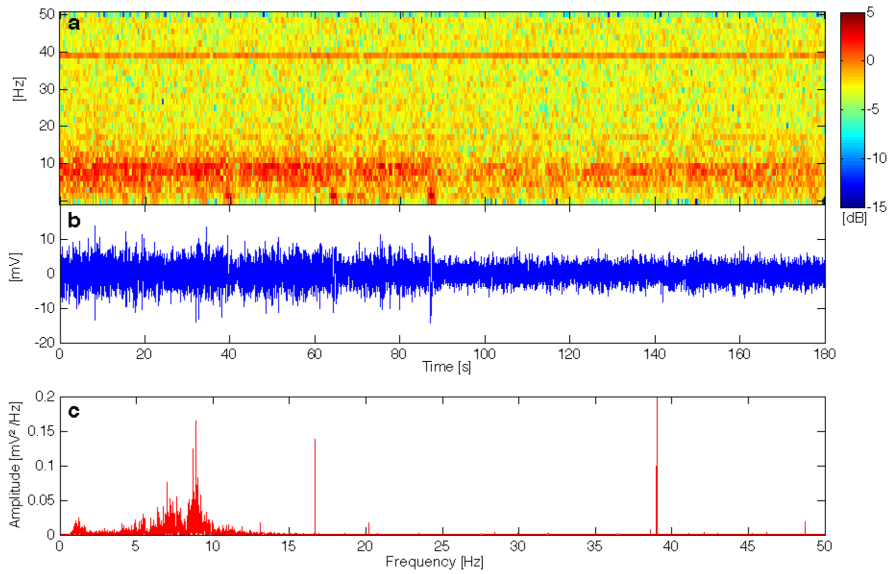

Figure 40: RS (a), time series (b) and PS (c) of the infrasound signal during a debris flow on 12/09/07 flow at Guxiang Glacier starting at 01:30:12am. Infrasound signal in mV, sensor sensitivity 50mV/Pa.

The absence of these increases may be due to the source-sensor distance. The placement indoors or the rheology of the flow could be further explanations for the constant signal amplitude. There are no expected differences due to the infrasound microphone, as this same device was used at the Illgraben torrent and only the data-logger differs.

Midui Glacier (China)

The Midui Glacier is one of the most famous glaciers in Tibet. It is situated east of the Guxiang Glacier, approximately 131 km upstream in the Podou Zhangpu River, and has a catchment area of 123,8 km^2. The channel has a N-S orientation and flows into the south bank of the Podou Zhangpu River (Fig. 41). The debris flows occurring here originate at the glacier. The first event occurred in 1988, resulting from a glacial lake outburst. The peak discharge was 1270 m^3/s. The river was blocked, the highway was destroyed and downstream villages and cities were flooded. Since 1988 several smaller viscous debris flows have occurred almost yearly, but they did not reach the monitoring point (Fig. 41, A).

As with the Guxiang Glacier, the infrasound monitoring unit DFW-I III was used (frequency range of 3 Hz to 200 Hz, sensitivity of 50 mV/Pa and sampling rate of 100 Hz).

Figure 41: Overview of the Midui Glacier - catchment area (red) debris flow channel and the Podou Zhangpu River. The distance between the infrasound sensor (A) and the area of debris flow origin (B) is 7.5km (Source: Google Earth).

For safety purposes, the equipment had to be placed in the local travel office, which is close to the debris flow channel. Figure 42 and 43 provide the infrasonic data recorded with the DFW-I III unit. As this device was developed for warning purposes, recording is initiated only if the amplitudes reach over a threshold value (3 mV). Figure 42 illustrates a 100 s window with recordings that are related to debris flow activity in the channel. Figure 43 provides a 17 s window that shows one debris flood surge (according to local witnesses). An increase in amplitude is observable in the time series as well as a change in the frequencies in the RS.

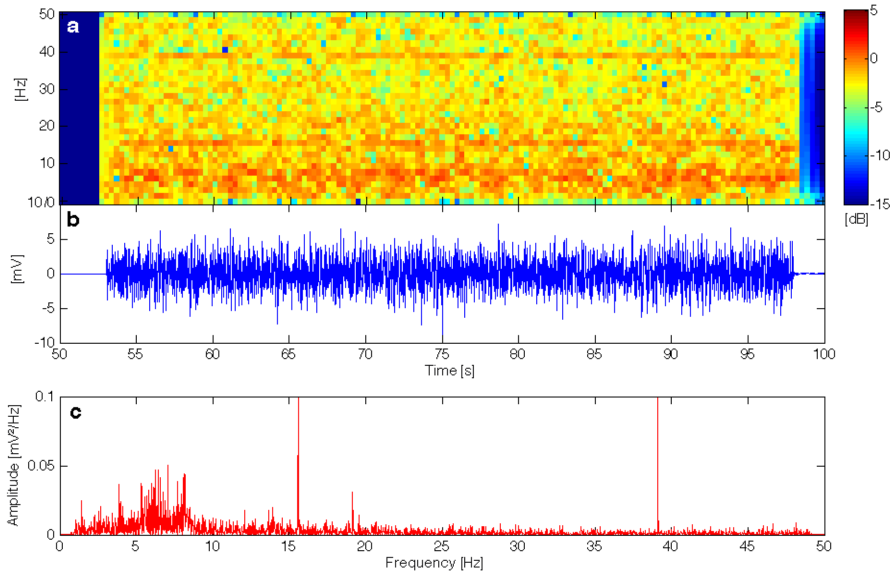

Figure 42: RS (a), time series (b) and PS (c) of the infrasound signal during a debris flow on 10/08/09 flow at Midui Glacier starting at 07:35:36am. Infrasound signal in mV, sensor sensitivity 50mV/Pa.

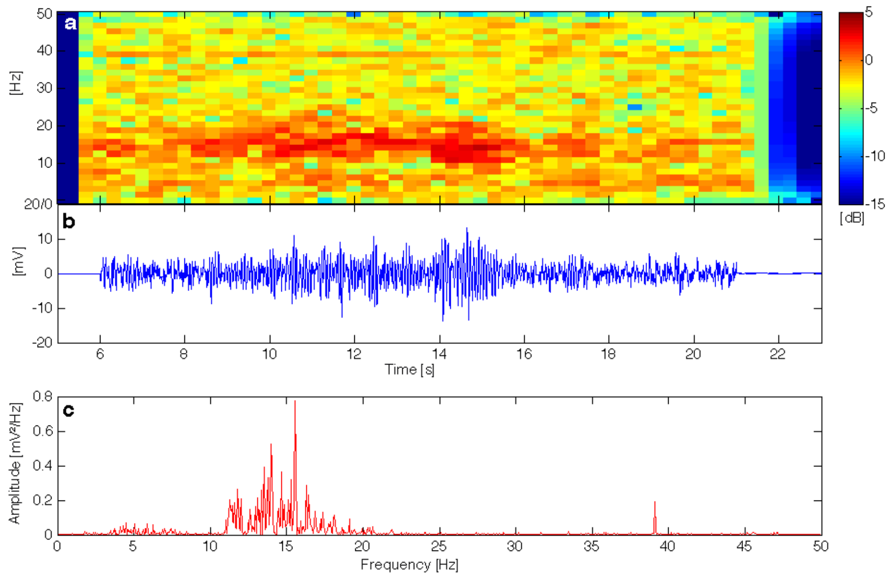

Figure 43: RS (a), time series (b) and PS (c) of the infrasound signal of a single surge during a debris flood on 05/09/08 at Midui Glacier starting at 09:07:38pm. Infrasound signal in mV, sensor sensitivity 50mV/Pa.

More interestingly, in the PS the main frequency content has shifted to 10 Hz to 20 Hz (similar to the Illgraben, Fig. 35) in comparison to the frequency shown in the larger time window (Fig. 42, 5 Hz to 10 Hz). No firm confirmation can be given due to a lack of supplementary data; it can only be assumed that the frequencies reflect a difference in flow characteristics (i.e. debris flood) of the single surge.

Conclusions

Infrasound monitoring of debris flows at different locations in Europe and China are presented in this study. The infrasound data could be correlated with seismic recordings and flow height measurements for the Lattenbach (Austria) and Illgraben (Switzerland) torrents. In all cases, the infrasound device was able to detect the event before passing the sensor location. At the Lattenbach torrent, the infrasound sensor detected the debris flow before the geophone (cut-off frequency 10 Hz), whereas the opposite was seen at the Illgraben torrent (geophone cut-off frequency 4.5 Hz). Further studies are required to clarify the relative detection capabilities of these sensors.

Data analysis for the two sites in China was more challenging and reference data were unavailable. Furthermore, the DFW-I III is a warning device that initiates recording only after the breach of a specific amplitude threshold and, as such, there is no knowledge of signal patterns below this threshold. For further studies at these two sites it is recommended to employ a seismic sensor in addition to the infrasound sensor, relocate the sensors to an outdoor location and implement a continuous recording scheme. These sites are promising and the warning device is nevertheless a powerful tool for debris flow alarming systems.

The preliminary results indicate that a combination of infrasound and seismic sensors and an analysis of the frequency evolution of the signal (RS) are the most promising for monitoring torrential hazards. Moreover, interfering noise in the signal arising from a local thunderstorm are presented in the Illgraben data. Variations in predominant infrasound and seismic frequencies of over 15 Hz were seen between study locations. It can be concluded that debris flows emit infrasound signals with a lower frequency spectrum (<10 Hz) than debris floods (>10 Hz), and that the frequency range is dependent on study site characteristics, sensor location and process characteristics.

References

Arattano, M. (1999): On the use of seismic detectors as monitoring and warning systems for debris flows, Natural Hazards and Earth System Sciences, 20,197–213

Badoux, A., Graf, C., Rhyner, J., Kuntner, R. and McArdell, B. (2009): A debris-flow alarm system for the alpine Illgraben catchment: design and performance, Natural Hazards and Earth System Sciences, 49, 517–539

Chou, H., Cheung, Y. and Zhang, S. (2007): Calibration of infrasound monitoring system and acoustic characteristics of debris-flow movement by field studies, in: Chenglung, C., Major, J. (eds.) Debris-flow Hazards Mitigation: Mechanics, Prediction, and Assessment, Millpress, Rotterdam, 571–580

Hübl, J., Zhang, S. and Kogelnig, A. (2008): Infrasound measurements of debris flow*,* In: De Wrachien, D., Brebbia, C.A., Lenzi, M.A. (Eds.), WIT Transactions on Engineering Sciences, 60, Second International Conference on Monitoring, Simulation, Prevention and Remediation of Dense and Debris Flows II*, 17.-19*. Juni 2008, The New Forest, 3-12; ISSN 1743-3533

Hungr, O., Evans, S., Bovis, M. and Hutchinson, J. (2001): A review of the classification of landslides of the flow type, Environmental and Engineering Geoscience, 7(3), 221–238, doi:10.2113/gseegeosci.7.3.22

Itakura, Y., Inaba, H. and Sawada T. (2005): A debris flow monitoring devices and methods bibliography, Natural Hazards and Earth System Sciences, 5, 971-977

Iverson, R. (1997): The physics of debris flow, Reviews of Geophysics, 35(3), 245–296

Kogelnig, A., Hübl, J., Suriñach, E., Vilajosana, I. and McArdell, B. (online first): Infrasound produced by debris flow: propagation and frequency content evolution, Natural Hazards, doi:10.1007/s11069-011-9741-8

Kogelnig, A., Hübl, J., Suriñach, E., Vilajosana, I., Zhang, S., Yun, N. and McArdell, B. (2011): A study of infrasonic signals of debris flows, in: Genevois, R., Hamilton, D. and Prestininzi, A. (Eds.), Italian Journal of Engineering Geology and Environment - Book, 563- 572, ISBN: 1825-6635; ISSN 978-88-95814-46-9

Lahusen, R. (2005): Debris-flow instrumentation, In: Jakob M. & Hungr O. (eds.), Debris-flow Hazards and Related Phenomena, 291-325, Springer Verlag Berlin, Germany in association with Praxis Publishing Ltd, Chichester, UK

Pilger, C. and Bittner, M. (2009): Infrasound from tropospheric sources: impact on mesopause temperature?, Journal of Atmospheric and Solar-Terrestrial Physics, 71(8-9), 816–822, doi:10.1016/j.jastp.2009.03.008

Zhang, S., Hong, Y. and Yu, B. (2004): Detecting infrasound emission of debris flow for warning purposes, International Symposium Interpraevent VII, Riva, Trient, 359–364

Chapter 9

On the complementariness of infrasound and seismic sensors for monitoring snow avalanches

Kogelnig, A., Suriñach, E., Vilajosana, I., Hübl, J., Sovilla, B., Hiller, M. and Dufour, F.

Published in: *Natural Hazards and Earth System Sciences*, 11(8), 2355-2370 (2011)

Abstract

This chapter analyses and compares infrasonic and seismic data from snow avalanches monitored at the Vallée de la Sionne test site in Switzerland from 2009 to 2010. Using a combination of seismic and infrasound sensors, it is possible not only to detect a snow avalanche but also to distinguish between the different flow regimes and to analyze duration, average speed (for sections of the avalanche path) and avalanche size. Different sensitiveness of the seismic and infrasound sensors to the avalanche regimes is shown. Furthermore, the high amplitudes observed in the infrasound signal for one avalanche were modeled assuming that the suspension layer of the avalanche acts as a moving turbulent sound source. Our results show reproducibility for similar avalanches on the same avalanche path. In the following pages the paper Kogelnig et al. (2011) is fully reproduced in an easy reading format.

Introduction

A number of studies have shown that snow avalanches generate seismic (e.g., Saint-Lawrence and Williams, 1976; Salway et al., 1978; Firstov et al., 1992; Sabot et al. 1998; Suriñach et al., 2000) and acoustic signals in the low frequency spectrum (Bedard, 1989; Firstov et al., 1992; Scott et al. 2004). Seismic signals of snow avalanches have been studied since the 1970s, focusing on monitoring (Saint-Lawrence and Williams, 1976; Salway, 1978; Suriñach et al., 2000) and warning systems (Leprettre et al., 1996; Bessason et al., 2007), investigation of their time and frequency evolution (Sabot et al., 1998; Suriñach et al., 2000; Suriñach et al., 2001; Biescas et al., 2003), and on the determination of avalanche speed and seismic energy estimation (Vilajosana et al., 2007a,b). Suriñach et al. (2000, 2001) studied the seismic signals produced by avalanches and found different signal behaviour for distinct types of avalanches. Research on the infrasound generated by snow avalanches has increased in the last two decades (e.g., Bedard 1989; Adam et al., 1997; Comey and Mendenhall, 2004; Scott et al., 2007) with a focus mainly on detection purposes.

Firstov et al. (1992) were one of the first researchers to study the acoustic and seismic emissions generated by snow avalanches. These authors concluded that the seismic signals recorded were generated mainly by the dense flow part of the avalanche, whereas the acoustic signals were generated principally by the turbulent snow-air flow (powder cloud). Recent studies using infrasound and seismic sensors for monitoring snow avalanches and debris flows (Suriñach et al., 2009; Chapter 7) have shown that infrasound and seismic signals can be correlated with each other and also with data from other measurements (e.g. flow depth for debris flows). However, an in-depth, study combining the infrasound and seismic wave fields generated by snow avalanches has not been carried out to date.

The aim of this study is to evaluate the potential of the combination of infrasound and seismic sensors for monitoring snow avalanches. We present an analysis of seismic and infrasound signals generated by four snow avalanches monitored at the Swiss Vallée de la Sionne (VDLS) test site (Sovilla et. al., 2008b; Kern et al., 2009; Barbolini and Issler, 2006). Mixed avalanches that often generate a well-developed powder-snow part are typical for the site. Note that these avalanches rarely flow in a pure wet- or dry-flow regime. In most cases both regimes are present. Typically, a plug flow core may be surrounded by diluted flow, particularly if the avalanche is released from altitudes where the snow is still dry. Thereafter, the snow in the path becomes wet at lower altitudes (Sovilla et al., 2010a).

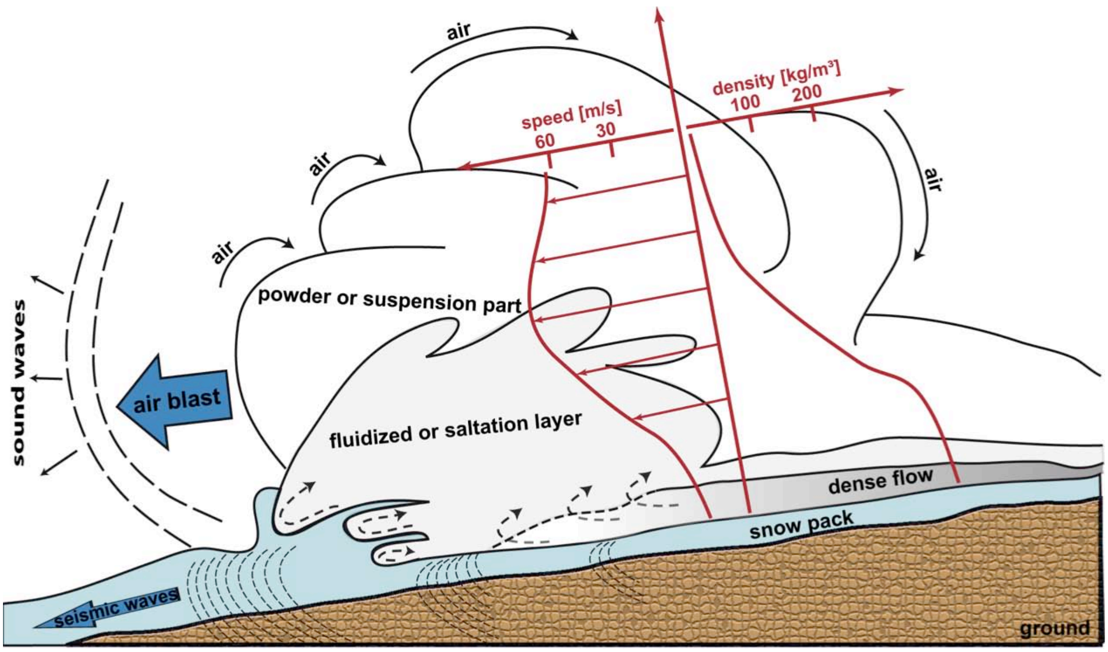

Figure 44: Cross section of a mixed avalanche, indicating the different parts (Modified after McClung and Schaerer (2006) and Gauer et al. (2008)). The sources of seismic and acoustic emissions are also indicated.

Mixed avalanches can be described as a three-layered structure (Fig. 44). Impact pressure measurements in VDLS show that the layer at the avalanche bottom is frequently dense and characterized by a continuous flow medium (Sovilla et al., 2008a). As we move higher up into the avalanche core, avalanche speed increases and particles at the surface of the dense flow are lifted due to the shear stress produced by the interaction with the air forming a saltation layer. Stresses are primarily transmitted by particle collisions and particle inertia. If the snow is dry and the avalanche speed is sufficiently high, a snow cloud of low density, the suspension layer, covers the exterior of the avalanche core (McClung and Schaerer, 2006). Small particles are suspended by turbulent eddies of air generated by the friction of the flowing snow interacting with the ambient air. This suspension layer behaves like a turbulent flow of a Newtonian fluid (Gauer et al., 2008).

In the following sections we present a description of the Vallée de La Sionne test site together with an overview of the measurement setup and the data analyzing methods. Section “Seismic and Infrasonic data” is devoted to the analysis of the measurements of four avalanches of different types and sizes released naturally at the VDLS during the winter seasons 08/09 to 10/11. We refer to these avalanches as avalanches 1 to 4. Their SLF archive numbers are listed in brackets to allow cross-reference with other publications. In the following section the sources of the infrasound and seismic signals generated by the snow avalanches are discussed, and the last section contains the conclusions of this study.

Test Site, Instrumentation and Data Treatment

Test site and instrumentation

The Vallée de La Sionne (VDLS) avalanche dynamic test site is located in central Valais (Switzerland) above the city of Sion and is operated by the WSL Swiss Federal Institute for Snow and Avalanche Research, SLF (Fig. 45). The different release areas cover about 30 ha with a slope varying between 32° to 45°. They are exposed to westerly and north-westerly winds.

At the site, avalanche dynamic measurements are routinely performed. In the runout zone, located at 1600 m a.s.l., a 20 m high pylon is instrumented with speed, pressure and flow-height sensors. Velocity, pressure and flow depth measurements performed at the pylon are used in this paper to facilitate the interpretation of the seismic and acoustic measurements. A detailed explanation of the velocity and pressure measurements is given in Kern et al. (2009) and Sovilla et al. (2008b), respectively. In a shelter opposite the avalanche slope, a pulsed Doppler radar (PDR) operated by the Federal Research and Training Centre for Forests, Natural Hazards and Landscape (BFW) measures avalanche velocities. The PDR data were used to obtain the speed profile of one avalanche. A detailed explanation of the radar system is given in Rammer et al. (2007). The measurement system is started automatically by seismic triggering whenever natural avalanches are released within the avalanche path.

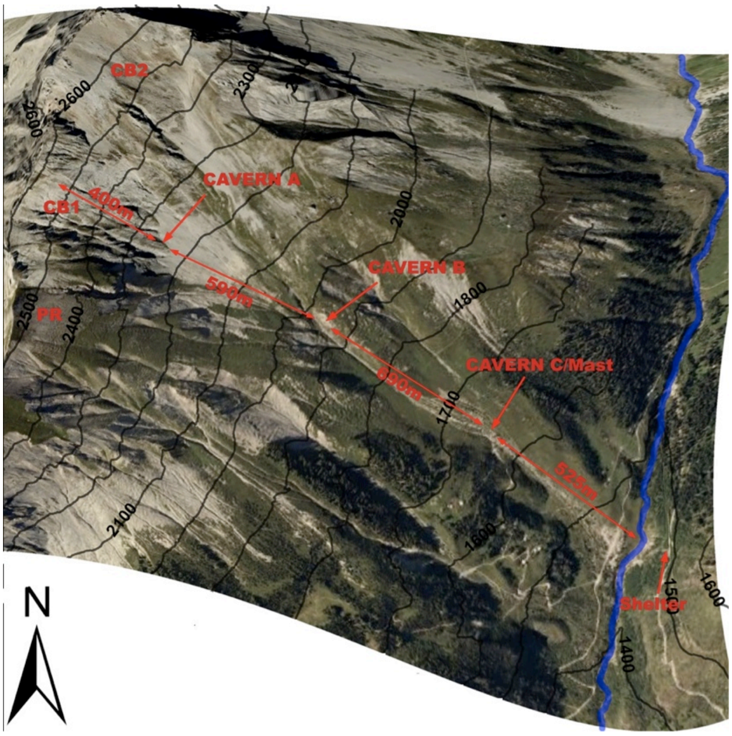

Figure 45: Overview of the VDLS test site. Caverns A, B and C are marked. The 20 m instrumented pylon is located near cavern C. PDR and the VDLS data acquisition systems are located in a shelter opposite the slope. Release areas are indicated as Pra Roua (PR), Crêta-Besse (CB1) and Crêta -Besse 2 (CB2). The La Sionne river is shown in blue (source: Google Earth).

The site has been equipped for several years with instruments to analyze the seismic signals generated by avalanches (Sabot et al., 1998; Suriñach, 2004). Infrasound (IS) sensors were first installed in 2008, close to the seismic sensor near the shelter. The infrasound sensors were attached to a star aligned porous garden hose setup to dampen wind noise. Figure 45 shows the location of the caverns along the avalanche path and the shelter on the counter slope where sensors are installed. The setup of the sensors and type of equipment varied over the years (Table 3). All data were continuously recorded during all the winter season with a sample rate of 100 Hz with a Reftek DAS130 data logger and common base of time.

Table 3: Overview of the setup of the seismometers and infrasound (IS) sensors used in this study. The position of caverns and shelter is shown in Figure 45.

	Cavern A	Cavern B	Cavern C	Shelter	
Aval. 1 **2009/2010**	SEISMOMETER Syscom MR 2002 1 Hz nat. freq. Sensit. 277V/m/s	SEISMOMETER Mark L4-3D 1 Hz nat. freq. Sensit. 277 V/m/s		SEISMOMETER Mark L4-3D 1 Hz nat. freq. Sensit. 277 V/m/s	IS-SENSOR Chaparral Model 24 0.1 Hz nat. freq. Sensit. 2V/Pa
Aval. 2 **2009/2010**		SEISMOMETER Mark L4-3D 1 Hz nat. freq. Sensit. 277 V/m/s		SEISMOMETER Mark L4-3D 1 Hz nat. freq. Sensit. 277 V/m/s	IS-SENSOR Chaparral Model 24 0.1 Hz nat. freq. Sensit. 2V/Pa
Aval. 3 **2008/2009**			SEISMOMETER Mark L4-3D 1 Hz nat. freq. Sensit. 277 V/m/s	SEISMOMETER Mark L4-3D 1 Hz nat. freq. Sensit. 277 V/m/s	IS-SENSOR Gefell WME 960H 0.5 Hz nat. freq. Sensit. 50mV/Pa
Aval 4 **2010/2011**		SEISMOMETER Mark L4-3D 1 Hz nat. freq. Sensit. 277 V/m/s	SEISMOMETER Mark L4-3D 1 Hz nat. freq. Sensit. 277 V/m/s	SEISMOMETER Mark L4-3D 1 Hz nat. freq. Sensit. 277 V/m/s	IS-SENSOR Chaparral Model 24 0.1 Hz nat. freq. Sensit. 2V/Pa

Data treatment

The methods used for data treatment in this study have been presented in previous publications (Suriñach et al., 2001, 2005; Vilajosana et al., 2007a). In line with their results, we have processed the data as following. First, the raw signals were converted into physical parameters, velocity of the ground (m/s) for seismic signals and air pressure (Pa) for infrasound signals. The signals were filtered (1 Hz to 40 Hz) with a 4th order Butterworth band-pass filter to homogenize the data. Furthermore, data were analysed using detailed time series analysis. The different wave packets in the time series allow us to determine the different sections. Total spectra using FFT (Fast Fourier Transformation) were used to analyze frequency content of these different sections. In addition, we used spectrograms for the analysis of the frequency content evolution in time because it facilitates the determination of wave time arrivals (Vilajosana et al, 2007a).

For the data interpretation we benefitted from the work of Biescas et al. (2003) and Suriñach et al. (2005) that associated an increase in the amplitudes in the time series with the avalanche approaching the sensor. This is also reflected in an increase of the presence of higher frequencies in time giving a triangular shape in the spectrograms. These features are due to the wave attenuation phenomenon (Stein and Wylesession, 2003; Suriñach et al., 2005). Seismic waves are attenuated due to geometrical spreading and anelastic attenuation in the ground. These effects are strongly dependent on the distance between source and receiver. In contrast to seismic signals, attenuation of infrasound signals at local distances (<5 km) is negligible (Chapter 8 and references therein).

Seismic And Infrasonic Data

Avalanche 1 (SLF #20100003)

Avalanche description

Avalanche 1 occurred naturally on 30 December 2009 at 13:30. Owing to bad visibility during and after the release, it was not possible to establish the exact position and extension of the release area. Photographs taken after the event showing part of the avalanche path and deposition extent, support the idea that the avalanche descended both right and left channels, and thus presumably released from Crêta-Besse 1 and at least part of Crêta-Besse 2 (Fig. 45 and 46).

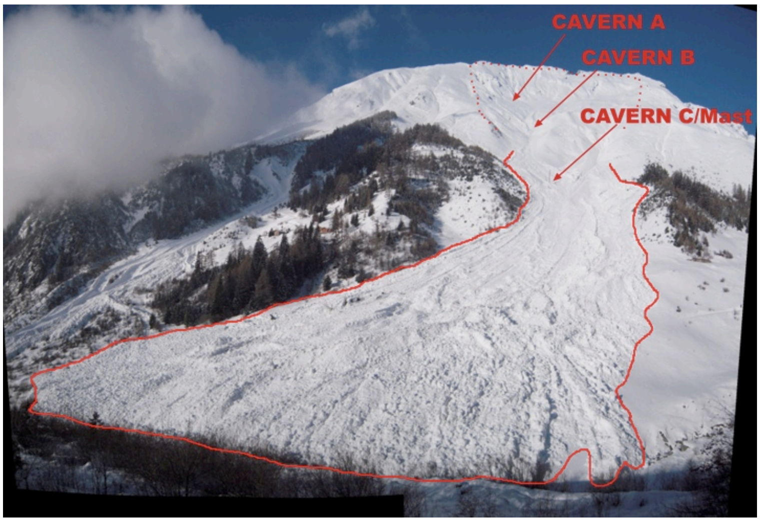

Figure 46: Avalanche 1 occurred on 30 December 2009 at 13:30. The avalanche path and deposition zone is indicated (solid red line). View is from the shelter. The photo was taken a few days later (photo source: F. Dufour).

The avalanche triggered the automatic data recording system located in cavern A, reached the instrumented pylon where internal velocities, flow depths and impact pressures were measured (Fig. 47), and stopped in the river bed in the valley bottom. The PDR, situated in the shelter, which was switched on by the automatic detection system located in cavern A, recorded the overall avalanche velocity from this cavern to the end of the path (Fig. 48).

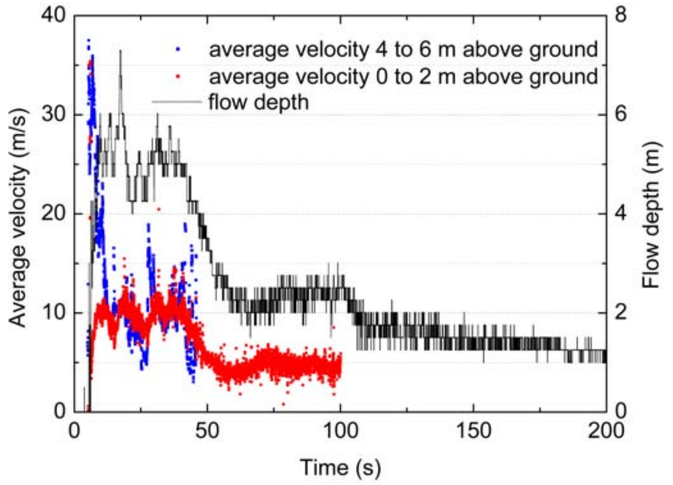

Figure 47: Flow depth and average velocities measured at the pylon, close to cavern C. The avalanche was characterized by a fast diluted front moving at 35m/s (blue dots) and a slow large dense core moving at about 10m/s (red dots). Undulations in velocity and flow depth indicate that the flow was characterized by successive surges. This large avalanche had maximum flow depths up to 6m to 7m at the pylon.

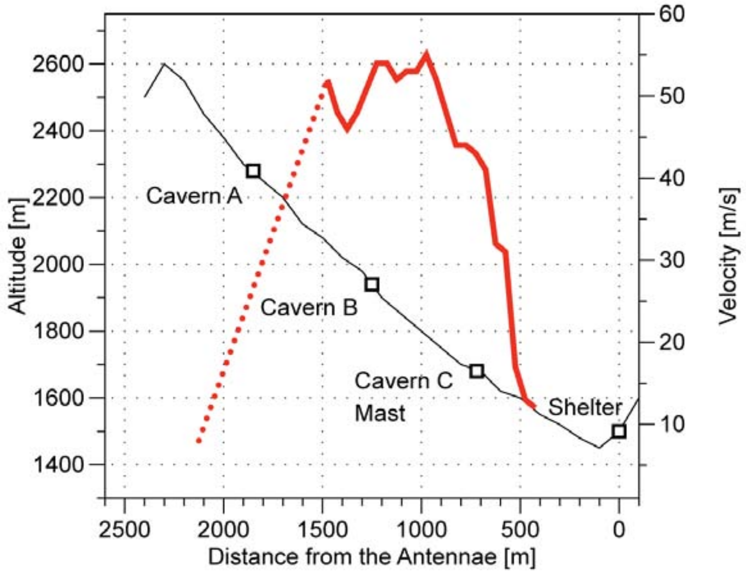

Figure 48: Avalanche front velocity measured with the PDR for Avalanche 1 (solid red line). Velocity was assumed to grow linearly in time (dotted red line) above Cavern B in the absence of data.

The avalanche was detected in the sensors placed in caverns A, B and in the shelter (Table 3). At the time of release, the weather station Donin du Jour (2390 m) reported ca. 0.20 m of new snow in the preceding 24h on a snow cover of 1.80 m, a snow temperature of –5°C at a snow height of 1.0 m and an air temperature of -

1.5°C. Air temperature in the release zone was -4°C according to the weather station at Crêta-Besse (2696 m). This would indicate that, at lower altitude, close to the deposition zone, the snow precipitation could have evolved into rain. According to measurements performed at the pylon, in the runout zone the avalanche was characterized by two main flow regimes (Fig. 47). The avalanche had a short, diluted front moving at about 35 m/s preceding a very large wet-dense flow, characterized by maximum flow depth in the order of 6-7 m, and velocity in the order of 10 m/s. Previous studies showed that the coexistence of the two regimes indicates that the avalanche had a large powder component in the first part of the path but evolved into a high-density flow as the avalanche entrained wet snow at lower altitudes (Sovilla et al., 2008a). The dense flow was characterized by surges recognizable in Figure 47 as variations of flow depth and velocity.

Punctual measurements at the pylon are in agreement with the PDR measurements performed from the shelter. The avalanche reached maximum velocities of up to 55 m/s in the area of cavern B, indicating the presence of a powder component. At the start of the runout zone, it decelerated suddenly to velocities typical of a slow dense flow. In the absence of PDR data in the area around cavern A, given the configuration of the triggering system, we assume that the avalanche, in this part of the path, had a constant acceleration and thus, the velocity grew linearly in time as shown in Figure 48. Note that this figure reports only the values for the avalanche front velocity. However, a detailed inspection of the PDR measurements of the entire avalanche path shows that this avalanche had a large turbulent component, which lasted for more than 50 s (Rammer, personal communication).

The deposition morphology was characterized by the typical patterns of a large wet-dense flow. The presence of numerous levees and complex structures suggests that the deposition was probably built up in several stages (Fig. 46). The earlier deposits were successively overrun by subsequent parts of the flow, as has been evidenced in other avalanches at this site (Sovilla et al., 2010b). In a first approximation, we estimate the avalanche to have a classification size of 5 (mass of the order of 10^5 t and path length 2000 m, Canadian snow avalanche size classification, McClung and Schaerer, (1980)).

Seismic and infrasonic data description

Figure 49 shows the seismic (N-S component) and infrasound signals measured during the avalanche. In the time interval [500 s to 620 s], the seismic signals of caverns A and B present numerous energy peaks (10^{-3} m/s), which are related to impacts produced by the avalanche flowing over the caverns (Figs. 49a, b). A detailed inspection of this time interval allowed us to determine the time at which the avalanche reached caverns A and B (534 s and 548 s, respectively) (Figs. 49a, b). Accordingly, the avalanche front covered the distance between caverns A and B, 590 m, in 14 s, yielding an average speed of the avalanche front of approximately 42 m/s. This value is consistent with the values obtained from the PDR, which shows velocities between 45 m/s to 48 m/s for this section (Fig. 48) and is also consistent with the maximum punctual velocity measured at the pylon, of 35 m/s (Fig. 47).

The average amplitudes recorded in cavern B are higher than those recorded in cavern A. The amplitudes of the seismic signals obtained in the shelter over the same time interval [500 s to 620 s] (Fig. 49d) are two orders of magnitude smaller and have a different shape (Fig. 49f). At the shelter, the amplitudes increase with time, yielding a maximum at a later interval [630 s to 740 s]. The increase in amplitudes in a triangular shape (Fig. 49d) indicates that the avalanche approached the sensor in the shelter.

Interestingly, infrasound sensors near the shelter detected the avalanche 25 s before it reached cavern A (Fig. 49a). In the time interval [500 s to 620 s], high amplitudes up to 5 Pa with a spindle shape were detected in the infrasound sensor (Fig. 49c). In this time interval, the avalanche flowed over caverns A and B and the signal amplitudes were the smallest in the seismic sensor near the shelter.

To interpret the infrasound signals in the time window [500 s to 620 s], we compared the time series from the infrasound and the seismic sensor located near the shelter (Figs. 49e, f, respectively). Figure 50 presents the total spectra of the seismic and infrasound signals. The maximum energy is centered at 1 Hz to 3 Hz in the infrasound signal, whereas it is shifted to 6 Hz to 8 Hz in the seismic signal. However, seismic data also have energy in the range of 1 Hz to 3 Hz as indicated in Figure 50c. After filtering the seismic signal between 1 Hz to 3 Hz, the time series shows in this interval a spindle shape, similar to that of the infrasound signal, with maximum amplitudes of the order of $3x10^{-7}$ m/s (Fig. 49g).

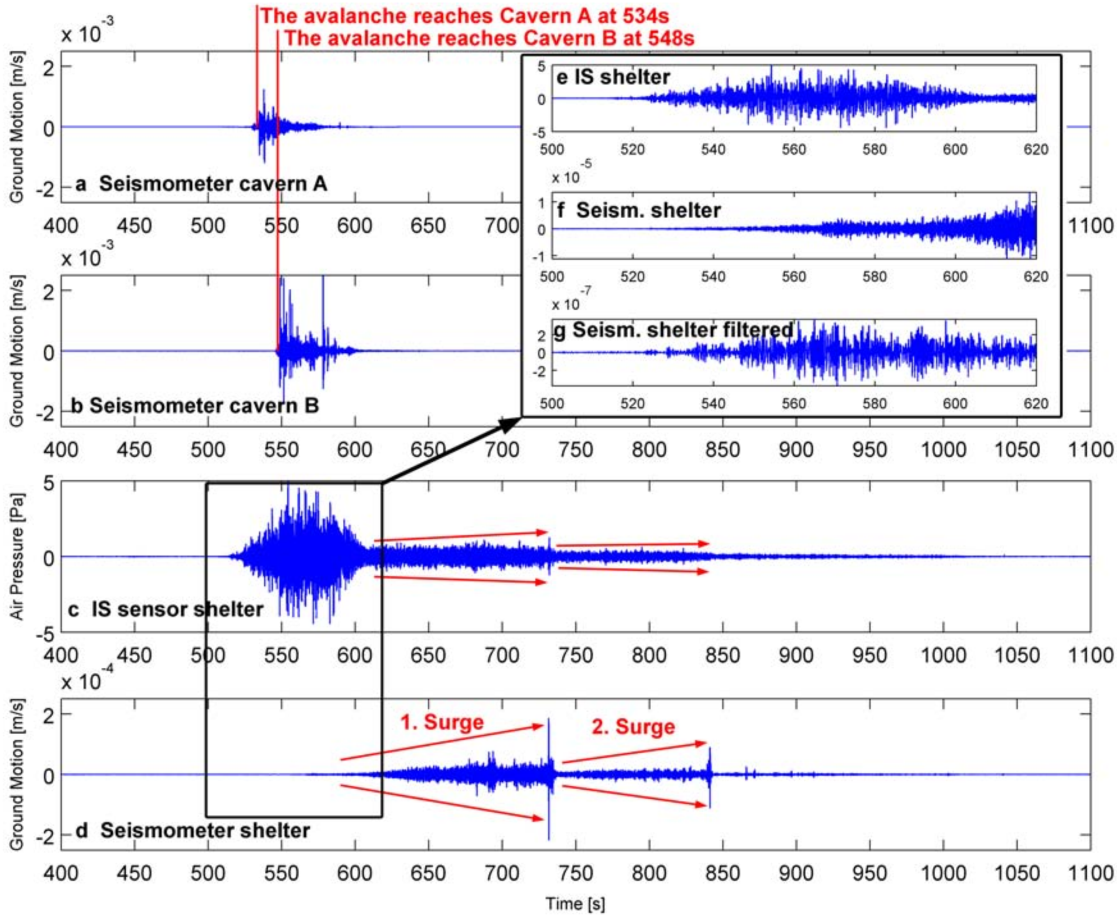

Figure 49: Seismic (N-S component) and infrasonic data from Avalanche 1. Signals are represented with a common base of time. (a) Seismogram in cavern A; (b) Seismogram in cavern B; (c) infrasound time series near the shelter; (d) Seismogram near the shelter; (e) magnified infrasound time series; (f) magnified Seismogram near the shelter; and (g) magnified filtered (1–3 Hz) Seismogram near the shelter. Red arrows indicate the infrasound signal associated with the different surges of the avalanche. Note the similar spindle shape between the seismic (g) and infrasound signals (e). Magnified time series are shown with a different scale of amplitude and all series are plotted on an arbitrary time scale.

At approx. 600 s, the amplitudes in the infrasound start to decrease and a value of ca. 1 Pa is maintained thereafter (arrows in Fig. 49c). By contrast, the amplitudes of the seismic signals in the shelter start to increase up to $1x10^{-4}$ m/s (Fig. 49d). Arrows in Figure 49d mark two different surges of the avalanche in agreement with the measurements at the pylon (Fig. 47). Seismic peaks at the end of the surges characterize the deposition processes as observed in earlier seismic studies (e.g., Suriñach et al., 2000). The two surges can also be identified in the infrasonic data with the same length and arrival time, but with lower amplitudes. The total duration of the avalanche based on the seismic and infrasonic data was approximately 500 s [500 s to 1000 s] (Fig. 49).

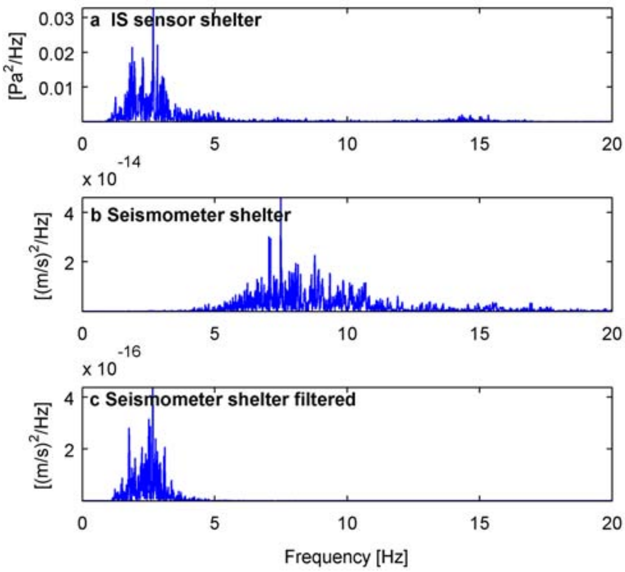

Figure 50: Total spectra for the time interval [500 s to 620 s] of Avalanche 1 (Fig. 49). (a) Infrasound time signal from the sensor near the shelter; (b) N-S component Seismogram near the shelter; and (c) N-S component filtered (1–3 Hz) Seismogram near the shelter. Note the different scale of amplitudes (10^{-16}).

Avalanche 2 (SLF #20100003b)

Avalanche description

On 30 December 2010, about 5 minutes before Avalanche 1, we detected an avalanche which was released in the area known as Pra Roua, situated immediately on the left of Crêta-Besse 1 (Fig. 45). The avalanche path is located to the south of caverns A and B and it is characterized by two narrow channels which join in a common deposition zone ca. 200 m southeast of the deposition area of Avalanche 1 (Fig. 51). Avalanches that release from Pra Roua, may also enter the gully where the seismic sensors and instrumented pylon are located. However, in this case, the avalanche did not trigger the automatic data recording system, and did not reach the instrumented pylon. Weather and snow cover characteristics are similar to those of Avalanche 1. No dynamical data are available for this event. The avalanche was detected in the sensors placed in cavern B and in the shelter (Table 3).

In the deposition zone, the avalanche self-formed a channel delimited by bounding levees and it flowed down to the river. Given the dimensions of the deposition zone shown in Fig 51, the classification size of the avalanche was approx. 4 (mass 10^4 t, path length 2000 m).

Figure 51: Left: Avalanche 2 occurred on 30 December 2009, at 13:25 in a path close to the monitored area. The avalanche release zone is indicated. Right: detail of the avalanche deposit (photo source: SLF).

Seismic and infrasonic data description

Figure 52 shows the time series of the seismic (N-S component) and infrasound signals. The total duration of the avalanche signals was approx. 230 s [180 s to 410 s]. The time series show two-wave packages of approx. 25 s to 30 s in the interval [200 s to 260 s] in all three sensors. Each wave packet has a spindle shape with high amplitudes and a similar shape (Fig. 52, curved lines). Note that the seismic signals obtained in cavern B show a shape that is markedly different from that of those obtained in Avalanche 1 because of the different paths of the avalanches.

In the interval [190 s to 260 s], the averaged amplitudes of the seismic signals in cavern B were slightly higher than those recorded in the shelter (all of the order of 10^{-6} m/s). The seismic amplitudes decrease rapidly at 260 s and remain almost constant ($2x10^{-7}$ m/s) between 260 s and 400 s, although peaks associated with the deposition phase are visible in the interval 300 s to 400 s (Figs. 52a, c, arrows). During this interval the amplitudes in the shelter were generally slightly higher than those in cavern B.

The maximum amplitudes of the infrasound signal were 1 Pa (average values 0.5 Pa). The amplitudes decrease drastically after 260 s (Fig. 52b). A detailed inspection of the signals in the time interval [180 s to 220 s] (Figs. 52d-f), which corresponds to the initial phase of the avalanche, shows that energetic infrasound signals arrive at the shelter approx. 5 s later than the seismic signals. This delay can be explained if the sources of the seismic and infrasound signals originated simultaneously. The observed delay matches the differences in the wave travel times if we consider the propagation speed of the seismic (approx. 2500 m/s in VDLS) and infrasound (343 m/s, at standard temperature and pressure) waves, and the distances involved between source and sensors. This result indicates that the start of the avalanche generated seismic and infrasound wave fields simultaneously.

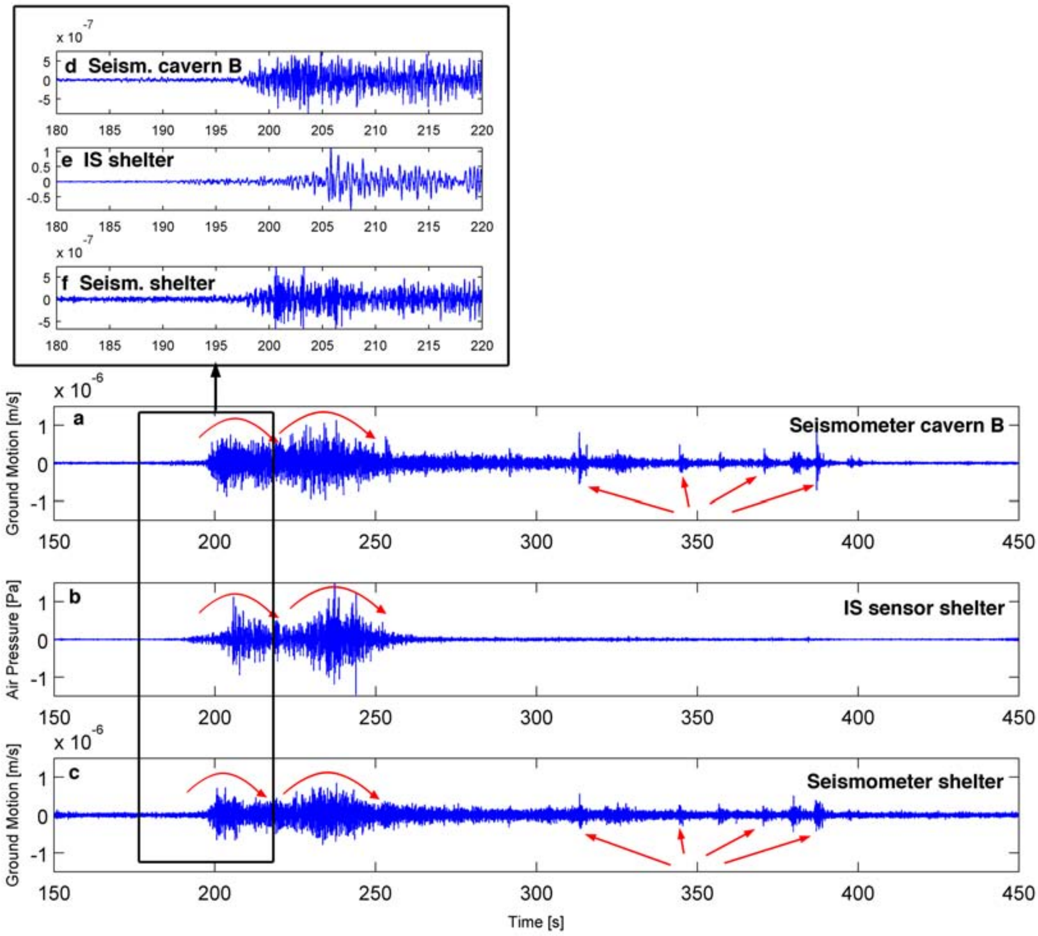

Figure 52: Seismic (N-S component) and infrasonic data from Avalanche 2. Signals are represented with a common base of time. (a) Seismogram in caverns B; (b) infrasound time series near the shelter; (c) Seismogram near the shelter; (d) magnified Seismogram in cavern C; (e) magnified infrasound time series; and (f) magnified Seismogram near the shelter. Curved arrows indicate two different surges of the avalanche and straight arrows indicate the seismic peaks associated with the stopping phase of the avalanche.

Avalanche 3 (SLF #20093025)

Avalanche description

Avalanche 3 occurred naturally on 11 February 2009 at 01:30. Owing to bad visibility during and after the release, it was not possible to establish the exact position and extension of the release area. Photographs (taken after the event) of part of the avalanche path and the deposition extent suggest that the avalanche was released from Crêta-Besse 1 (Fig. 53).

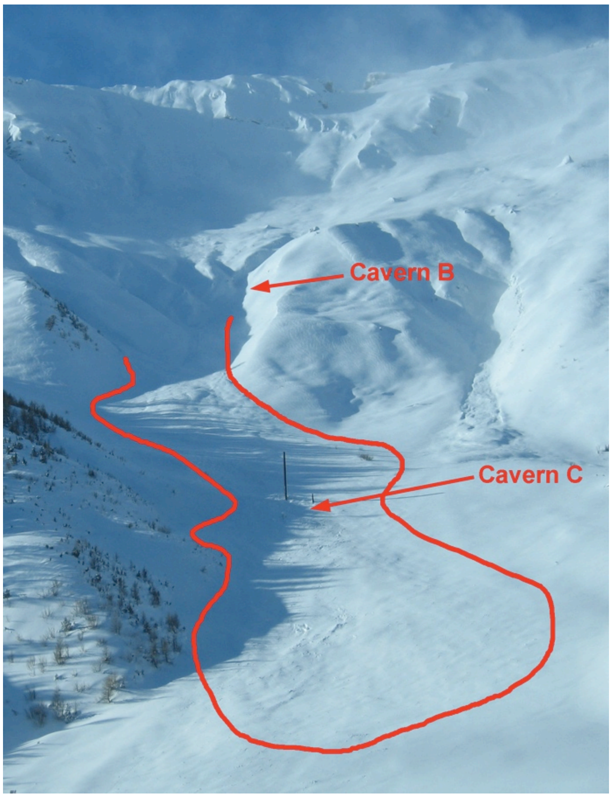

Figure 53: Avalanche 3 viewed from the shelter. Avalanche 3 occurred on 11 February 2009 at 01:30 (photo source: F. Dufour). The avalanche deposit is outlined in red. The 20 m measurement pylon is visible above the red arrow indicating the location of cavern C. Deposit boundaries are difficult to identify.

The avalanche triggered the automatic data recording system in cavern A, reached the instrumented pylon where internal velocity, flow depth and impact pressure were measured, and stopped at a short distance from the pylon (Fig 53). The records from the weather station at Donin du Jour (2390 m) reported ca. 0.40 m of new snow in the preceding 48 h on a snow cover of 2.00 m and a snow temperature of -3°C at a snow height of 1.00 m. Air temperature in the release zone was -14°C.

The measurements at the pylon indicates that the avalanche was characterized by a low density, diluted flow regime (Fig. 54) with a velocity up to 30 m/s and flow depths between 1 and 2 m. Two main surges [1s to 7s, 8s to 14s] are visible in Figure 54 as variations of flow depth and velocity. The thin deposition and the difficulty of detecting precise deposition boundaries indicate that the avalanche does not have an important dense core at the site of the pylon. Given the dimensions of the deposition zone shown in Figure 53, the classification size of the avalanche is approx. 3 (mass 10^3 t, path length 1000 m, although the path length exceeded 1000 m in this case). This avalanche was detected in the sensors placed in cavern C and shelter (Table 3).

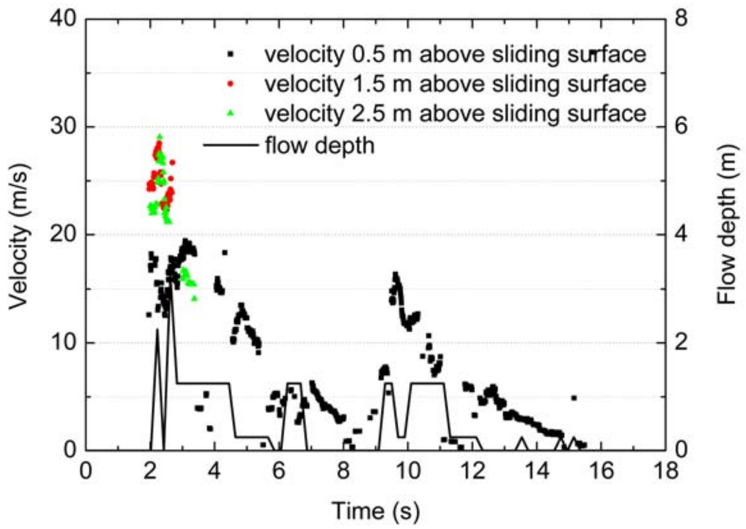

Figure 54: Avalanche 3, flow depth and internal velocities measured at the pylon, close to cavern C. The avalanche was characterized by a low density, diluted flow moving up to 30 m/s (dots). The flow depth was small. Undulations in velocity and flow depth indicate that the flow had two surges.

Seismic and infrasonic data description

Figure 55 shows the seismic (Z component) and infrasound signals. The impact of the avalanche against the pylon and the passage of the avalanche over cavern C, situated approx. 50 m below the pylon, are observed by the sudden increase in amplitudes (approx. $1x10^{-4}$ m/s) at 103 s (Fig. 55a). This is also observed in the seismic sensors near the shelter (Fig. 55c). The impact against the pylon is less noticeable in the infrasonic data (Fig. 55b). The seismic energy is detected at approx. 55 s in cavern C (Fig. 55d, red arrow), whereas it is not significant in the two sensors near the shelter at this time. The energy is detected in these sensors approx. 15 s later (70s) (Figs. 55e, f, red line). The high amplitude energy disappears at approx. 120 s in cavern C, whereas seismic signal increases at this time (up to 150 s) in the sensor near the shelter.

Infrasonic energy is observed in the whole interval [70 s to 150 s]. The shape of the time series obtained in the infrasound and seismic sensor near the shelter is very similar. Both have a spindle shape (Figs. 55b, c) and the duration [70 s to 150 s] and arrival time of the avalanche signals are similar.

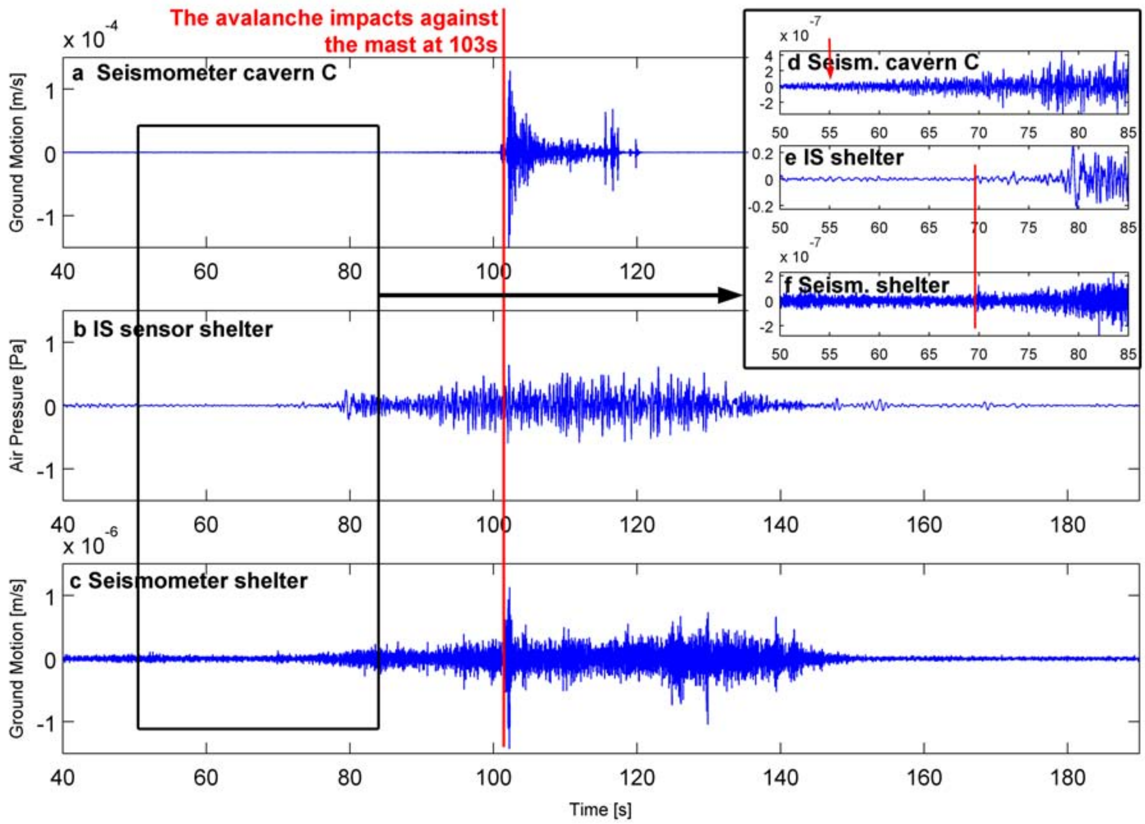

Figure 55: Seismic Z component and infrasonic data from Avalanche 3. Signals are represented with a common base of time. (a) Seismogram in cavern C; (b) infrasound time series near the shelter; (c) Seismogram near the shelter; (d) magnified Seismogram in cavern C, the arrow indicates the signal arrival (e) magnified infrasound time series; and (g) magnified Seismogram near the shelter, the red line indicates the signal arrival. Note the spindle shape of the signal in (b) and (c). Magnified time series are shown with a different scale of amplitude and all series are plotted on an arbitrary time scale.

Avalanche 4 (SLF #20103004)

Avalanche description

During the days of 6 and 7 December 2010 three avalanches were released naturally at the Vallée de La Sionne test site. On 6 December two avalanches occurred, one at 06: 22 (SLF #20103002) and the second at 18:31(SLF #20103003). The third avalanche (SLF #20103004), known as Avalanche 4, occurred a few hours later on the 7 December at 03:36. The avalanches were released after a snow precipitation of ca. 0.50 m in the preceding 48 h on a snow cover of 0.80 m and a snow temperature of -3°C at a snow height of 1.00 m. Air temperature in the release zone was -4°C.

Owing to poor visibility during and after the release, it was not possible to establish the exact position and extension of the different release areas. However, a laserscanning campaign undertaken a day later indicates that the avalanches were released from Crêta-Besse 1 and from part of Crêta-Besse 2 (Sovilla et al., 2010). Automatic pictures taken each ½ hour in the area of the pylon indicate that avalanche SLF #20103003 followed the left couloir and was probably released from Crêta-Besse 1. Avalanche 4 descended the left couloir and was probably released from the area of Crêta-Besse 1 and form part of Crêta-Besse 2. The release area and the path of the first avalanche (#20103002) are very uncertain but we assume that it followed the left and partly the right channel. However, no clear information on the path followed by these avalanches is available at the moment. Figure 56 shows an estimate of the release boundaries and the extension of the area affected by the three avalanches.

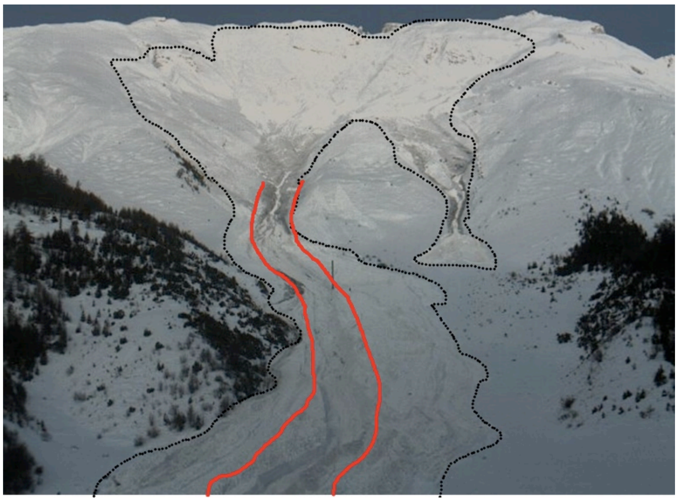

Figure 56: Estimated boundaries of avalanches on 6 and 7 December 2010. Red line: Channel of Avalanche 4, delimited by levees. Avalanche 4 was probably released from the far left of Crêta-Besse 1 and from part of Crêta-Besse 2. The dashed black line indicates the total area affected by the avalanche activity on 6 and 7 December2010 (photo source: SLF).

Avalanches #20103003 and Avalanche 4 triggered the automatic recording system and hit the measurement pylon, where internal velocities, flow depth and impact pressure were measured. However, no data are available for the avalanche that occurred in the morning on 6 December. Only Avalanche 4 will be analyzed in detail.

Figure 57 shows velocity and flow depth measured at the pylon for Avalanche 4. At the pylon, the avalanche had a slow dense flow regime characterized by a velocity of up to 5 m/s and flow depths in the order of 1 m. Because this avalanche reached the valley bottom, we expect velocity in the upper part of the path to be high enough to develop a suspension layer. The low velocity at the pylon suggests that this layer disappeared before reaching the pylon. An explanation for this behaviour is that the preceding avalanches had already entrained all the snow cover along the left channel, hindering the development of a suspension layer in Avalanche 4 in the lower avalanche path. This behaviour has been observed in other studies (Sovilla et al., 2006).

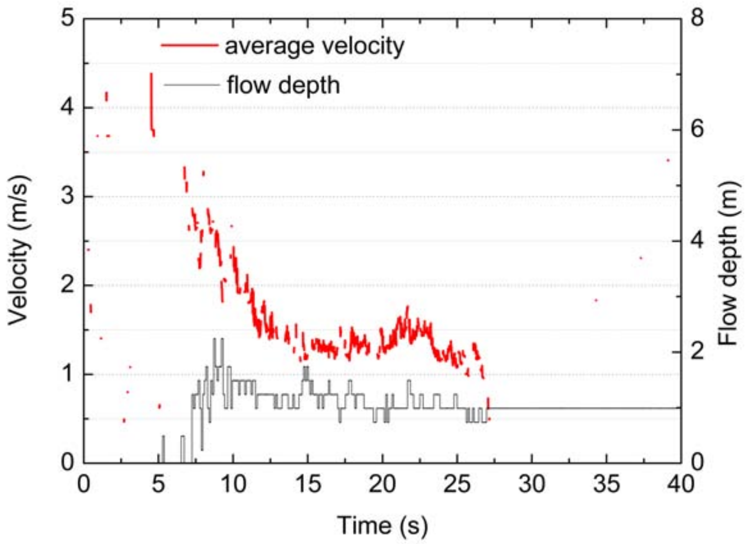

Figure 57: Avalanche 4. Flow depth and internal velocities measured at the pylon, close to cavern C. This avalanche was characterized at the beginning of the runout zone by a small dense flow with velocity up to 4 m/s to 5 m/s and flow depth in the order of 1 m.

Figure 56 shows the deposits of the avalanches as pictured in the early morning of 7 December. From the analysis of pictures taken after this avalanche, we deduce that Avalanche 4 self-formed a channel delimited by levees engraved into the deposit of the previous avalanches (Fig 56). From laserscanning measurements performed after both avalanches we estimated a total deposit volume of about 115000 m^3. Assuming a density of 400 kg/m^3 we can estimate that the avalanches have a total mass of about 46000 t. Thus, in first approximation, the classification size of both avalanches is approx. 4 (mass 104 t, path length 2000 m). Avalanche 4 was detected in the sensors placed in caverns B, C and shelter (Table 3).

Seismic and infrasonic data description

Figure 58 presents the seismic and infrasound signals recorded during Avalanche 4. A preliminary glance at the signals shows that the signal shapes are similar to those of Avalanche 1, which suggests a similar behaviour of both avalanches. The sudden increase in amplitudes, up to 10^{-4} m/s, in the time series in cavern B, at 103 s, and in cavern C, at 137 s (Figs. 58a, b) reflects the passage of the avalanche. Figures 58a and 55b also show that seismic signal amplitudes decrease more slowly in cavern C than in cavern B.

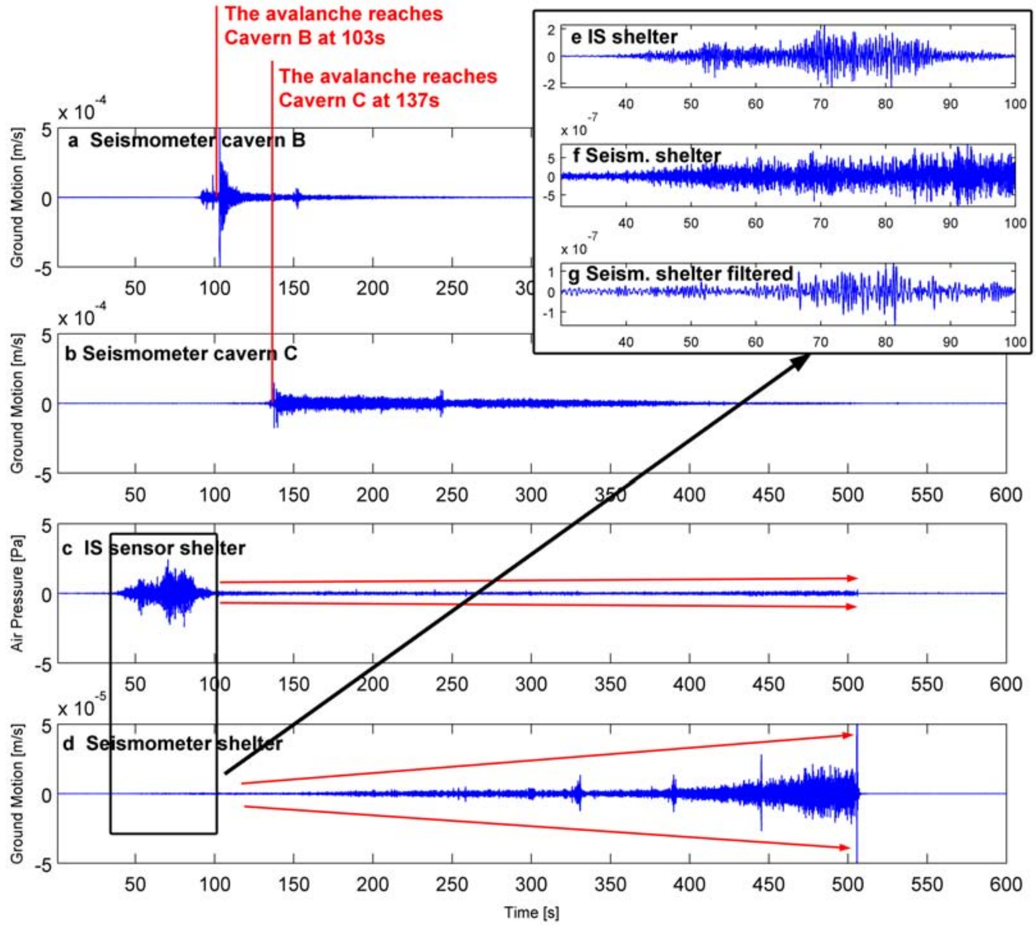

Figure 58: Seismic (N-S component) and infrasonic data from Avalanche 4. Signals are represented with a common base of time. (a) Seismogram in cavern B; (b) Seismogram in cavern C; (c) infrasound time series near the shelter; (d) Seismogram in cavern B (red arrows indicate the infrasound signal associated with the different surges of the avalanche); (e) magnified infrasound time series; (f) magnified Seismogram near the shelter; (g) magnified Seismogram (1 Hz to 3 Hz) near the shelter. Note the similar spindle shape between the seismic (g) and infrasound signals (e). Magnified time series are shown with a different scale of amplitude and all series are plotted on an arbitrary time scale.

Avalanche 4 travelled a distance of 690 between caverns B and C with an average speed of approx. 20 m/s. Measurements at the pylon show (Fig. 57) that Avalanche 4 reached the pylon at a velocity of about 5 m/s. One explanation for this difference in the speed is that the avalanche decelerated in the gully. This sudden deceleration was probably due to the lack of snow to entrain in the lower part of the path after the passage of the previous avalanches. This also accounts for the slower amplitude decrease in seismic signals in cavern C in comparison to cavern B. At the shelter, the seismic time signal has a triangular shape, which indicates that the avalanche was approaching the sensor. The arrows in Figure 58d indicate the increase in amplitudes of the seismic signal and the presence of peaks associated with the stopping phase of the avalanche. The signals also suggest that Avalanche 4 underwent only one surge.

In the infrasound signal, two wave packages of different amplitudes are observed (Fig. 58c). The amplitudes in the infrasound signal rapidly decrease in the time interval [90 s to 100 s] just before the avalanche reaches cavern B. The time series of the infrasound and filtered seismic signals behave in the same manner (spindle shape) when the avalanche is in the upper avalanche path (Figs. 58e, g).

Based on the seismic and infrasonic data, the total duration of the avalanche was approx. 495 s [40 s to 535 s] (Fig. 58).

Summary of the seismic and infrasonic data

In the previous sections, signals generated by avalanches of varying sizes at VDLS are described. Table 4 shows that the maximum amplitudes of the infrasound and seismic signals change from avalanche to avalanche.

The seismometers located in the caverns provide information about the position of the avalanche along the path and about the duration of the flow over the caverns. The maximum seismic amplitudes generated by an avalanche depends on its size, velocity, density and distance source - sensors (Suriñach et al., 2001; Biescas et al., 2003; Vilajosana et al., 2007b). As expected, Avalanche 1 had the largest amplitudes with a similar flow duration in both caverns (Table 4). The amplitudes in cavern B were slightly higher than those in cavern A, indicating that the avalanche speed and size were increasing. Avalanche 3 had smaller amplitudes attributable to the smaller size and a more diluted flow. Finally, for Avalanche 4 the seismic amplitudes monitored in cavern B were slightly higher than those observed in cavern C, whereas the flow duration over cavern C was much longer. This can be explained by a deceleration of the avalanche before cavern C and a more dense flow regime in the lower avalanche path.

As the avalanche approached the seismometer in the shelter, an increase in the seismic amplitudes was produced. Again, the large dense flow of Avalanche 1 yielded higher amplitudes than the smaller diluted Avalanche 3, which stopped further away from the shelter than Avalanche 1. In the seismic data of Avalanche 3, the impact of the avalanche against the pylon can be clearly identified. This can be attributed to the fact that the avalanche had a large diluted part that impacted against the pylon, generating a significant seismic signal. This signal is well observed over the relatively smaller seismic amplitudes caused by the friction in the snow cover. In Avalanches 1 and 4, the seismic signal produced by the impact of the avalanches against the pylon was masked by the higher signal amplitudes generated by the flow of the dense part. An increase in seismic amplitudes in the shelter is also clearly observed in Avalanche 4. The maximum amplitudes attained values smaller than those of Avalanche 1, which is in accordance with the avalanche size. In contrast to Avalanche 1, the signals suggest that Avalanche 4 had only one surge. Avalanche 2, whose path was further away from the sensors, yielded smaller amplitudes in the seismic sensors placed in the shelter and in cavern B. The peaks due to the stopping phase of the avalanche are detected only in the seismic signal.

Infrasound signals at the shelter are observed before the avalanche passed over the caverns in the upper avalanche path. In the lower avalanche path, the infrasound amplitudes rapidly decreased. Avalanche 1 yielded the largest infrasound amplitudes, up to 5 Pa. According to PDR velocity measurements, in the upper part of the path, the avalanche had the highest velocities, up to 55 m/s, and probably developed a large suspension layer. Avalanche 2 released from the Pra Roua, in similar meteorological and snow cover conditions had much smaller infrasound amplitudes, up to 1 Pa. The smallest infrasound signal amplitude, up to 0.6 Pa, was recorded for Avalanche 3, probably indicating a smaller suspension layer. Again, these data are in agreement with the measurements at the pylon and with the total duration of the flow, which indicates that Avalanche 3 had the smallest volume of all the avalanches studied (Fig. 54).

Finally, we recorded maximum infrasound amplitudes of 2.5 Pa for Avalanche 4. The average avalanche speed between cavern B and C obtained from the seismic signals was 20 m/s. This value indicates that Avalanche 4 was able to form a suspension layer in the upper part of the path. This is also consistent with the duration of the high amplitudes in the infrasound signals that rapidly decrease before the avalanche reaches cavern B (Fig. 58c). The simultaneous decrease in the amplitudes in the infrasound signal and the increase in the amplitudes of the seismic signal is also a common characteristic for Avalanches 1 and 4, (Figs. 49c, d and 58c, d).

Interestingly, infrasound signals showed a spindle shape in all the avalanches studied. The length of this spindle wave packet is of the order of 60 s to 80 s in all cases regardless of the length of the seismic signals, which depends on the size of the avalanche. The spindle shape is also observed in the signals of the seismic sensor placed near the infrasound sensor for all avalanches. In Avalanche 3, the smallest avalanche, the seismic and infrasound signals with a spindle shape have the same length. In Avalanche 2, a clear correlation between seismic and infrasound signals is observed although the seismic part is longer. In Avalanches 1 and 4, however, it was necessary to filter the seismic signal to observe this shape because it was masked by the seismic energy of higher frequency produced by the basal friction of the dense part of the avalanche. Despite the varying amplitudes in the infrasound signal because of the avalanche size (0.6 Pa to 5 Pa), the magnitude of the amplitudes of the spindle shape in the seismic signals is always of the same order (10^{-7} m/s).

Table 4: Summary of the maximum amplitudes (MA) of the seismic signals (m/s) and the infrasound signal (Pa). Also summarized is the flow duration (FD) of the avalanches flow over the caverns and the total duration based on seismic and infrasonic data. The maximum available velocities for each avalanche are also displayed: (1) PDR data in cavern B, (2) measurement at the pylon, (3) average velocity between caverns B-C from seismic data.

		Avalanche 1	Avalanche 2	Avalanche 3	Avalanche 4
Size		5	4	3	4
Cavern A	FD	50s			
	$MA_{SEIS.}$	$1x10^{-3}$ m/s			
Cavern B	FD	50s	No flow over cavern		25s
	$MA_{SEIS.}$	$2x10^{-3}$ m/s	$1x10^{-6}$ m/s		$5x10^{-4}$ m/s
Cavern C	FD			20s	300s
	$MA_{SEIS.}$			$1x10^{-4}$ m/s	$2x10^{-4}$ m/s
Shelter	$MA_{SEIS.}$	$1x10^{-4}$ m/s	$0.5x10^{-6}$ m/s	$1x10^{-6}$ m/s	$5x10^{-5}$ m/s
	$MA_{IS.}$	5 Pa	1 Pa	0.6 Pa	2.5 Pa
Total duration		500s	230s	80s	495s
Velocity		55m/s(1)		36m/s(2)	20m/s(3)

The source of infrasound and seismic signals

In the previous sections it has been shown that seismic and infrasound signals generated by snow avalanches have a significantly different temporal behaviour during the avalanche descent. For example, Figures 49c and d (Avalanche 1) highlight clear differences between seismic and infrasound signals recorded at the same place.

This is a consequence of the different avalanche flow regimes that interact differently with the environment and hence yield different types of seismic and infrasonic emissions. The main sources of the seismic energy generated by snow avalanches are the basal friction produced by the dense body inside the flow in contact with the ground or snow cover and the changes in the slope of the path (Suriñach et al., 2000; Biescas et al., 2003; Vilajosana et al., 2007b; Schneider et al., 2010). Wet snow avalanches generate especially large and long signals owing to the high-density snow and the relatively slow speed of propagation. In contrast, powder snow avalanches produce comparatively smaller seismic amplitudes because of the low-density snow and high speed of propagation (Biescas et al., 2003).

Despite the large number of studies on avalanche seismic signals, the source of infrasonic emissions of snow avalanches is poorly documented. Since infrasonic emissions are a component of acoustic emission ($f< 20$ Hz), the application of the general theory of the acoustic emissions to our study is appropriate. Firstov et al. (1992) carried out one of the first studies on acoustic emissions of snow avalanches. These authors suggest that the acoustic signal is generated by the turbulent snow air flow (powder cloud) and that the sound intensity emitted is proportional to the eighth power of the flow velocity, as proposed by Lighthill (1954). In Firstov et al. (1992) the acoustic sound source was considered stationary and was generated by a single eddy. While the approach of Firstov et al. (1992) is consistent with our measurements, which indicate that the acoustic emissions are strongly correlated with the presence of a suspension layer and thus with high avalanche velocities, we believe that the hypothesis of a stationary source is too simplistic. In particular, the avalanche motion will have two effects on the sound emissions in relation to the stationary approach suggested by Firstov et al. (1992): a change of frequency and a change in the effective source length in the direction of motion.

In this regard, a more appropriate approach has been proposed by Ffowcs (1963). To account for a limited source volume and acoustic frequency shift, the Doppler factor $(1-M\cos\Theta)$ was introduced; where $\cos\Theta$ indicates the direction between source motion and acoustic propagation. Ffowcs (1963) describe the acoustic intensity generated by a moving turbulent source by:

$$I \approx \frac{\rho^2 U^8}{\rho_0 a_0^5}\left(\frac{D}{|y|}\right)^2 \frac{1}{|1-M\cos\theta|^5} \tag{7}$$

where I is the intensity, ρ the fluid density, ρ_0 the atmospheric density, a_0 the atmospheric speed of sound, U the flow speed, D the flow dimension, y the distance travelled by the sound wave and M the Mach number $M=(U/a_0)$. Following Eq. 7, the acoustic emission intensity is proportional to the eighth power of the flow speed corrected by the Mach number and by the flow dimension.

In the previous section, we observed that the strong increase in infrasound signal emissions was apparently in correlation with the presence of a fluidised avalanche layer characterized by high speed. In the infrasound time series of Avalanche 1, high amplitudes are observed for the first 120 s of avalanche motion (Fig. 49c), whereas relatively low amplitudes exist in the seismic signal (Fig 49d). This behaviour was also observed during Avalanche 4 (Fig. 58c, d).

In order to prove that these high-energy amplitudes in the infrasound signal are attributed to a large turbulent volume of snow with a high flow speed, we calculated the expected acoustic emissions for Avalanche 1 according to Eq. 7 and compared it with the measured values (Fig. 59).

The avalanche front speed gathered from the PDR measurements (Fig. 48) was used for the flow speed U. The flow dimension D was fixed assuming that the avalanche behaves like a compact source with *M<<1*, i.e. the sound frequency equals the source frequency as proposed by Crighton (1975). In this case, the flow dimension D can be calculated by $D=U/f$ where frequency f can be deduced from the total spectra of the infrasound measurements (Fig. 50). Using this expression, D varies from 14 m to 18 m and is in good agreement with the aerosol height measurements previously obtained for powder snow avalanches at the VDLS test site (Vallet et al., 2004).

High uncertainty exists in the density ρ of the avalanche turbulent layer. According to the literature, the density values may vary from 1-2 kg/m^3 for the suspension layer to up to 50 kg/m^3 for the saltation layer (Nishimura et al., 1993; Issler, 2003; Turnbull and McElwaine, 2007). The best fit in Fig. 59 between measured and calculated values was obtained with a density ρ of 2.5 kg/m^3. This is consistent with the calculated flow dimension D, which corresponds to the typical height of avalanche suspension layers. Finally, we assumed a value of $\Theta = 10^\circ$ to describe the direction between source motion and acoustic propagation. We used equation $I = p^2 / \rho_0 a_0$ (e.g., Hirschberg and Rienstra, 2004) for plane waves to convert sound intensity I to pressure p.

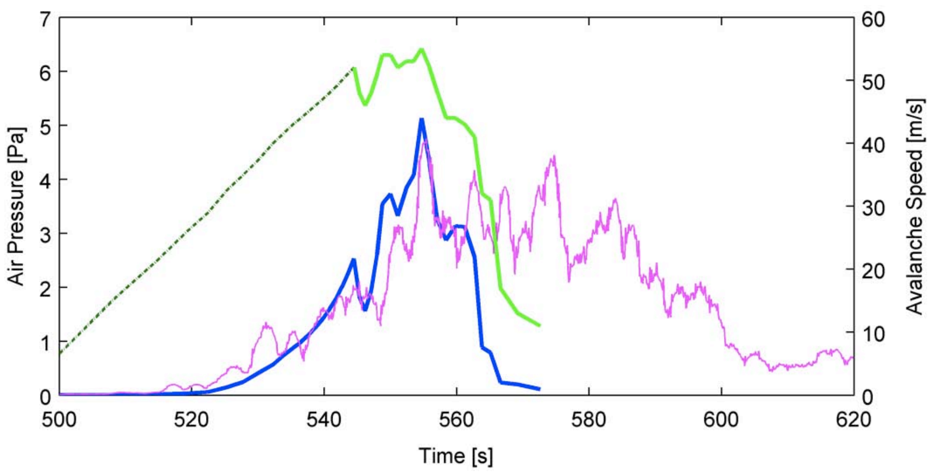

Figure 59: Air pressure profile in time generated by Avalanche 1 illustrating the infrasound time series (pink line), pressure calculation from Eq. (7) (blue line) and PDR front speed (solid green line) assuming a linear velocity growth in time (dotted green line). The origin of time is the same as in Figure 48.

Figure 59 shows the calculated pressure values for Avalanche 1 (blue line) against the envelope of our infrasound measurements (pink line). In the time interval [540 s to 560 s], the calculated and measured values are in agreement. The calculated signal decreases in amplitude after 560 s due to the rapid fall in the avalanche front speed. The monitored values (pink line) however, remain high (5 Pa). This apparent discrepancy can be explained by recalling that values calculated from Eq. 7 (blue line) represent only the avalanche front and do not take into account the possibility that the suspension layer spreads over a large area of the avalanche path. In fact, while the avalanche front suddenly decelerated at the start of the runout zone, radar measurement reveals that there were still high velocities for about 50 s in the upper avalanche path (see section Avalanche 1/Avalanche description).

The relatively small seismic amplitudes in the sensor near the shelter for Avalanche 1 [500 s to 600 s] (Fig. 49d) are also in line with the existence of a low-density flow regime in the initial phase of this avalanche. According to earlier studies, seismic observations of powder snow avalanches show that the generated ground vibrations are very weak (Nishimura et al., 1993; Suriñach et al., 2001). In particular, seismic waves are relatively small during the initial acceleration of the avalanche because a certain amount of snow mass is necessary to generate sufficient seismic energy for detection by seismometers (Suriñach et al., 2000).

A similar behaviour of infrasound and seismic amplitudes can be observed for Avalanche 4 (Fig. 58c, d). The amplitudes in the infrasound rapidly decrease before Avalanche 4 reaches Cavern B. At the same time the amplitudes in the seismic signal in the shelter increase. The analysis of the seismic signals in the caverns indicates that Avalanche 4 had still an average speed of 20 m/s between Cavern B and C, which rapidly decreased to 5 m/s at the pylon. Using the same reasoning as in the case of Avalanche 1, it may be concluded that the high amplitudes in the infrasonic data are related to the presence of a suspension layer in the upper avalanche path.

The smaller amplitudes in the infrasound of Avalanche 2 with respect to those of Avalanche 1 can also be explained if we assume that most of the infrasound signals come from the suspension part. As for Avalanche 2 (Pra Ruoa), the potential erosion area was smaller than that of Avalanche 1 (Crêta Besse). Consequently, the erosion of snow along the path of Avalanche 2 was limited, and as a result, the development of the suspension layer (Sovilla et al., 2006). Pressure changes in the seismic sensor or infrasound-seismic coupling as observed in other sources (e.g., Hayward and Pankow, 2008; Negraru, 2010) may account for the spindle shape of the seismic data (filtered or not) at the start of the avalanche.

Conclusions

The infrasound and seismic signals generated by four different snow avalanches released naturally at the Vallée de La Sionne test site were analysed. We showed that infrasound and seismic signals are correlated with each other and that the combination of both sensors is a valuable tool for detecting snow avalanches. Both sensors can detect avalanches despite being sensitive to different avalanche regimes. Infrasound sensors are more sensitive to the aerosol fluctuations (powder part), whereas seismic sensors are more sensitive to the vibrations generated by the dense flow. Thus, while infrasound sensors readily perceive avalanches in the early stages of an event, provided that the suspension part is present, the seismic sensors detect avalanches as soon as they have enough mass to generate signals that can be discriminated from the ambient noise.

In addition, the main findings of this study may be summarized as follows:

1. The combination of infrasound and seismic sensors used allowed us to estimate the total avalanche duration with high reliability and accuracy. The infrasound sensor proved more suitable for detecting avalanche initiation and the seismic sensors more suitable for estimating the end of the avalanche motion. The avalanche stopping phase was only detected by the seismic sensors.
2. High amplitudes in the infrasound measurement were related to the suspension layer in the upper avalanche path. For one of the measured avalanches, we were able to reproduce the measured infrasound signal, assuming that the suspension layer acted as a moving turbulent sound source and that the infrasonic emission intensity was proportional to flow speed and to the height of the suspension layer.
3. The amplitudes of the infrasound and seismic signals were roughly correlated with the size of the suspension and dense layer, respectively.
4. The combination of infrasound and seismic sensors not only detected the avalanches but also differentiated between the different flow regimes.

References

Adam, V., Chritin, V., Rossi, M. and Bolognesi, R. (1997): Acoustic detection system for operational avalanche forecasting, in: Proceedings International Snow Science Workshop, Banff, Alberta, 149–153

Barbolini, M. and Issler, D. (2006): Avalanche Test Sites and Research Equipment in Europe: An Updated Overview, Final-report deliverable D8, SATSIE avalanche studies and model validation in Europe

Bedard, A. (1989): Detection of avalanches using atmospheric infrasound, in: Proceedings of the Western Snow Conference, edited by: Shafer, B., Western Snow Conference, Colorado State University, 52–58

Bessason, B., Eirìksson, G., Thoŕorinsson, Ò., Thoŕorinsson, A. and Einarsson, S. (2007): Automatic detection of avalanches and debris flows by seismic methods, Journal of Glaciology, 53, 461–472

Biescas, B. (2003): Aplicacíon de la sismología al estudio y detección de aludes de nieve, Ph.D. thesis, Universitat de Barcelona, Grup d'Allaus UB, Departament de Geodinàmica i Geofísica

Biescas, B., Dufour, F., Furdada, G., Khazaradze, G. and Suriñach, E. (2003): Frequency content evolution of snow avalanche seismic signals, Surveys in Geophysics, 24, 447–464

Comey, R. and Mendenhall, T. (2004): Recent Studies Using Infrasound Sensors to Remotely Monitor Avalanche Activity, in: Proceedings of the International Snow Science Workshop, Jackson Hole, Wyoming, 640–646

Crighton, D. (1975): Basic Principles of Aerodynamic Noise Generation, Progress in Aerospace Sciences, 16, 31–96

Ffowcs Williams, J. (1963): The noise from Turbulence Convected at High Speed, Philosophical Transactions of the Royal Society of London A, 255(1061), 469–503, doi: 10.1098/rsta.1963.0010

Firstov, P., Sukhanov, L., Pergament, V. and Rodionovskiy, M. (1992): Acoustic and seismic signal from snow avalanches, Transactions (Doklady) of the U.S.S.R., Academy of Sciences: Earth Science Sections, 312, 67–71

Gauer, P., Issler, D., Lied, K., Kristensen, K. and Sandersen, F. (2008): On snow avalanches flow regimes: Inferences from observations and measurements, in: Proceedings International Snow Science Workshop, 717–723, Whistler

Hayward, C. and Pankow, K. (2008): Obervations of infrasound to seismic coupling at Earthscope stations using co located infrasound microphones, AGU Fall Meeting Abstracts, abstract #S33B-1945

Hirschberg, A. and Rienstra, S. (2004): An introduction to aeroacoustics, Technical report, Eindhoven University of Technology, Dept. of App. Physics and Dept. of Mathematics and Comp. Science

Issler, D., (2003): Experimental information on the dynamics of dry-snow avalanches, in: Hutter, K. and N. Kirchner (eds.), Dynamic Response of Granular and Porous Materials under Large and Catastrophic Deformations, Lecture Notes in Applied and Computational Mechanics 11, Springer, 109–160

Kern, M., Bartelt, P., Sovilla, B. and Buser, O. (2009): Measured shear rates in large dry and wet snow avalanches, Journal of Glaciology, 55, 327–338

Kogelnig, A., Hübl, J., Suriñach, E., Vilajosana, I. and McArdell, B. (online first): Infrasound produced by debris flow: propagation and frequency content evolution, Natural Hazards, doi:10.1007/s11069-011-9741-8

Kogelnig, A., Suriñach, E., Vilajosana, I., Hübl, J., Sovilla, B., Hiller, M. and Dufour, F. (2011): On the complementariness of infrasound and seismic sensors for monitoring snow avalanches, Natural Hazards and Earth System Sciences, 11(8), 2355-2370

Leprettre, B., Martin, N., Glangeaud, F. and Navarre, J. (1998): Three-Component Signal Recognition Using Time, Time-Frequency and Polarization Information-Application to Seismic Detection of Avalanches, IEEE Transactions on Signal Processing, 46, 83–102

Lighthill, M. (1954): On sound generated aerodynamically II. Turbulence as a source of sound, Proceedings of the Royal Society A, 222(1148), 1–32

McClung, D. and Schaerer, P. (1980): Snow Avalanche Size Classification, in: Proceedings of Avalanche Workshop, edited by Comittee, C. A., vol. Technical Memorandum 133,12–27, Associate Committee on Geotechnical Research, Ottawa: National Research Council of Canada

McClung, D. and Schaerer, P. (2006): The Avalanche Handbook, The Mountaineers Books

Negraru, P. T. (2010): Application of Seismo-Acoustic Signals to the Study of Local Site Effects, Acta Geophysica, 58(6), 1021-1039, doi:10.2478/s11600-010-0025-6

Nishimura, K., Maeno, N., Kawada, K. and Izumi, K. (1993): Structures of snow cloud in dry-snow avalanches, Annals of Glaciology, 18, 173–178

Rammer, L., Kern, M., Gruber, U. and Tiefenbacher, F. (2007): Comparison of avalanche-velocity measurements by means of pulsed Doppler radar, continuous wave radar and optical methods, Cold Regions Science and Technology, 50, 35–54

Sabot, F., Naaim, M., Granada, F., Suriñach, E., Planet, P. and Furdada, G. (1998): Study of avalanche dynamics by seismic methods, image processing techniques and numerical models, Annals of Glaciology, 26, 319–323

Saint-Lawrence, Y. and Williams, T. (1976): Seismic signals associated with avalanches, Journal of Glaciology, 17, 521–526

Salway, A. (1978): A Seismic and Pressure Transducer System for Monitoring Velocities and Impact Pressure of Snow Avalanches, Arctic Antarctic and Alpine Research, 10, 769–774

Schneider, D., Bartelt, P., Caplan-Auerbach, J., Christen, M., Huggel, C. and McArdell, B. (2010): Insights into rock-ice avalanche dynamics by combined analysis of seismic recordings and a numerical avalanche model, Journal of Geophysical Research, 115, doi:10.1029/2010JF001734

Scott, E., Hayward, C., Kubichek, R., Hamann, J. and Pierre, J. (2004): Results of Recent Infrasound Avalanche Monitoring Studies, in: International Snow Science Workshop, Jackson Hole, Wyoming, 696–704

Scott, E., Hayward, C., Kubichek, R., Hamann, J., Comey, R., Pierre, J. and Mendenhall, T. (2007): Single and multiple sensor identification of avalanche-generated infrasound, Cold Regions Science and Technology, 47, 159–170

Sovilla, B., Burlando, P. and Bartelt, P. (2006): Field experiments and numerical modeling of mass entrainment in snow avalanches, Journal of Geophysical Research, 111, doi:10.1029/2005JF000391

Sovilla, B., Schaer, M., Kern, M. and Bartelt, P. (2008a): Impact pressures and flow regimes in dense snow avalanches observed at the Vallée de la Sionne test site, Journal of Geophysical Research, 113, 1–14, doi:10.1029/2006JF000688

Sovilla, B., Schaer, M. and Rammer, L. (2008b): Measurements and analysis of full-scale avalanche impact pressure at the Vallèe de la Sionne test site, Cold Regions Science and Technology, 51, 122–137

Sovilla, B., Kern, M. and Schaer, M. (2010a): Slow drag in wet snow avalanche flow, Journal of Glaciology, 56, 587–592

Sovilla, B., McElwaine, J., Schaer, M. and Vallet, J. (2010b): Variation of deposition depth with slope angle in snow avalanches: Measurements from Vallée de la Sionne, Journal of Geophysical Research, 115, doi:10.1029/2009JF001390

Stein, S. and Wylesession, M. (2003): An Introduction to seismology, earthquakes and earth structure, Blackwell Publishing

Suriñach, E., Sabot, F., Furdada G. and Vilaplana, J. (2000): Study of seismic signals of artificially released snow avalanches for monitoring purposes, Physics and Chemistry of the Earth, 25(9), 721–727

Suriñach, E., Furdada, G., Sabot, F., Biescas, B. and Vilaplana, J. (2001): On the characterization of seismic signals generated by snow avalanches for monitoring purposes, Annals of Glaciology, 32, 268–274

Suriñach, E. (2004): Spanish avalanche research: Experimental sites and seismic measurements, in: Snow and Avalanche Test Sites, edited by Naaim, M. and Naaim-Bouvet, F., 71–183, Cemagref

Suriñach, E., Vilajosana, I., Khazaradze, G., Biescas, B., Furdada, G. and Vilaplana, J. (2005): Seismic detection and characterization of landslides and other mass movements, Natural Hazards and Earth System Sciences, 5, 791–798

Suriñach, E., Kogelnig, A., Vilajosana, I., Hübl, J., Hiller, M. and Dufour, F. (2009): Incorporación de la señal de infrasonido a la detección y estudio de aludes de nieve y flujos torrenciales, in: VII Simposio Nacional sobre Taludes y Laderas Inestables, edited by Alonso, E., Corominas, J., and Hürlimann, M., Barcelona, Spain

Turnbull, B. and McElwaine, J. (2007): A comparison of powder-snow avalanches at Vallée de la Sionne, Switzerland, with plume theories, Journal of Glaciology, 53, 30–40

Vallet, J., Turnbull, B., Joly, S. and Dufour, F. (2004): Obervations on powder snow avalanches using videogrammetry, Cold Regions Science and Technology, 39, 153–159

Vilajosana, I., Khazaradze, G., Suriñach, E., Lied, E. and Kristensen, K. (2007a): Snow avalanche speed determination using seismic methods, Cold Regions Science and Technology, 49, 2–10

Vilajosana, I., Suriñach, E., Khazaradze, G., and Gauer, P. (2007b): Snow avalanche energy estimation from seismic signal analysis, Cold Regions Science and Technology, 50, 72–85

Chapter 10

Summary of signals from snow avalanches and debris flows

In the previous chapters infrasound and seismic signals of different alpine mass movements have been discussed. The following chapter summarizes the most important characteristics of infrasound and seismic signals of snow avalanches and debris flows. For this purpose data of one snow avalanche (Fig. 60) and one debris flow (Fig. 61) has been chosen, which can be considered as typical for the respective process. Table 5 summarizes the main characteristics of infrasound and seismic data of alpine mass movements in view of the subsequent Chapter 11, which introduces other common sources of infrasound signals.

Figure 60 shows infrasound and seismic data (time series, total spectra, running spectra) of a natural snow avalanche monitored at the VDLS test site on 07.12.2010. The infrasound data was monitored with a Chaparral Model 24 microphone and the seismic data with a Mark 3D seismometer, both recorded with a Reftek DAS 130 datalogger and placed at the shelter in the VDLS test site. For further information about the VDLS test site the reader is referred to Chapter 4 and 9. For the purpose of this chapter only the vertical component is presented. This avalanche has been discussed in detail previously in Chapter 9 (Avalanche 4, SLF #20103004) and can be considered as a good example of a dry-mixed motion avalanche at the VDLS test site.

Figure 61 shows infrasound and seismic data (time series, total spectra, running spectra) of one debris flow monitored at the Lattenbach test site on 01.09.2008. The infrasound data was monitored with the Gefell microphone and the seismic data was recorded with the Sensor SM4 geophone. Both sensors were connected to a Campbell CR1000 datalogger. This debris flow has been analysed in detail in Chapter 7 and represents a typical debris flow event at this test site. In the time series the maximum amplitudes of the infrasound signals produced by debris flows and snow avalanches are similar (up to 5 Pa). Both processes present a spindle shape in the time series of the infrasound data, although in case of the debris flow the increase in amplitudes is more rapid and the total duration of the high amplitude wave package is much longer (up to 2000 s). In case of the snow avalanches high amplitude infrasound wave packages are only observed for approximately 50 s to 80 s, corresponding to the powder part (see Chapter 9).

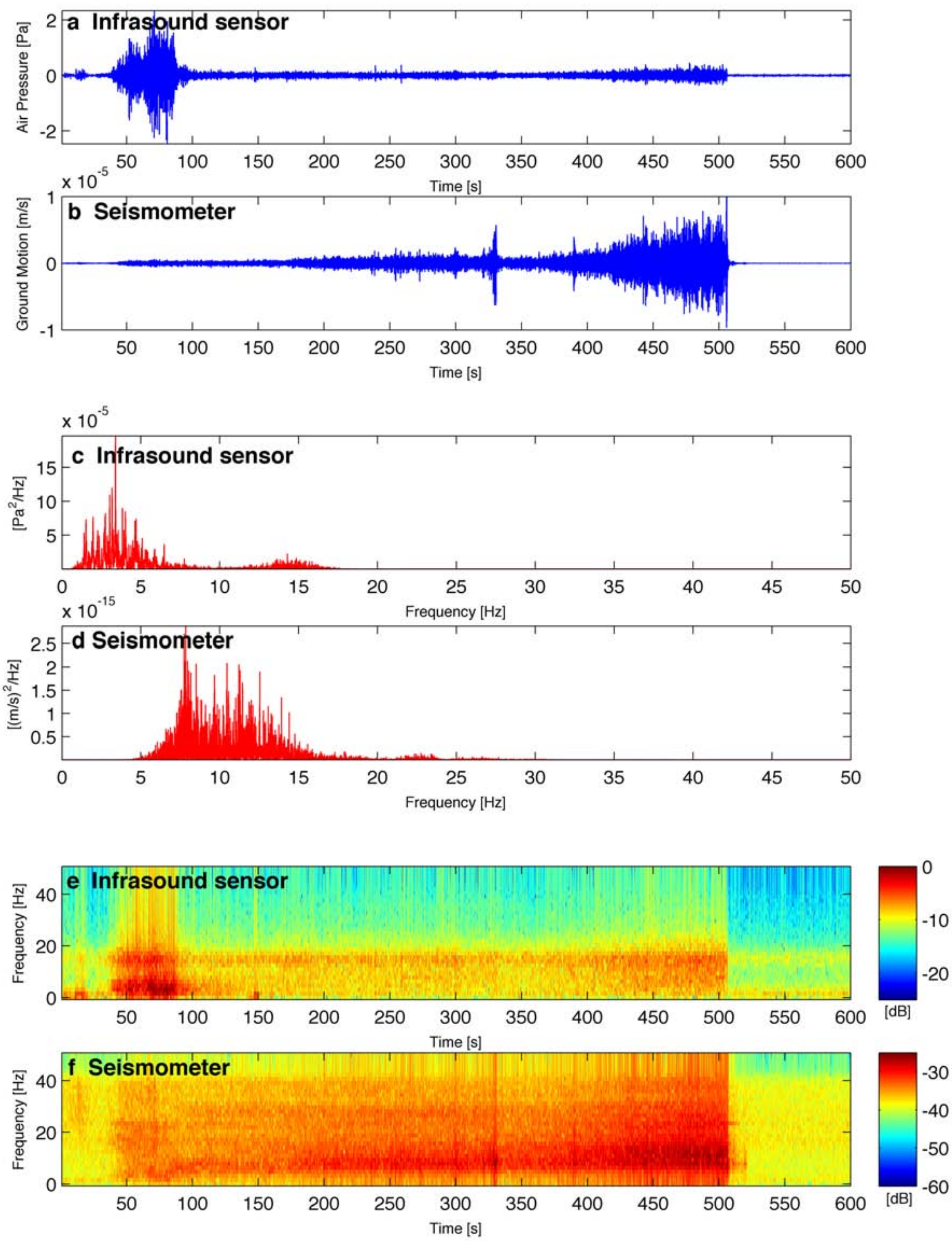

Figure 60: Infrasound and seismic (Z-component) data of an avalanche on 07.12.2010 (Avalanche 4, SLF #20103004, see Fig. 58, Chapter 9) at the VDLS test site. Signals are represented with a common base of time. (a) Infrasound time series near the shelter; (b) Seismogram near the shelter; (c) Total spectrum of the infrasound signal; (d) Total spectrum of the seismic signal; (e) Running spectrum of the infrasound signal; (f) Running spectrum of the seismic signal.

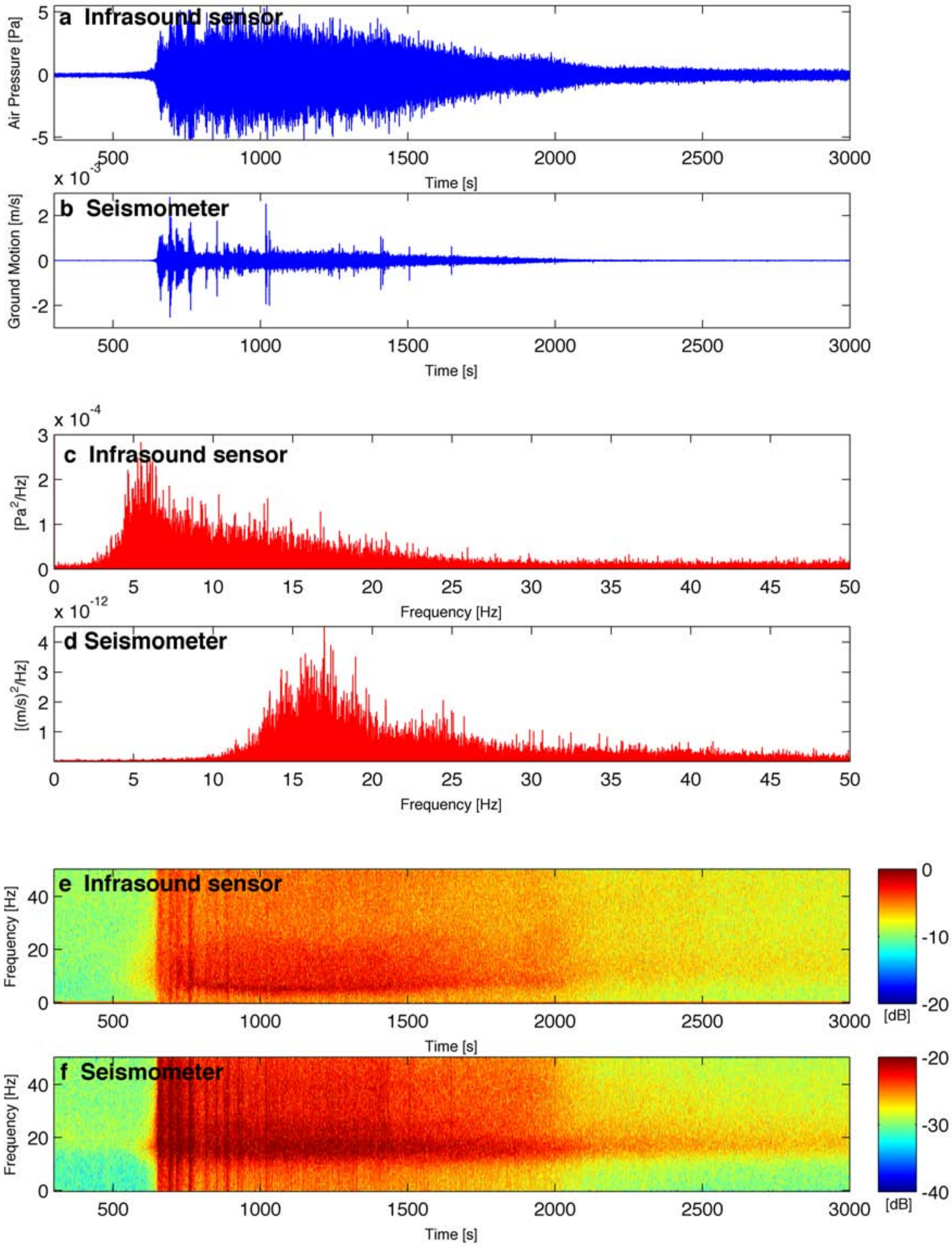

Figure 61: Infrasound and seismic (Z-component) data of a debris flow monitored at the Lattenbach test site on 01.09.2008 (see Fig. 16, Chapter 7). Signals are represented with a common base of time. (a) Infrasound time series near the shelter; (b) Seismogram near the shelter; (c) Total spectrum of the infrasound signal; (d) Total spectrum of the seismic signal; (e) Running spectrum of the infrasound signal; (f) Running spectrum of the seismic signal.

For debris flows the seismograph shows a similar shape to the infrasonic data. The maximum seismic amplitudes in the time series observed for debris flow are in the order of 10^{-3} m/s when the sensor location is close to the channel (< 30 m). Snow avalanche seismic data monitored at the shelter at the VDLS test site show a typical triangular shape indicating that the avalanche approaches the shelter. Seismic amplitudes for snow avalanches are in the order of order of 10^{-3} m/s if monitored in the caverns or approximately 10^{-5} m/s to 10^{-6} m/s if monitored at the shelter at the VDLS test site. The amplitudes of both, seismic and infrasound data, depend on the type and size of the process and on the distance source-sensor.

For both processes the total spectra (Fig 60, 61 c, d) show that infrasound and seismic signals are complementary. Debris flow infrasonic signals have peak frequencies from 3 Hz to 10 Hz whereas seismic signals have peak frequencies from 10 Hz to 20 Hz. A similar behaviour can be observed for snow avalanches. Infrasound signals of snow avalanches have peak frequencies between 2 Hz to 8 Hz and seismic signals 5 Hz to 15 Hz. These values do not depend on the characteristics of the sensor nor the datalogger; they are a characteristic of the process. Biescas et al. (2003) studied the frequency content of snow avalanches seismic signals and reported a frequency varying between 1 Hz to 45 Hz on the type and size of recorded avalanches.

The running spectra of snow avalanche seismic and infrasound data show a different signal pattern. In the infrasound spectrum (Fig. 60 e) the most energy is observed at the beginning, depicted by the dark red colors (1 Hz to 5 Hz), due to high amplitudes corresponding to the powder part. This is followed by some low energy signal associated with avalanche activity until the end of avalanche motion in the frequency band from 1 Hz to 20 Hz. The running spectrum of the seismic data (Fig. 60f) presents a triangular shape depicted by the dark red colors, due to the increase in high frequency content as the avalanche approaches the sensor. This behaviour is typical for seismic signals monitored at the shelter and similar results have already been reported in previous studies (Biescas et al., 2003).

The running spectra of the debris flow (Fig. 61e, f) show a similar signal pattern in the seismic and infrasonic data. Both have a spindle shape with a rather sudden increase in frequencies and energy as the debris flow approaches the sensor location. The frequency content slowly decreases again in both sensors when the debris flow moves downstream far from the monitoring station.

Table 5: Summary of the recorded maximum amplitudes (MA) of the seismic signals (m/s) and infrasound signals (Pa) of snow avalanches and debris flows. Also summarized is the total duration (s) based on the seismic and infrasound data, the peak frequency content (Hz) and the typical pattern in the running spectra (RS).

	Debris Flows	Snow Avalanches
MA_{IS}	1 Pa to 4.8 Pa	0.6 Pa to 5 Pa
MA_{SEIS}	10^{-3} m/s	10^{-6} m/s to 10^{-3} m/s [(a)]
Total Duration	1500 s to 5500 s [(b)]	80 s to 500 s
Peak Freq. $_{IS}$	3 Hz to 10 Hz 10 Hz to 20 Hz [(b)]	2 Hz to 8 Hz
Peak Freq. $_{SEIS}$	10 Hz to 20 Hz	1 Hz up to 45 Hz [(c)]
Pattern in RS_{IS}	Spindle shape	Spindle shape passing to broad horizontal band
Pattern in RS_{SEIS}	Spindle shape	Triangular shape [(d)]

[(a)] Monitored at the VDLS test site in the caverns with avalanche flow above the seismometer.
[(b)] Debris flood events monitored at Illgraben test site.
[(c)] According to Biescas et al (2003).
[(d)] Seismometer location at the shelter VDLS test site.

References:

Biescas, B., Dufour, F., Furdada, G., Khazaradze, G. and Suriñach, E. (2003): Frequency content evolution of snow avalanche seismic signals, Surveys in Geophysics, 24, 447–464

Chapter 11

Examples of other sources of infrasound

Monitoring mass movements in an alpine region inherently involves different sources of background noise. Some of them could be monitored and identified during this study. In order to clearly differentiate the mass movement signal of interest from interfering noise, in a first step, a study of the background noise signals in both the time and the frequency domain at the study site was conducted. In the following chapter different infrasound sources, which could be relevant for monitoring debris flows or snow avalanches are discussed. As already explained in Chapter 5 we used different infrasound sensors for monitoring throughout this study. If possible, we recorded seismic data with 3D seismometers or geophones and if available, all 3 components were studied. For the purpose of this chapter, to introduce different sources of infrasound, only the vertical component of the seismic data is represented.

Helicopters

In wintertime, helicopters are often used in avalanche control work for protection of roads, ski slopes and other infrastructure. As a consequence helicopters present a possible noise source when monitoring artificially released snow avalanches. The acoustic and seismic signature of helicopters has been previously studied mostly in relation to detection on the battlefield for military purposes (Stubbs, 2005; Becker and Güdesen, 2000).

Figure 62 presents 20 s of infrasound and seismic (Z component) data from a helicopter at the VDLS test site on 25.01.2009. The data was obtained at the shelter using the Gefell infrasound microphone and a Mark 3D seismometer, both recorded with a Reftek DAS 130 datalogger. The helicopter noise is not visible in the time series of both sensors without detailed analysis (Fig. 62a, b). The amplitudes in the time series are very small in both sensors (0.02 Pa and 10^{-8} m/s) similar to the background noise level at this site and do not present any particular shape. The total spectrum of the infrasound data (Fig 62c) presents a significant peak at 19 Hz, which can be associated with the helicopter signal. There is another peak of very small amplitude present at 38 Hz, which is the harmonic of the 19 Hz signal and some low energy associated with background noise between 1 Hz to 3 Hz.

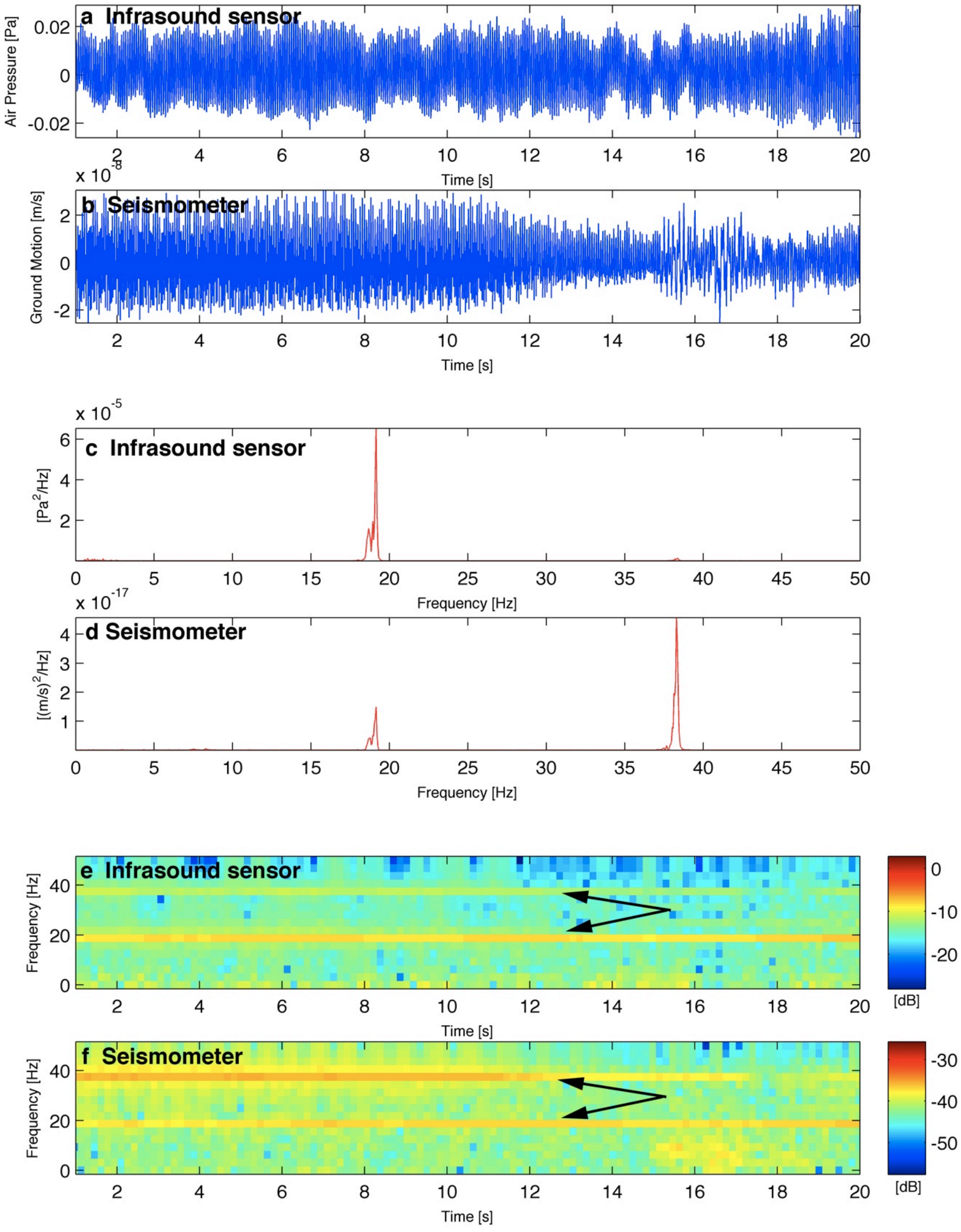

Figure 62: Infrasound and seismic (Z-component) data of a helicopter in VDLS on 25.01.2009. Signals are represented with a common base of time. (a) Infrasound time series near the shelter; (b) Seismogram near the shelter; (c) Total spectrum of the infrasound signal; (d) Total spectrum of the seismic signal; (e) Running spectrum of the infrasound signal; (f) Running spectrum of the seismic signal. The black arrows indicate signal associated with the helicopter.

The total spectrum of the seismic data (Fig 62d) shows the same energy peak at 19 Hz and with more energy the harmonic at 38 Hz. However, looking at the maximum amplitudes in Figure 62c and d the total amount of energy is very small. In the running spectra (Fig. 62e, f) the helicopter noise is presented by two narrow lines at 19 Hz and 38 Hz (marked by arrows) in the seismic and infrasonic data. For the seismic data the peak frequencies obtained (19 Hz and 38 Hz) are consistent with values reported by Biescas et al. (2003) at the same test site, who found signals of helicopters in the data while monitoring snow avalanches with seismometers.

Previous studies have already investigated the source of acoustic emissions from helicopters. Long (1983) developed a theoretical formulation describing the acoustic and aerodynamic characteristics of rotating blades. He showed that the main source of acoustic emissions from helicopters originate from the rotating blades, which are thin and usually operate at high speeds, therefore creating pressure perturbation in the air. Following the work of previous studies (Lighthill, 1952, 1954; Ffowcs Williams 1963) Long (1983) showed that these perturbations act as a quadropole turbulent sound source, as described by the third term on the right hand side of Eq. 1 (see Chapter 3, infrasound waves). As already mentioned before (Chapter 3, coupling effects), the source of the seismic signals is most probably sound waves generated by the helicopter coupled into the ground.

Infrasound and seismic signals from helicopters have negligibly low amplitudes in the time series and a characteristic signal pattern (narrow horizontal lines) in the frequency domain, with peak frequencies at 19 Hz and 38 Hz. These features can be used to easily differentiate helicopter signals from alpine mass movement signals. Previous studies (Biescas et al., 2003; Suriñach et al., 2009; Chapter 9) reported that the main energy of mass movement generated seismic and infrasound signals is significantly higher and expected to be at lower frequencies (<19 Hz).

The reader is also referred to the following section, where Figure 64 shows the infrasound and seismic data of a helicopter and an explosion.

Explosions

Explosive charges of different size are commonly used to trigger snow avalanches in different applications (e.g. hand charges or avalanche towers). The detonation of an explosive charge causes a shockwave in its immediate surroundings (Gubler, 1977). With increasing distance from the point of detonation this shockwave develops into a N-shaped pressure wave (an elastic wave with large amplitude), and finally becomes a sound wave (Gubler, 1977) (Fig. 63). Within the snow cover and within the ground these disturbances propagate as different kinds of displacement waves (P-, S-waves) and seismic waves, respectively.

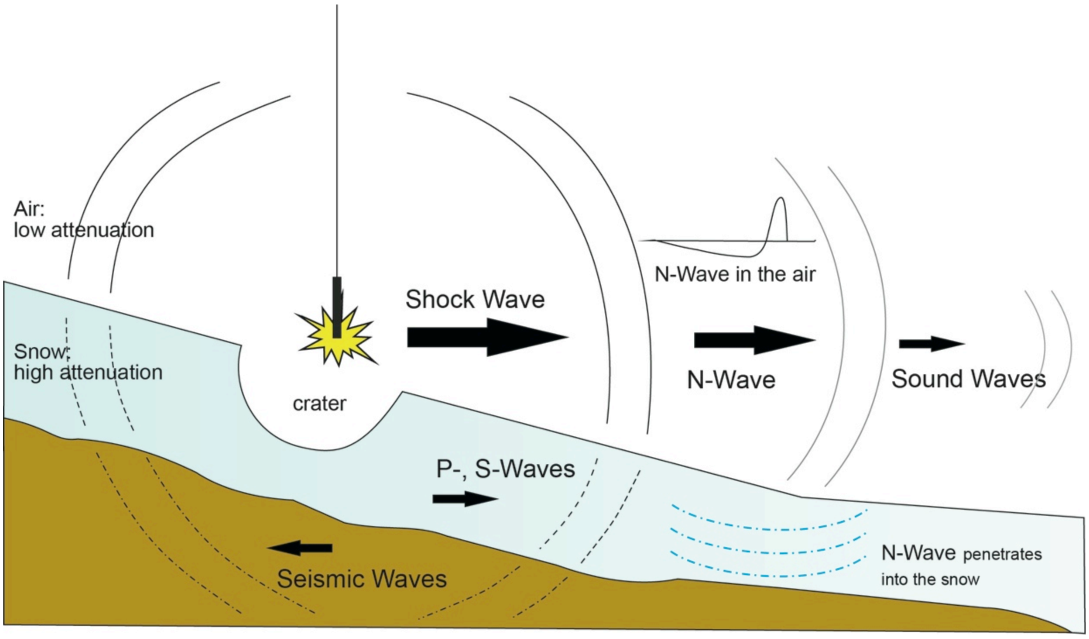

Figure 63: Overview of pressure waves caused by an explosive charge in different media such as air, snow and soil (modified after Gubler, 1977).

Therefore it is necessary to investigate the seismic and infrasound signal from explosions to allow differentiation from avalanche signals. Seismic signals of explosions and as a consequence artificially triggered snow avalanches have been analysed and discussed in previous studies (Suriñach et al., 2000, 2001). Scott and Lance (2002) monitored artificially triggered snow avalanches using infrasound sensors and reported that large explosive mechanisms produce higher amplitude pressure fluctuations that are longer in duration than those produced by smaller explosive mechanisms.

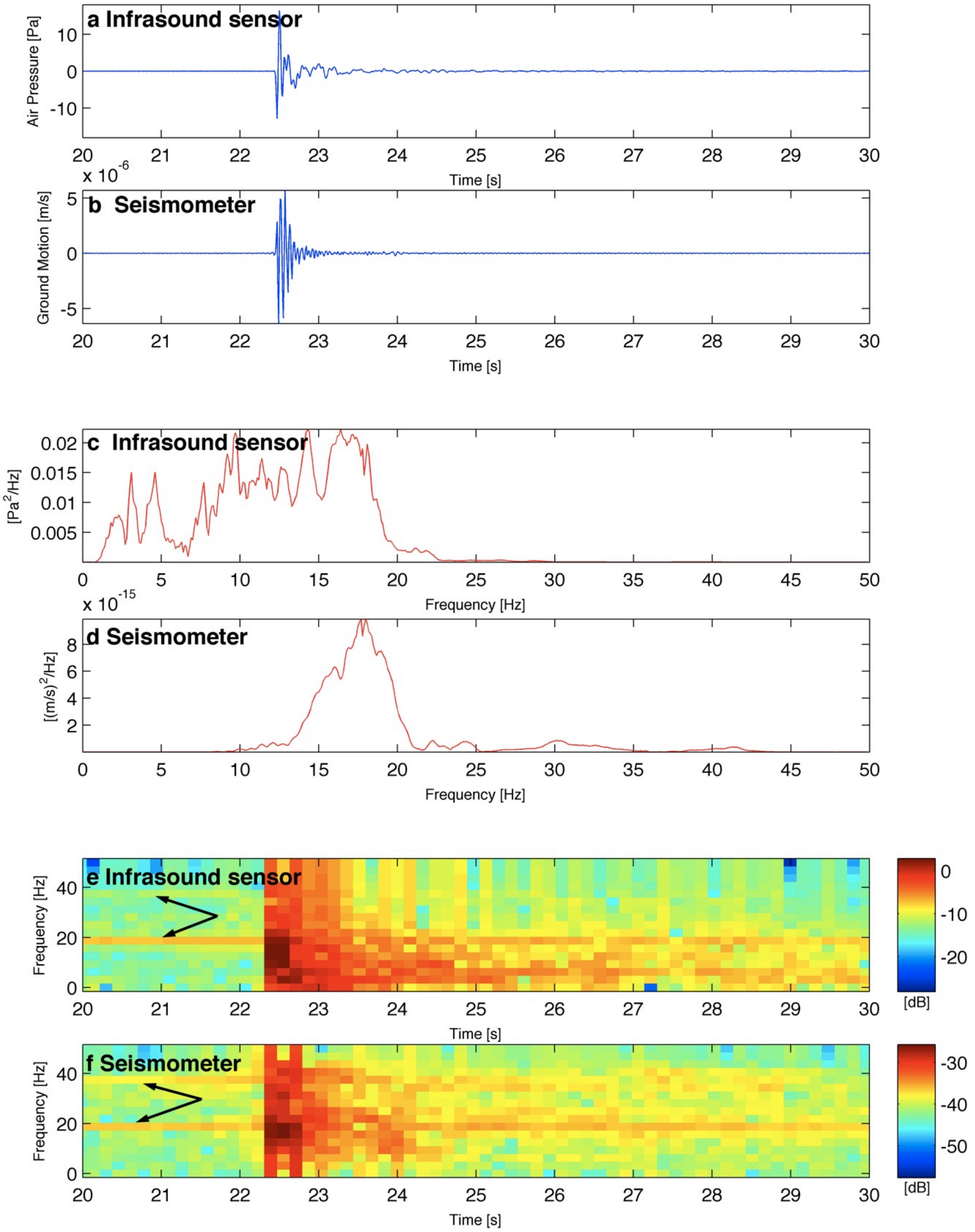

Figure 64: Infrasound and seismic (Z-component) data of an explosion in VDLS on 25.01.2009. Signals are represented with a common base of time. (a) Infrasound time series near the shelter; (b) Seismogram near the shelter; (c) Total spectrum of the infrasound signal; (d) Total spectrum of the seismic signal; (e) Running spectrum of the infrasound signal; (f) Running spectrum of the seismic signal. The black arrows indicate signal associated with the helicopter.

Figure 64 presents infrasound and seismic (Z component) data from an explosion (hand charge from a helicopter) to artificial trigger avalanches in VDLS on 25.01.2009. Unfortunately, in this case only a very small snow slide was released. The helicopter signal is not visible in the time series nor in the total spectra of both sensors. The explosion is clearly visible in the seismic (Z component) and infrasonic time series by a sudden increase in amplitudes for about one second (Fig 64a, b). The maximum amplitudes in the infrasound data are 12 Pa and in the seismic data $5x10^{-6}$ m/s in this case. However, the maximum amplitudes of the seismic and infrasound signals depend on the distance explosion-sensors and on the type and amount of explosive used. For comparison, the maximum infrasound amplitudes monitored in this study for snow avalanches are around 5 Pa (see Chapter 9). Maximum seismic amplitudes may vary from 10^{-3} m/s to 10^{-7} m/s depending on the location of the sensor.

The total spectrum of the infrasound data (Fig 64c) shows an energy distribution between 1 Hz to 20 Hz, whereas the most energy is concentrated between 12 Hz to 22 Hz in the seismic signal (Fig 64d).

In the running spectra of both sensors the explosion produces a significant increase in energy and frequency depicted by the dark red colors (Fig. 64e, f). The black arrows mark signal associated with helicopters, characterized by the two narrow horizontal lines at 19 Hz and 38 Hz in the seismic and infrasonic data. It can be concluded that infrasound signals produced by explosives are short in the time scale (about 1 s) and of higher energy and therefore significantly different from what can be expected from snow avalanches as reported above (Chapter 9).

Ski lifts

Ski lifts are a common source of audible sound. The movement of the single chairs over the wheels at the lift pillars is a source of sound as well as the sound emitted by the engines in the top- and valley stations. To study the acoustic emissions of ski lifts in the infrasonic frequency range the Chinese microphone MK 224 together with the Campbell CR100 datalogger were placed in between two valley stations (distance ca. 70 m from each) of two chair lifts in the ski resort Obertauern (Austria) in winter 2008. Please note that the sampling rate in this case was 60 Hz. Unfortunately no seismic sensor was available for this survey.

Figure 65 presents 100 s of infrasound data collected. In the time series (Fig. 65a) three periodic wave packages in the intervals [0 s to 15 s], [40 s to 50 s] and [80 s to 90 s] of similar amplitude (ca. 0.2 Pa) and length (ca. 10 s) are observed. These wave packages are separated by a constant period of ca. 30 s of low signal amplitude. Without having any additional measurements, it may be concluded that these periodic wave packages correspond to signals emitted by the chair lift.

The total spectrum (Fig. 65b) shows high energy in the frequency range between 1 Hz to 5 Hz, which can be attributed to the wave packages discussed above and a single energetic peak at 23 Hz of unknown source.

In the running spectrum (Fig. 65c) the three wave packages can be identified by the dark red colors in the same time intervals as in the time series, although less significant due to the little difference in signal energy compared to the ambient noise at this site.

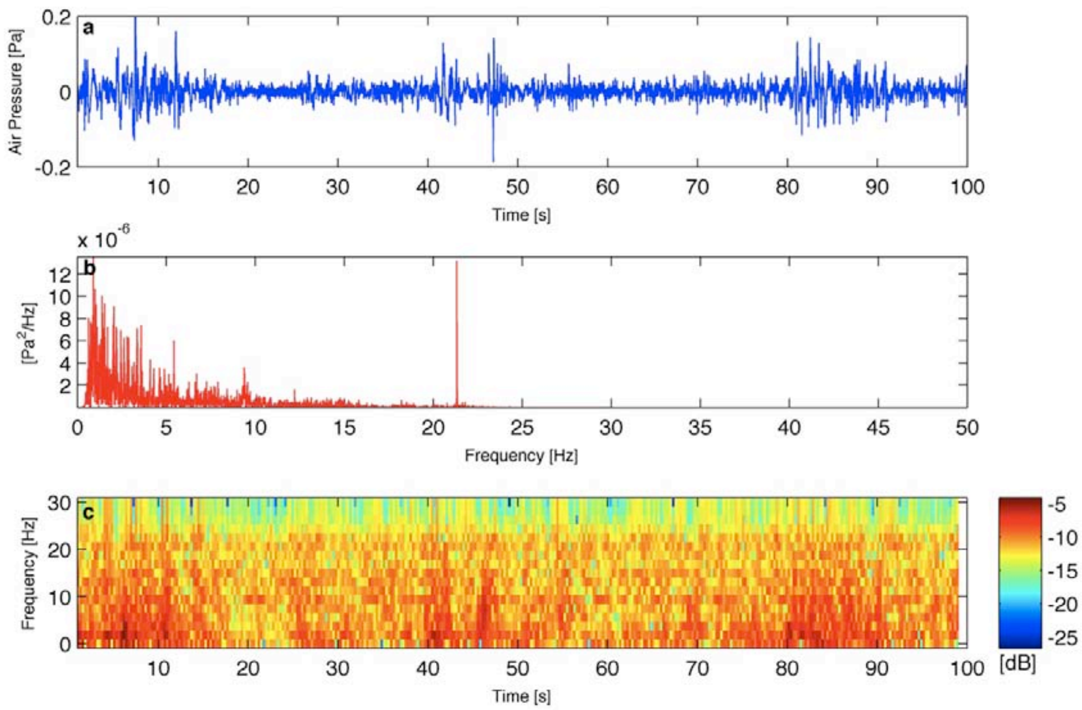

Figure 65: Infrasound data of a ski lift collected during winter 2008 in the ski resort Obertauern (Austria). (a) Infrasound time series; (b) Total spectrum of the infrasound signal; (c) Running spectrum of the infrasound signal. Please note that the sampling rate was 60 Hz

The maximum amplitudes in the time series are below 0.2 Pa, which is very small compared to other sources (e.g. snow avalanches, debris flows, explosions). The amount of data available from this study is limited and no seismic data was recorded; therefore further studies are needed, preferably in combination with a seismometer in order to classify the infrasound signals emitted by ski lifts.

Trains

Previous studies have primarily analysed infrasound signals produced by high-speed trains hitting a tunnel (Howe, 2002; Iida M. et al., 2007), and concluded that pressure fluctuations generated by high-speed trains are adversely affecting the area close to a tunnel portal. Cato (1976) analysed noise produced by the vibration of the train wheels and concluded that wheels are the dominant sources of noise and radiate as resonant dipoles. Takami and Kikuchi (2010) showed that the most significant source of low frequency noise from high-speed trains in the far field is aerodynamically generated unsteady flow, which is analogous to a line source.

However, not much work has been performed on infrasonic emissions in the near field of trains traveling at moderate velocities of about 90 km/h, as is the case in Austria or Switzerland and other Alpine regions. To investigate if trains produce significant infrasound and seismic emissions at low distances, which could possibly effect monitoring of alpine mass movements, we co-located seismic and infrasonic sensors with a distance of 30 m to the rails near the village of Pressbaum (Austria). At this location the trains pass with a velocity between 70 km/h and 90 km/h. We used the Chaparral Model 24 microphone with a sensitivity of 2 V/Pa and a natural frequency of 0.1 Hz and the geophone Sara GS 11 with a sensitivity of 90 V/m/s and a natural frequency of 4.5 Hz, both connected to a Reftek DAS 130 datalogger.

Figure 66 shows a time interval of 150 s with one train passing the sensor location. The total duration according to the infrasound and mainly the seismic data was 50s [1500 s to 1550 s]. The train signal can be identified in the time series of the infrasound sensor through an increase in energy but the maximum amplitudes are very low 0.4 Pa, not significantly higher from what can be expected due to ambient noise (ca. 0.2 Pa) at this location. In the seismogram an increase and decrease of amplitudes (spindle shape) is clearly observed and the maximum amplitudes are significantly higher ($5x10^{-6}$ m/s) than the ambient noise level (ca. $3x10^{-7}$ m/s).

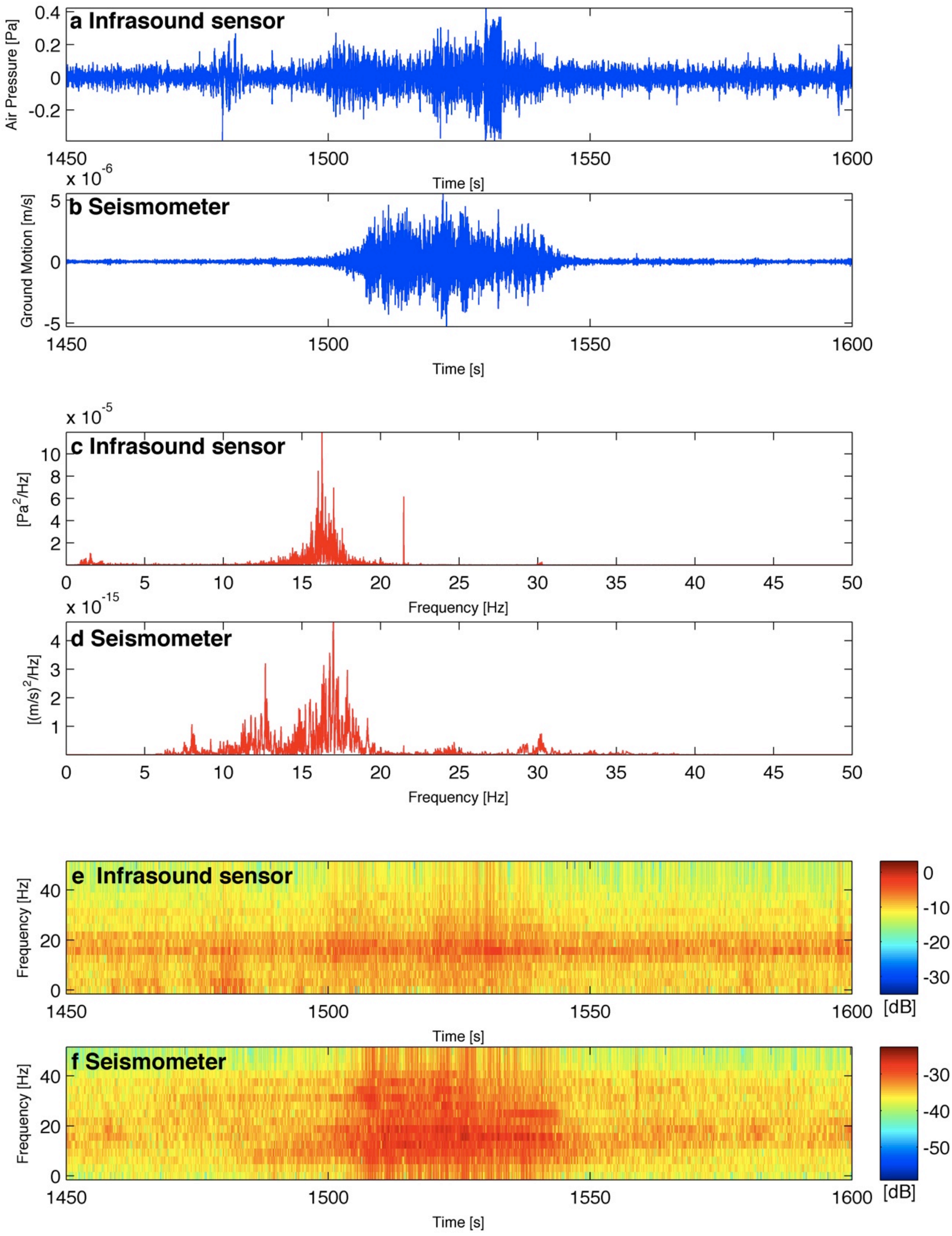

Figure 66: Infrasound and seismic (Z-component) data of a train passing the sensors, placed close to the rails, near Pressbaum (Austria). Signals are represented with a common base of time. (a) Infrasound time series; (b) Seismogram; (c) Total spectrum of the infrasound signal; (d) Total spectrum of the seismic signal; (e) Running spectrum of the infrasound signal; (f) Running spectrum of the seismic signal.

The total spectrum of the infrasound data presents a peak at 16 Hz, which can be associated with the railway electrification system (frequency of 16⅔ Hz in Austria)

(Fig. 66c). This peak at 16 Hz was also observed at other moments without trains. On the other hand the total spectrum of the seismic signal has energy in the frequency range between 5 Hz to 30 Hz with the most energy between 10 Hz to 20 Hz (Fig. 66d). In the running spectrum of the infrasound data the train produces no significant pattern (Fig. 66e). The most energy is concentrated in a band of noise between 15 Hz to 20 Hz. On the other hand in the running spectrum of the seismometer the train produces an increase in frequency and energy as it is approaching the sensors location and a decrease as it is moving away. It can be concluded that trains produce more energetic pressure fluctuations in the ground than in the air. The seismic signal of trains in the time series and in the running spectrum can be similar to alpine mass movements if not analysed in detail.

Monitoring with a combination of infrasound and seismic sensors, it is possible to identify a train mainly through the seismic signals but also to differentiate it from mass movement signals using the infrasound sensor. Infrasound signals of snow avalanches or debris flows mostly have higher amplitudes (>1 Pa) in the time series and a characteristic signal pattern in the running spectrum. Most importantly, for snow avalanches and debris flows the greatest infrasound signal energy is concentrated below 15 Hz, which should allow differentiation from train noise in the frequency domain.

Cars

Cars are a well-known source of audible sound as the countless kilometers of noise barriers along the main traffic routes depict. In previous studies the infrasound emissions of battlefield vehicles (trucks, tanks etc.) have been analysed for military detection purposes (Stubbs, 2005). Stubbs (2005) reported that he was not able to obtain significant acoustic energy for vehicles with a length of 10 m at frequencies below 20 Hz, the typical infrasound region. In order to investigate the acoustic emissions of cars and trucks in the infrasonic frequency range the Chinese microphone MK 224 with a Campbell CR1000 datalogger were placed close (distance <50 m) to the Autobahn A1 near the city of Vienna, Austria. Unfortunately no seismic sensor was available for this study.

Figure 67 shows 600 s of collected infrasound data. In the time series (Fig. 67a) multiple packages of 1 s to 5 s of higher amplitudes are observed, which can be associated with cars or trucks passing the sensor location. The maximum infrasound amplitudes produced are in the order of 0.2 Pa. Note that the cars passing the monitoring location probably have an average velocity of 120 km/h. The total spectrum (Fig. 67b) shows the most energy between 1 Hz to 20 Hz with a significant peak at 15 Hz. The running spectrum (Fig 67c) shows several vertical bands of high energy depicted by the dark red colors associated with the passing of cars or trucks.

In summary, infrasonic signals of cars are short-period peaks, with amplitudes smaller than what has been reported previously for Alpine mass movements (Chapters 7 to 9).

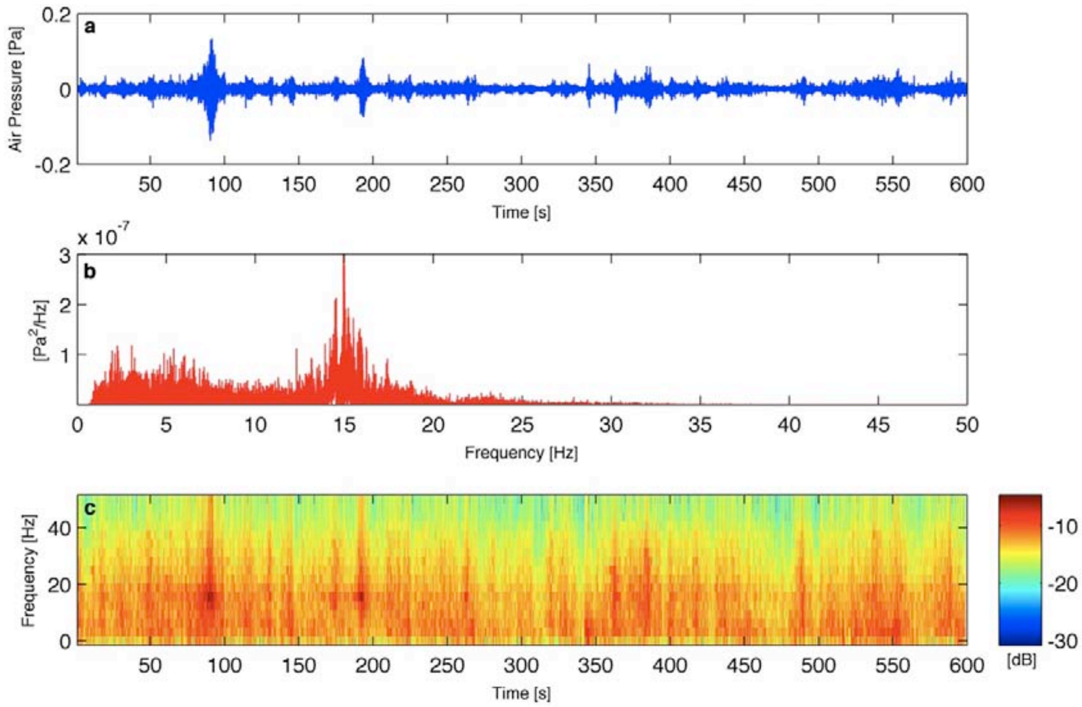

Figure 67: Infrasound data monitored close to the Autobahn A1 near the city of Vienna, Austria. (a) Infrasound time series; (b) Total spectrum of the infrasound signal; (c) Running spectrum of the infrasound signal.

Airplanes

Due to the great demand on mobility of the modern society, airplanes are ubiquitous in the sky and therefore their noise emission has to be considered when monitoring acoustic signals outdoors.

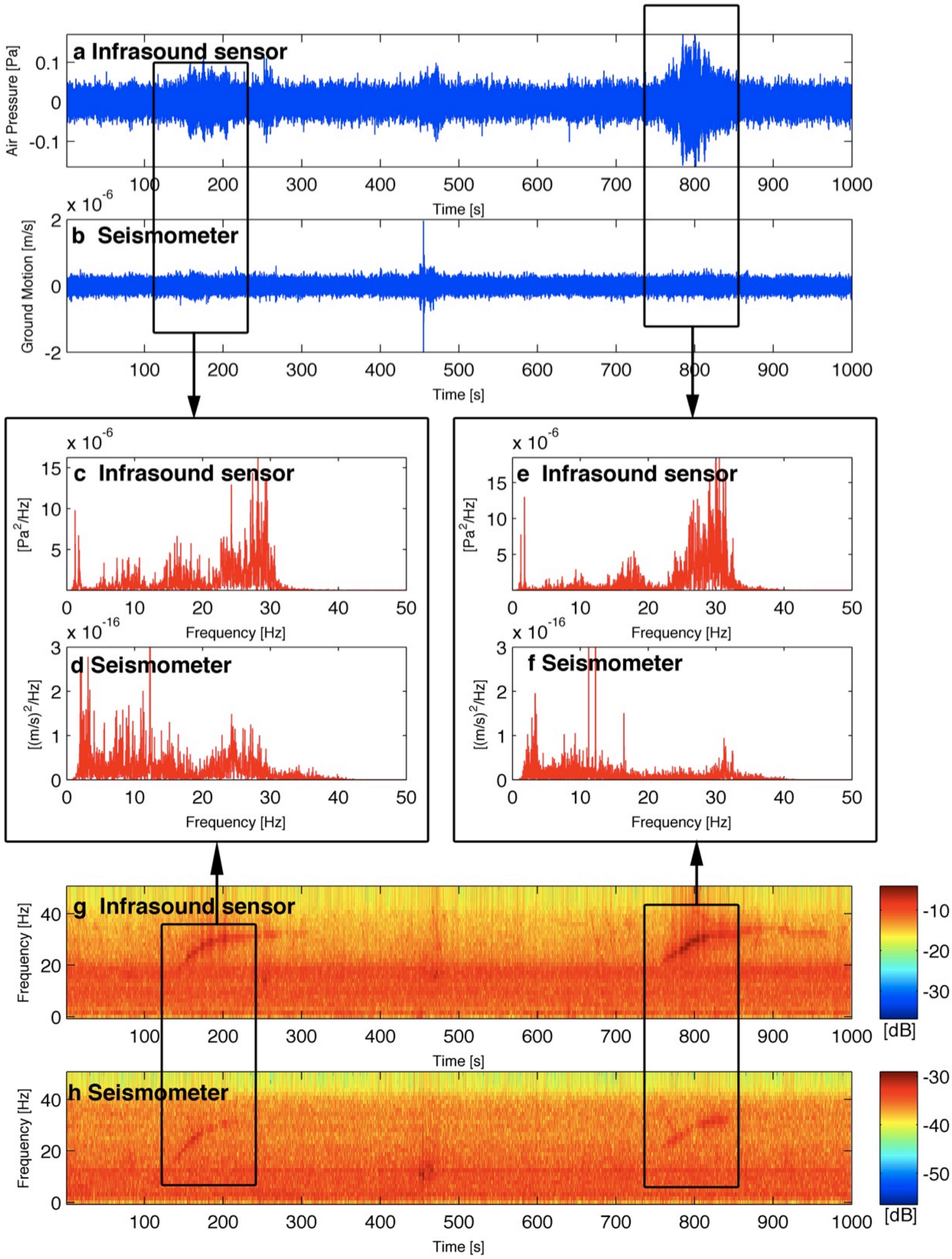

Figure 68: Infrasound and seismic (Z-component) data of airplanes monitored at the Illgraben test site in summer 2010. Signals are represented with a common base of time. The black rectangles mark signals associated with airplanes. (a) Infrasound time series; (b) Seismogram; (c) Total spectrum of the infrasound signal of the first rectangle; (d) Total spectrum of the seismic signal of the first rectangle; (e) Total spectrum of the infrasound signal of the second rectangle; (f) Total spectrum of the seismic signal of the second rectangle; (g) Running spectrum of the infrasound signal; (h) Running spectrum of the seismic signal.

Infrasonic signals originating from a sonic boom in the form of a N-wave pressure signature are frequently detected under the flight path of a supersonic aircraft (Grover, 1973; Donn, 1978).

As the shock wave propagates away from the aircraft, higher frequencies are attenuated and the resulting infrasonic components may be detected, depending on conditions, at distances of up to at least 4000 km from the flight path of the aircraft (Campus and Christie, 2010, and references therein). Infrasonic waves generated by commercial jet aircrafts at cruising altitude are frequently observed at many infrasound stations. In contrast with signals from supersonic aircrafts, the energy content of the waves is lower and therefore the range of detection is limited to about 40 km (Campus and Christie, 2010).

Figure 68 presents data monitored at the Illgraben test site in summer 2010 with the Chaparral Model 24 microphone and the Mark L4-3D seismometer, both connected to a Campbell CR 1000 datalogger. In the time series of the infrasound sensor (Fig. 68a) two wave packages associated with an airplane can be detected, [150 s to 250 s] and [750 s to 850 s] with a maximum amplitude of 0.15 Pa. No particular shape is visible in the time series of the seismic (Z component) data (max. amplitude 10^{-6} m/s) (Fig 68b). The total spectra of both sensors are calculated for the time interval of the two wave packages associated with airplanes, marked by the black rectangles. The total spectra of the infrasound data exhibit a similar shape and energy distribution. The most energy is in the frequency range between 25 Hz to 35 Hz (Fig. 68c, e). Also for the seismic data the two total spectra show a similar shape but the energy is concentrated at lower frequencies (< 10 Hz), probably associated with background noise (Fig 68d, f). The total spectra of both time intervals associated with airplane signals are similar and repetitiveness is seen. In the running spectra of both sensors the airplane is depicted by a thin red line of increasing frequency (Fig 68g, h). The signal is not very significant in both sensors due to similar energy content as the background noise level at this site.

The maximum amplitudes in the time series (0.15 Pa, 10^{-6} m/s), the frequency range of the signals in the total spectra (25 Hz to 35 Hz) and the pattern of the signals in the running spectra (thin line) are significantly different to infrasound and seismic signals observed from debris flows or snow avalanches.

Earthquakes

It is well known that earthquakes produce seismic as well as infrasound signals. While the seismic wavefield from earthquakes is comparatively well understood, the corresponding infrasonic wavefield is less well known (Arrowsmith et al., 2010). Atmospheric pressure changes associated with earthquakes have been observed in many previous studies (Mikumo, 1968; Olson et al., 2003; Kim et al., 2004; Le Pichon et al., 2005, Campus and Christie, 2010). Infrasound signals caused by earthquakes can be divided into three different types (Arrowsmith et al., 2010):

1. "local infrasound", i.e. infrasound generated by Rayleigh waves passing the receiver;
2. "epicentral infrasound", i.e. infrasound generated by surface pumping above the epicentre; and
3. "secondary infrasound", i.e. infrasound generated by the interaction of surface waves with topography such as a range of mountain.

Generation of atmospheric disturbance by earthquakes is often modeled by a simple relationship between ground velocity and the pressure change at the surface with an assumption that the time scale of the vertical motion is short compared with the acoustic cut-off period (Watada et al., 2006). Excess pressure in a homogenous fluid medium caused by the vertical motion is given by (Lighthill, 1978): $p = \rho * c_s * w$, where p is the excess pressure, ρ is the air density, c_s is the sound velocity and w is the velocity of the ground motion.

Figure 69 shows seismic (Z component) and infrasound data of the 2010 Chile earthquake monitored at the VDLS test site (Latitude: 46.2915802; Longitude: 7.37799978). The earthquake occurred off the coast of either the Maule Region or the Biobío Region of Chile (Latitude: -35.909; Longitude: -72.733) on February 27th, 2010, at 06:34 UTC, with a magnitude of 8.8 on the moment magnitude scale. The calculated travel time for Body waves is about 860 s and for Surface waves 3127 s to the VDLS test site (Δt= 2267 s). Figure 69a and b show the time series of the infrasound sensor and the seismometer, respectively.

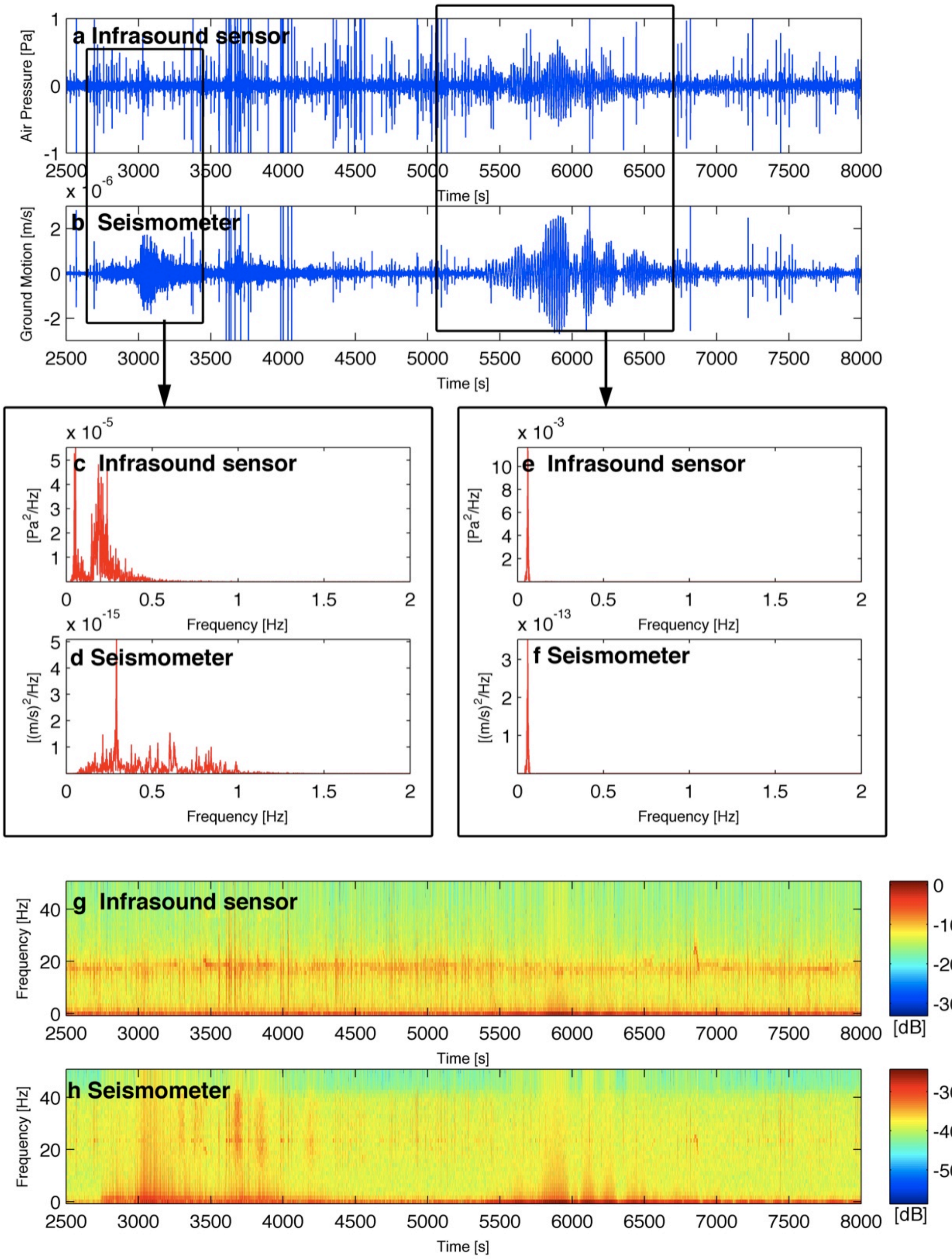

Figure 69: Infrasound and seismic (Z-component) data of the 2010 Chile earthquake monitored at the VDLS test site. Signals are represented with a common base of time. The black rectangles mark signals associated with the passing of seismic Body- and Surface waves, respectively. (a) Infrasound time series near the shelter; (b) Seismogram near the shelter; (c) Total spectrum of the infrasound signal of Body waves; (d) Total spectrum of the seismic signal of the Body waves; (e) Total spectrum of the infrasound signal of the Surface waves; (f) Total spectrum of the seismic signal of the Surface waves; (g) Running spectrum of the infrasound signal; (h) Running spectrum of the seismic signal.

The left rectangle marks the arrival of the Body waves at 2733 s. In the seismogram (Z component) in the shelter (Fig. 69b) an increase in amplitudes is visible whereas in the infrasound data nothing is observed (Fig. 69a). The right rectangle marks the passing of the Surface waves at 5024 s in the time series. Wave packages of similar shape and amplitude can be observed in both sensors (Fig. 69a, b).

The difference in arrival time $\Delta t = 2291$ s between the wave packages matches the calculated value ($\Delta t = 2267$ s). According to the classification of Arrowsmith et al. (2010) this would be type 1 “local infrasound” generated by Rayleigh waves near the receiver. Many short-period, high-energetic peaks can be observed in the time series of both sensors as well. The source of these peaks is unknown.

The total spectra (Fig. 69c, d) for the time interval corresponding to the passing of the Body Waves shows energy in the low frequency range (<1 Hz) in both sensors. For the time interval corresponding to the passing of the Surface waves (Fig. 69e, f) the energy band is even narrower showing a single peak in both sensors (ca. 0.1 Hz). Please note that the natural frequency of the Chaparral Model 24 infrasound microphone is 0.1 Hz and of the Mark L4 3D seismometer is 1 Hz. Therefore these sensors are not best for monitoring low frequency signals (<1 Hz). Signals below the natural frequency of the respective equipment can be considered as noise.

The running spectra of both sensors do not show any characteristic pattern (Fig. 69g, h). In the running spectrum of the infrasound data (Fig. 69g) a narrow band of noise centered at 19 Hz can be observed, which is associated with background signals at the site. In the running spectrum of the seismic data (Fig. 69h) higher energy below 1 Hz, depicted by the dark red colors, is observed in the time intervals of the passing of the Body- and Surface Waves [2700 s to 3500 s] and [5000 s to 6500 s] respectively.

Figure 70 shows infrasound and seismic data of the Lausanne earthquake (Latitude: 46.05; Longitude: 6.94) on 06.12.2010 at 06:41 UTC with a magnitude of 3.1, recorded at the VDLS test site. The distance between Lausanne and VDLS is 62 km. Unfortunately only data of the arrival of the Body waves is available. The Body wave arrival is clearly visible in the seismogram (Z component) by a sudden increase in amplitudes up to 2 x 10^{-5} m/s (Fig. 70b). In the infrasound data a slight increase in amplitudes can be observed (0.2 Pa), but not as significant as in the seismic data (Fig. 70a).

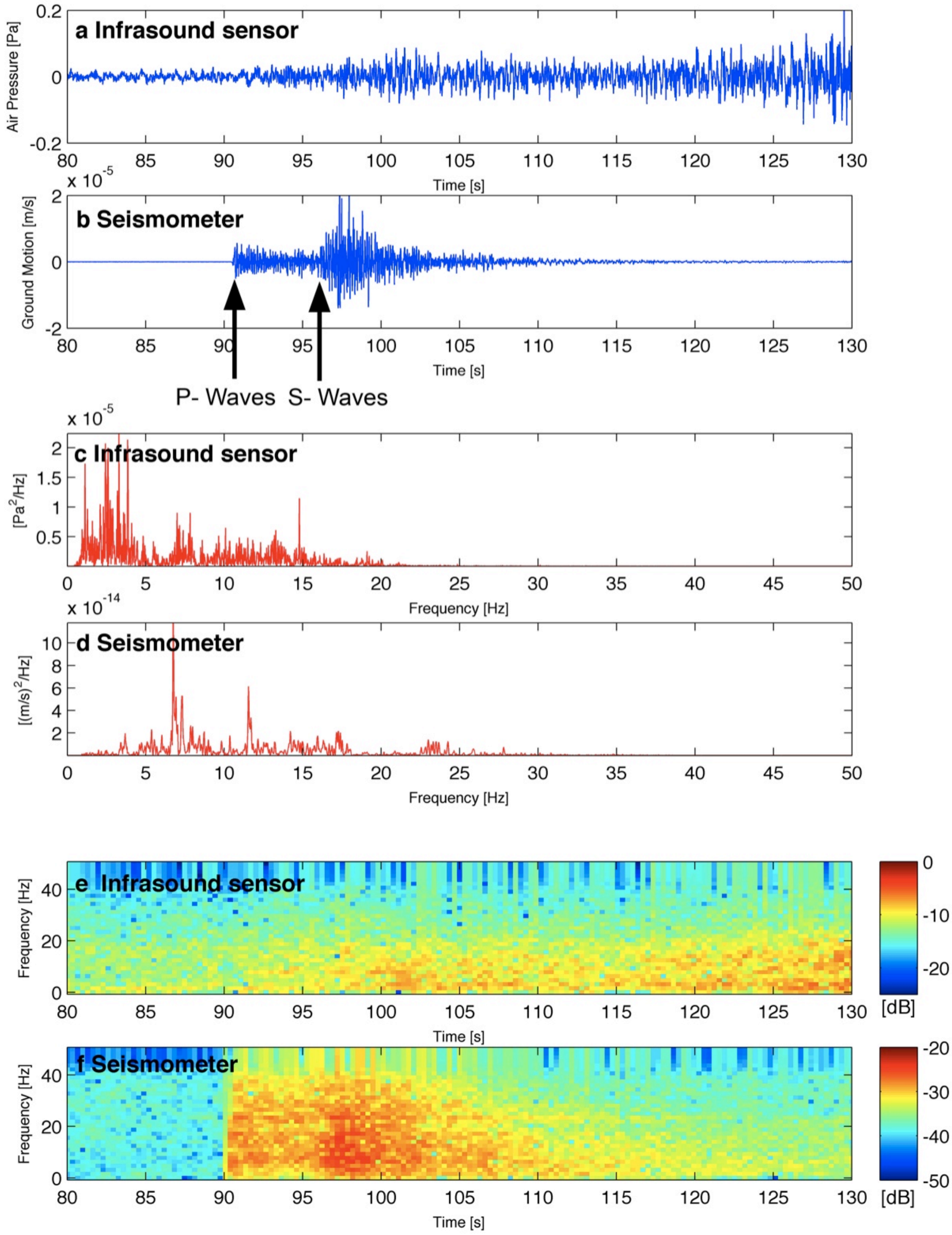

Figure 70: Infrasound and seismic (Z-component) data of the 2010 Lausanne earthquake monitored at the VDLS test site. Signals are represented with a common base of time. (a) Infrasound time series near the shelter; (b) Seismogram near the shelter, the arrival of P- and S Waves is indicated; (c) Total spectrum of the infrasound signal; (d) Total spectrum of the seismic signal; (e) Running spectrum of the infrasound signal; (f) Running spectrum of the seismic signal.

The total spectrum of the infrasound data shows an energy distribution between 1 Hz to 15 Hz (Fig. 70c), which can be associated with background noise. The seismic total spectrum shows two significant peaks at 7 Hz and 12 Hz (Fig. 70d).

In the running spectrum of the seismic signal the arrival of the Body waves (P- and S Waves) is observed by a sudden increase in energy depicted by the dark red colors (Fig. 70f). Please note that this shape is similar to the shape observed from explosions for seismic signals (see Fig. 64f). In the running spectrum of the infrasound data no characteristic pattern is observed (Fig. 70e). As the distance to the epicenter of the earthquake is low (<80 km) type 2, “epicentral infrasound” would be expected. However, probably the magnitude of the earthquake (3.1) was to create significant signals. The seismic signal of Body waves of local earthquakes in the time series and in the running spectrum can be confounded with signals from alpine mass movements if not analysed in detail. Monitoring with a combination of infrasound and seismic sensors, it is possible to identify earthquakes mainly through the seismic signals but also to differentiate it from mass movement signals using the infrasound sensor. Infrasound signals of snow avalanches or debris flows mostly have higher amplitudes (>1 Pa) in the time series and a characteristic signal pattern in the running spectrum.

Thunder

Thunderstorms are usually accompanied by strong winds and more importantly, heavy rain. These are possible sources of interfering noise when monitoring debris flows. Thunder is the acoustic emission produced by lightning. The sudden increase in pressure and temperature from lightning produces rapid expansion of the air surrounding and within a bolt of lightning (Few, 1985). In turn, this expansion of air creates a shock wave, which then propagates as audible thunder through the atmosphere (Assink et al., 2008). In contrast to “audible thunder” as described above, infrasonic thunder is produced by the conversion of the thundercloud electrostatic field to sound waves (Farges and Blanc, 2010).

Infrasound signals associated with thunderstorm and lightning have been analysed extensively in previous studies (e.g., Bowman and Bedard, 1971; Assink et al., 2008; Campus and Christie, 2010; Farges and Blanc, 2010).

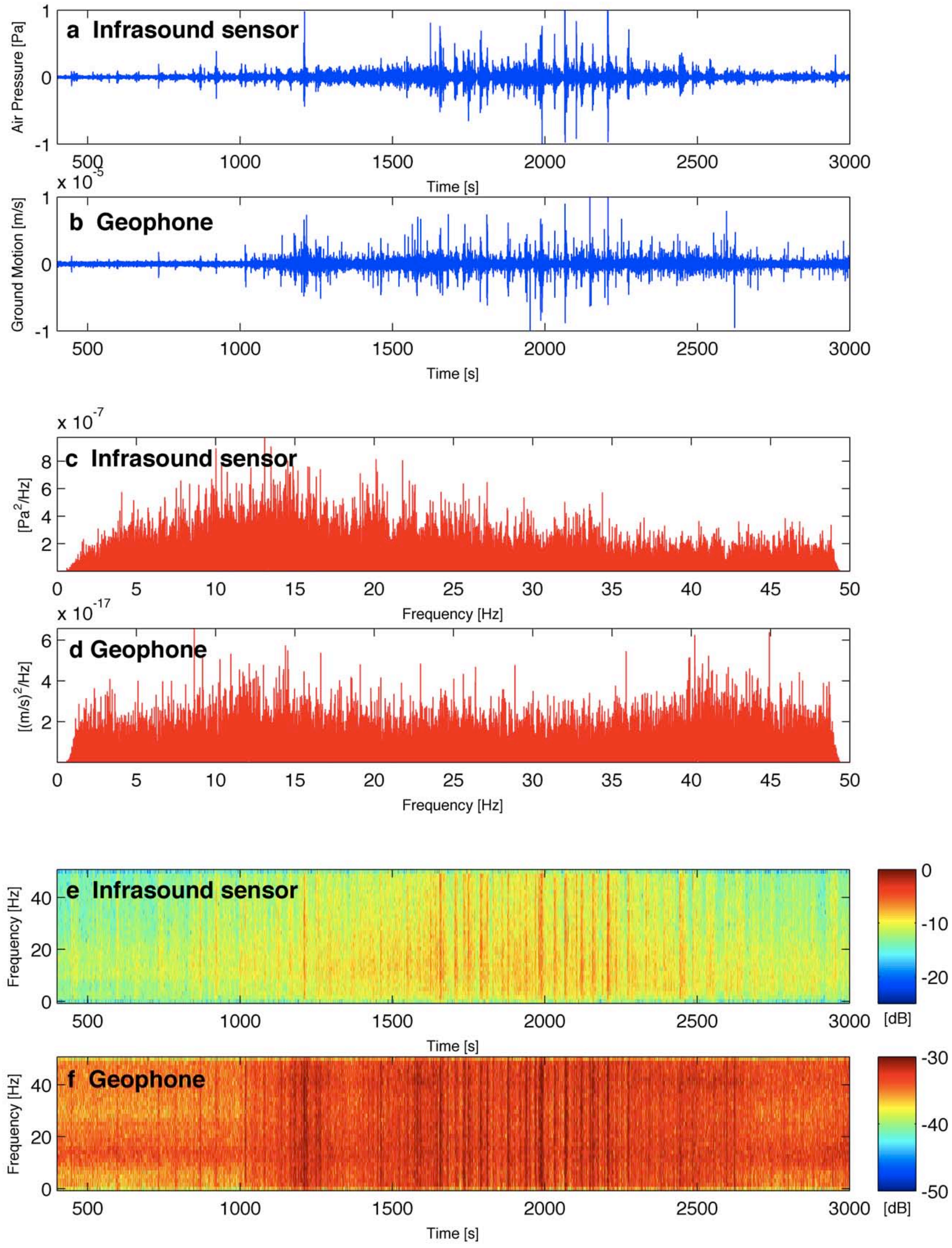

Figure 71: Infrasound and seismic (Z-component) data monitored during a thunderstorm at the Illgraben test site on 28.07.2009 (see Chapter 8, Fig. 35 and following). Signals are represented with a common base of time. (a) Infrasound time series; (b) Seismogram; (c) Total spectrum of the infrasound signal; (d) Total spectrum of the seismic signal; (e) Running spectrum of the infrasound signal; (f) Running spectrum of the seismic signal.

Infrasound waves generated by thunder propagate towards the ground and generate air to ground coupled seismic signals. Lin and Langston (2007) studied the seismic wave field produced by thunder concluding that thunder appears to be a useful seismic source to empirically determine site resonance characteristics.

Figure 71 presents infrasound and seismic data monitored during a thunderstorm at the Illgraben test site on 28.07.2009. The data has already been shown in Chapter 8 (see Fig. 35 and following). The data were collected using the Chinese MK224 infrasound microphone and a GS11 geophone, both connected to a Campbell CR23 datalogger. The intense rainfall produced by the thunderstorm caused a debris flood, which has already been discussed in Chapter 8. In the time series of both sensors (Fig 71a, b) several pulses lasting from 0.3 s to 1 s are simultaneously observed. The maximum amplitudes in the infrasound data are 1 Pa and $1x10^{-5}$ m/s in the seismogram. The passing of the thunderstorm over the sensors produces an increase and decrease of the amplitudes in both sensors.

In the total spectra of both sensors no significant peaks are observed, and the energy is spread over the whole frequency band (Fig 71c, d). In the running spectra of both sensors the thunder pulses are observed. Many dark-red vertical lines depict the short-period, high-energy pulses (Fig 71e, f).

The length of the signal in the time series (1 s) and the wide frequency distribution (1 Hz to 50 Hz) in both sensors is significantly different to what can be expected from debris flows. Infrasound and seismic signals of debris flows have a duration of several minutes and a lower frequency content (<20 Hz) as described in Chapter 7 and 8. Although it has to be considered, that an infrasound thunderstorm signal could mask the signal of a debris flow.

References:

Arrowsmith, S., Johnson, J., Drob, D. and Hedlin M. (2010): The seismoacoustic wavefield: A new paradigm in studying geophysical phenomena, Reviews of Geophysics, 48, RG4003, doi:10.1029/2010RG000335

Assink, J., Evers, L., Holleman, I. and Paulssen, H. (2008): Characterization of infrasound from lightning, Geophysical Research Letters, 35, L15802, doi:10.1029/2008GL034193

Becker, G. and Güdesen, A. (2000): Passive sensing with acoustics on the battlefield, Applied Acoustics, 59, 149-178

Biescas, B., Dufour, F., Furdada, G., Khazaradze, G. and Suriñach, E. (2003): Frequency content evolution of snow avalanche seismic signals, Surveys in Geophysics, 24, 447–464

Bowman, H. and Bedard, A. (1971): Observations of infrasound and subsonic disturbances related to severe weather, Geophysical Journal of the Royal Astronomical Society, 26 (1-4), 215-242

Campus, P. and Christie, D. (2010): Worldwide observations of infrasonic waves, in: Infrasound Monitoring for Atmospheric Studies, edited by: Le Pichon, A., Blanc, E. and Hauchecorne, A., Springer, 185-235

Cato, D. (1976): Prediction of environmental noise from fast electric trains, Journal of sound and vibration, 46(4), 483-500

Donn, W. (1978): Exploring the atmosphere with sonic booms, American Scientist, 66, 724-733

Farges, T. and Blanc, E. (2010): Characteristics of infrasound from lightning and sprites near thunderstorm areas, Journal Of Geophysical Research, 115, A00E31, doi:10.1029/2009JA014700.

Few, A. (1985): The production of lightning-associated infrasonic acoustic sources in thunderclouds, Journal Of Geophysical Research, 90(D4), 6175-6180, doi:10.1029/JD090iD04p06175

Ffowcs Williams, J. (1963): The noise from Turbulence Convected at High Speed, Philosophical Transactions of the Royal Society of London A, 255(1061), 469–503, doi: 10.1098/rsta.1963.0010

Grover, F. (1973): Geophysical effects of Concord sonic boom, Quarterly Journal of the Royal Astronomical Society, 14, 141-160

Gubler, H. (1977): Artificial release of avalanches by explosives, Journal of Glaciology, Vol. 19(81), 419-429

Howe, M. (2002): On the infrasound generated when a train enters a tunnel, Journal of Fluids and Structures, 17, 629-642

Iida, M., Kikuchi K. and Takami H. (2007): Infrasound Generated by a High-Speed Train Running Through a Short Tunnel, Journal of Low Frequency Noise, Vibration and Active Control, 26(3), 177-194

Kim, T., Hayward, C. and Stump, B. (2004): Local infrasound signals from the Tokachi-Oki earthquake, Geophysical Research Letters, 31, L20605, doi: I0.1 02912004GL021178

Le Pichon, A., Herry, P., Mialle, P., Vergoz, J., Brachet, N., Garcés, M., Drob, D. and Ceranna, L. (2005): Infrasound associated with 2004-2005 large Sumatra earthquakes and tsunami, Geophysical Research Letters, 32, L19802, doi: 10.1 029/2005GL023893

Lighthill, M. (1952): On sound generated aerodynamically I, General Theory, Proceedings of the Royal Society A, 211(1107), 564–587

Lighthill, M. (1954): On sound generated aerodynamically II. Turbulence as a source of sound, Proceedings of the Royal Society A, 222(1148), 1–32

Lighthill, J. (1978): Waves in Fluids, Cambridge University Press, New York

Lin, T. and Langston, C. (2007): Infrasound from thunder: A natural seismic source, Geophysical Research Letters, 34, L14304, doi:10.1029/2007GL030404

Long, L. (1983): The Compressible Aerodynamics of Rotating Blades Based on an Acoustic Formulation, NASA Technical Paper 2197, The George Washington University Joint Institute for Advancement of Flight Sciences Langley Research Center Hampton, Virginia

Mikumo, T. (1968): Atmospheric pressure waves and tectonic deformations associated with the Alaskan earthquake of March 28, 1964, Journal of Geophysical Research, 73, 2009-2025

Olson, J., Wilson, C. and Hansen, R. (2003): Infrasound associated with the 2002 Denali fault earthquake, Alaska, Geophysical Research Letters, 30(23), 2195, doi:lO.1029/2003GLOI8568

Scott, E. and Lance, C. (2002): Infrasonic Monitoring of Avalanche Activity, in: Proceedings International Snow Science Workshop, Penticton, British Columbia

Stubbs, C. (2005): Tactical infrasound, Technical report, The MITRE Corporation, Department of the Army United States Army Intelligence and Security Command National Ground Intelligence Center, Charlottesville, Virginia

Suriñach, E., Sabot, F., Furdada G. and Vilaplana, J. (2000): Study of seismic signals of artificially released snow avalanches for monitoring purposes, Physics and Chemistry of the Earth, 25(9), 721–727

Suriñach, E., Furdada, G., Sabot, F., Biescas, B. and Vilaplana, J. (2001): On the characterization of seismic signals generated by snow avalanches for monitoring purposes, Annals of Glaciology, 32, 268–274

Takami, H. and Kikuchi, K. (2010): Experimental investigation of low-frequency wayside noise from high-speed train, Quarterly Report of Railway Technical Research Institute, 51(1), 23-28

Watada, S., Kunugi, T., Hirata, K., Sugioka, H., Nishida, K., Sekiguchi, S., Oikawa, J., Tsuji, Y. and Kanamori, H. (2006): Atmospheric pressure change associated with the 2003 Tokachi-Oki earthquake, Geophysical Research Letters, 33, L24306, doi: 10.1029/2006GL027

Chapter 12

Conclusions

This study deals with the application of infrasound and seismic sensors for monitoring and characterization of snow avalanches and debris flows. For the first time, an in-depth study combining the infrasound and seismic wave fields generated by alpine mass movements has been carried out. We showed that the combination of infrasound and seismic sensors is a valuable tool for monitoring alpine mass movements and that: i) infrasound and seismic signals are correlated with each other and also with other measurements (e.g. flow depth for debris flows), ii) relevant information concerning the dynamics of the process can be gathered from the data and iii) the combination of both sensor technologies increases the detection probability.

The equipment used improved with the progress of the study, because of the problems encountered and knowledge gathered. More sensitive infrasound microphones (Chaparral Model 24) and seismic sensors (Mark L4 3D) along with high-resolution dataloggers (Reftek DAS 130) have significantly increased the quality of the data and thus the information gathered. However, the application of seismic and infrasound sensors for monitoring alpine mass movements is not a straightforward task. Thorough investigations of the study site and the background noise characteristics are necessary to determine the suitability for acoustic monitoring. Understanding the propagation and attenuation mechanisms of seismic and infrasonic waves in the study conditions is crucial for the interpretation of the recorded seismic and infrasonic signals. The equipment and the placement of the sensors (see Chapter 4 and 5) have to be chosen carefully, as shown by the results obtained in China (see Chapter 8, Guxiang Glacier and Midui Glacier).

During this study infrasound and seismic data of more than 10 snow avalanches were recorded at the VDLS test site and more than 5 torrential processes (debris flows and debris floods) were recorded in Switzerland and Austria. In addition, numerous sources of interfering signals were studied and discussed in Chapter 11. The detailed analysis of all the seismic and infrasonic signals allowed not only to find a characteristic evolution in the time and frequency domain for the specific processes studied, but also to make a clear differentiation from interfering signals. Our observations confirm results obtained for seismic signals produced by snow avalanches at VDLS (Switzerland), Nùria (Spain) and Ryggfonn (Norway) in previous studies (Biescas et al., 2003; Vilajosana 2007a, b). The present study confirms that snow avalanches and debris flows produce seismic and infrasonic signals characteristics that are reproducible at very different experimental sites and under different environmental conditions.

Besides the purpose of detection, seismic and infrasonic signals were used to determine relevant physical information related to the dynamics of the process.

For torrential processes it has been shown that the frequency content of the infrasound signals vary between debris flows and debris floods. Debris flows generally have lower peak frequencies in the infrasound signal (around 5 Hz) compared to debris floods (>7 Hz). The amplitude and frequency content of the seismic and infrasound signals increase as the debris flow moves towards the sensors. During the passage of the debris flow, the ultrasonic gauges identified several surges. The time series and the running spectra of the seismic and infrasonic data also recognize these surges. Concerning debris flows the relative detection capabilities of both sensors are strongly dependent on the terrain. At the Lattenbach torrent the infrasound sensor detects the debris flow before the seismic sensor, whereas at the Illgraben the opposite was observed. We believe that high mountain ridges, as is the case at the Illgraben, produce a natural sound barrier with an acoustic shadow zone behind. If the infrasound sensor is placed within this shadow zone the forecast time is significantly reduced. Seismic sensors provide signals in near real time due to the high seismic speed in the ground, but they are more sensitive to signal attenuation effects, strongly depending on the characteristics of the ground and the distance between source and receiver.

Concerning snow avalanches the sensors are sensitive to different avalanche regimes. More specifically we showed that infrasound sensors are more sensitive to the aerosol fluctuations (powder part), whereas seismic sensors are more sensitive to the vibrations generated by the dense flow. Thus, while infrasound sensors readily perceive avalanches in the early stages of an event, provided that the suspension part is present, the seismic sensors detect avalanches as soon as they have enough mass to generate signals that can be discriminated from the ambient noise. Infrasound signals showed a typical spindle shape in all the avalanches studied. Seismic signals monitored at the shelter showed an increase in amplitudes in a triangular shape as the avalanche approaches the sensor and high-energy peaks at the end associated with the stopping phase of the avalanche. Moreover seismic sensors seem more capable of monitoring wet dense flow avalanches. The combination of infrasound and seismic sensors allowed us to determine the total avalanche duration with high reliability and accuracy. The infrasound sensor proved more suitable for detecting avalanche initiation in the starting zone and the seismic sensor more suitable for estimating the end of the avalanche motion in the run out area.

We demonstrated that it was possible in all situations to clearly differentiate the infrasound and seismic signal of alpine mass movements from ambient noise. The most common sources of interfering signals have been summarized in Chapter 10 and their characteristic discussed in view of acoustic monitoring of alpine mass movements.

In summary, the initial motivation for this study, i.e. to investigate for the first time a combination of infrasound and seismic sensors for monitoring alpine mass movements, showed promising results. The combined analysis of the emitted infrasonic and seismic wavefield gives further insights on the process monitored. The author hopes that this study will stimulate interest in the field and encourage other scientists to get active in the fascinating work of low frequency monitoring.

References:

Biescas, B., Dufour, F., Furdada, G., Khazaradze, G. and Suriñach, E. (2003): Frequency content evolution of snow avalanche seismic signals, Surveys in Geophysics, 24, 447–464

Vilajosana, I., Khazaradze, G., Suriñach, E., Lied, E. and Kristensen, K. (2007a): Snow avalanche speed determination using seismic methods, Cold Regions Science and Technology, 49, 2–10

Vilajosana, I., Suriñach, E., Khazaradze, G., and Gauer, P. (2007b): Snow avalanche energy estimation from seismic signal analysis, Cold Regions Science and Technology, 50, 72–85

Chapter 13

Possible future implications

At the end of the present work, we are conscious that many scientific questions remain unresolved. It is obvious that new advanced data analysis techniques, the recent progresses in data communication technology and the development of wireless and energy efficient monitoring devices have the potential to provide new and valuable tools for monitoring and detection of alpine mass movements.

The present study showed that seismic and infrasound signals are correlated and complementary when monitoring natural hazards. Some characteristic features of the analysed signals could be used as statistical parameters for a detection process. This may include, for example: i) the signal duration, defined as the duration of the amplitude above a certain threshold value, ii) the frequency distribution, considering that alpine mass movements have signals varying over multiple frequencies, whereby elimination of narrow banded signals such as e.g. helicopters must be considered, and iii) the outline and the area of the mass movement signal pattern in the running spectrum. In addition, the obtained results show the potential of the combination of infrasonic and seismic sensors for detection of alpine mass movements.

Several signal-processing techniques have been developed in the recent years and proved to be useful for natural hazards detection. For example Bessason et al. (2007) suggested, based on statistical methods, a methodology to detect avalanche and debris flow activity. The authors used recorded seismic signals of snow avalanches and debris flows to identify statistical features of a given dataset as a calibration system. New snow avalanches and debris flows were then detected based on a nearest-neighbor method. Bessason et al. (2007) used ten parameters, such as peak value, power, total duration, etc., to characterize the statistical properties of the different events. Leprettre et al. (1998) used a similar approach but considered time, time-frequency and frequency representation of the different signals to identify statistical features of the data. Based on these parameters, the detection/no detection decision was made by implementing a fuzzy logic system.. Alasonati et al. (2006) used Markov chain systems to identify the seismic activity in Volcanoes, after a feature extraction techniques based on wavelet analysis. Vilajosana and Alasonati (2008) extended this approach to snow avalanche detection. Scott et al. (2007) used beam-forming techniques to detect snow avalanches through arrays of infrasonic sensors.

However, no joint approach of infrasonic and seismic sensors has been performed to date. The presented results suggest that the joint analysis of seismic and infrasonic signals could provide better information for alpine mass movement detection. As already suggested by Suriñach et al. (2005) the evolution of the frequency content in time of known events could be exploited for detection purposes. Vilajosana (2008) showed that three clearly identifiable parts (signal onset, signal body, signal tail) on the avalanche seismic signals exist. In Chapter 7 and 8 we showed that infrasonic signals of debris flows also show this behaviour. Both seismic and infrasonic signals showed specific features that may be suited for detection purposes (e.g. frequency content, signal length, signal parts such as onset, body, tail, signal shape). For example, a pattern recognition and classification algorithm may be suited to identify these features after being extracted.

Among the classification techniques Alasonati et al. (2006) showed the potential of Hidden Markov models. Gómez and Kavzoglu (2005) showed that artificial neural networks can be used for the classification of signals from landslide for detection purposes. The big advantage of artificial neural networks is the possibility of learning. The large database, which has been collected throughout this study, may help on training the system through semi-supervised learning techniques.

Finally, the computational power of new embedded devices has allowed a tremendous upsurge in recent years and new wireless sensor devices become more and more efficient (e.g., Swami et al. 2007). The combination of seismic and infrasound sensors suggest the possibility of building complex detection schemes for the extraction and classification of signal features which could be computed almost in real time with wireless, battery powered devices in remote areas.

References

Alasonati, P., Wassermann, J. and Ohrnberger, M. (2006): Signal classification by wavelet-based hidden Markov models: application to seismic signals of volcanic origin, Mader, H.M., Coles, S.G., Conner, C.B. and Conner, L.J. (eds.), Statistics in Volcany, 161-173, Geological Society, London

Bessason, B., Eirìksson, G., Thoŕorinsson, Ò., Thoŕorinsson, A. and Einarsson, S. (2007): Automatic detection of avalanches and debris flows by seismic methods, Journal of Glaciology, 53, 461–472

Gómez, H. and Kavzoglu, T. (2005): Assessment of shallow landslide susceptibility using artificial neural networks in Jabonosa River Basin, Venezuela, Engineering Geology, 78, 11-27

Leprettre, B., Martin, N., Glangeaud, F. and Navarre, J. (1998): Three-Component Signal Recognition Using Time, Time-Frequency and Polarization Information-Application to Seismic Detection of Avalanches, IEEE Transactions on Signal Processing, 46, 83–102

Scott, E., Hayward, C., Kubichek, R., Hamann, J., Comey, R., Pierre, J. and Mendenhall, T. (2007): Single and multiple sensor identification of avalanche-generated infrasound, Cold Regions Science and Technology, 47, 159–170

Suriñach, E., Vilajosana, I., Khazaradze, G., Biescas, B., Furdada, G. and Vilaplana, J. (2005): Seismic detection and characterization of landslides and other mass movements, Natural Hazards and Earth System Sciences, 5, 791–798

Swami, A., Zhao, Q., Hong, Y. and Tong, L. (2007): Wireless sensor networks, signal processing and communications perspectives, John Wiley and Sons Ltd, England

Vilajosana, I. (2008): Seismic detection and characterization of snow avalanches and other mass movements, PhD thesis, Universitat de Barcelona, Department de Geodinámica i Geofísica, Facultat de Geologia

Chapter 14

References

Adam, V., Chritin, V., Rossi, M. and Bolognesi, R. (1997): Acoustic detection system for operational avalanche forecasting, in: Proceedings International Snow Science Workshop, Banff, Alberta, 149–153

Aki, K. and Richards, P. (1980): Quantitative Seismology, A Series of Books in Geology,1, W.H. Freeman and Company, New York, USA

Alasonati, P., Wassermann, J. and Ohrnberger, M. (2006): Signal classification by wavelet-based hidden Markov models: application to seismic signals of volcanic origin, Mader, H.M., Coles, S.G., Conner, C.B. and Conner, L.J. (eds.), Statistics in Volcany, 161-173, Geological Society, London

Albert, D. and Orcutt, J. (1989): Observations of low frequency acoustic to seismic coupling in the summer and winter, Journal of the Acoustical Society of America, 86(1), 352-359

Albert, D. and Orcutt, J. (1990): Acoustic pulse propagation above grassland and snow: Comparison of theoretical and experimental waveforms, Journal of the Acoustical Society of America, 87 (1), 93-100

Albert, D., Decato, S. and Carbee, D. (2008): Snow cover effects on acoustic sensors, Cold Regions Science and Technology, 52, 132–145

Alcoverro, B., Martysevich, P. and Starovoit, Y. (2005): Mechanical sensitivity of microbarometers MB2000 (DASE, France) and Chaparral5 (USA) to vertical and horizontal ground motion, Inframatics, 9, March 2005, 1-10

Amundson, J., Truffer, M., Lüthi, M., Fahnestock, M., West M. and Motyka R. (2008): Glacier, fjord, and seismic response to recent large calving events, Jakobshavn Isbræ, Greenland, Geophysical Research Letters, 35, L22501, 1-5, doi:10.1029/2008GL035281

Arattano, M. (1999): On the use of seismic detectors as monitoring and warning systems for debris flows, Natural Hazards and Earth System Sciences, 20,197–213

Arattano, M. (2000): On debris flow front evolution along a torrent, Natural Hazards and Earth System Sciences, 25(9), 733–740

Arattano, M. and Marchi, L. (2000): Video-derived velocity distribution along a debris flow surge, Physics and Chemistry of the Earth, Part B, 25, 781–784

Arattano, M. (2003): Monitoring the presence of the debris-flow front and its velocity through ground vibrations detectors, Proceedings of the Third International Conference on Debris-Flow Hazards Mitigation: Mechanics, Prediction and Assessment, Millpress, Rotterdam, 2, 731-743

Arnoult, K., Wilson, C., Olson, J. and Szuberla, A. (2005): Infrasound associated with Mt. Steller Avalanche, Inframatics, 12, December 2005, 4-7

Arrowsmith, S., Hedlin, M., Stump, B. and Arrowsmith, M. (2008): Infrasonic signals from large mining explosions, Bulletin of the Seismological Society of America, 98(2), 768-777 doi:10.1785/0120060241.

Arrowsmith, S., Burlacu, R., Whitaker, R. and Randall G. (2009): A repeating secondary source of infrasound from the Wells, Nevada, earthquake sequence, Geophysical Research Letters, 36, L11817, doi:10.1029/2009GL038363

Arrowsmith, S., Johnson, J., Drob, D. and Hedlin M. (2010): The seismoacoustic wavefield: A new paradigm in studying geophysical phenomena, Reviews of Geophysics, 48, RG4003, doi:10.1029/2010RG000335

Artru, J., Farges, T. and Lognonné P. (2004): Acoustic waves generated from seismic surface waves: propagation properties determined from Doppler sounding observations and normal-mode modelling, Geophysical Journal International, 158, 1067–1077

Assink, J., Evers, L., Holleman, I. and Paulssen, H. (2008): Characterization of infrasound from lightning, Geophysical Research Letters, 35, L15802, doi:10.1029/2008GL034193

Aulitzky, H. (1980): Preliminary two-fold classification of debris torrents, International Symposium Interpraevent IV, Bad Ischl, Austria, 285-309 (translated to English by G. Eisbacher)

Badoux, A., Graf, C., Rhyner, J., Kuntner, R. and McArdell, B. (2009): A debris-flow alarm system for the alpine Illgraben catchment: design and performance, Natural Hazards and Earth System Sciences, 49, 517–539

Barbolini, M. and Issler, D. (2006): Avalanche Test Sites and Research Equipment in Europe: An Updated Overview, Final-report deliverable D8, SATSIE avalanche studies and model validation in Europe

Bass, H., Bauer, H. and Evans, L. (1972): Atmospheric absorption of sound: Analytical expressions, Journal of the Acoustical Society of America, 52, 821-825

Becker, G. and Güdesen, A. (2000): Passive sensing with acoustics on the battlefield, Applied Acoustics, 59, 149-178

Bedard, A., Greene, G., Intrieri, J. and Rodriguez, R. (1988): On the Feasibility and Value of Detecting and Characterizing Avalanches Remotely by Monitoring Radiated Sub-Audible Atmospheric Sound at Long Distances, in Proceedings: A Multidisciplinary Approach to Snow Engineering, Santa Barbara, CA, 1-9

Bedard, A. (1989): Detection of avalanches using atmospheric infrasound, in: Proceedings of the Western Snow Conference, edited by: Shafer, B., Western Snow Conference, Colorado State University, 52–58

Bedard, A. (1994): An Evaluation of Atmospheric Infrasound for Monitoring Avalanches, Proceedings; 7th International Symposium on Acoustic Sensing and Associated Techniques of the Atmosphere and Oceans, Boulder, CO

Benioff, H., Ewing, E. and Press, F. (1951): Sound wave in the atmosphere generated by a small earthquake, Proceedings of the National Academy of Sciences of the United States of America, 37, 600-603.

Bessason, B., Eirìksson, G., Thoŕorinsson, Ò., Thoŕorinsson, A. and Einarsson, S. (2007): Automatic detection of avalanches and debris flows by seismic methods, Journal of Glaciology, 53, 461–472

Biescas, B. (2003): Aplicacíon de la sismología al estudio y detección de aludes de nieve, Ph.D. thesis, Universitat de Barcelona, Grup d'Allaus UB, Departament de Geodinàmica i Geofísica

Biescas, B., Dufour, F., Furdada, G., Khazaradze, G. and Suriñach, E. (2003): Frequency content evolution of snow avalanche seismic signals, Surveys in Geophysics, 24, 447–464

Blackstock, D. (2000): Fundamentals of Physical Acoustics, Wiley Interscience Publications

Bowman, H. and Bedard, A. (1971): Observations of infrasound and subsonic disturbances related to severe weather, Geophysical Journal of the Royal Astronomical Society, 26 (1-4), 215-242

Brachet, N., Brown, D., Le Bras, R., Cansi, Y., Mialle, P. and Coyne, J. (2010): Monitoring the Earth's Atmosphere with the Global IMS Infrasound Network, in: Infrasound Monitoring for Atmospheric Studies, edited by: Le Pichon, A., Blanc, E. and Hauchecorne, A., Springer, 77-119

Brodsky, E., Gordeev, E. and Kanamori, H. (2003): Landslide basal friction as measured by seismic waves, Geophysical Research Letters, 30(24), 2236, doi:10.1029/2003GL018485

Campus, P. and Christie, D. (2010): Worldwide observations of infrasonic waves, in: Infrasound Monitoring for Atmospheric Studies, edited by: Le Pichon, A., Blanc, E. and Hauchecorne, A., Springer, 185-235

Cato, D. (1976): Prediction of environmental noise from fast electric trains, Journal of sound and vibration, 46(4), 483-500

Che, I., Shin, J. and Kang, I. (2009): Seismo-acoustic location method for small-magnitude surface explosions, Earth Planets Space, 61, e1–e4

Cho, C., Chou, P., Chung, Y., King, C., Tsai, M., Lee, B. and Chou T. (2008): Wireless Sensor Networks for Debris Flow Observation, in: Proceedings 2nd International Conference on Urban Disaster Reduction, IEEE Xplore, 615-617

Chou, H., Cheung, Y. and Zhang, S. (2007): Calibration of infrasound monitoring system and acoustic characteristics of debris-flow movement by field studies, in: Chenglung, C., Major, J. (eds.) Debris-flow Hazards Mitigation: Mechanics, Prediction, and Assessment, Millpress, Rotterdam, 571–580

Christen, M., Kowalski, J. and Bartelt, P. (2010): RAMMS: Numerical simulation of dense snow avalanches in three dimensional terrain, Cold Regions Science and Technology, 63, 1–14, doi:10.1016/j.coldregions.2010.04.005

Chritin, V., Rossi, M., Bolognesi, R. (1996): Acoustic Detection System for Operational Avalanche Forecasting, in: Proceedings of the International Snow Science Workshop, Banff, Alberta

Comey, R. and Mendenhall, T. (2004): Recent Studies Using Infrasound Sensors to Remotely Monitor Avalanche Activity, in: Proceedings of the International Snow Science Workshop, Jackson Hole, Wyoming, 640–646

Crighton, D. (1975): Basic Principles of Aerodynamic Noise Generation, Progress in Aerospace Sciences, 16, 31–96

Curle, N. (1955): The influence of solid boundaries upon aerodynamic sound, Proceedings of the Royal Society London A, 231(1187), 505–514, doi: 10.1098/rspa.1955.0191

Donn, W. (1978): Exploring the atmosphere with sonic booms, American Scientist, 66, 724-733

Drob, D. and Picone, J. (2003): Global morphology of infrasound propagation, Journal of Geophysical Research, 108(21), 4680, doi:10.1029/2002JD003307

Edwards, W., Eaton, D., McCausland, P., ReVelle, D. and Brown, P. (2007): Calibrating infrasonic to seismic coupling using the Stardust sample return capsule shockwave: Implications for seismic observations of meteors, Journal of Geophysical Research, 112, B10306, doi:10.1029/2006JB004621

Edwards, W., Eaton, D. and Brown, P. (2008): Seismic observations of meteors: Coupling theory and observations, Reviews of Geophysics, 46, RG4007, doi:10.1029/2007RG000253

Embleton, T., Piercyand, J. and Olson, N. (1976): Outdoor sound propagation over ground of finite Impedance, Journal of the Acoustical Society of America, 59, 267-277

Evans, L., Bass, H. and Sutherland, L. (1972): Atmospheric absorption of sound: theoretical predictions, Journal of the Acoustical Society of America, 51 (5), 1565-1575

Evernden, J., Archambeau C. and Cranswick E. (1986): An evaluation of seismic decoupling and underground nuclear test monitoring using high-frequency seismic data, Reviews of Geophysics, 24(2), 143–215, doi:10.1029/RG024i002p00143

Farges, T. and Blanc, E. (2010): Characteristics of infrasound from lightning and sprites near thunderstorm areas, Journal Of Geophysical Research, 115, A00E31, doi:10.1029/2009JA014700

Few, A. (1985): The production of lightning-associated infrasonic acoustic sources in thunderclouds, Journal Of Geophysical Research, 90(D4), 6175-6180, doi:10.1029/JD090iD04p06175

Ffowcs Williams, J. (1963): The noise from Turbulence Convected at High Speed, Philosophical Transactions of the Royal Society of London A, 255(1061), 469–503, doi: 10.1098/rsta.1963.0010

Ffowcs Williams, J. and Hawkings, D. (1969): Sound Generation by Turbulence and Surfaces in Arbitrary Motion, Philosophical Transactions of the Royal Society of London A, 264(1151), 321–342, doi:10.1098/rsta.1969.0031

Ffowcs Williams, J. (1977): Aeroacoustics, Annual Review of Fluid Mechanics, 9, 447–468, doi: 10.1146/annurev.fl.09.010177.002311

Firstov, P., Sukhanov, L., Pergament, V. and Rodionovskiy, M. (1992): Acoustic and seismic signal from snow avalanches, Transactions (Doklady) of the U.S.S.R., Academy of Sciences: Earth Science Sections, 312, 67–71

Gauer, P., Kern, M., Kristensen, K., Lied, K., Rammer, L. and Schreiber, H. (2007): On pulsed Doppler radar measurements of avalanches and their implication to avalanche dynamics, Cold Regions Science and Technology, 50, 55–71

Gauer, P., Issler, D., Lied, K., Kristensen, K., Iwe, H., Lied, E., Rammer, L. and Schreiber, H. (2007): On full-scale avalanche measurements at the Ryggfonn test site, Norway, Cold Regions Science and Technology, 49(1), 39–53

Gauer, P., Issler, D., Lied, K., Kristensen, K. and Sandersen, F. (2008): On snow avalanches flow regimes: Inferences from observations and measurements, in: Proceedings International Snow Science Workshop, 717–723, Whistler

Genevois, R., Tecca, P., Breti, M. and Simoni, A. (2000): Debris-flow in the Dolomites: Experimental data from a monitoring system, in: Debris-Flow Hazards Mitigation: Mechanics, Prediction, and Assessment, edited by: Wieczorek, G. F. and Naeser, N. D., Proc. 2nd Intern. Conf., Taipei, Taiwan, 16–18 August 2000, Rotterdam, Balkema Press, 283–291

Genevois, R., Gaigaro, A. and Tecca, P. R. (2001): Image analysis for debris flow properties estimation, Physics and Chemistry of the Earth, Part C, 26, 623–631

Gómez, H. and Kavzoglu, T. (2005): Assessment of shallow landslide susceptibility using artificial neural networks in Jabonosa River Basin, Venezuela, Engineering Geology, 78, 11-27

Graf, C., Badoux, A., McArdell, B., Dufour, F., Rhyner, J. and Kuntner, R. (2006): A warning system for natural hazards in summer at the Illgraben, 4th Swiss Geoscience Meeting, Bern

Grover, F. (1973): Geophysical effects of Concord sonic boom, Quarterly Journal of the Royal Astronomical Society, 14, 141-160

Gubler, H. (1977): Artificial release of avalanches by explosives, Journal of Glaciology, Vol. 19(81), 419-429

Günther, B., Hansen, K. and Veit, I. (2002): Technische Akustik- Ausgewählte Kapitel, 7,Expert Verlag

Hadley, K. and Lahusen R. (1991): Deployment of an acoustic flow monitor system and examples of its application at Mount Pinatubo, Philippines (abstract), Eos Trans, AGU, 72(44), F67.

Hagerty, M., Kim, W. and Martysevich, P. (2002): Infrasound detection of large mining blasts in Kazakhstan, Pure and Applied Geophysics, 159, 1063–1079, doi:10.1007/s00024-002-8673-3.

Harrison, J. (1976): Seismic Signals from Avalanches, Chapter 7 in: Avalanche Release and Snow Characteristics, San Juan Mountain, Colorado, Final Report San Juan Avalanche Project, Institute of Arctic and Alpine Research, U. of Colorado, Boulder, CO, Editors: R. L. Armstrong and J. D. Ives, 145-152

Hayward, C. and Pankow, K. (2008): Obervations of infrasound to seismic coupling at Earthscope stations using co located infrasound microphones, AGU Fall Meeting Abstracts, abstract #S33B-1945

Hedlin, M. and Berger, J. (2001): Evaluation of infrasonic noise reduction filters, in: Proceedings 23rd Seismic Research Review: Worldwide Monitoring of Nuclear Explosions, 121-130

Hirschberg, A. and Rienstra, S. (2004): An introduction to aeroacoustics, Technical report, Eindhoven University of Technology, Dept. of App. Physics and Dept. of Mathematics and Comp. Science

Howe, M. (2002): On the infrasound generated when a train enters a tunnel, Journal of Fluids and Structures, 17, 629-642

Huang, C., Yin, H. and Shieh, C. (2003): Experimental study of the underground sound generated by debris flow, in: Proceedings of the Third International Conference on Debris-Flow Hazards Mitigation: Mechanics, Prediction and Assessment, Millpress, Rotterdam, 2, 731-743

Huang, C., Yin, H., Chen, C., Yeh, C. and Wang C. (2007): Ground Vibrations produced by rock motions and debris flow, Journal of Geophysical Research, 112, F02014, doi:10.1029/2005JF000437

Huang, C., Yeh, C., Chen, C. and Chang, S. (2008): Ground vibrations and airborne sounds generated by motion of rock river bed, Natural Hazards and Earth System Sciences, 8, 1139-1147

Hübl, J. and Moser, M. (2006): Risk management in Lattenbach: a case study from Austria. In: Lorenzi G, Brebbia C, Emmanouloudis D (eds.) Monitoring, Simulation, Prevention and Remediation of Dense and Debris Flows, WIT Press, Southamption, 333-342

Hübl, J., Zhang, S. and Kogelnig, A. (2008): Infrasound measurements of debris flow, In: De Wrachien, D., Brebbia, C.A., Lenzi, M.A. (Eds.), WIT Transactions on Engineering Sciences, 60, Second International Conference on Monitoring, Simulation, Prevention and Remediation of Dense and Debris Flows II, *17.-19*. Juni 2008, The New Forest, 3-12; ISSN 1743-3533

Hungr, O., Evans, S., Bovis, M. and Hutchinson, J. (2001): A review of the classification of landslides of the flow type, Environmental and Engineering Geoscience, 7(3), 221–238, doi:10.2113/gseegeosci.7.3.22

Hurlimann, M., Rickenmann, D. and Graf, D. (2003): Field and monitoring data of debris-flow events in the Swiss Alps, Canadian Geotechnical Journal, 40, 161–175

Hutchinson, J. (1988): General Report: morphological and geotechnical parameters of landslides in relation to geology and hydrogeology. In: Bonnard, C. (Editor), Proceedings, Fifth International Symposium on Landslides, A.A: Balkema, Rotterdam, 1, 3-36

Iida, M., Kikuchi K. and Takami H. (2007): Infrasound Generated by a High-Speed Train Running Through a Short Tunnel, Journal of Low Frequency Noise, Vibration and Active Control, 26(3), 177-194

Inaba, H., Uddin, M. S., Itakura, Y. and Kasahara, M. (1997): Surface velocity vector field measurement of debris flow based on spatio temporal derivative space method, in: Debris-Flow Hazards Mitigation: Mechanics, Prediction, and Assessment, edited by: Chen, C. L., Proc. First Intern. Conf., San Francisco, USA, 7–9 August 1997, New York, ASCE, 757–766

Issler, D., (2003): Experimental information on the dynamics of dry-snow avalanches, in: Hutter, K. and N. Kirchner (eds.), Dynamic Response of Granular and Porous Materials under Large and Catastrophic Deformations, Lecture Notes in Applied and Computational Mechanics 11, Springer, 109–160

Itakura, Y., Koga, Y., Takahama, J. and Nowa, Y. (1997): Acoustic detection sensor for debris-flow, in: Debris-Flow Hazards Mitigation: Mechanics, Prediction, and Assessment, edited by: Chen, C. L., Proc. First Intern. Conf., San Francisco, USA, 7–9 August 1997, New York, ASCE, 747–756

Itakura, Y., Fujii, N. and Sawada, T. (2000): Basic characteristics of ground vibration sensors for the detection of debris-flow, Physics and Chemistry of the Earth, Part B, 25, 717–720

Itakura, Y., Inaba, H. and Sawada T. (2005): A debris flow monitoring devices and methods bibliography, Natural Hazards and Earth System Sciences, 5, 971-977

Iverson, R. (1997): The physics of debris flow, Reviews of Geophysics, 35(3), 245–296

Johnson, J. (2003): Generation and propagation of infrasonic airwaves from volcanic explosions, Journal of Volcanology and Geothermal Research, 121,1–14

Kanamori, H. and Rivera, L. (2008): Source inversion of W-phase: speeding up seismic tsunami warning, Geophysical Journal International, 175, 222–238

Kenneth, M., Wilson, C., Olson, J. and Szuberla C. (2005): Infrasound Associated with Mt. Steller Avalanche, Inframatics, 12, December 2005, 4-7

Kern, M., Tiefenbacher, F. and McElwaine J. (2004): The rheology of snow in large chute flows, Cold Regions Science and Technology, 39, 181–192

Kern, M., Bartelt, P., Sovilla, B. and Buser, O. (2009): Measured shear rates in large dry and wet snow avalanches, Journal of Glaciology, 55, 327–338

Kim, T., Hayward, C. and Stump, B. (2004): Local infrasound signals from the Tokachi-Oki earthquake, Geophysical Research Letters, 31, L20605, doi: I0.1 02912004GL021178

Kishimura, K. and Izumi, K. (1997): Seismic signals induced by snow avalanche flow, Natural Hazards, 15, 89-100

Kogelnig, A., Hübl, J., Suriñach, E., Vilajosana, I. and McArdell, B. (online first): Infrasound produced by debris flow: propagation and frequency content evolution, Natural Hazards, doi:10.1007/s11069-011-9741-8

Kogelnig, A., Hübl, J., Suriñach, E., Vilajosana, I., Zhang, S., Yun, N. and McArdell, B. (2011): A study of infrasonic signals of debris flows, in: Genevois, R., Hamilton, D. and Prestininzi, A. (Eds.), Italian Journal of Engineering Geology and Environment - Book, 563- 572, ISBN: 1825-6635; ISSN 978-88-95814-46-9

Kogelnig, A., Suriñach, E., Vilajosana, I., Hübl, J., Sovilla, B., Hiller, M. and Dufour, F. (2011): On the complementariness of infrasound and seismic sensors for monitoring snow avalanches, Natural Hazards and Earth System Sciences, 11(8), 2355-2370

La Rocca, M., Galluzzo, D., Saccorotti, G., Tinti, S., Cimini, G. and Del Pezzo, E. (2004): Seismic signals associated to landslides and to tsunami at Aeolian islands, Italy, Geophysical Research Abstracts, Vol. 6, 00738

Lee, P. and Wang, J. (2010): The simulation of acoustic radiation from a moving line source with variable speed, Applied Acoustics, 71, 931–939

Le Pichon, A., Garcés, M., Blanc, E., Barthélémy, M. and Drob, D. (2001): Acoustic propagation and atmosphere characteristics derived from infrasonic waves generated by the Concorde, Journal of the Acoustical Society of America, 111 (1), 629-641

Le Pichon, A., Herry, P., Mialle, P., Vergoz, J., Brachet, N., Garcés, M., Drob, D. and Ceranna, L. (2005): Infrasound associated with 2004-2005 large Sumatra earthquakes and tsunami, Geophysical Research Letters, 32, L19802, doi: 10.1 029/2005GL023893

Le Pichon, A., Blanc, E. and Hauchecorne, A. (2010): Infrasound Monitoring for Atmospheric Studies, Springer

Leprettre, B., Martin, N., Glangeaud, F. and Navarre, J. (1998): Three-Component Signal Recognition Using Time, Time-Frequency and Polarization Information-Application to Seismic Detection of Avalanches, IEEE Transactions on Signal Processing, 46, 83–102

Lied, K., Moe, A., Kristensen, K. and Issler, D. (2002): Ryggfonn: Snow Avalanche Research Program SIP-6: Full scale avalanche test site and the effect of the catching dam, Tech. Rep. NGI report 581200-35, Norwegian Geotechnical Institute, Oslo

Lighthill, M. (1952): On sound generated aerodynamically I, General Theory, Proceedings of the Royal Society A, 211(1107), 564–587

Lighthill, M. (1954): On sound generated aerodynamically II. Turbulence as a source of sound, Proceedings of the Royal Society A, 222(1148), 1–32

Lighthill, J. (1978): Waves in Fluids, Cambridge University Press, New York

Lin, T. and Langston, C. (2007): Infrasound from thunder: A natural seismic source, Geophysical Research Letters, 34, L14304, doi:10.1029/2007GL030404

Long, L. (1983): The Compressible Aerodynamics of Rotating Blades Based on an Acoustic Formulation, NASA Technical Paper 2197, The George Washington University Joint Institute for Advancement of Flight Sciences Langley Research Center Hampton, Virginia

Major, J. and Pierson, T. (1992): Debris flow rheology: experimental analysis of fine-grained slurries, Water Resources Research, 28, 841-857

Marchi L., Arattano M. and Deganutti, A. (2002): Ten years of debris-flow monitoring in the Moscardo Torrent (Italian Alps), Geomorphology, 46(1-2), 1-17

Martinez, A., Fortuny, J. and Gruber, U. (2005): Monitoring of the snow cover with a ground-based synthetic aperture radar, European Association of Remote Sensing Laboratories, eProceedings, 4, 171-178

McClung, D. and Schaerer, P. (1980): Snow Avalanche Size Classification, in: Proceedings of Avalanche Workshop, edited by Comittee, C. A., vol. Technical Memorandum 133,12–27, Associate Committee on Geotechnical Research, Ottawa: National Research Council of Canada

McClung, D. and Schaerer, P. (2006): The Avalanche Handbook, The Mountaineers Books

Mikumo, T. (1968): Atmospheric pressure waves and tectonic deformations associated with the Alaskan earthquake of March 28, 1964, Journal of Geophysical Research, 73, 2009-2025

Nakamura, Y. (1988): On the urgent earthquake detection and alarm system, in: Proceedings of ninth world conference on earthquake engineering, Tokyo, Japan, 7, 673-678

Naugolnykh, K. and Bedard, A. (2002): A model of the avalanche infrasonic radiation, in: Geoscience and Remote Sensing Symposium, 2, 871–872, doi:10.1109/IGARSS.2002.1025713

Navarre, J., Bourova, E., Roulle, J. and Deliot, Y. (2009): The seismic detection of avalanches: an information tool for the avalanche forecaster, in: Schweizer, J. and A. van Herwijnen, (eds.) Proceedings of the International Snow Science Workshop, 27 September–2 October 2009, Davos, Switzerland. Davos, WSL Institute for Snow and Avalanche Research SLF, 379–383

Negraru, P. T. (2010): Application of Seismo-Acoustic Signals to the Study of Local Site Effects, Acta Geophysica, 58(6), 1021-1039, doi:10.2478/s11600-010-0025-6

Nicolas, J., Berry, J. and Daigle, G. (1985): Propagation of sound above a finite layer of snow, Journal of the Acoustical Society of America, 77, 67–73

Nishimura, K., Maeno, N., Kawada, K. and Izumi, K. (1993): Structures of snow cloud in dry-snow avalanches, Annals of Glaciology, 18, 173–178

Okuda, S., Suwa, H., Okunishi, K., Yokoyama, K., Ogawa, K. and Hamana, S. (1979): Synthetic observation on debris-flow, Part 5, Observation at Valley Kamikamihorisawa of Mt. Yakedade in 1978, Annuals of Disaster Prevention Research Institute, Kyoto University, 22B-1, 157–204

Okuda, S., Okunishi, K. and Suwa, H. (1980): Observation of debris flow at Kamikamihori Valley of Mt. Yakedade, Excursion Guidebook of the Third Meeting of IGU commission on Field Experiment in Geomorphology, 127-130

Olson, J., Wilson, C. and Hansen, R. (2003): Infrasound associated with the 2002 Denali fault earthquake, Alaska, Geophysical Research Letters, 30(23), 2195, doi:IO.1029/2003GLOI8568

Ponceau, D. and Bosca, L. (2010): Low-Noise Broadband Microbarometers, in: Infrasound Monitoring for Atmospheric Studies, edited by: Le Pichon, A., Blanc, E. and Hauchecorne, A., Springer, 119-141

Pilger, C. and Bittner, M. (2009): Infrasound from tropospheric sources: impact on mesopause temperature?, Journal of Atmospheric and Solar-Terrestrial Physics, 71(8-9), 816–822, doi:10.1016/j.jastp.2009.03.008

Prokop, A. (2008): Assessing the applicability of terrestrial laser scanning for spatial snow depth measurements, Cold Regions Science and Technology, 54(3), 155-163

Prokop, A (2009): Terrestrial laser scanning for snow depth observations: An update on technical developments and applications, in: Schweizer, J. and Herwijnen, A. van (Eds.), ISSW 09 - International Snow Science Workshop: Proceedings, 192-196

Proudman, I. (1952): The generation of noise by isotropic turbulence, Proceedings of the Royal Society A, 214(1116), 119-132, doi: 10.1098/rspa.1952.0154

Rammer, L., Kern, M., Gruber, U. and Tiefenbacher, F. (2007): Comparison of avalanche-velocity measurements by means of pulsed Doppler radar, continuous wave radar and optical methods, Cold Regions Science and Technology, 50, 35–54

Sabatier, J., Bass, H. and Bolen, L. (1986): Acoustically induced seismic waves, Journal of the Acoustical Society of America, 80(2), 646-649

Sabot, F., Naaim, M., Granada, F., Suriñach, E., Planet, P. and Furdada, G. (1998): Study of avalanche dynamics by seismic methods, image processing techniques and numerical models, Annals of Glaciology, 26, 319–323

Saint-Lawrence, Y. and Williams, T. (1976): Seismic signals associated with avalanches, Journal of Glaciology, 17, 521–526

Salway, A. (1978): A Seismic and Pressure Transducer System for Monitoring Velocities and Impact Pressure of Snow Avalanches, Arctic Antarctic and Alpine Research, 10, 769–774

Santana, V. and Olson, J. (2004): A Study of the Effects of Snow Cover on Infrasonic Signal Levels: Variations in the RMS Levels, Inframatics, 7, September 2004, 22-25

Schlunegger, F., Badoux, A., McArdell, B., Gwerder, C., Schnydrig, D., Rieke-Zapp, D. and Molnar, P (2009): Limits of sediment transfer in an alpine debris-flow catchment, Illgraben, Switzerland, Quaternary Science Reviews, 28, 1097-1105

Schneider, D., Bartelt, P., Caplan-Auerbach, J., Christen, M., Huggel, C. and McArdell, B. (2010): Insights into rock-ice avalanche dynamics by combined analysis of seismic recordings and a numerical avalanche model, Journal of Geophysical Research, 115, doi:10.1029/2010JF001734

Scott, E. and Lance, C. (2002): Infrasonic Monitoring of Avalanche Activity, in: Proceedings International Snow Science Workshop, Penticton, British Columbia

Scott, E., Hayward, C., Kubichek, R., Hamann, J. and Pierre, J. (2004): Results of Recent Infrasound Avalanche Monitoring Studies, in: International Snow Science Workshop, Jackson Hole, Wyoming, 696–704

Scott, E., Hayward, C., Colgan, T., Hamann, J., Kubichek, R., Pierre, J. and Yount, J. (2006): Practical implementation of avalanche infrasound monitoring technology for operational utilization near Teton pass Wyoming, in: Proceedings International Snow Science Workshop

Scott, E., Hayward, C., Kubichek, R., Hamann, J., Comey, R., Pierre, J. and Mendenhall, T. (2007): Single and multiple sensor identification of avalanche-generated infrasound, Cold Regions Science and Technology, 47, 159–170

Sikora, T., Kogelnig, A., Vilajosana, I., Suriñach, E., Hiller, M. and Dufour, F. (2009): Monitoring of snow avalanches - a new approach to measuring flow induced vibrations in the ground and in the air, Geophysical Research Abstracts, Vol. 11, EGU2009-12327

Sovilla, B., Burlando, P. and Bartelt, P. (2006): Field experiments and numerical modeling of mass entrainment in snow avalanches, Journal of Geophysical Research, 111, doi:10.1029/2005JF000391

Sovilla, B., Schaer, M., Kern, M. and Bartelt, P. (2008a): Impact pressures and flow regimes in dense snow avalanches observed at the Vallée de la Sionne test site, Journal of Geophysical Research, 113, 1–14, doi:10.1029/2006JF000688

Sovilla, B., Schaer, M. and Rammer, L. (2008b): Measurements and analysis of full-scale avalanche impact pressure at the Vallèe de la Sionne test site, Cold Regions Science and Technology, 51, 122–137

Sovilla, B., Kern, M. and Schaer, M. (2010a): Slow drag in wet snow avalanche flow, Journal of Glaciology, 56, 587–592

Sovilla, B., McElwaine, J., Schaer, M. and Vallet, J. (2010b): Variation of deposition depth with slope angle in snow avalanches: Measurements from Vallée de la Sionne, Journal of Geophysical Research, 115, doi:10.1029/2009JF001390

Starovoit, Y. and Martysevich P. (2005): Different observed mechanisms of correlation between seismic and pressure signals, Inframatics, 9, March 2005, 11-16

Stein, S. and Wylesession, M. (2003): An Introduction to seismology, earthquakes and earth structure, Blackwell Publishing

Stubbs, C. (2005): Tactical infrasound, Technical report, The MITRE Corporation, Department of the Army United States Army Intelligence and Security Command National Ground Intelligence Center, Charlottesville, Virginia

Strachey, R. (1888): On the air waves and sounds caused by the eruption of Krakatoa in August, 1883, in: The Eruption of Krakatoa and Subsequent Phenomena, edited by G. J. Symons, 57–88,Trubner, London

Suriñach, E., Sabot, F., Furdada G. and Vilaplana, J. (2000): Study of seismic signals of artificially released snow avalanches for monitoring purposes, Physics and Chemistry of the Earth, 25(9), 721–727

Suriñach, E., Furdada, G., Sabot, F., Biescas, B. and Vilaplana, J. (2001): On the characterization of seismic signals generated by snow avalanches for monitoring purposes, Annals of Glaciology, 32, 268–274

Suriñach, E. (2004): Spanish avalanche research: Experimental sites and seismic measurements, in: Snow and Avalanche Test Sites, edited by Naaim, M. and Naaim-Bouvet, F., 71–183, Cemagref

Suriñach, E., Vilajosana, I., Khazaradze, G., Biescas, B., Furdada, G. and Vilaplana, J. (2005): Seismic detection and characterization of landslides and other mass movements, Natural Hazards and Earth System Sciences, 5, 791–798

Suriñach, E., Kogelnig, A., Vilajosana, I., Hübl, J., Hiller, M. and Dufour, F. (2009): Incorporación de la señal de infrasonido a la detección y estudio de aludes de nieve y flujos torrenciales, in: VII Simposio Nacional sobre Taludes y Laderas Inestables, edited by Alonso, E., Corominas, J., and Hürlimann, M., Barcelona, Spain

Sutherland, L. and Bass, H. (2004): Atmospheric absorption in the atmosphere up to 160 km, Acoustical Society of America, 3(115), 1012-1032

Suwa, H., Yamakoshi, T. and Sato, K. (2000): Relationship between debris-flow discharge and ground vibration, in: Debris-Flow Hazards Mitigation: Mechanics, Prediction, and Assessment, edited by: Wieczorek, G. F. and Naeser, N. D., Proceedings 2nd International Conference, Taipei, Taiwan, 16-18 August 2000, Rotterdam, Balkema Press, 311–318

Takahashi, T. (2007): Debris Flow: Mechanics, Prediction and Counter measurements, Taylor and Francis Group, London, UK

Takami, H. and Kikuchi, K. (2010): Experimental investigation of low-frequency wayside noise from high-speed train, Quarterly Report of Railway Technical Research Institute, 51(1), 23-28

Thorne, L. and Wallace, T. (1995): Modern Global Seismology, Academic Press, San Diego, USA

Tipler, P. (1994): Physics for scientists and engineers, Worth Publishers Inc., New York, USA

Turnbull, B. and McElwaine, J. (2007): A comparison of powder-snow avalanches at Vallée de la Sionne, Switzerland, with plume theories, Journal of Glaciology, 53, 30–40

Uddin, M. S., Inaba, H., Itakura, Y., Yoshida, Y. and Kasahara, M. (1999): Adaptive computer-based spatial filtering method for more accurate estimation of the surface velocity of debris-flow, Applied Optics, 38, 6714–6721

Udías, A. (1999): Principles of Seismology, Cambridge University Press

Vallet, J., Turnbull, B., Joly, S. and Dufour, F. (2004): Observations on powder snow avalanches using videogrammetry, Cold Regions Science and Technology, 39, 153–159

VanDine, D. (1985): Debris flows and debris torrents in the southern Canadian Cordillera, Canadian Geotechnical Journal, 22, 44-68

VanHerwijnen, A. and Schweizer, J. (2011): Seismic sensor array for monitoring an avalanche start zone: design, deployment and preliminary results, Journal of Glaciology, 57(202), 267-276

Vilajosana, I., Khazaradze, G., Suriñach, E., Lied, E. and Kristensen, K. (2007): Snow avalanche speed determination using seismic methods, Cold Regions Science and Technology, 49, 2–10

Vilajosana, I., Suriñach, E., Khazaradze, G., and Gauer, P. (2007): Snow avalanche energy estimation from seismic signal analysis, Cold Regions Science and Technology, 50, 72–85

Vilajosana, I. (2008): Seismic detection and characterization of snow avalanches and other mass movements, PhD thesis, Universitat de Barcelona, Department de Geodinámica i Geofísica, Facultat de Geologia

Vilajosana, I., Suriñach, E., Abellán, A., Khazaradze, G., Garcia, D. and Llosa, J. (2008): Rockfall induced seismic signals: case study in Montserrat, Catalonia, Natural Hazards and Earth System Sciences, 8(4), 805–812

Vilajosana, I. and Alasonati, P. (2008): Seismic Detection of snow Avalanches using Wavelet-Based Hidden Markov Models, Geophysical Research Abstracts, 10, EGU2008-A-08940

Walker, K. and Hedlin, M. (2010): A Review of Wind-Noise Reduction Methodologies, in: Infrasound Monitoring for Atmospheric Studies, edited by: Le Pichon, A., Blanc, E. and Hauchecorne, A., Springer, 119-141

Watada, S., Kunugi, T., Hirata, K., Sugioka, H., Nishida, K., Sekiguchi, S., Oikawa, J., Tsuji, Y. and Kanamori, H. (2006): Atmospheric pressure change associated with the 2003 Tokachi-Oki earthquake, Geophysical Research Letters, 33, L24306, doi: 10.1029/2006GL027967

Wu, J., Kang, Z., Tian, L. and Zhang, S. (1990): Observation and investigation of debris flows at Jiangjia Gully in Yunnan Province (China), Science Press, Beijing, China

Zhang, S. (1993): A Comprehensive Approach to the Observation and Prevention of Debris Flow in China, Natural Hazards, 7, 1-23

Zhang, S., Hong, Y. and Yu, B. (2004): Detecting infrasound emission of debris flow for warning purposes, International Symposium Interpraevent VII, Riva, Trient, 359–364

Arnold Kogelnig

Development of acoustic monitoring for alpine mass movements

Snow avalanches and debris flows (alpine mass movements) are processes that occur in high alpine regions with consequences on infrastructure and settlements. This study presents a new approach to gather knowledge about alpine mass movements using a combination of two acoustic sensors: seismic sensors and infrasound microphones. Both sensors have been individually used in many previous studies. But the potential combination of infrasonic and seismic sensors for monitoring natural hazards, which could take advantage of the benefits of both sensor technologies, has not been evaluated to date. As a consequence, the aim of the present work is an in-depth, combined study considering both the infrasonic and the seismic wave field generated by alpine mass movements.

A detailed analysis of seismic and infrasonic signals generated by snow avalanches and debris flows monitored at different locations in the Austrian, Swiss Alps and China will be presented. Additionally, the data will be compared with other measurements, such as flow depth (for debris flows) or flow velocity and pressure (snow avalanches), for the interpretation, verification and validation of the seismic and infrasonic data.

The most important characteristic of acoustic signals from alpine mass movements are summarized and possible interfering signals are presented. At the end an outlook to the future of monitoring alpine mass movements is given.

Arnold Kogelnig (Master Degree in Land and Water Management and Engineering, Master Degree in Mountain Risk Engineering) Since 2008 scientific stuff and PhD student at the Institute of Mountain Risk Engineering, University of Natural Resources and Applied Life Sciences, Vienna